DEPARTMENT OF ELECTRICAL AND ELECTRONIC ENGINEERING
FACULTY OF ENGINEERING
LOUGHBOROUGH UNIVERSITY

NON-INVASIVE VASCULAR ASSESSMENT USING PHOTOPLETHYSMOGRAPHY

BY

VINCENT PETER CRABTREE

A Doctoral Thesis
Submitted in partial fulfilment of the requirements for the award of
Doctor of Philosophy of Loughborough University

March 2003

Supervisor: Professor Peter R. Smith
Department of Electrical Engineering

For the Trueman family,

Who showed me real faith and kindness.

Abstract

Photoplethysmography (PPG) has become widely accepted as a valuable clinical tool for performing non-invasive biomedical monitoring. The dominant clinical application of PPG has been pulse oximetry, which uses spectral analysis of the peripheral blood supply to establish haemoglobin saturation. PPG has also found success in screening for venous dysfunction, though to a limited degree.

Arterial Disease (AD) is a condition where blood flow in the arteries of the body is reduced, a condition known as ischaemia. Ischaemia can result in pain in the affected areas, such as chest pain for an ischeamic heart, but does not always produce symptoms. The most common form of AD is arteriosclerosis, which affects around 5% of the population over 50 years old. Arteriosclerosis, more commonly known as 'hardening of the arteries' is a condition that results in a gradual thickening, hardening and loss of elasticity in the walls of the arteries, reducing overall blood flow.

A subset of AD, Peripheral Arterial Disease (PAD), is caused by reduced blood flow in the arteries supplying the leg. The most common symptom of PAD is pain in the leg or foot during exercise, subsiding upon cessation of exercise. PAD often results in loss of mobility caused by uncomfortable pains and cramps. Severe PAD can result in reduced healing ability in the extremities, often producing ulcers which are slow to heal, which can in extreme cases become gangrenous and require amputation.

The Ankle Brachial Pressure Index (ABPI) is a common technique for diagnosing PAD in the legs and feet, employing the detecting changes in blood pressure in the extremities as a result of arteriosclerosis. This thesis investigates current PAD diagnosis methods including the ABPI protocol, providing an overview and identifying weakness in current methodologies.

This thesis investigates the possibility of employing PPG to perform vascular assessment, specifically arterial assessment, in two ways. PPG based perfusion monitoring may allow identification of ischaemia in the periphery. To further investigate this premise, prospective experimental trials are performed, firstly to assess the viability of PPG based perfusion monitoring and culminating in the development of a more objective method for determining ABPI using PPG based vascular assessment.

A complex interaction between the heart and the connective vasculature, detected at the measuring site, generates the PPG signal. The haemodynamic properties of the vasculature will affect the shape of the PPG waveform, characterising the PPG signal with the properties of the intermediary vasculature. This thesis investigates the feasibility of deriving quantitative vascular parameters from the PPG signal. A quantitative approach allows direct identification of pathology, simplifying vascular assessment. Both forward and inverse models are developed in order to investigate this topic. Application of the models in prospective experimental trials with both normal subjects and subjects suffering PVD have shown encouraging results.

It is concluded that the PPG signal contains information on the connective vasculature of the subject. PPG may be used to perform vascular assessment using either perfusion-based techniques, where the magnitude of the PPG signal is of interest, or by directly assessing the connective vasculature using PPG, where the shape of the PPG signal is of interest.

It is argued that PPG perfusion based techniques for performing the ABPI diagnosis protocol can offer greater sensitivity to the onset of PAD, compared to more conventional methods. It is speculated that the PPG based ABPI diagnosis protocol could provide enhanced PAD diagnosis, detecting the onset of the disease and allowing a treatment plan to be formed sooner than was possible previously.

The determination of quantitative vascular parameters using PPG shape could allow direct vascular diagnosis, reducing subjectivity due to interpretation. The prospective trials investigating PPG shape analysis concentrated on PVD diagnosis, but it is speculated that quantitative PPG shaped based vascular assessment could be a powerful tool in the diagnosis of many vascular based pathological conditions.

Keywords: Photoplethysmography, arterial disease, vascular assessment, dual-channel

Acknowledgements

I would like to express my sincere gratitude and respect to my supervisor, Professor Peter Smith, for his guidance and support throughout my research. Additionally, I would like to thanks both Current and Previous members of the Optical Engineering Group for their assistance and advice.

Thanks must also be given to the Engineering and Clerical staff at Loughborough University, whose assistance proved invaluable during my time there.

Acknowledgement is given to the Engineering and Physical Sciences Research Council; without their sponsorship, this research would not have been possible.

Contents

Optical Engineering Group
Loughborough University

Chapter One

Introduction

1 Introduction

1.1 Introduction

Photoplethysmography (PPG) is the non-invasive electro-optic method for detecting the cardiovascular pulse wave, generated by quasi-periodic contractions of the heart, which propagates through the body. PPG has found considerable use in the fields of non-invasive physiological monitoring; the most successful application of PPG being pulse oximetry, but PPG has found lesser applications in the field of vascular assessment, where the dominant diagnosis technique is Ultrasound imaging.

The complex interaction between the heart and connective vasculature are the principle components of the mechanism that generates the PPG signal. Although the PPG signal is known to be sensitive to vascular changes, such as ageing, hypertension and peripheral vascular disease, pertinent methods of identifying an index of vascular health are currently the subject of research.

This thesis is a contribution to the field of vascular assessment, providing an appraisal of which aspects of the PPG signal are most compatible with vascular assessment. In deciding this question, novel methodologies have been developed for performing vascular assessment using PPG, based on assessment of perfusion and vascular parameterisation, which is the quantification of vascular haemodynamics.

1.1.1 Thesis Overview

The area of vascular assessment is multidisciplinary, requiring knowledge of biology, physiology and engineering in order to investigate the premise fo vascular assessment using PPG. This thesis goes some way to unifying these differing fields to provide a coherent argument for the feasibility of PPG vascular assessment.

The first chapter contains an in-depth review of the fundamental aspects of PPG. These include generation of the actual PPG waveform and the relationship between optical density changes registered by PPG to anatomical blood volume changes in the periphery.

The elementary *modus operandi* of arterial PPG, that perfusion, and thus arterial PPG proper, are proportional to arterial pulse pressure, will be discussed. The proportionality of

PPG to arterial pulse, in that arterial PPG is correlated to arterial pressure, is the fundamental limitation of PPG, since a lack of absolute quantification causes the PPG signal level to be un-calibrated, or relative.

Chapter One will also discuss the effects of peripheral vascular disease (PVD) on both subject life-style and mortality. Current primary identification means of physiology and PVD will be discussed, and the limitations regarding error evaluated. Peripheral arterial disease, a subset of PVD, will be introduced, and the primary diagnostic tools investigated.

The development of heuristic models in order to employ PPG for vascular assessment will be performed in Chapter Two. A simple perfusion model, based on light and tissue interaction, will be developed, allowing blood volume changes to be evaluated across differing subjects.

A review of blood pressure models will be discussed in order to apply blood pressure based models in the context of PPG. This is a novel concept since the un-calibrated nature of PPG has previously limited applications of this type. Development of the pressure based forward model will give an expression for arterial pressure, based on model parameters, dependant on the haemodynamic properties of the arterial system. An argument will justify the application of the pressure model to the PPG signal, allowing indirect determination of quantified vascular parameters using numerical fits. The actual relationship between the vascular parameters will be described, in order to provide a correlation between actual vessel anatomy and vascular parameters.

Chapter Three will extend the vascular parameter forward model, developed in chapter two, in order to develop a novel inverse model that provides information on the vasculature without the need for fitting. This methodology will be applied to PPG signals, and will be independent of the magnitude of the PPG signal, allowing determination of vascular parameters by way of relationship. The concept of dual channel analysis will be introduced, whereby comparative vascular assessment may be performed. Comparative assessment of dual distal sites could offer self-normalisation advantages, reducing PPG calibration problems.

The perfusion-based models (developed in chapter two) will be assessed for validity in Chapter Four, with the aid of experimental trials. A sport science based trial will attempt to identify changes in perfusion as a result of exercise. The sport science trial will evaluate the

developed methodologies regarding perfusion analysis, identifying the suitability of these techniques for perfusion assessment.

A clinical trial will attempt to enhance current peripheral arterial disease (PAD) diagnosis techniques, the most common of which is the ankle-brachial pressure index (ABPI) protocol. As part of the clinical trial, a novel methodology of performing automatic PPG based systolic blood pressure (SBP) determination will be developed. This will allow operator independent automatic SBP and ABPI determination using a modified sphygmomanometry protocol, based on the simple PPG perfusion model and perfusion trend analysis. The novel procedure will be argued more sensitive to the onset of PAD, as the peripheral nature of PPG affords diagnosis of the microvasculature; these vessels being most susceptible to the effects of PAD.

The vascular models developed in chapters two and three will be incorporated into experimental subject trials in Chapter Five. A small prospective trial study was conducted on known subject groups in order to determine the feasibility applying blood pressure forward model to PPG in order to obtain quantified vascular parameters by numerical fitting. The inverse model will be examined in relation to differing subject groups, and the suitability of the inverse model to vascular assessment investigated.

A clinical trial will investigate the suitability of the forward and inverse models for the assessment of vascular disease – in this case, occlusive PAD in the feet. This feasibility trial will be the culmination of the quantitative methods developed in previous chapters, to investigate whether PPG can indeed offer increased functionality for vascular assessment.

Chapter Six will briefly reiterate the major achievements of the work and provide concluding remarks. Suggestions for further extensions and enhancements to the work will be made, together with suggestions for further studies in order to reinforce the reliability of the initial trial results tentatively presented here.

1.2 Photoplethysmography

The term 'Photoplethysmography' (PPG) is derived from ancient Greek 'plethysmos', meaning increase; 'plethys' meaning mass, 'photo' meaning optical along with the ancient Greek for write, 'graph'. The fundamental *modus-operandi* of this technology is the detection of the dynamic cardiovascular pulse-wave, generated by the heart, as it travels throughout the body.

First developed by Hertzman[1], PPG is used to describe the detection by photoelectric methods of this pulse wave. Commonly called *blood volume pulse*[2] in the USA, the cardiovascular pulse wave is generated by the elastic nature of the peripheral vascular arteries excited by the quasi-periodic contractions of the heart. The heart instigates a pulse pressure wave that propagates throughout the arteries into deeper vasculature. A stationary probe on the skin can detect a time varying dynamic blood volume change as caused by the cardiovascular wave; resulting in a corresponding inverse change in the optical absorption of this tissue under inspection. Well-perfused peripheral tissue has a blood-volume increase during the *systole* (contraction of the heart ventricles) thereby reducing light transmission through peripheral vasculature[3]. These optical changes are detectable qualitatively using an electronic photo sensor and electronic signal processing equipment.

1.2.1 PPG Signal Generation

This section describes PPG signal generation. It is important to understand the complex interaction of the various physiological subsystems of the body and how these may affect PPG signal generation. To do so requires knowledge of the human/PPG system interface, which is the skin.

1.2.1.1 Background Physiology

The skin is the largest organ of the body, possessing excellent self-healing capabilities. It not only provides mechanical protection in the form of abrasion resistance for the underlying vasculature and tissue, it also provides environmental protection, preventing the underlying tissue from dying out. Additionally, the skin is the body's first line of defence against external bacteria and viruses.

Figure 1-1 shows an idealised cross section of the outer layer of the skin. The organisation of the skin goes some way in revealing how changes in body physiology may affect PPG signal generation.

The skin is divided into four main parts: the *stratum corneum*, the *epidermis*, the *dermis* and finally subcutaneous tissue. The *stratum corneum* is the outermost skin layer and comprises dead skin cells, usually less than 50μm thick. A pigment, melanin, is present in the *epidermis* which determines skin tone; its function is to absorb short wavelength ionising radiation, typically UV radiation. Due to the small size of the cells present in this layer, absorption rather than scattering is the dominant light-tissue interaction; this layer is usually less than 100 μm thick. The dermis is between 1 and 4mm thick, and comprises a highly scattering

combination of proteinus fibres, dermal cells and blood vessels contained in interstitial fluid, which is a viscous yellow gel containing various essential salts and sugars. Subcutaneous tissue is deeper still, comprising yellow fat globules used for mechanical protection and energy storage. Subcutaneous tissue is well perfused with vessels and is both highly scattering and absorbing. Subcutaneous tissue offers the mechanical protection required by the body, and as thus is differing thickness in different body locations. It may be several centimetres thick covering the buttocks but unfortunately only a few mm thick covering the shin bone. Underneath subcutaneous tissue is the red tissue of muscles, organs or even the white structure of bone, depending on location.

1.2.1.2 Skin Involvement in CNS temperature regulation

Epidermal tissue contains around 5% blood[4], a value that far exceeds its metabolic requirement. The primary reason for this excess perfusion is to maintain the central nervous system (CNS) at an acceptable operational temperature[5]; put simply, brain temperature regulation. The skin can accommodate a wide range of blood flows dependent on the body's needs to either dissipate or conserve heat, depending on environmental and other conditions. Conservation of heat is achieved by employing counter-current heat exchange blood vessel pairs[6]; each vessel pair containing blood travelling to and returning from the epidermis. This methodology reduces skin blood temperature by warming returning blood (i.e. transferring heat from skin bound blood to returning blood) from the skin, reducing the skin/air temperature gradient therefore minimising radiative heat loss.

Moreover, arterio-venous shunts may be employed to reduce blood flow to the skin. This short-term event is reversed as time progresses so as not to cause physiological damage by oxygen deprivation. The skin initially becomes blanched when cold, due to this bypassing of blood to the skin, but then becomes redder after several minutes when epidermal blood flow has returned and counter-current heat exchangers are employed to reduce the temperature of the blood passing to the skin surface.

If the body needs to dissipate excess heat in order to maintain the CNS at acceptable levels, blood may pass through a superficial network of veins with the purpose of transferring heat to the surrounding tissue. This triggers other physiological effects, such as sweating, in an attempt to reduce skin temperature by evaporative cooling. Figure 1-1 illustrates these features, such as the deep plexus and superficial plexus with an exemplary counter current heat exchanger.

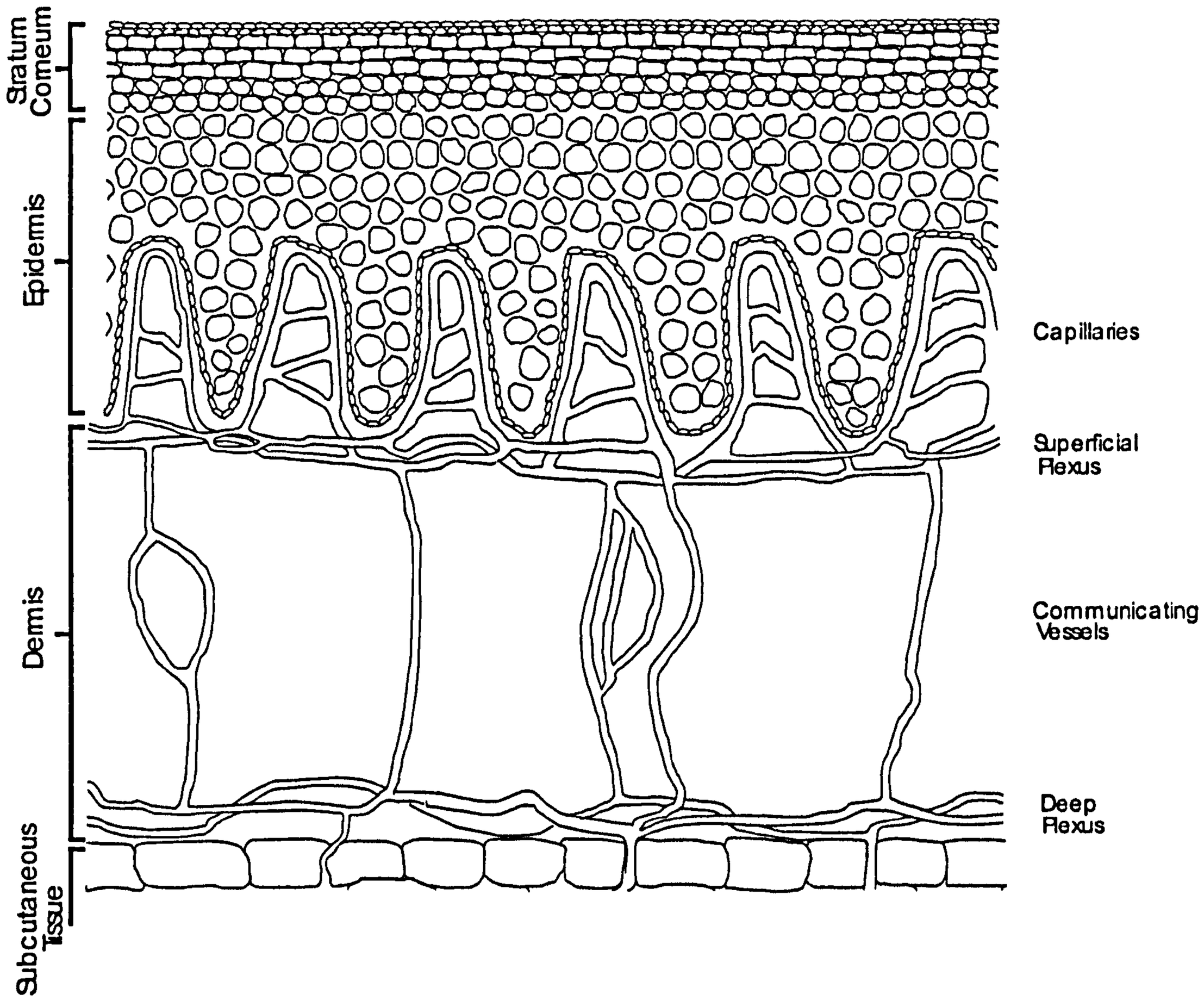

Figure 1-1. Idealised cross sectional view of the skin.

1.2.1.3 Generation of the Pulse Pressure Wave

During *systole*, the contraction of the left ventricle of the heart ejects the contained blood within it 'into' passed the semi lunar check valves into the ascending aorta. Blood present within the aorta is stationary compared to the velocity of the blood leaving the heart. As the aorta attempts to contain the ejected volume of blood, blood within the aorta will be displaced further 'into' the arterial vasculature, creating a pressure wave front that travels along the arterial circulatory system. Since the front of the pressure wave travels down the elastic arterial circulatory system, the transient increased pressure generated during systole causes the vessel walls to expand, thereby accommodating an extra volume of blood over the quiescent volume. During *diastole*, the arteries release this stored blood further into the vasculature, first noted in 1733 by Rev. Stephen Hales[7]. The blood volume increase caused by the elastic nature of the arteries will flow further 'into' the vasculature since the closed heart valve prevents backflow, thereby returning blood volume to quiescent values, ready for

the next cycle. This periodic expansion and 'contraction' may be imagined as a bolus of blood travelling along the arterial system starting with expansion of the aorta. Since the heart contracts quasi-periodically, the arteries will oscillate in size but opposite in phase to the rhythmic contractions of the heart. Harvey[8] used this observation in his 1628 treatise on the circulatory system, which up until that point in time had not been described.

In contrast, the venous system receives an almost steady flow of blood from the microcirculation, gradually collecting this slow return of blood into a significant volume for re-circulation by the heart. If a little blood is lost, blood pressure in the arteries remains fairly constant meaning arteries and the heart contain the same amount of blood as before. Since 80% of the blood[9] is contained in the veins, collapsing veins (which form a non-circular shape when only partially full) control the volume levels of the blood. In short, arteries form the circulatory system pressure buffer and veins form the circulatory volume buffer.

1.2.1.4 Light and Tissue Interaction

If we now consider a controlled light source illuminating the vascular bed, any light interactions, either transmission or reflection (see section 1.2.2 below), between the light penetrating the skin and the vasculature within the skin will be modulated periodically.

As described previously, during *systole* the increased volume of blood forced into the arterial vasculature will cause a corresponding increase in optical absorption, with a decrease in any light reaching a photo sensor. During *diastole*, the increased arterial blood volume returns to quiescent values, as does optical absorption.

A photo sensor may be employed to detect these alternate expansions and contractions of the arteries by detection of the associated inverse change in light transmission or reflectance caused by these blood volume changes, generating an arterial PPG waveform.

1.2.2 PPG Modes of Operation

The vascular bed, responsible for dynamic optical absorption changes as discussed in section 1.2.1.4 above, may be illuminated with an appropriate wavelength in order to produce the PPG signal. Generally, the illuminating PPG wavelength is chosen based upon weak absorption by tissue and stronger absorption by blood (relatively speaking) to give a high degree of optical contrast. Near infra red (NIR) radiation is often employed since an LED provides a convenient illumination source, NIR light poses little subject hazard at the low intensities employed in PPG and NIR light can penetrate up of 20 mm in tissue[10].

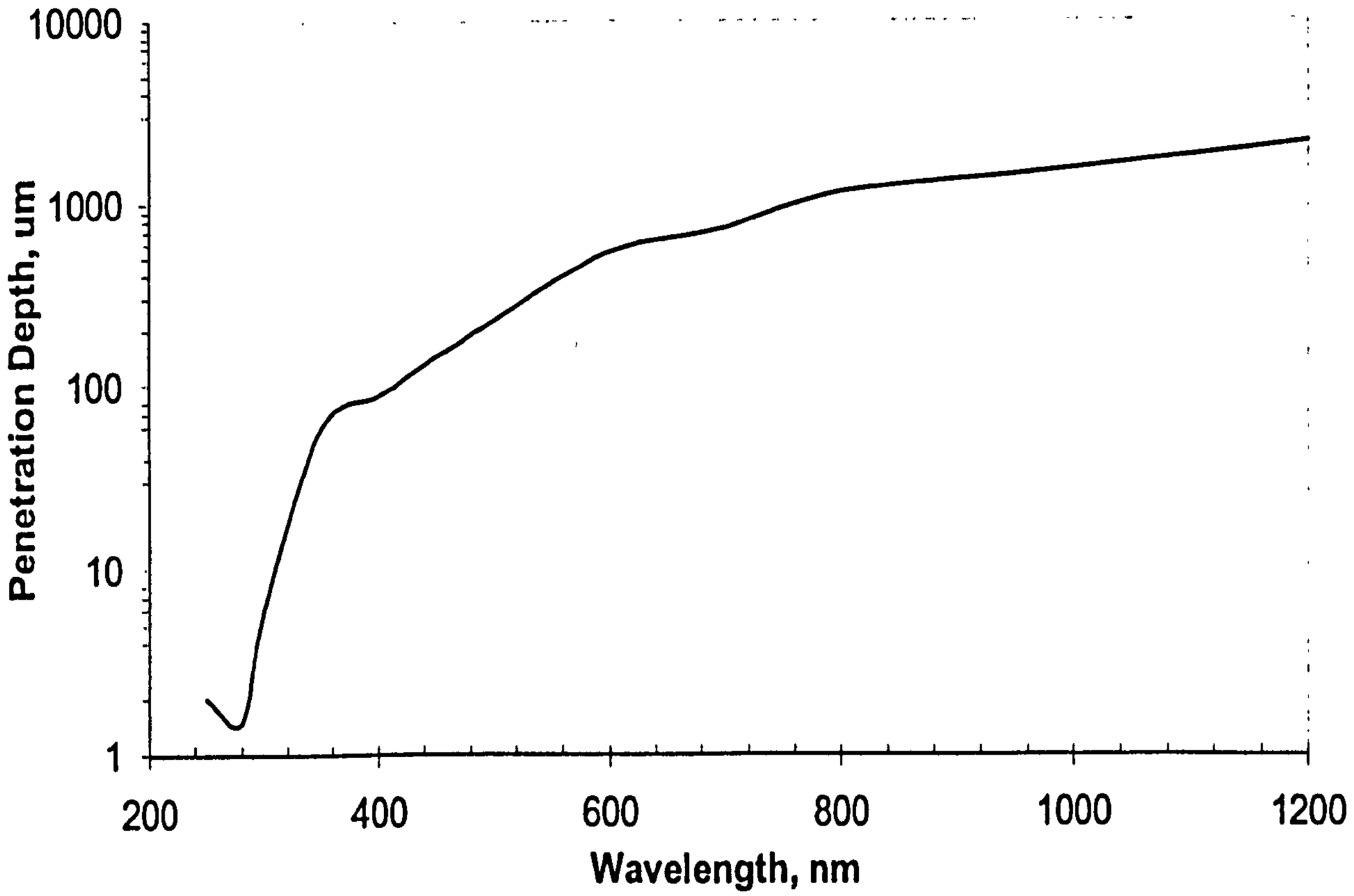

Figure 1-2. Penetration depth of light versus wavelength in epidermal tissue for e^{-1} incident light energy density.

Figure 1-2 shows typical transmission ranges through fair Caucasian skin for e^{-1} ratio of incident light energy density. A photo-sensor may be used to detect dynamic changes in absorption caused by the dynamic blood volume pulse. Suitable illumination points are usually well-perfused areas where the surface dermal layer is relatively thin, which allows interaction of the illuminating light source and peripheral vasculature. Commonly, areas of analysis have been fingers[13], ears and toes[11].

These sites may be distinguished by the mode[12] of optical detection:

Transmission mode is where light passes through tissue to be detected by a sensor (usually diametrically) opposite the illumination source. Examples of this technique are finger probes, toe probes, penile probes, and ear probes.

Reflection mode is where light from the illumination source is reflected from pulsatile tissue to be detected by a sensor usually adjacent to the illumination source. Consequently, the active side of both the photo sensor and illumination source face the same general direction. Typical examples of reflectance mode probes are venous pooling sensors, muscle oximetry sensors, and forehead sensors.

1.2.2.1 Transmission Mode PPG

Monitoring sites for transmission mode[13] PPG are limited to areas where the perfused tissue is relatively transparent, allowing transmitted light to be detected through the tissue volume.

Commonly toes, fingertips, ears and feet or hands in the case of neonates are favourable probe placement areas. One of the most common designs of transmission mode PPG probe (used extensively in pulse oximetry) employs a finger clip with a light physical clamping action that helps keep finger, photo sensor and illumination source fixed relative to one another, thereby reducing both motion and ambient light artefact. The probe mounts to contra-lateral side of the fingertip; one half of the probe illuminates the nail matrix while the other half detects transmitted light through the finger. The advantage in using transmission mode probes over reflection mode probes is also its main disadvantage. Signal recovery electronic circuitry is generally simpler, therefore less expensive, for transmission mode probes; transmission mode probes generally illuminate a large tissue volume which results in a large returned pulsatile signal component due to light being modulated as it passes through the entire pulsatile tissue. The direct disadvantage with transmission mode probes is the increased sensitivity to motion artefact caused by changes in the field of view of the probe due to probe/tissue movement.

1.2.2.2 Reflection Mode PPG

In reflection mode PPG[14] both source and detector are usually positioned adjacently at the skin contact surface. In the case of reflection mode PPG, back scattered rather than transmitted light is responsible for generating the detected PPG signal. PPG allows monitoring of central sites, such as forehead, limbs, and chest. A reflection mode probe may be successfully employed on a subject in a state of peripheral circulatory shutdown, such as a hypothermic patient, by applying a reflection mode probe to the forehead, where the reflected light is fully modulated by the pulsating vascular bed.

It is the viability of reflection mode PPG in sites where transmission mode PPG is inapplicable, which is the methods main advantage. However, since the reflected component only interacts with a relatively small tissue volume, the received signal requires more processing to extract signals of interest, therefore more complex electronics. An application of reflection mode PPG is deep tissue oximetry.

1.2.3 Breakdown of the PPG signal

Dermal tissue contains approximately 5% blood, and this blood experiences only a small volumetric change due to the pulsatile pressure wave. Therefore, the PPG signal recovered from the photo-sensor contains a pulsatile component of between 1-5%[4], the rest of the recovered signal being attributable to other light/tissue interaction. Table 1-1 presents the relative component signal levels.

Absorption Component	Relative absorption index
Pulsatile due to dynamic arterial blood	0 to 1
Static due to arterial blood	1 to 5
Static due to venous blood	5 to 50
Static due to skin, bone and tissue	50 to 500

Table 1-1. Vascular bed dynamic absorption, taken from [4].

From Table 1-1 it is apparent that the significant absorption is due to the very tissue itself; this absorption characteristic has yet to provide useful information. The next largest proportion of the recovered signal is due to venous non-pulsatile blood. Whilst static absorption due to venous blood is difficult to distinguish from static absorption due to skin and other anatomical components, this component has found use in comparative venous testing[15]. It may be deduced from Table 1-1 that the recovered PPG signal contains a minor time varying (in the short-term) dynamic signal that represents arterial pulsations. Since dynamic arterial volume pulsation is dependent on the skin blood supply, peripheral microcirculation may be assessed using PPG[16]. A much larger quasi-static component attributable to venous blood volume is the underlying trend of any recovered PPG signal. Generally, clinical PPG equipment (such as pulse oximeters) isolates arterial pulsations for analysis and venous quasi-static signal for calibration purposes.

1.2.4 Applications of PPG

Currently, the dominant application of PPG is pulse-oximetry[13]. This non-invasive technique uses the differences between the relative absorption of differing haemoglobin species to obtain an indication of arterial oxygen saturation.

Studies using arterial PPG have investigated physiological factors such as pulse and respiration rate[17,18], vasomotion[19], blood flow[3], arterial blood pressure[20] and visco-elastic properties of vessels[21]. Quasi-static (venous) PPG allows a variety of functional venous haemodynamic tests to be performed[22], with renewed clinical interest in this technique being stimulated by the introduction of calibration[23,24]. Several typical applications of PPG are discussed in detail below.

1.2.4.1 The Muscle Pump

General muscle activity causes compression of the venous vasculature surrounding these active muscles. This compression causes displacement of venous blood - check-valves in the

venous vasculature (first identified by Hieronymus Fabricus 1537-1619) convert this displacement into a flow – venous blood is literally squeezed from small veins into larger veins ('towards' the heart) by the contraction of skeletal muscles around them. This positive flow effort is given the term 'muscle pump'[25] and assists venous return to the heart. The operation of the muscle is essential in the legs since venous pressure in the extremities is often sub-atmospheric[9] and venous blood will not return to the heart when the subject is standing. Venous insufficiency is a disease where the venous return check valves mentioned above are faulty, resulting in venous back flow ('away' from the heart) immediately after muscle pumping, causing venous oedema, or pooling of blood in the extremities. Venous pooling causes fluid leakage into adjacent tissue resulting in swollen and bruised extremities. Venous PPG monitors the blood volume in the feet both before and after dorsaflex (repeated calf extension and contraction) extensions. A healthy subject will illustrate venous refilling by arterial inflow alone[26], whereas a diseased patient will suffer shortened venous reflux[27]. Remedial action, such as wearing compression stockings, helps limit venous pooling and encourages 'forward' motion of venous blood.

1.2.4.2 Deep Vein Thrombosis

If the patient is suffering a potentially limb threatening venous obstruction, such as a deep vein thrombosis (DVT), then a vein occlusion test is used to screen for this so called venous occlusion. Venous return is restricted by inflation of a cuff around the periphery to a level greater than the venous pressure, more than around 20mmHg. A reduced PPG transmission results from the increased blood volume due to venous pooling. The cuff is then released allowing the 'drainage' time to be monitored and compared against known healthy values. If the drainage time exceeds known healthy drainage times then venous return is compromised and a DVT is a possible diagnosis[28]. Combinations of DVT and venous insufficiency may be detected by comparing both refilling and drainage times in the same test.

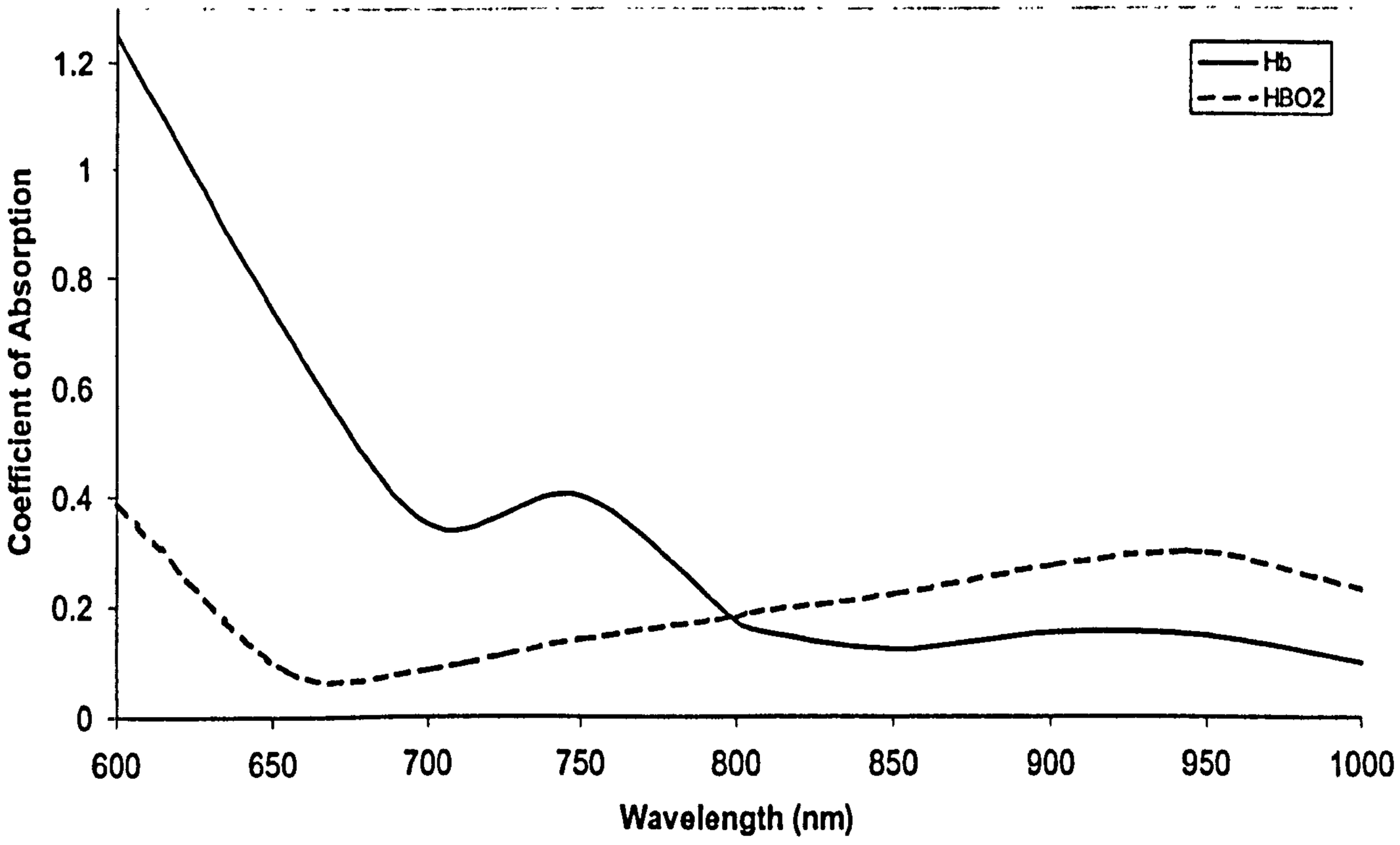

Figure 1-3. Haemoglobin Species optical absorption.

1.2.4.3 Pulse Oximetry

The first recorded instance of an Oximeter[29] was a device that measured the oxygen saturation of the blood using a continuously illuminated system operating in transmission mode on a heated earlobe. Dual wavelength spectroscopy is performed since haemoglobin (Hb) and oxy-haemoglobin (HbO_2) have differing absorption characteristics with respect to wavelength; this fact allows calculation of blood oxygen saturation, usually termed SpO_2.

When the vascular bed is illuminated with two light sources (using either transmission or diffuse reflection mode[30]) of appropriate wavelength, a contrast is observed dependent on the relative concentration of the two species, thus oxygen saturation. Commonly, NIR and red wavelengths are chosen around the isosbestic (crossover) point, which is the wavelength where both species have identical absorption; Figure 1-3 illustrates optical absorption of the two species[31]. Some research suggests it may be advantageous to use illuminating wavelengths either side of the isosbestic point[32]. The Oximeter was improved by recognising the change in absorbency ratio caused by arterial pulsations, which removed the need for heated probes[33]. Here, the arterial pulsations are used to differentiate between static and dynamic signals (effectively spectral PPG). This approach removes the optical properties of

skin, bone, and tissue from the calibration procedure. Incorporation of PPG and oximetry in 1980 produced the first pulse oximeter using a transmission mode finger probe[13].

The use of a pulse Oximeter in the operating theatre has become mandatory in many countries in order to detect anaesthesia-induced hypoxia. Pulse Oximetry is also used in many neonatal intensive care units for apnoea detection. Many variants of pulse oximetry have been developed, such as reflection mode oximetry[34] and a fibre based Oximeter[35] suitable for use in MRI equipment, and multi-wavelength Oximeter[36] used to detect arterial pulsations in the presence of artefact.

1.2.5 Assumptions of PPG

The fundamental assumption with PPG is that a change in received optical intensity is caused by a corresponding change in blood volume in the field of view of the probe. This assumption allows modelling of blood volume changes assuming an average uniform distribution of blood in the vascular tissue within the field of view. Dynamic blood volume changes cause a corresponding change in the homogeneous and macroscopic optical properties of the tissue. Blood volume changes may be detected with a greater contrast, than for example plasma volume changes, by employing a corresponding illumination wavelength with greater absorption by the blood than plasma. The dominant effect in any recovered PPG signal will then be attributable to blood volume changes since this has a greater contrast than other physiological effects.

Previous studies have reported a strong correlation between dynamic PPG and dynamic strain gauge plethysmography[37] providing strong evidence that the dynamic PPG signal is a measure of dynamic blood volume change. However, though the amplitude of the PPG signal is shown to relate to variations in blood flow and cardiac cycle, the precise relationship between physiological dynamics and the observed signal is not yet determined[4]. Attempts at showing a direct correlation between the contours of the arterial pressure waveform and the received pulsatile PPG signal waveform have been somewhat unsuccessful when directly analysing skin capillaries[38]. However, other models have been developed[39,40], with more success, that relate the PPG waveform to more major arteries, demonstrating that this area is active in the research field. Although the output of the PPG photo sensor depends on many factors (such as physiological, sensor design, probe coupling etc) it can be shown that with appropriate control of the source intensity[23] (compensating for skin absorption), a quasi-static PPG signal that is generally attributable to the total

illuminated blood volume may be obtained, as discussed previously. Components of the PPG signal attributable to dynamic arterial blood volume changes may be isolated from static and quasi-static components by spectral or filtering techniques.

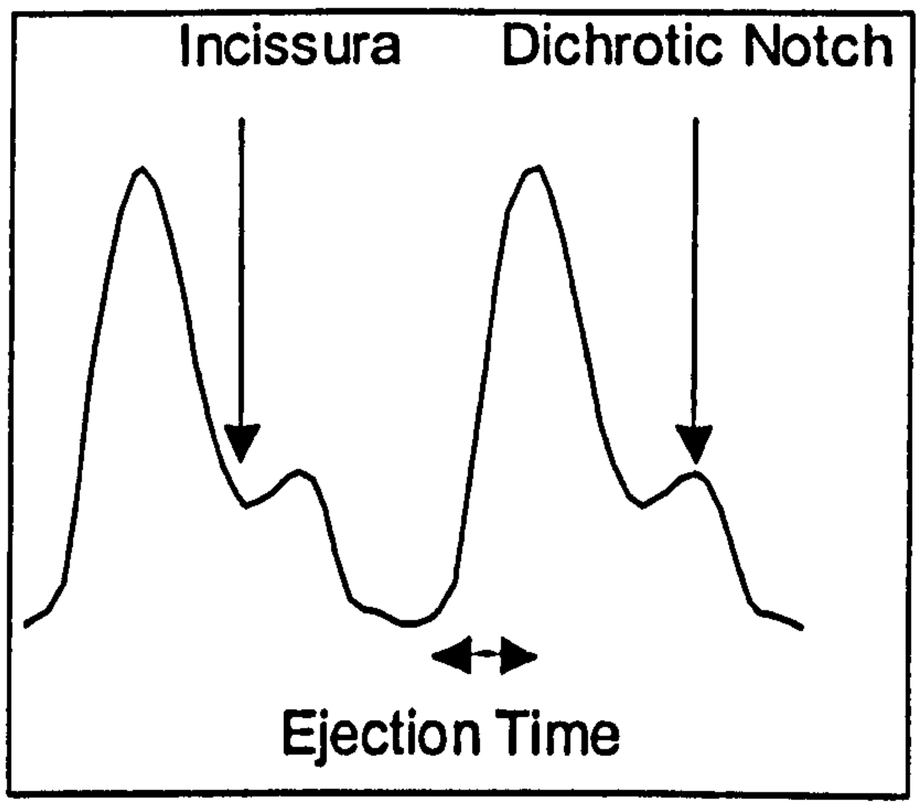

Figure 1-4. Typical Arterial PPG pulsations obtained from a finger probe.

1.2.6 Conclusions on PPG

Temporal and Fourier analysis of PPG signal waveform allows inference of physiological parameters, the most obvious being heart rate. Low frequency trends in PPG signals permit the determination of respiration rate and other slow rhythmic body functions[41].

The clinical area of vascular assessment using PPG has been introduced. Venous testing, both for DVT and venous insufficiency, require analysis of the quasi-static PPG term, attributed to venous effects and tissue absorption. Interpretation of results is required with these methods, since the tests require knowledge of the underlying physiology. The main clinical application of arterial PPG is pulse oximetry, whereby spectroscopic detection of the pulsatile oxygenated and deoxygenated PPG signal components eliminates signal components attributed to skin, bone and venous blood volume changes.

Reviewing the current literature, relatively little research has been applied to the shape of the arterial PPG waveform. Figure 1-4 shows a typical arterial PPG signal waveform (obtained using a finger transmission probe) with key points noted. It is reasonable to suspect that the connective vasculature between the heart and distal PPG measuring site must have an effect on the shape of the PPG waveform. Contours of the arterial pressure waveform have been attributable to energy storage in arterial vasculature[42]. One explanation of the shape of the contour waveform has been attributed to travelling waves caused by the abrupt closure of the heart valves[43]. If the arterial PPG waveform is proportional to the pressure waveform, these effects must also be observable in the PPG waveform. The distal pressure waveform shape appears very similar to the distal arterial PPG waveform shape when compared.

It can therefore be argued that the connective tissue of the arterial vasculature directly affect the contours of the arterial PPG waveform, allowing inference of vascular parameters by assessment of the arterial PPG waveform.

The proportionality to the pulse pressure has been described as the reason why PPG has not received greater popularity, since the PPG waveform is un-calibrated. Little research appears to have been conducted on dual channel PPG[44]. Comparative vascular assessment[45] is currently the subject of research using dual channel PPG, since the potential for self normalisation is possible with this technique in the same manner as the ABPI protocol discussed later.

1.3 Introduction to PVD

Peripheral Vascular disease (PVD), of which peripheral arterial disease (PAD) is a subset, affects a large percentage of the elderly population. PVD patients with intermittent claudication[46] (exercise induced pain) have a five-year mortality rate two to three times higher than age and sex matched controls, resulting in the death of approximately one third of claudicants in follow up studies[47,48].

Lifestyle modifications, such as cessation of smoking[49], increased exercise[50] and a prudent diet are obvious factors in the reduction of atherosclerotic disease[51]. Symptoms of occlusive PAD vary from muscle tightness, tingling in the feet, 'pins and needles', and cramp ranging from intermittent (usually during exercise) to continuous pain, depending on PVD severity. Complications of reduced perfusion (ischemia) in the extremities can also reduce wound-healing capability, so a minor injury may become infected, requiring partial or full amputation of the toe or foot[52], and without amputation may lead to death.

Additionally, a strong association[53] exists between PVD and undiagnosed renal artery stenosis, with the consequence that diagnosis of PVD should be followed by renal arterial screening.

With the implications mentioned above, early screening of suspected occlusive PAD in patients is essential to reduce both the severity of symptoms and the occurrence of associated problems mentioned above.

1.3.1 Blood Pressure and Arterial Disease

The most common indicator of overall patient physiology is the blood pressure tests. This procedure obtains the limits to the pulse pressure by means of a widely used non-invasive technique. Central blood pressure may be obtained by performing a blood pressure determination test on the upper arm, since with the patient upright hydrostatic effects are cancelled and the pressure obtained will be approximately equal to ascending aorta blood pressure. This gives an indication of the vascular properties for the central circulatory system.

Blood pressure determination obtained from the extremities, such as arms and feed, reveal if any upstream obstructions are present, since blood pressure drops after obstructions in the same manner as voltage drops after a resistor, a concept to be further developed in chapter two.

1.3.1.1 What is Blood Pressure?

Blood pressure is the name given to the transmural (intra arterial) pressure as it oscillates between the two limits: diastolic blood pressure (DBP) is the lower limit of pressure within the artery, and is the internal quiescent pressure when the heart is relaxed after any transients have passed. Systolic blood pressure (SBP) is the maximal transmural pressure generated during contraction of the heart. Pulse pressure is the difference between the SBP and DBP.

Blood pressure is usually measured using a sphygmomanometer, derived from ancient Greek 'sphygmos', meaning pertaining to the pulse, 'manos', meaning thin or rarefied and meter (i.e. a manometer measures the pressure of a gas.) The sphygmomanometer applies a pressure, measured as the height in mm of a column of mercury (with units of mmHg) to an occluding cuff that is usually placed around a limb. A typical value for 'normal' blood pressure is 120/80, meaning SBP is 120 mmHg, and DBP is 80mmHg.

Arterial blood pressure was first quantified by Rev. Stephen Hales in 1733 by demonstrating the blood of a horse rose to a height of 8 feet 3 inches when a glass tube was placed in a major artery. Since blood has a density of around 1.05 g/cc, we can convert this to mmHg (Hg has a density of 13.6g/cc) giving the blood pressure of the horse to be around 188mmHg.

The physiological condition of high blood pressure is given the clinical term Hypertension. Since the distribution of blood pressure amongst the population is continuous (bell shaped), there will be no clear bins indicating normotensive and hypertensive subjects. However, hypertensive resting blood pressure are generally accepted to be greater than SBP of

140mmHg and/or and a DBP of 100mmHg or more, but these figures are dependent on subject age.

1.3.1.2 Cause and Effects of Hypertension.

Blood pressure regulation is exceedingly complex, with localised and systemic control. Localised control is maintained by small arteries, which both dilate and constrict in order to maintain pressure, but this can be affected by hormones released by the muscles during exercise, demanding more blood. One cause of hypertension is arteriosclerosis, or build-up of lipids on the arteries. This extra arterial wall thickness reduces arterial compliance as discussed in chapter two. One component of the pressure regulation system is the arterial blood pressure sensors, termed baroreceptors. Baroreceptors are comprised of stretch sensors in the walls of the large arteries, and form a closed loop blood pressure regulatory system, indirectly modifying the hearts pace and rate of contraction. However, in the case of arteriosclerosis causing reduced arterial compliance, the stiffer arterial walls can 'fool' the blood pressure sensors into instructing the circulatory system to increase blood pressure, to a value that is physiologically unhealthy, since the baroreceptors have not 'stretched' enough. Hypertension has effects ranging from damage to the small capillaries within the organs, causing plasma leakage due to the higher system pressure, stroke, renal failure, insanity, retinopathy and heart failure. As discussed, the arteries form a pressure buffer, absorbing the pulsatile flow from the heart and converting it into a smoother flow into the vasculature, cushioning the blood pressure pulses. With hypertension, the increased arterial stiffness fails to smooth the flow and cushion the pressure; resulting in higher fatigue loading on the heart[54] and pressure damaged tissue, which causes conditions mentioned previously[55]. Finally, the coronary arteries, which supply the heart muscle with oxygenated blood, are occluded by the ventricular contraction during systole, preventing filling during this time. The coronary arteries therefore fill during diastole, where the pressure gradient is much lower, with corresponding effects on perfusion of oxygen and other substances. The pressure difference caused by hypertension effectively reduces the oxygen and nutrient supply to the heart[56]. The compound effects of hypertension on the heart explain why hypertension is viewed seriously, and why blood pressure monitoring is routine.

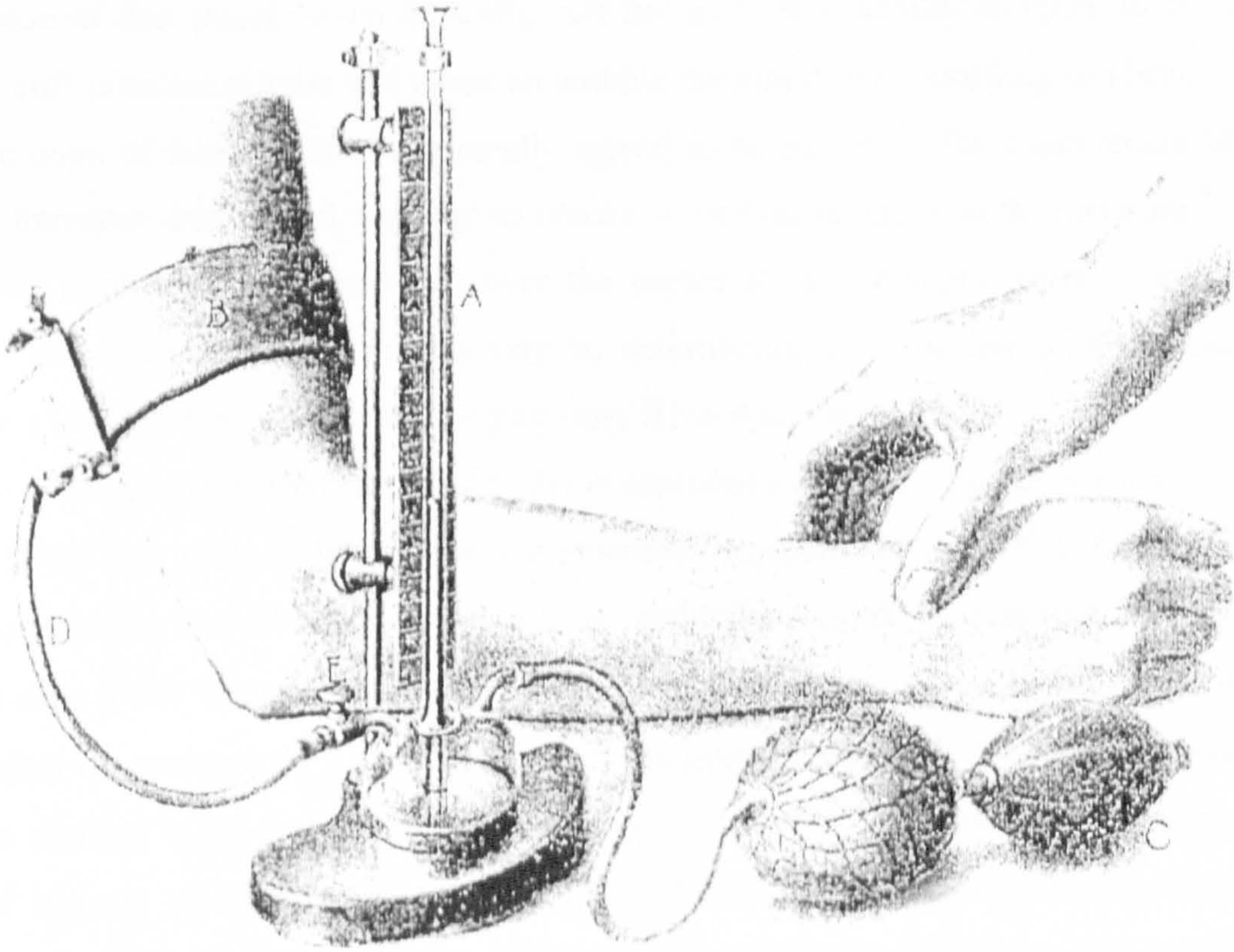

Figure 1-5. Riva-Rocci sphygmomanometry, from Janeway[57], *c.* 1904. Key:- *A* is Mercury sphygmomanometer, *B* is occluding cuff, *C* is inflation bulb, *D* is connective pressure pipe, *E* is pressure control valve.

1.3.1.3 The Auscultatory method of Blood Pressure Determination.

The first clinical apparatus for measuring systolic blood pressure, the arm occluding mercury sphygmomanometer, was developed by Riva-Rocci in 1896, by palpating the radial artery downstream of the occluding cuff – Figure 1-5 demonstrates the principle components of this technique. Korotkoff[58] extended this procedure in 1905, developing the auscultatory method for measuring both the systolic and the diastolic blood pressures. The Korotkoff procedure employs an occluding cuff (a sphygmomanometer cuff), usually placed around the upper arm, in order to occlude the brachial artery. A stethoscope is then placed on or close to the brachial artery downstream of the cuff to monitor blood flow in the brachial artery. The cuff is inflated to a pressure greater than the expected SBP (often called supra-systolic pressure), occluding blood flow through the brachial artery. Slow release of the cuff will reveal a sphygmomanometer pressure where blood is just pushing past the 'pinch' in the brachial artery caused by the cuff. At this instant, a noise should be heard through the stethoscope, caused by blood turbulence generated by pressurised blood flowing from the obstruction colliding with a static column of blood downstream of the obstruction, in sympathy with the heartbeat so causing a 'tapping' sound. The pressure value at the first

occurrence of this sound (when releasing cuff pressure) is generally accepted to be SBP. Further cuff pressure release will cause an audible transition from muffling to silence. The pressure point of this transition is generally agreed to be the DBP. The exact nature of the audible transition from initial 'tapping' to silence is well documented in the literature[59]. The Korotkoff procedure has advantages over the earlier Riva-Rocci procedure in that both systolic and diastolic blood pressure may be determined, with the use of a stethoscope providing increased sensitivity over the palpatory Riva-Rocci method.

Various problems have been identified with the auscultory method[60]. Obviously, the hearing acuity of the user must be good for low frequencies, typically 20 to 300Hz. Any systemic condition causing low arterial pressure, such as cardiogenic shock for example, will cause a shift to even lower frequencies of the so called Korotkoff sounds. The DBP itself has been the subject of controversy[61], since it has been suggested that when the Korotkoff sounds become muffled is the true diastolic pressure but this too has been criticised as too high[62]. Typical sources of these errors are usually attributable to operator variance, since the cessation or muffling of a sound is very subjective; especially if a linear change in volume or 'muffled', quality is present. Other operator errors have been attributed to 'terminal digit preference', meaning the operator subconsciously prefers least significant digit of the pressure height to be either zero, even, odd, or five[63]. Other errors attributable to skin thickness and cuff design[64] and arterial stiffness[65] have been reported when compared to invasive intra-arterial blood pressure monitoring. Blood pressure values derived by the auscilatory method must therefore be taken as approximate, but the ease of use and convenience in performing these measurements has resulted in this procedure being adopted virtually worldwide.

1.3.1.4 Other methods of Obtaining Blood Pressure

For true accuracy in determining arterial pressure, invasive pressure probes must be used. However, this means introducing foreign material into the human body, with associated mortality risk[66]. The implications of this, such as infection, shock etc and also the extra preparation of equipment (sterilising etc) and hazard to staff (from contagious disease) involved when using invasive probes has led some researchers to look at non-invasive methods of accurately determining arterial pressure.

1.3.2 PAD and ABPI

Currently, if a patient reports leg pain or tingling during exercise, the most common form of screening is the Ankle Brachial pressure index[67] (ABPI) test, in order to differentiate

between other diseases such as arthritis or neurosis. ABPI also provides an objective baseline to monitor progress of APD and treatment-plan. The ABPI uses SBP readings taken in the feet to form a ratio with the brachial SBP reading taken as the normal, assuming upper limb stenosis is absent. Significant changes in SBP between sites indicate reduced blood flow caused by stenosis. Table 1-2 shows expected ABPI values and corresponding diagnosis[68,69]. Often, pre and post exercise ABPI values are taken in order to determine severity of occlusion[70], since dilation of the arteries following exercise reduces pressure, emphasising the effect of the stenosis.

Resting Ankle/Brachial Index	Diagnosis
≥ 1 to 0.98	Normal
0.9 – 0.98	Asymptomatic obstructive Disease
0.5 – 0.9	Claudication
≤ 0.5	Rest Pain, severe arterial Disease

Table 1-2. ABPI diagnosis, from

1.3.2.1 Doppler and Cuff ABPI technique

Generally, a handheld constant wave (CW) Doppler ultrasound probe with an audio output is used to detect flow downstream of an occluding sphygmomanometer pressure cuff, similar in principle to the Korotkoff technique mentioned in section 1.3.1 above. A Doppler probe is used to detect blood flow after pressure release from supra-systolic since a more sensitive system is required – smaller arteries in the feet combined with disease renders the stethoscope insensitive to the audible events of interest. The cuff may be placed either on the brachial artery, with the Doppler ultrasound probe placed on the brachial, ulna, or radial artery in order to detect blood flow and from this SBP. This technique assumes a subclavian stenosis is absent – if suspected, brachial pressure should be determined in both arms and the higher of the two readings used. To determine ankle pressures, the cuff is placed around the lower calf, and usually three SBP readings are taken corresponding to the dorsalis pedis, posterior tibial or peroneal (poplital in U.S.A.) arteries: the highest pressure reading is used in calculating the ABPI.

If exercise testing is required, the subject performs exercises such as treadmill tests[70] or dorsoflex extensions using a localised calf exercise device such as the Stress'Ter[71]. After exercise, the arteries producing the greatest SBP readings (both ankle and systemic) are used to determine the post exercise ABPI. Comparison of before and after exercise ABPI should

reveal a pronounced effect in claudicants whereas normal before and after ABPI values indicate the problem lies elsewhere, such as arthritic joint pain.

1.3.2.2 Problems with ABPI

When using the 'Doppler and Cuff' technique for determining ABPI, several problems arise. Locating diseased arteries in the feet is the main problem; generally, the arteries feeding the foot are small on the outset, and proximal arterial narrowing or occlusion reduces arterial flow further. Oedema and obesity are two factors causing further signal attenuation, whilst arterial calcification, especially in diabetic patients[72], is another source of difficulties associated with this method. Reduced peripheral circulation will result if the ABPI test is conducted when the patient is cold; an additional limiting factor.

Furthermore, since this method require audio acuteness on behalf of the clinician performing the test, subjectivity errors[73,74] are introduced in a similar manner to errors discussed in the Korotkoff procedure discussed in section 1.3.1 above. Moreover, oscillometric automatic sphygmomanometers (which are becoming increasingly popular in the GP surgery for blood pressure determination by the District Nurse rather than the GP thus reducing 'White Coat' hypertension[75]) do not function in cases of proximal stenosis since the pressure waveform is reduced: hence the requirement for the Doppler probe and vascular technician.

1.3.3 Alternative Solutions to the Auscultatory BP Determination Method

Photoplethysmography has been previously employed in the assessment of ABPI[70,76,77] with promising results. Additionally, investigations have been performed using PPG in the determination of blood pressure specifically within the foot[52,78,79]. However, these methods, as reviewed, require interpretation of the data presented by the PPG instrument; most require inspection of the PPG waveform, or listening to the signal in the case of audio-photoplethysmography, in order to determine blood flow return. This methodology raises the same problem of subjectivity amongst users. Obviously, experience counts in determining false positives, but these same factors also apply when using the Doppler probe. An automatic method for determining SBP based on arterial PPG could be developed which would eliminate these subjectivity errors. This technique could then be applied to the arm and toe in order to generate an ankle and brachial pressure index, suitable for evaluation of peripheral arterial disease.

The advantages of this technique would be in elementary screening since a trained operator would not be required to perform ABPI evaluations; unlike the current technique for a

specialised operator using the clumsy CW Doppler system with its inherent sensitivity to operator variability. This would make early screening easy and simpler to perform at the General Practitioners (GP) level, the so-called 'primary health care', without referral to a vascular specialist.

1.3.3.1 Automatic Systolic Blood Pressure Determination using PPG

In order to determine SBP more accurately, an investigation into blood pressure determination using PPG was performed. Usually, the comparative method for determining SBP is by using the Korotkoff procedure, as discussed earlier, but the Korotkoff procedure introduces subjectivity errors in blood pressure measurement due to operator involvement. A review of current methodologies for PPG determined SBP was conducted, allowing evaluation of these technologies.

1.3.3.2 Direct determination of Finger Blood Pressure

Several papers have reported methods for determining finger SBP using a basal phalanx finger cuff and PPG system, termed the volume oscillometric method[80], and the volume-compensation method[81] based on the vascular unloading principle[82]. The volume oscillometric method can determine pressure points by monitoring the PPG waveform, such as SBP and mean arterial pressure, whereas the compensation method can provide a pressure waveform over the entire cardiac cycle[83] using a servo volume compensation technique. A commercial device, the *Finapres*, originally manufactured by Datex-Ohmeda, uses the servo compensation technique, and has shown good agreement[84] with invasive blood pressure measurements. However, these techniques cannot be correlated with the Korotkoff method since SBP is found in the finger, whereas the Korotkoff procedure cannot be applied simultaneously to the finger.

1.3.3.3 Indirect determination of finger blood pressure

The paper by Giltveldt[85] uses two PPG illumination wavelengths in order to measure perfusion in varying depths of the skin. A sphygmomanometer pressure cuff is placed on the forearm over the brachial artery in the normal position, and a dual source (950nm infrared and 560nm green) reflection mode probe placed on the finger pad. The cuff is inflated to a supra-systolic pressure then gradually deflated. The pressure values at the instant of PPG pulsatile return values for the two colour channels, corresponding to systolic return, were noted and seen to be different for the two-channels. The infrared channel gave a mean

systolic return of 80mmHg. Since the penetration depth of infrared light at 950nm has a penetration depth of around 1.5mm. This was attributed to systolic pressure in the dermis.
The mean pulsatile return of the green channel was 60mmHg, attributed to arterioles since the penetration depth of this channel was approximately 0.5mm deep.
The paper by Nielsen *et al*[86] follows a similar methodology to the previous paper. However, dual PPG probes are employed, one distal to the sphygmomanometer cuff, the other local to it. Cuff inflation is taken supra-systolic pressure as before, and the instant of AC pulsatile return observed as the systolic pressure return. Agreement with the auscultory method is also shown, with good results. Both these techniques may be performed in parallel with the standard Korotkoff auscultatory SBP determination method, using dual observers in order to provide a correlation measure. However, interpretation of supra-systolic threshold and PPG signal return requires interpretation in order to determine SBP.

1.3.4 Conclusion on PVD

This section has looked at the impact of peripheral vascular disease on the population, and the long-term effects associated with it. The ABPI technique has been shown to be the predominant screening technique for PAD in the legs and feet. Known problems with ABPI, in that it uses a subjective method of determining SBP, a key component of the ABPI calculation, has been found. Alternatives techniques using ABPI have been investigated and reported. An automatic method of determining SBP, and from this ABPI, will be developed in a later chapter. This protocol will employ a supra diastolic cuff-deflation procedure since any protocol employing cuff-inflation does not allow correlation with other non-invasive blood pressure determination techniques, i.e. the standard Korotkoff/Riva-Rocci procedure unless an invasive pressure catheter is employed. For logistical reasons, invasive pressure monitoring was deemed inappropriate.

1.4 Thesis Aims and Objectives

The concept and major applications of Photoplethysmography have been introduced, and brief details of PVD provided. With these in mind, the primary aims of the thesis can now be succinctly stated.

1. Develop a technique to give a measure of blood perfusion using PPG. This fundamental concept is required for all subsequent methodologies. A relationship must be developed between changes in blood volume and changes in the arterial PPG waveform.

2. Develop an automatic method of determining SBP using arterial PPG. Investigate the sensitivity of the automatic method compared to conventional auscultatory SBP methods, since the peripheral nature of the PPG may prove more sensitive to PAD. The automatic nature of the technique should also reduce operator subjectivity and variability errors, giving increased reliability and accuracy. This automatic technique should allow non-specialised operators to obtain accurate SBP determinations.

3. Quantify vascular physiology with the development of a forward model. The forward model will relate changes in the haemodynamic properties of the vasculature, as excited by the heart, to the PPG signal, and allow investigation into the differing effects of pathology on subject vasculature and PPG waveforms.

4. Develop an inverse vascular model to directly assess vascular physiology by analysing the PPG waveform. This will allow indications of the quantified vascular parameters developed in the forward model to be assessed based on the PPG waveform alone.

5. Evaluate the prospect of comparative evaluation techniques using dual channel PPG in all the models developed. The comparative technique has the potential to provide a vascular health index through the normalising techniques.

6. Evaluate the feasibility of speculative hypothesis and the functionality of the models developed in previous aims with prospective subject trials. Small subject trials will provide a first indication of the validity of the assumptions and hypothesis developed in earlier aims, providing evidence to assess the viability of vascular assessment using PPG.

1.5 Conclusion

The principles of Photoplethysmography have been introduced in this chapter, and the advantages of this perfusion monitoring technique are readily apparent. It is assumed the inter-connective vasculature between the heart and measuring site will modulate the arterial PPG waveform. Decoding of this modulation should allow inference of the properties of the connective vasculature, giving insight into any pathology that may be present.

The field of PAD has been briefly introduced, with the indication that early assessment monitoring of disease is essential for long-term management, with the goal of increasing lasting subject health. Current PAD diagnosis methods, though long established, have been found inaccurate and suffer variability due to differing operator acuity and interpretation.

It is anticipated that monitoring of perfusion alone could serve as a valuable tool for vascular assessment, since reduced perfusion in the extremities is an indication of ischaemia. It is predicted that a combining PPG and sphygmomanometry based automatic SBP determination system could reduce operator variability and increase reliability.

A quantitative approach to vascular assessment would eliminate operator subjectivity problems, and increase diagnostic specificity. Furthermore, statistical data-mining techniques could be developed, based on population analysis, which would allow the onset of vascular abnormality to be detected parametrically. This would form a valuable tool for both clinical and non-clinical vascular assessment, such as PAD or exercise perfusion monitoring, respectively.

Although PPG has been in existence for approximately 60 years, little attention has been paid to the shape of the arterial waveforms. Most current extant applications employ spectrographic arterial amplitude techniques (pulse-oximetry) or focus on low frequency blood volume trends (venous testing). As described, it is conjectured that information is contained within the shape of the arterial PPG signal that can provide information directly related to the parameters of the connective arterial vasculature. A further conjecture can be made that the arterial PPG contains information on the physiology of the heart, but this will not be investigated here.

This thesis will investigate these features and determine if useful information regarding arterial vascular health may be obtained using non-invasive PPG technology. This will involve investigations into both physical light/tissue interaction models and physiological models in order to derive information on the haemodynamic system under analysis.

Currently, little work in the literature has been conducted using simultaneous distal site multi-channel PPG. Asymmetric vascular disease may be detectible by comparative analysis of distal sites using this technique. Comparative evaluations of perfusion changes could offer the potential for self-normalisation in the same manner as the ABPI measurement. Ratiometric evaluation of vascular parameters could offer the prospect for determination of an index of vascular health, simplifying vascular assessment, and allowing unspecialised personnel to perform vascular diagnosis.

1.6 Chapter References

[1] A.B. Hertzman, "Photoelectric Plethysmography of the Fingers and Toes in Man", Proc. Soc. Exp. Biol. Med., **37**, pp.529 (1937)

[2] Barreto A.B., Aguilar C.D., Jakubzick E.E., "Adaptive LMS Delay Measurement in Dual Blood Volume Pulse Signals for Non-Invasive Monitoring", Proc. 16th Southern BI, IEEE, pp. 117-120 (1997)

[3] Challoner A.V.J, "Photoelectric Plethysmography for Estimating Cutaneous Blood Flow" In: Rolf P, "Non-Invasive Physiological Measurements", **1**, London Academic, pp. 125-151 (1979)

[4] Hurch A, Hurch R, Kourg V, "Limitations of Pulse Oximetry [Letter]", Lancet, **1**, pp. 357-359 (1988)

[5] Brengelmann G.L., "Specialized Brain Cooling in Man?", FASAB J., 7:, pp. 1148-1153 (1993)

[6] Schmidt-Nielson K, "Counter current systems in Animals", Sci. Amer., 244(5), pp. 118-128 (1981)

[7] Hales S, "Statistical Essays: Containing Haemostaticks", Innyes & Manby, London, UK, vol. II (1733)

[8] Harvey W, "On the motion of the Heart and Blood in Animals", Willis's translation, 1962 Chicago, Henry Regnery Co., pp.213, (originally 1628)

[9] Vogel S., "Vital Circuits", Oxford University Press, New York, UsA,(1992)

[10] Cartwright C.M, "Infrared transmission of the flesh", J. Opt. Soc. Amer., 20, pp. 81-84 (1930)

[11] Jago J.R, Murray A,"Repeatability of periperal pulse measurement on ears, fingers,and toes using photoelectric plethysmography", Clin. Phys. Physiol. Meas., 9, pp. 319-29 (1988)

[12] Nijboer J.A, Dorlas J.C, Mahieu H.F, "Photoelectric plethysmography – some fundamental aspects of the reflection and transmission method", Clin. Phys. Meas., 2, pp.205-215 (1981)

[13] Yoshiya I, Shimada Y, Tanaka K, "Spectrophotometric monitoring of arterial oxygen saturation in the finger tip", Med. Biol. Eng. Comput., 18, pp. 27-32 (1980)

[14] Yelderman M, New W, "Evaluation of pulse oximetry", Anesthesiology, 59, pp. 349-352 (1983)

[15] Abramowitz H.B, Queral L.A, Flinn W.R, Nora P.F, et al., "The use of photoplethysmography in the assessment of venous insufficiency: a comparison to venous pressure measurement", Surgery, 86, pp. 434-441 (1979)

[16] Hertzman A.B, "The blood supply of various skin areas as estimated by the photoelectric plethysmograph", Am. J. Physiol., 124, pp. 329-340 (1938)

[17] Nakajima K, Tamura T, Miike H, "Monitoring of heart and respiratory rates by photoplethysmography using a digital filtering technique", Med. Eng. Phys., 18(5), pp. 365-372 (1996)

[18] Olsson E., Ugnell H., Oberog P.A., Sedin G., "Photoplethysmography for simultaneous recording of heart and respiratory rates in newborn infants", Acta Paediatr, Jul 89, pp. 853-61 (2000)

[19] Nitzan M, Babchenko A, Khanokh B, Landau D, "The Variability of the Photoplethysmographic signal – a Potential Method for the Evaluation of the Autonomic Nervous System", Physiol. Meas., **19**, pp. 93-102 (1998)

[20] Yamakoshi K, Shimazu H, Shibata M et al., "A new oscillometric method for indirect measurement of systolic and mean arterial pressure in the human finger", Med. Biol. Eng. Comput., 20, pp. 307-313 (1982)

[21] Shimazu H, Fukuoka M, Ito H et al., "Noninvasive measurement of beat-to-beat vascular viscoelastic properties in human fingers and forearms", Med. Biol. Eng. Comput., 23, pp. 43-47 (1985)

[22] Schmeink U, Schmeink T, Lossau I, Roschansky V, "D-PPG and Duplex Ultrasound: Correlation of results in the diagnosis of Deep Vein Insufficiency", in *Proceedings of the Seventh International Symposium CNVD (Computer-aided Noninvasive Vascular Diagnostics)*, Blažek V and Schultz-Ehrenburg U Eds. (Verein Deutscher Ingenieure, Düsseldorf, Germany, 1998), **263**, pp. 161-164 (1997)

[23] Fronek A, Blažek V, "Automatic calibration of the D-PPG: Its meaning and effectiveness", Report by Third Annual Congress of NASP, Phoenix, USA (1990)

[24] Blažek V, Schmitt H.J, Schultz-Ehrenburg U, Kemer J, "Digitale Photoplethysmographie (D-PPG) für die Beinvenendiagnostik", Medizinischtechnische Grundlagen, Phlebol. u., 18, pp. 91-97 (1989)

[25] Aughlin M.H., Schrage W.G., "Effects of muscle contraction on skeletal muscle blood flow: when is there a muscle pump?", Med. Sci. Sports Exerc., 31, 7, pp. 1027-1035 (1999)

[26] Sarin S, Shields D.A, Scurr J.H, Coleridge-Smith P.D, "Photoplethysmography: a valuable non-invasive tool in the assessment of venous dysfunction?", J. Vasc. Surg, 16:2, pp. 154-162 (1992)

[27] McMillin G.M, Coleridge-Smith P.D, "An Evaluation of Doppler Ultrasound and Photoplethysmography in the investigation of Venous insufficiency", Aust N.Z. J Surg, 62:4, pp. 270-275 (1992)

[28] Tan Y.K, da Silva A.F, "Digital Photoplethysmography in the Diagnosis of Suspected Lower Limb DVT: Is it Useful?", Eur. J. Endovasc Surg, 18, pp. 71-79 (1999)

[29] Millikan G.A., "Oximeter, instrument for measuring continuously oxygen saturation of arterial blood in man", Rev. Sci. Instrum., 13, pp. 434 (1942)

[30] Mendelson Y., Ochs B.D., "Non-invasive Pulse Oximeter Utilizing Skin Reflectance Photoplethysmography", IEEE Trans. Biomed. Eng., Vol. 35(10), pp. 798-805 (1988)

[31] Lindberg L.G, Öberg P.Å, "Photoplethysmography. II. Influence of light source wavelength", Med. Biol. Eng. Comput., 29, pp. 48-54 (1991)

[32] Manheimer P.D., Casciani J.R., Fein M.E., Nierlich S.L., "Wavelength selection for low saturation pulse oximetry", IEEE Trans. Biomed. Eng., 44(3), pp. 148-158 (1997)

[33] Aoyogi T, Kishi M, Yamaguchi K, Watanabe S, "Improvements of the Ear Piece Oximeter", Abstracts Jpn. Soc. Med. Electronics Biol. Engineer, pp. 90-91 (1974)

[34] Takatani S., Davies C., Sakakibara N., Zurik A., "Experimental and Clinical evaluation of a non-invasive reflectance pulse oximeter"., J. Clin. Monit., 8(4), pp. 257-266 (1992)

[35] Polyani M.L., Hehir R.M., "New Reflectance Oximeter", Rev. Sci. Instrum., 31, pp. 401-403 (1960)

[36] Aoyogi T, "Apparatus for measuring predetermined data of living tissue", US Patent No: 5385143 (1995)

[37] Trafford J. de, Lafferty K, "What does Photoplethysmography Measure?[Letter]", Med. Biol. Eng. Comput., **22**, pp. 479-480 (1984)

[38] Heubach T, Czastrau C, Klysc T, Blazek V, Junger M, Hahn M, "Synchronous Measurements of Capillary Blood Pressure and Arterial Photoplethysmography", Int. J. of Microcir. Clin. Exp., **16**(1), pp. 121 (1996)

[39] Allen J, Murray A., "Modelling the relationship between peripheral blood pressure and blood volume pulse using linear and neural network system identification techniques", Physiol. Meas, 20, pp.287-301 (1999)

[40] Millasseau S.C, Guigui F.G, Kelly R.P, Prasad K, Cockcroft J.R, Ritter J.M, Chowienczyk P.J, "Non-invasive Assessment of the Digital Volume Pulse – Comparison with the Peripheral Pressure Pulse", Hypertension, 36, pp.952-956 (2000)

[41] Nitzan M, de Boer H, Turivenko S, Babchenko A, Sapoznikov D, "Spontaneous oscillations in the peripheral circulation system, as measured by photoplethysmography", SPIE, 2328, pp. 188-195 (1994)

[42] Goldwyn R.M., Watt T.B., "Arterial Pressure Pulse Contour analysis Via a Mathematical Model for Clinical Quantification of Human Vascular Properties", IEEE Trans. Biomed. Eng., BME-14, 1, pp 11-17 (1967)

[43] Iketani T, Iketani Y, Takazawa K, Yamashina A. , ""The influence of the peripheral reflection wave on left ventricular hypertrophy in patients with essential hypertension", Hypertens Res., 23, pp.451-8 (2000)

[44] Allen J, Murray A, "Similarity in Bilateral Photoplethysmography Peripheral Pulse Wave Characteristics as the Ears, Thumbs and Toes", Physiol. Meas., 21, pp.369-377 (2000)

[45] Nitzam M, Khanokh B, Slovik Y, "The Difference in Pulse Transit Time to the Toe and Finger Measured by Photoplethysmography", Physiol. Meas., 21, pp. 85-93 (2002)

[46] Dodds S.R, Chant A.D.B, "The Haemodynamic Mechanism of Intermittent Claudication", Cardiovascular Surgery, 5, 1002, pp. 13 (1997)

[47] Smith F.B., Rumley A., Lee A.J. et al, "Haemostatic factors and prediction of ischaemic heart disease and stroke in claudicants", Br. J., Haematol, 100, pp.758-63 (1998)

[48] O'Riordain D.S, O'Donnel J.A, "Realistic expectations for patients with intermittent claudication", Br. J. Surg, 78, pp. 861-863 (1991)

[49] McVeigh G.E, Morgan D.J, Finkelstein S.M, Lemay L.A, Cohn J.N, "Vascular abnormalities associated with long term cigarette smoking identified by arterial waveform analysis", Am. J. Med., 102(3), pp. 207-231 (1997)

[50] Kingwell B.A, Berry K.L, Cameron J.D, Jennings G.L, Dart A.M, "Arterial compliance increases after moderate-intensity cycling", Am. J. Physiol, Heart Circ. Physiol, 273 (42), H2186-H2191 (1997)

[51] Fowkes F.G.R., "Epidemiology of atherosclerotic arterial disease in the lower limbs", Eur. J. Vasc. Surg, 2, pp.283-91 (1988)

[52] Bone G.E., Pomajzl M.J., "Toe Blood pressure by Photoplethysmography: an index of healing in forefoot amputation", Surgery, 89, pp. 569-74 (1981)

[53] O'Brien E.T, Beevers D.G, Marshall H.J, "ABC of Hypertension", BMJ, 3rd Ed, London, (1996)

[54] Guyton A.C, "Arterial Pressure and Hypertension", Ch. 17, W.B. Saunders Co., Philadelphia (1980)

[55] Domanski M.J, Davis B.R, Pfeffer M.A, Kastantin M, Mitchell G.F, "Isolated Systolic Hypertension : Prognostic Information provided by Pulse Pressure", Hypertension, 34, pp. 375-380 (1999)

[56] Gregg D.E, Fisher L.C, "Blood Supply to the heart", in Hamilton W.R, Dow P, eds.: Handbook of Physiology. Sect. 2: Circulation, Vol. 2, Washington, DC: American Physiology Society, pp. 1517-1584 (1963)

[57] Janeway T.C, "The Clinical Study of Blood-Pressure", D. Appleton and Co., New York, London, pp. 79 (1904)

[58] Korotkof N.S., "A Contribution to the Problem of Methods for the Determination of Blood Pressure", Rep. Imper. Milit-Med. Acad., St. Petersburg, **11**, pp. 365 (1905)

[59] Petrie J.C, O'Brien E.T, Littler W.A, de Swiet M, Dillon M.J, Padfield P.L, "Recommendations on blood pressure measurement", BML Publishing Group, 2nd Ed, (1990)

[60] Musso N.R, Giacchè M, Galbariggi G, Vergassola C, "Blood pressure evaluation by non-invasive and traditional methods. Consistencies and discrepancies among Photoplethysmography, office sphygmomanometry, and ambulatory monitoring. Effects of blood pressure measurement", Am. J. Hypertension, 9, pp. 293-299 (1996)

[61] Short D, "The Diastolic Dilemma", BMJ, ii, pp. 685-686 (1975)

[62] London S.B, London R.E, "Critique of indirect diastolic end point", Arch. Intern. Med, 119, pp. 39-49 (1967)

[63] Rose G, "Standardisation of observers in blood pressure measurement", Lancet, i, pp.673-674 (1965)

[64] Stolt M, Sjonnel G, Astrom H, Hansson L, "Factors affecting the validity of the standard blood pressure cuff", Clin. Physiol., 13(6), pp. 611-620 (1993)

[65] Sheahan N.F., MacMahon M., Colgan M.P., Walsh J.B., Coakley D, Malone J.F., "Measurement of arterial closing pressure", Physiol. Meas, 14, pp. 7-12 (1993)

[66] Connors A.F, Speroff T, Dawson N.V. et al, "The effectiveness of right heart catheterisation in the initial care of critically ill patient", J. Am. Med. Assoc., 276, pp. 889-897 (1996)

[67] Prineas R.J., Harland W.R., Janzon L, Kannel W., "Recommendation for use of non-invasive methods to detect atheroscloretic peripheral arterial disease in population studies", Circulation, 65, pp. 1561A-1566A (1982)

[68] Carter S.A., "Role of pressure measurements", In Bernstein E.F., ed: Vascular Diagnosis, Fourth Ed. Chapter 55, St. Loius, M.O., Moseby Year Book Inc. (1993)

[69] Hooi JD, Stoffers HE, Kester AD, van RJ, Knottnerus JA, "Peripheral arterial occlusive disease: prognostic value of signs, symptoms, and the ankle-brachial pressure index", Med. Decis. Making, 22(2), pp. 99-107 (2002)

[70] Duprez D., Missault L., Van Wassenhove A., Clement D.L., "Comparison between ankle and toe index in patients with peripheral arterial disease", Int. Angiol., 6, pp. 295-7 (1987)

[71] Manning BJ, McGreal G, Crowley H, Redmond HP, O'Donnell JA, "A prospective comparison of pedal ergometry with conventional treadmill testing in the investigation of lower extremity pain", Ir. J. Med. Sci., 170(3), pp. 169-171 (2001)

[72] Apelqvist J., Castenfors J., Larsson J., Strenstrom A., Agardh C.D., "Prognostic value of systolic ankle and toe blood pressure levels in outcome of diabetic foot ulcer", Diabetes Care, 12, pp. 373-8 (1989)

[73] Stoffers H.E, Kester A.D, Kaiser V, Rinkens P.E, Kitslaar P.J, Knotterus J.A, "The diagnostic value of ankle-brachial systolic pressure index in primary health care", J. Clin. Epidemiol., 49, pp. 1401-1405 (1996)

[74] Ray S.A, Srodon P.D, Taylor R.S, Dormandy J.A, "Reliability of ankle:brachial pressure index measurements by junior doctors", Br J Surg, 81, pp.188-190 (1994)

[75] Pickering T.G, James G.D, Boddie C, Harshfield G.A, Blank S, Laragh J.H, "How common is white coat hypertension", JAMA, 2, pp. 584-586 (1988)

[76] Whitteley M.S., Fox A.D., Horrocks M., "Photoplethysmography can replace hand held Doppler in the measurement of ankle/brachial indices", Ann. R. Coll. Surg. Engl., 80, pp.96-8 (1998)

[77] Sadiq S., Chithriki M., "Arterial pressure measurements using infrared photosensors: comparison with CW Doppler", Clin Physiol, 21(1), pp. 129-32 (2001)

[78] Fronek A, Blazek V, Curran B., "Toe Pressure determination by audio-photoplethysmography", J. Vasc Surg, 20, pp.267-70 (1994)

[79] Tsai F.W., Tulsyan N., Jones D.N., Abdel-Al N., Castronuovo J.J., Carter S.A., "Skin perfusion pressure of the foot is a good substitute for toe pressure in the assessment of limb ischemia.", J Vasc Surg, 32, pp. 32-6 (2000)

[80] Yamakoshi K, Shimazu H, Shibata M et al., "A new oscillometric method for indirect measurement of systolic and mean arterial pressure in the human finger", Med. Biol. Eng. Comput., 20, pp. 307-313 (1982)

[81] Yamakoshi K, Rolfe P, Murphy C, "Current Developments in Non-Invasive measurements of Arterial Blood Pressure", J. Biomed. Eng, 10, pp. 130-137 (1988)

[82] Penáz J, "Photoelectric measurements of blood pressure, volume and flow in the finger", Dig 10th Int Conf Med Biol Eng, Dresden pp.104- (1973)

[83] Molhoek G.P, Wesseling K.H, Settels J.J, van Vollenhoven E, Weeda H.W, de Wilt B, Arntzenius A.C, "Evaluation of the Penáz servo-plethysmo-manometer for the continuous, non-invasive measurement of finger blood pressure", Basic Res. Cardiol, 79, pp. 598-609 (1984)

[84] Jones RD, Brown AG, Roulson CJ, Smith ID, Chan SC, "The upgraded Finapres 2300e. A clinical evaluation of a continuous non-invasive blood pressure monitor", Anaesthesia, 47(8), pp. 701-705 (1992)

[85] Giltveldt J, Sira A, Helme P, "Pulsed Multi-frequency photoplethysmography", Med. Biol. End. Comput., 22, pp.212-215 (1984)

[86] Nielsen P.E, Poulson H, Gyntelberg F, "Arterial blood pressure in the skin measured by a photoelectric probe and external counterpressure", VASA, Band 2, Heft 1, pp. 65-74 (1973)

Optical Engineering Group
Loughborough University

Chapter Two

PPG Models

2 Introduction to Modelling

2.1 Introduction to Modelling

The term 'model' is derived from ancient Greek 'modas', meaning an object representing accurately something to be made or already existing. Academically, modelling usually refers to the technique of creating a mathematical equation that may be used to represent a system, codifying any observations made. In the case of PPG, a model is used to predict the complex light-tissue interactions as detected by the photo-sensor.

The science psychologist Sir Karl Popper (1902-1994) proposed the positivist theory, where a model will describe a large range of phenomenon based on a few simple postulates. The model will allow predictions to be made that may be tested with the system being modelled. The validity of the model may be determined by comparing the actual system response and the predicted (model) response. Often, the model is not 100% validated, meaning the model must be tested; each test increases confidence in the model when the predicted and actual results are compatible, conversely decreasing model confidence when the predicted results are vastly different.

If the system to be modelled is exceptionally complex, a simpler model is often employed which can predict part of the output of the system under test or provide acceptable results within a reduced input parameter set. These simpler models are usually employed when the full system is either too difficult or time consuming to model in its entirety. This often happens when the system contains many input parameters, and a full model could take too long to set up and analyse, with the added complexity not necessarily giving any extra useful information over a simpler model.

When discussing models, two types are often considered, the forward model, and the reverse or inverse model. The forward model gives predicted outputs from known inputs, whereas the inverse model uses the system output to predict either the driving input or the parameters of the system.

This chapter will demonstrate typical PPG models currently employed. Additionally, it will demonstrate the development of pressure based forward models, which employ a parametricated vascular system. This pressure model will be applied to arterial PPG in order to obtain a forward PPG model, based on mechanical and physical properties of the arterial vascular system.

2.2 Current PPG Models

Models traditionally applied to PPG have represented light/tissue interaction. These models generally consider the tissue as a homogeneous slab, without boundaries and quite often without layers. These models ignore underlying physiological variations within the tissue, leaving open the interpretation of results.

Two classical forward analytic models exist for the interaction between light and matter, the Beer-Lambert Law[1] and Diffusion[2] theory. The Beer-Lambert law is based on one-dimensional optical density calculations, assuming a classical, empirical interpretation of the illuminating light source. Diffusion theory assumes the light and tissue interaction can be modelled as a diffusion of photon density as described by macroscopic absorption and scattering parameters.

2.2.1 Beer Lambert Model applied to PPG

The relationship between the interaction of light and tissue may be modelled using the Beer-Lambert law[3,4], which has been described as over simplistic[5]. However, the Beer-Lambert law has been shown to give good results to first order[6]. It will be useful to explore the classical representations of the Beer-Lambert law in order to aid understanding of models to be developed later.

The classical representation of the Beer-Lambert law is shown in equation [2.1].

$$I(\lambda) = I_o(\lambda)\beta(\lambda)\exp\left(-\mu_{eff}(\lambda)r\right) \qquad [2.1]$$

Equation [2.1] couples path length r and effective absorption μ_{eff} (as a function of wavelength λ) into a single measure of optical density, source intensity represented by I_o with wavelength dependency, and finally optical coupling β with wavelength dependency.

A primary assumption when applying the Beer-Lambert law to PPG is that the optical path length through tissue comprises two distinct components. The major part of this absorption is due to structural components of the vascular periphery (such as differing tissue features) and venous return, and is quasi-static, varying over several seconds. A small dynamic component[7] is formed by absorption from arterial blood across a dynamically varying path length due to blood volume changes during *systole*.

Equation [2.2] below shows decomposition of the macroscopic optical density μ_{eff} into two separate components. Here μ_t representing a quasi-static component related to venous absorption and tissue structures with a fixed path length r and μ_b represents wavelength

absorption due to arterial blood and dynamic path length *z(t)*, dependent on blood volume changes.

$$\mu_{eff}(\lambda)r = \mu_b(\lambda)z(t) + \mu_t(\lambda)r \quad [2.2]$$

Equation [2.3] shows decomposition of optical density expanded in the Beer-Lambert expression of equation [2.2] above. Equation [2.4] shows that overall recovered signal intensity is a product of the two terms, with wavelength dependency removed due to assumption of single illuminating wavelength.

$$I = I_O \beta \exp\left(-\left(\mu_b z(t) + \mu_t r\right)\right) \quad [2.3]$$

$$I = I_O \beta \exp(-\mu_t r)\exp(-\mu_b z(t)) \quad [2.4]$$

Various techniques exist for separating absorption due to these two multiplicative terms. Absorption due to the time varying dynamic component is termed pulsatile or arterial photoplethysmography, whereas absorption due to the quasi-static component is almost steady state, and often used for venous analysis.

Referring to equation [2.4], some assumptions can be in order to arrive at a Beer-Lambert based model that expresses blood volume changes, as expression [2.4] in its current form, being a product term, is non linear.

Assuming $\mu_b z(t)$ is small (typically 1 to 5% as discussed[7]) and recalling that $e^x \approx 1 + x$ if x is also small (truncated Taylor series), equation [2.4] may be rewritten, equation [2.5] below.

$$I \approx I_O \beta \exp(-\mu_t r)(1 - \mu_b z(t)) \quad [2.5]$$

Remembering that *z(t)* may be both positive and negative, equation [2.5] may be expressed as a quasi-static *DC* term with a superimposed time varying pulsatile *AC* signal, i.e. $I = DC + AC(t)$, equation [2.6].

$$I \approx I_O \beta \exp(-\mu_t r) + I_O \beta \exp(-\mu_t r)\mu_b z(t) \quad [2.6]$$

This *AC* term may be extracted electronically from the received intensity *I* using a band limited differentiation (high pass filtering) of the received signal, $\Delta I(t)$, By taking the ratio *AC(t)/DC* an expression is obtained which is directly proportional to the pulsatile path length, equation[2.7] below.

$$[2.7] \qquad \frac{\Delta I(t)}{I} = \frac{AC(t)}{DC} \approx \frac{I_o \beta \exp(-\mu_t r)\mu_b z(t)}{I_o \beta \exp(-\mu_t r)} \approx \mu_b z(t)$$

Equation [2.7] shows that by dividing the pulsatile component, obtained by amplifying and high pass filtering the recovered PPG signal, by the quasi static recovered signal, it is possible to obtain a quantity directly proportionally to path length changes caused by blood volume change that is insensitive to both source intensity and optical coupling.

2.2.2 Generalised Light/Tissue Interaction Model

The Beer Lambert model, described above, has found considerable use in the field of optics in order to describe the interaction of light with matter in simple terms. However, it is more appropriate in this case to develop an alternative model, inspired by the Beer-Lambert model, which can be applied to PPG signals and integrates factors not accounted for in the standard Beer-Lambert model. This model has the advantages of being more general, as no attempt at describing the exact *nature* of signal intensity changes are made. The Beer-Lambert model is mainly criticised for representing a one-dimensional geometric model, whereas this model does not specify the spatiality of the dynamic components of the model. Additionally, experiments conducted by the author shows equation [2.7] is still influenced by probe coupling effects. A more general model will be developed which considers these effects in more detail, ultimately eradicating probe-coupling problems from the PPG system. Equation [2.8] shows the generalised model in its basic form, using the notation developed previously, with *p(t)* expressing small path length changes due to arterial pressure changes, a function of cardiac rhythm.

$$[2.8] \qquad I(\lambda) = I_o(\lambda)\left[\mu_t(\lambda)\beta(\lambda) + \mu_b(\lambda)p(t)\right]$$

Equation [2.8] may be expanded, revealing the PPG waveform is again composed of a large quasi-static DC component with a small-superimposed pulsatile AC component. It may be observed that the coupling coefficient β dependency is eliminated between venous and arterial systems, since the pulsatile function *p(t)* contains AC coupling. Wavelength dependency can again be eliminated with the assumption of a single illuminating wavelength, expressed in equation [2.9].

$$I = I_O \beta \mu_t + I_O \mu_b p(t) \quad [2.9]$$

Using the same procedure developed in the Beer-Lambert modelling, the separate *AC(t)* and *DC* signal components can be manipulated in order to arrive at an expression describing blood volume, equation [2.10].

$$\frac{\Delta I(t)}{I} = \frac{I_O \mu_b p(t)}{I_O\left[\beta \mu_t + \mu_b p(t)\right]} = \frac{\mu_b p(t)}{\beta \mu_t + \mu_b p(t)} \quad [2.10]$$

Equation [2.10] may be developed further, equation [2.11].

$$\frac{\Delta I(t)}{I} = \frac{\mu_b p(t)}{\mu_b p(t)\left[\beta \frac{\mu_t}{\mu_b p(t)} + 1\right]} = \frac{1}{\beta \frac{\mu_t}{\mu_b p(t)} + 1} \quad [2.11]$$

We may form a ratio constant from equation [2.11] to express absorption coefficients for both tissue (μ_t) and blood (μ_b) at the chosen wavelength as a proportion termed κ, shown in equation [2.12].

$$\frac{\Delta I(t)}{I} = \frac{1}{\beta\kappa \frac{1}{p(t)} + 1} \cong \frac{1}{\beta\kappa \frac{1}{p(t)}} \cong \frac{\kappa^{-1}}{\beta} p(t) \propto p(t) \quad [2.12]$$

Equation [2.12] shows that, since the pulsatile component *p(t)* is small, the inverse will be large, allowing an approximation in the denominator to be made. This simplifies to give a constant based on the absorption coefficient constant developed above (which is ratiometric anyway) divided by the probe coupling coefficient, multiplied by the pulsatile component itself, which gives a direct proportionality. Equation [2.12] will be named relative volume change (RVC) index. This equation incorporates the probe coupling coefficient term while still remaining independent from source intensity.

The RVC index gives increased generality compared to the Beer Lambert model of equation [2.7] since independence between venous and arterial coupling is provided, which was deemed necessary by experiment as discussed. The RVC index will be significant utilised in later chapters since it expresses the pulsatile component of the PPG signal and may be used to derive blood perfusion changes in tissue.

2.2.3 Diffusion Theory Modelling applied to PPG

Diffusion theory[8] affords a more in-depth insight into general tissue optics. The extra generality of diffusion theory affords more flexibility in defining terms, but this extra flexibility results in a more complex model. Generally, diffusion theory consists of an approximation to the Boltzmann[9] transport equation. This generalisation assumes the tissue to be a semi-infinite slab (to eliminate boundary conditions) and of homogeneous material. The fact that tissue conforms to neither of these two assumptions does not detract from the usefulness of the model. Tissue illumination is usually defined as a point source at a depth corresponding to the point where the first scattering events would occur for collimated radiation. This methodology eliminates problems associated with the use of a diffuse source, such as an LED.

Unfortunately, the added flexibility generalised diffusion theory offers gives an increased complexity of models. In many cases, increased model complexity is essential for accurate prediction of light and tissue interaction, but in this instance, diffusion theory is unnecessarily complex, and will not be discussed further.

2.3 Blood Pressure Models

Although the models discussed previously provide an insight into light/tissue interactions, they provide no information on physiological conditions actually modulating the light source. Both models contain time varying dimensional elements (attributable to vasculature) within the tissue slab, which produce time varying outputs from either model; any results from these forward models must be *interpreted* in a physiological manner. Since physiological parameters are involved in either model, the interpretation of these signal changes must be performed with knowledge of the underlying physiological functions. Given that these forward models do contain physiological parameters, any inverse model generated from the forward model cannot be used to provide an heuristic model based on direct physiological parameters.

It would be of great advantage to use PPG to imply actual physiological information from the vasculature. The fact that PPG provides relative un-calibrated outputs is one of the reasons PPG is employed more frequently in non-invasive vascular diagnostics[10]; indeed PPG has been viewed with suspicion by some[11]. Obviously the PPG signal is generated by the interaction of the physiology of the subject with the illuminating light source; examination of the recovered PPG signal may reveal information on the subjects physiology

directly, without inferring details as must be performed when using the simpler optical models discussed above.

Much work has been undertaken using blood pressure models, so called Pulse Contour Models (PCM). Often, the primary aim of PCM is to determine cardiac output (CO), which is the volumetric output of the heart over time, and is a product of stroke volume and heart rate. The monitoring of CO is routine in subjects undergoing intensive therapy, usually employing highly invasive catheterisation techniques, where probes are placed directly into the heart of the subject[12]. One aim of PCM is to reduce the dangers inherent in heart catheterisation[13] by using less invasive catheterisation of, for example, the brachial artery in order to derive the same information.

PCM have also been developed in order to assess the state of the vascular system. This allows evaluation of haemodynamic parameters, such as diastolic after load on the ventricles of heart[14].

2.3.1 Important Physiological Parameters

Pressure models generally employ parameters derived from the circulatory system in order to investigate loading effects on the heart, as briefly described above. Given that blood vessels are effectively distensible organic tubes, they will characteristics of elasticity and resistance; the values of which depending on the location and type of vessel. Definitions of hydraulic parameters will assist both the derivation and understanding of pressure models later.

The resistance of a tube R may be defined as the pressure drop P across the two ends, divided by the volume flow Q, equation [2.13], with units of pressure over volume flow.

$$R = \frac{\Delta P}{Q} \qquad [2.13]$$

Resistance may also be expressed in terms of the properties of the fluid passing through the vessel, first observed by Hagen and Puisuille[15] in 1840, stated in Equation [2.14] below.

$$R = \frac{8\mu}{r^4 \pi} \qquad [2.14]$$

Equation [2.14] above states the resistance per unit length is proportional to fluid viscosity μ (the ratio of force resisting flow to the force pushing the flow) divided by the fourth power of the tube inner radius r. Viscosity μ can be taken as the viscosity of blood, i.e. 4 cP (centiPoise, in honour of Poiseuille) at 37°C. The non-linear relationship of resistance with

respect to radius explains why blood flow is severely compromised by arterial blockages. The Hagen-Poiseuille equation assumes a homogenous Newtonian fluid with a constant laminar[16] flow in a rigid tube, which will be assumed for the sake of hydraulic understanding.

An arterial wall is partially comprised of the proteinous fibres elastin, which has an elastic quality, and collagen, which has a rigid quality, permitting the artery to expand whenever it receives a bolus of blood during systole, but with special characteristics discussed later. This elasticity, termed *arterial compliance*, allows the arterial system to smooth the pulsatile flow from the heart into a semi-constant flow[17] that supplies the periphery during diastole, since the heart valve prevents backflow.

Specific vascular compliance V_C may be defined[18] as the fractional change in vessel cross sectional area A per unit change in pressure P, equation [2.15] below.

$$V_C = \partial A / \partial P \qquad [2.15]$$

It may be shown[18] that V_C is related to the ratio of vessel wall thickness and vessel diameter and the modulus of elasticity (Young's modulus) of the vessel wall. Therefore, arterial wall thickness affects vascular compliance since a thicker vessel wall will be less distensible (for a given elastic constant) than a thinner vessel wall. It is for this reason that atherosclerotic plaque build up is so serious – plaque causes vascular compliance to be reduced, therefore greater loading is placed on the heart, not to mention the profound effects on flow caused by increased vessel resistance due to decreased vessel diameter.

The expression for vascular compliance, equation [2.15] above, neglects an important haemodynamic factor. As stated earlier, the construction of the arterial vessel employs both elastin and collagen arranged in such a manner as to limit the total available vessel expansion. Therefore, blood vessels do not follow Hooke's (1635 - 1703) law for tension in the vessel wall, where the change in *stress* (ratio of 'stretch' to cross sectional area of sample) divided by the change in *strain* (ratio of change in length to original length) is a constant up to the elastic limit. Nor do they follow conventional 'elastic-band' stress over strain rate of change observations, which follows an approximately quadratic law. Arterial blood vessels have an increasing rate of change of stress as strain increases[19]. This quality of arteries is essential in order to ensure any localised high pressures, quite possible in a multiple branched network such as the arterial system, does not cause localised 'ballooning' of the artery during systole. If localised ballooning does occur, this is known as an aneurysm;

the consequences of having an aortic aneurysm are dire for the patient, with high mortality rates if the aneurysm should rupture[20]. This therefore means that vascular compliance is not constant, since compliance is a function of pressure, and thus non-linear, but a linear relationship shall be assumed in this case.

If the arteries were fully rigid vessels, the circulatory system could not operate; blood is effectively incompressible (as the heart works by squeezing blood from itself) and if there were no elastic reservoirs in the rest of the system, blood ejected by the heart would have no where to go. The arterial system works as a pressure buffer, alternately stretching and relaxing, storing and releasing energy, smoothing variations in both pressure and flow[17]. As the venous system is not required to store energy, its vessels are generally non-compliant, but are filled with check valves as discussed previously. The venous system receives an almost steady flow of blood from the microcirculation, gradually collecting this slow return of blood into a significant volume for re-circulation by the heart.

2.3.2 Windkessel Model

Hales[17] qualitatively described a compliant arterial system in 1733. Frank[21], following on from Euler, quantified this concept, presenting a vascular model based on conservation of mass. This model portrayed the heart driving a simple reservoir and an output load resistance, as shown in Figure 2-1. The major arteries, including the aorta, are depicted as the reservoir, which, during diastole, discharges into a peripheral resistance representing the vascular bed. Frank's model was termed the 'windkessel' model after its similarities with anti-resonance reservoirs present in plumbing, used to reduce water hammer effects. This model was originally derived to obtain stroke volume (left ventricular ejection of the heart) by measuring aortic pressure. Implicit in this model is the gross simplification made of the circulatory system; infinite wave velocity is also assumed. It will be useful to analyse the windkessel model as the simplest blood pressure model since later sections draw from this initial work.

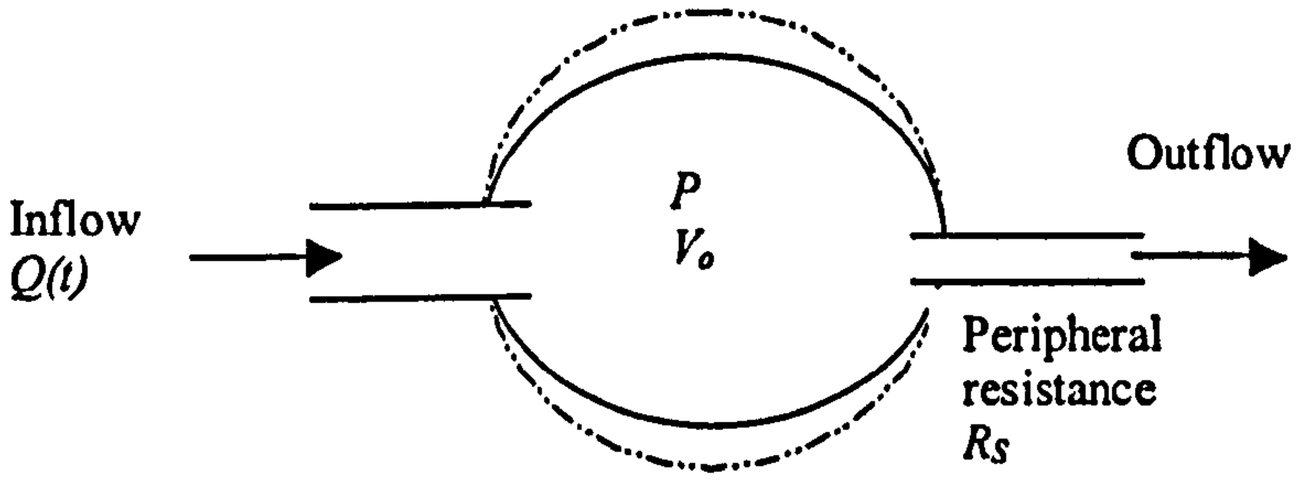

Figure 2-1 Windkessel analogy of the arterial circulatory system.

Referring to Figure 2-1, blood enters the windkessel on the left by ventricular contraction, and a relatively steady venous return flows out of the windkessel through the exit resistor R_S. The starting assumptions about the windkessel model are that ventricular ejection $Q(t)$ and intra-windkessel pressure P are related by the difference between inflow and outflow, and the volume elastic modulus E'. Frank himself suggested, from observations, that E' is not constant but a function of pressure, mentioned previously with regard to vascular compliance, but this example will assume E' is constant. We may define outflow from equation [2.13] as the internal windkessel pressure divided by the peripheral resistance R_s, since we shall assume the external pressure is zero. An expression may be developed which encompasses these concepts, as shown in equation [2.16].

[2.16] $$Q(t)-\frac{P}{R_s}=\frac{1}{E'}\frac{dP}{dt} \qquad E'=\frac{dP}{dV_o}$$

However, E' may be expanded since equation [2.17] shows that inflow and outflow are related to change in V_O, which is a dependent on volume elastic modulus and pressure.

[2.17] $$\frac{1}{E'}\frac{dP}{dt}=\frac{dV_o}{dP}\frac{dP}{dt}=\frac{dV_o}{dt}$$

The difference between inflow and outflow is the product of a material property of the windkessel and the change in pressure, an observable quantity. In order to determine pressure, by re-arranging equation [2.16] the differential equation must be solved. Doing so requires initial conditions to be specified and the system to be noted - this is a simple first order system resulting in an exponential decay. If, during systole, inflow Q_O is constant then equation [2.18] shows pressure during systole.

[2.18] $$P(t)=R_sQ_o-(R_sQ_o-P_o)\exp\left(\frac{-E't}{R_s}\right)$$

Equation [2.18] is only valid when time t is between zero and the duration of *systole* t_S, the initial conditions are specified as initial pressure P_O. Equation [2.13] shows that $R_S Q_O$ represents windkessel pressure P.

Conversely, equation [2.19] shows pressure during *diastole*: obviously during *diastole* flow Q is zero since the heart valves are closed, therefore any observable pressure is due to the elastic storage of the windkessel, and windkessel input flow is not required in this expression.

[2.19] $$P(t) = P_T \exp\left(\frac{E'}{R_S}(T-t)\right)$$

Equation [2.19] is valid for time t after systole but before the end of the cycle period T, with P_T being the arterial pressure at the end of *systole*. Stroke volume is simply defined as the total flow over the systolic period, and may be found by integrating equation [2.18] for flow. This windkessel model was developed further by first assuming a more accurate driving waveform from the heart – half sinusoids and other analytically definable waveforms were developed, without actually knowing the true driving flow pattern. Further expansions from this model were a non-linear relationship between reservoir pressure and volume, and the development of a dual reservoir model with two windkessel elements in series[22] (but significantly neglecting any inertial effects due to the mass of the column of blood from the proximal to distal site) in an attempt to represent differing compliances of the arterial system. However, these improvements could not explain the physical undulation of the dichrotic notch often present in pressure curves, and present in the arterial PPG waveform. The application of Fourier analysis[23] to pressure and flow in the circulatory system brought about the realisation of resonance in the vasculature, with the ultimate implementation of inertial effects into a model[24].

2.3.3 Lumped Blood Pressure Models

The term lumped applies to the technique of attributing a particular haemodynamic phenomenon, say peripheral vasculature resistance, into a particular element of the model. This technique was first developed by Frank, as shown above, attributing the distributed effects of the vasculature to discrete entities for analysis. While it is recognised that treating the vasculature in this manner is a gross simplification of the vasculature system, as the hydraulic parameters are *distributed* (see section 2.3.4) over the entire vasculature, lumped models have been shown to provide good results and have aided understanding[25].

The equations presented in section 2.3.2 above could have been solved using network theory, specifically Laplace transformations. Laplace transforms are generally used to convert an expression from the time domain, usually containing differential equations, into the frequency domain or '*s*' plane. Established methods for solving differential equations in the Laplace domain have been developed over time[26]. Direct parallels of hydraulic circulatory with electrical circuitry allow vasculature to be modelled using electrical engineering concepts.

Circuit voltage can represent arterial pressure; circuit current represents blood flow. The inertia of the column of blood between the heart and measuring site may be represented by an electrical inductance, the value of which is the ratio of blood density to lumen area. Resistance is the ratio of pressure gradient and flow rate; a change in pressure over flow is comparable to the voltage difference over current of Ohms law. Arterial compliance may be represented by a capacitor whose value depends on Young's modulus of the arterial wall and the vessel size parameters. The advantages in creating theses parallels are that abstract electrical engineering techniques, such as schematic diagrams, may be employed instead of mechanical-centric drawings such as Figure 2-1, which attempt to represent the arterial system in a conceptual manner. This abstract methodology allows established electrical engineering analysis techniques, such as nodal analysis[27], to be performed by treating the vasculature as a circuit. This section will employ this methodology in order to develop and analyse a more advanced lumped model.

2.3.3.1 Derivation of Electrical Engineering Analogies

Section 2.3.1 above discussed the derivation of physiological parameters, such as resistance and vascular compliance. Direct equivalencies between the haemodynamic parameters developed above and electrical engineering analogies must be defined. The simplest parameter, resistance, remains unchanged since this may be modelled directly using Ohms law, which states resistance is the ratio of voltage gradient and current, directly equivalent to equation [2.13]. However, electrical engineering equivalents, which have energy storage capabilities, are termed 'reactive', and have complex equivalencies that must be explicitly defined.

The inertia of a column of blood may be modelled using an electrical engineering parallel, the inductor. Inertia is the inherent property of a body to continue in its current state, be it rest or in motion. Inertia must be overcome to change that state; meaning mechanical inertia is a requirement for a force to accelerate a mass, i.e. mass opposes change of velocity, from

Newtons[28] Second Law which states force is the product of mass and velocity. An electrical inductor opposes change in current by its specific capacity 'inductance'; 'inertance' will be defined here as the specific capacity of inertia. In the case of vessels, inertia is modelled by a cylindrical mass of fluid, which may be defined[29] (per unit length) as the ratio of blood density ρ and vessel cross sectional area, equation [2.20].

$$L = \frac{\rho}{\pi r^2} \qquad [2.20]$$

Noted that inertance is unlikely to vary significantly between identical sites, assuming similar vessel characteristics such as length and diameter, since the density of blood is relatively constant over the entire physiological range of haematocrit values.

If the basic components of the system mentioned above are analysed further, it becomes apparent that the elastic nature of a vessel forms a storage reservoir, i.e. a tube with elastic walls that distend under pressure. Electrical engineering terminology defines a capacitor as a charge storage device: a direct analogy to an artery with distensible tubes forming a fluid storage device. This allows us to define arterial capacitance C as the ratio of change in volume V to change in pressure P, equation [2.21].

$$C = \frac{\partial V}{\partial P} \qquad [2.21]$$

Equation [2.21] expresses arterial capacitance, a haemodynamic property, and is closely related to vessel compliance, a mechanical property. If arterial capacitance is normalised with respect to unit length, then the change in volume simplifies to change in area (since volume of a cylinder is area multiplied by length), making capacitance C mathematically equivalent to Vascular Compliance V_C as defined in equation [2.15]. As stated previously, vascular compliance V_C in reality is not constant, but is a function of pressure. This implies arterial capacitance C will also be a function of pressure – but, in this case, arterial capacitance per unit length will be assumed constant.

To express arterial capacitance in terms of vessel parameters, the pressure to diameter relationship for elastic tubes must be determined. The Navier-Stokes[30] equations were developed for describing fluid-dynamic systems, based on Newtons second law. These equations may be simplified by neglecting second order terms and assuming blood is incompressible (which is valid for physiological pressures) in order to arrive at an analytical

solution. Equation [2.22] employs these generalisations in order to express arterial capacitance as a function of the arterial mechanical properties.

$$C = \frac{2r^3\pi}{Eh} \qquad [2.22]$$

Equation [2.22] depicts arterial capacitance C per unit length in terms of physical vessel parameters, where h is the ratios of vessel cross-sectional area to vessel wall thickness and E is the modulus of elasticity (ratio of stress over strain, Young's modulus) for the vessel. If the modulus of elasticity for the vessel E was a function of vessel wall strain, discussed above in section 2.3.1, then arterial compliance would be more accurate, depending on applied pressure. However, arterial capacitance in this case will be assumed constant.

2.3.3.2 Development of Lumped Parameter Model

The vascular model may now be expressed as a lumped electrical engineering system in terms of real physiological parameters. These parameters have a direct relationship with the actual mechanical and physical properties of the vasculature under investigation, albeit using a gross simplification of the circulatory system.

Referring to section 2.3.2, the developments of the windkessel model may be drawn schematically using electrical engineering terminology as shown in Figure 2-2. In all models of Figure 2-2, the source, i.e. the left ventricle of the heart, would be connected to the open ended circuit on the left, and the peripheral resistance is shown on the right. Model A is the electrical engineering equivalent of the windkessel model developed in section 2.3.2. The voltage across the resistor represents pressure as determined in the periphery. The capacitor charges during systole (analogous to the reservoir expanding in section 2.3.2) and discharges via the resistor during diastole.

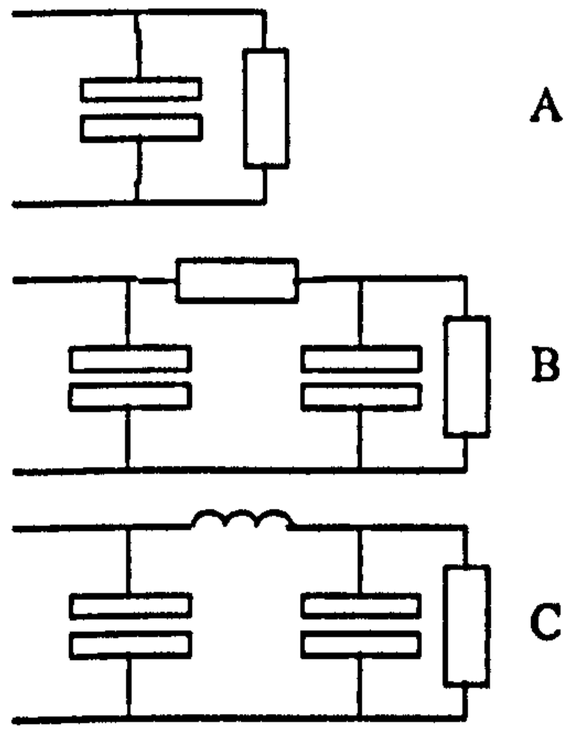

Figure 2-2. Electrical engineering analogues of circulatory systems in ascending order of complexity.

Model *B* shows the more complex model developed by Rashevsky[22], the dual windkessel model, expressed in electrical engineering terms, with the output of one windkessel (the intermediary resistance) feeding the input of the second windkessel. The left hand capacitor represents arterial compliance by the major arteries and its branches, with the right hand parallel resistor – capacitor representing the impedance to flow of these vessels and the distal vessel compliance respectively. As discussed, this model is technically more accurate but still does not model the undulations in the pressure curve frequently seen when examining arterial pressure in distal locations.

Model *C* was finally developed[31] to encompass frequency selectiveness of the arterial system. The central inductor represents the inertance of the column of blood within the major arteries. This configuration is recognisable as a tuned π circuit in electrical filter terminology, allowing resonance effects to produce peaks in the pressure waveform.

It is a relatively trivial matter to analyse the annotated circuit presented in Figure 2-3 using nodal analysis, taking Laplace equivalents of the inductance and capacitors, in order to derive a transfer function for the circuit in the Laplace (frequency) domain, then invert to the time domain. The steps involved for performing this will be now be performed.

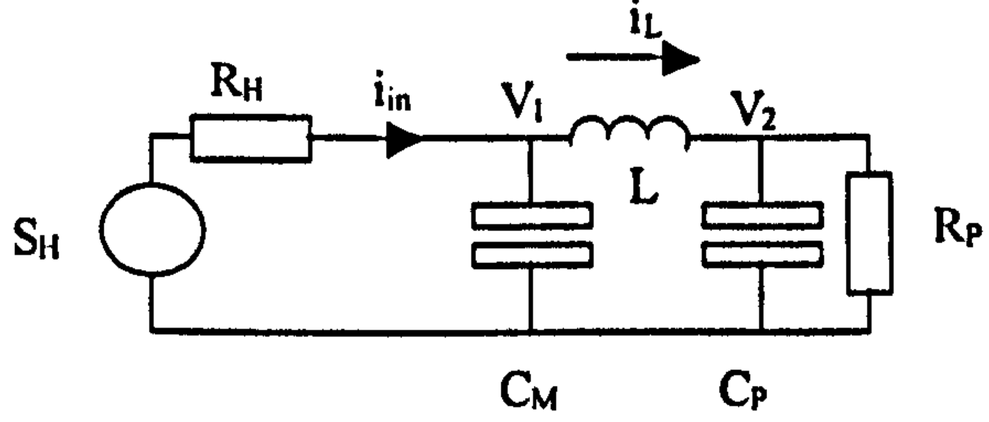

Figure 2-3. Four Element Lumped Parameter Arterial Model, with source S_H and source impedance R_H.

Figure 2-3 shows a more complete annotated version of model C from Figure 2-2, featuring inertance effects, where C_M is a capacitance representing the compliance effects of the major

arteries. The inductor L represents the inertia of the column of blood between the heart and the periphery. The capacitor C_P represents small arterial compliance, and R_P represents the resistance of the peripheral vasculature. Additionally, a source S_H and source impedance R_H have also been shown. Note the source form, current or voltage, is not explicityly defined, and will be discussed in detail later. The forward model time domain solution for this circuit must be developed to derive the physically observable output voltage across the resistor. It is more common when performing nodal analysis to represent the circuit under analysis as complex impedances, as shown in Figure 2-4.

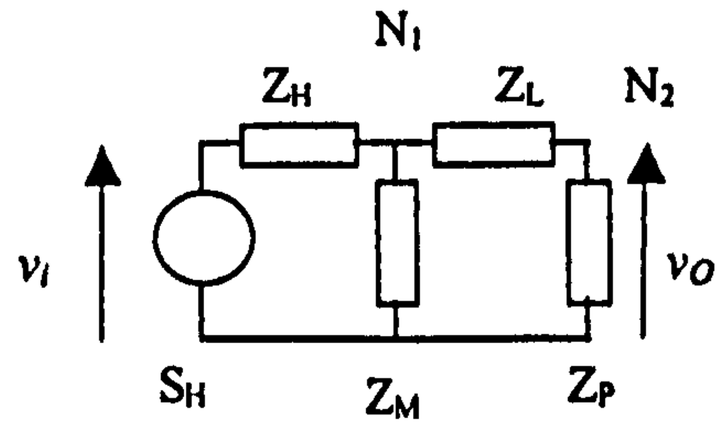

Figure 2-4. Complex impedance model of Figure 2-3

Figure 2-4 shows the complex impedance model, where Z_H is the impedance of the source, Z_M is the impedance of the major compliance, Z_L is the impedance of the inertance and Z_P is the combined peripheral impedance. Also shown are the two analysis nodes, N_1 and N_2. The output for this system is the voltage across Z_P, which shall be termed v_O, and the input will be the voltage across the source, termed v_I. The complex impedances are represented by their conventional Laplace transform equivalents, and are shown in equation [2.23].

$$
\begin{aligned}
Z_H &= R_H \\
Z_M &= \frac{1}{sC_M} \\
Z_L &= sL \\
Z_P &= \frac{R_P}{sR_PC_P+1}
\end{aligned}
\qquad [2.23]
$$

Note in equation [2.23] periperal impedance Z_P is the equivalent of R_P and C_P in parallel. Nodal analysis monitors the currents at junctions (nodes), recalling Kirchoffs (1824 – 1887) current law, stating total sum of currents at a junction (node) is zero. This allows expressions in current to be developed for the two nodes, N_1 expressed in equation [2.24] and N_2 in equation [2.25].

[2.24] $$\frac{v_{Z_M} - v_I}{Z_H} + \frac{v_{Z_M}}{Z_M} + \frac{v_{Z_M} - v_O}{Z_L} = 0$$

[2.25] $$\frac{v_O}{Z_P} + \frac{v_O - v_{Z_M}}{Z_L} = 0$$

Consequently, solving equations [2.24] and [2.25] for a transfer function requires a pair of simultaneous equations, equation [2.26] and equation [2.27].

[2.26] $$v_{Z_M}\left[\frac{1}{Z_H} + \frac{1}{Z_M} + \frac{1}{Z_L}\right] + v_O\left[\frac{-1}{Z_L}\right] = v_I\left[\frac{1}{Z_H}\right]$$

[2.27] $$v_{Z_M}\left[\frac{-1}{Z_L}\right] + v_O\left[\frac{1}{Z_L} + \frac{1}{Z_P}\right] = 0$$

In order to simplify further calculations, complex admittance rather than complex impedance will be employed, where complex admittance G_X is the reciprocal of complex impedance Z_X. Using this notation, equation [2.26] and equation [2.27] may be re-written as equation [2.28] and equation [2.29].

[2.28] $$v_{Z_M}[G_H + G_M + G_L] + v_O[-G_L] = v_I G_H$$

[2.29] $$v_{Z_M}[-G_L] + v_O[G_L + G_P] = 0$$

In order develop a system transfer equation of the form output over input, equation [2.29] must be solved for v_{ZM} and substituted into equation [2.28], shown in equation [2.30].

[2.30] $$v_O\left[\frac{G_P}{G_L} + 1\right](G_H + G_M + G_L) - v_O G_L = v_I G_H$$

Equation [2.30] may be re-arranged to obtain a transfer function in terms of complex admittance, equation [2.31].

[2.31] $$\frac{v_O}{v_I} = \frac{G_L G_H}{G_P[G_H + G_M + G_L] + G_L[G_H + G_M]}$$

Substituting the complex admittances developed earlier into equation [2.31] gives a transfer function in terms of the Laplace domain, equation [2.32].

$$[2.32] \qquad \frac{v_O}{v_I}(s) = \frac{R_P}{As^3 + Bs^2 + Cs + D} \quad where... \quad \begin{aligned} A &= R_P C_P C_M R_H L \\ B &= L(R_P C_P + C_M R_H) \\ C &= L + R_P R_H (R_P + R_M) \\ D &= R_H + R_P \end{aligned}$$

Equation [2.32] must be divided out to create a denominator that can be factored, and is shown in equation [2.32].

$$[2.33] \qquad \frac{v_O}{v_I}(s) = K \frac{1}{s^3 + Xs^2 + Ys + Z} \quad where... \quad \begin{aligned} K &= \frac{1}{C_P C_M R_H L} = Gain \\ X &= \frac{1}{C_M R_H} + \frac{1}{C_P R_P} \\ Y &= \frac{1}{C_P C_M R_P R_H} + \frac{1}{C_M L} + \frac{1}{C_P L} \\ Z &= \frac{1}{C_P C_M R_P L} \end{aligned}$$

Equation [2.33] gives the ratio of the output voltage (peripheral pressure, P_{Rp}) divided by the input voltage (pressure across source, P_{Source}, or aortic pressure), in the Laplace domain. A constant gain K has been introduced to express the scaling effects of the circuit. Unfortunately, this solution is of no practical use, because of complications brought about by the driving source of the system, i.e. the heart, which is unlike usual electrical engineering modelling challenges where the source is either a constant current or constant voltage device. This problem was briefly discussed in section 2.3.2, refinements of Frank's windkessel, with attempts at producing a more accurate driving waveform.

There are two main problems with the electrical engineering equivalent circuit, and thus the windkessel model from which it is developed. The first problem is the lack of a definable circuit source driving waveform, i.e. output from the heart. The pressure waveform is observed at the periphery, i.e. voltage, at the output resistor, but the driving waveform i.e. flow from the heart, is an unknown current flow, and therefore unknown voltage. We cannot then form an analytic expression for the driving waveform, nor perform a Laplace transform of the expression in the conventional manner when solving a problem of this type. Associated with the driving waveform is the problem of unknown initial conditions from the previous cycle, which are required when inverting Laplace transforms in order to determine the time domain solution. The second problem when analysing this circuit is a result of employing such a simple lumped model, in that the non-linearity of the semi-lunar heart

valve is not directly represented. To overcome these problems and limitation in the model, several arguments can be developed.

In the windkessel example given above, two equations were developed for pressure; equation [2.18] gives pressure during *systole* and equation [2.19] gives pressure during *diastole*. It was noted that the expression for pressure during *diastole* is independent of input flow during *systole*, only requiring post *systole* windkessel pressure in order to determine peripheral diastolic pressure. A similar approach can be performed here by only considering the circuit during diastole, which will eliminate the problem of unknown drive source.

If the electrical engineering equivalent circuit is only considered during *diastole*, then there will be flow neither into nor out of the heart (in our isolated vasculature section) since the semi-lunar heart valve is closed. The electrical equivalent circuit states therefore that there will be no current flowing into or out of the source, in the same manner, eliminating the driving waveform problems. It was proposed above to only consider the circuit during diastole, and the circuit can be modified in order to account for the arguments developed. Figure 2-3 shows the electrical circuit for which the transfer function was found. If the source impedance R_H is now assumed large, this effectively isolates the source (heart) from the circuit, as described above. A modified transfer function can be derived with these assumptions, as shown in equation [2.34], with K_D defined as the overall system gain of the system, and is not of major concern here.

$$X = \frac{1}{C_P R_P}$$

$$[2.34] \qquad v_O(s)_{Diastole} = K_D \frac{1}{s^3 + Xs^2 + Ys + Z} \quad where... Y = \frac{1}{C_M L} + \frac{1}{C_P L}$$

$$Z = \frac{1}{C_P C_M R_P L}$$

Equation [2.34] shows the system during diastole, when the only energy available is stored by the circuit reactive inertance and capacitance. The system is obviously 3rd order, which results in several possible time domain solutions. An unforced 3rd order system will have three modes, the response of the system being determined by the sum of the modes. With the general shape of the pressure waveform already known, the roots of the third order system model are expected to be either entirely real (since solutions producing complex results are not physically realisable or observable) or more likely one real root plus a complex conjugate pair. This is probable since the premise with this model is that some oscillation exists to

deliver the dichrotic notch, hence the incorporation of inertial effects into the model. A partial fraction expansion of equation [2.34] could be written, giving an expression shown in equation [2.35], which helps understand the form of the resulting time domain solution by providing further proof for the above statement.

$$v_o(s)_{Diastole} = K_D\left(\frac{A}{s+m}+\frac{B}{s^2+ns+p}\right) \qquad [2.35]$$

Reviewing the paragraph above, equation [2.35] implies that the time domain solution of equation [2.34] will show a decaying first order system and a conjugate second order system, equation [2.36], with K_D representing system gain as defined previously, and A and B representing coefficients of partial fraction expansion. Using the arguments developed above, a departure from traditional electrical engineering circuit solving procedures is made here, since as stated the inverse Laplace transform of equation [2.35] will not produce time domain solution as the driving waveform and initial conditions are unknown in this case. However, by inspection, the general diastolic solution will be the summation of the two part solutions, equation [2.36], shown in full in equation [2.37], with magnitude a_1, a_2, a_4 and phase a_7 representing end systolic initial conditions.

$$\begin{aligned} x_1(t) &= a_2\exp(-a_3t) \\ x_2(t) &= a_4\exp(-a_5t)\cos(a_6t-a_7) \end{aligned} \qquad [2.36]$$

$$p(t)_{Diastole} - a_1 = a_2\exp(-a_3t)+a_4\exp(-a_5t)\cos(a_6t-a_7) \qquad [2.37]$$

Equating coefficients is an alternative to partial fraction expansion, and the method used here for deriving a time domain solution. Equation [2.38] shows the standard solution for a third order equation with one real and a pair of complex roots, justified above, in terms of the coefficients of the time-domain solution equation [2.37].

$$\begin{aligned} &[s+a_3][s+(a_5+ja_6)][s+(a_5-ja_6)] = \\ &s^3+(2a_5+a_3)s^2+\left(a_6^{\,2}+a_5^{\,2}+2a_3a_5\right)s+\left(a_5^{\,2}+a_6^{\,2}\right)a_3 \end{aligned} \qquad [2.38]$$

Equation [2.39] shows the roots s_n of the system in terms of time domain system parameters introduced in equation [2.37].

[2.39]
$$s_1 = -a_3$$
$$s_{2,3} = -a_5 \pm ja_6$$

Equating coefficients of the diastolic third order Laplace solution, equation [2.34], gives a real solution, shown in equation [2.40].

[2.40]
$$X = a_3 + 2a_5$$
$$Y = 2a_3a_5 + a_5^2 + a_6^2$$
$$Z = a_3\left(a_5^2 + a_6^2\right)$$

Combining equations [2.25] and [2.40] gives the lumped parameter values (normalised in terms of peripheral resistance R_P) as shown in equation [2.41], with coefficients referenced to equation [2.34].

[2.41]
$$C_M = \frac{XY - Z}{XZ}\frac{1}{R_P}$$
$$C_P = \frac{1}{X}\frac{1}{R_P}$$
$$L = \frac{X^2}{XY - Z}\frac{1}{R_P}$$

Observation of equation [2.37] allows interpretation of the components of the function. The magnitude of the systolic pressure, corresponding to P_T in the windkessel model of section 2.3.2, is determined by taking $t=0$ and solving equation [2.37]. The reference pressure, which is the constant pressure offset, is modelled by parameter a_1. Parameter a_2 and a_3 represents the magnitude and exponential decay nature for the dominant section of the diastolic waveform, previously developed in the windkessel model. The magnitude and damping period of the dichrotic portion of the diastolic waveform is given by parameters a_4 and a_5 respectively. The frequency and phase respectively of the dichrotic oscillatory component is governed by parameters a_6 and a_7; units are radians per second and radians respectively. Table 2-1 shows this information in tabular form with typical[24] values.

Parameter	Typical Value	Description	Units	Status
a_1	60	Static Pressure	mmHg	Transient
a_2	60	Systolic Offset	mmHg	Transient
a_3	10	Dominant decay	mmHg	System
a_4	0.5	Dichrotic Magnitude	s^{-1}	Transient
a_5	5	Oscillatory damping	s^{-1}	System
a_6	20	Oscillatory period	Rad s^{-1}	System
a_7	-1	Phase	Rad	Transient

Table 2-1. Typical[24] Parameters of the lumped constant arterial model.

Numerical curve fits of pressure waveforms using equation [2.37] allow determination of system parameters a_3, a_5 and a_6. From these, the determination of the system tuned parameters i.e. physiological compliance and inertance, according to equation [2.41] may be performed. Parameters a_1, a_2, a_4 and a_7 are initial conditions needed only to calculate the voltages and currents (corresponding to pressure and flow in real vasculature) present in the system at the beginning of diastole. Typical[24] values of C_M and C_P indicate C_M is much greater than C_P, showing that the elastic energy storage capability of the aorta and major arteries is much greater than that of the peripheral compliance. Under these conditions, the value a_3, a_5 and a_6 may be approximated[24] as shown in equation [2.42].

$$a_3 \approx \frac{1}{C_M R_P}$$

[2.42]

$$a_5 \approx \frac{1}{2C_P R_P}$$

$$a_6 \approx \frac{1}{\sqrt{C_P L}}$$

The approximations in equation [2.42] allow a more direct interpretation between the systems physical parameters and the shape of the pressure curve. Now, a_3 is observable as a function of the major compliance C_M and the peripheral resistance R, and not of the inertance L or peripheral compliance C_P. Both the oscillatory frequency and decay, a_6 and a_5 respectively, are dominated by the peripheral compliance C_P, and are mainly independent of the major compliance C_M. Interestingly; a_6 is the only system parameter mainly independent of the peripheral resistance R_P.

2.3.4 Distributed Pressure Models

If one examines the basic components of the circulatory system, it becomes apparent that the system parameters are not grouped together in the simple manner suggested above. A far more accurate description would be a distribution of these circulatory components over the length of the system. A modelling approach to such a system would be transmission line theory[32], first proposed by Moens[33] and Korteweg[34], where the resistance, compliance, and inertance of the system are distributed over the length of the model. Figure 2-5 indicates these concepts diagrammatically, with the distal peripheral resistance R_P terminating the circulation.

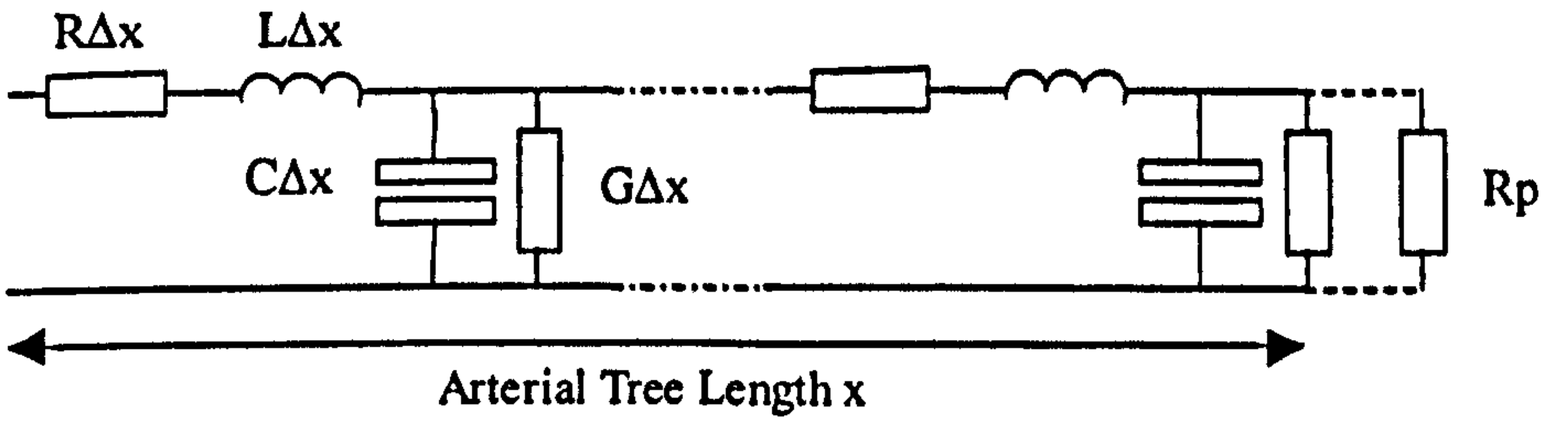

Figure 2-5. Distributed model of Arterial System.

The electrical analogue is characterised by four variables distributed along the length of the arterial tree, with parameters described as a function of x along the tree. An extra parameter G is included in the transmission line model not discussed previously, representing arterial leakage, termed conductance in electrical engineering terminology, and is assumed linearly proportional to transmural pressure. The development of the distributed model allows observation of the transformation of the pulse waves as they travel to the periphery. This model may employ several sections, which represent the various branches and bifurcation of a non-uniform circulatory system.

Differential equations representing each section may be developed[35] as shown in equation [2.43] using the electrical engineering analogies developed earlier. In equation [2.43], p and q represent pressure and flow (phasors) respectively, analogous to voltage and current.

$$-\frac{d\tilde{p}(x)}{dx} = -\frac{d\tilde{v}(x)}{dx} = (R + j\omega L)\tilde{i}(x)$$
$$-\frac{d\tilde{q}(x)}{dx} = -\frac{d\tilde{i}(x)}{dx} = (G + j\omega C)\tilde{v}(x) \qquad [2.43]$$

Complex impedance Z is often used when dealing with values of resistance. The eigenvalues and eigenvectors of equation [2.43] are shown in equation [2.44] and [2.45] respectively.

$$\lambda_1, \lambda_2 = \frac{Z_2 \pm \sqrt{Z_2^{\,2} + 4Z_1 Z_2}}{2} \text{ where } \begin{matrix} Z_1 = R + j\omega L \\ Z_2 = G + j\omega C \end{matrix} \quad [2.44]$$

$$\tilde{p}_{O+}(x)\begin{bmatrix} 1 \\ \frac{}{Z_2} \\ -\lambda_1 \end{bmatrix}, \tilde{p}_{O-}(x)\begin{bmatrix} 1 \\ \frac{}{Z_2} \\ -\lambda_2 \end{bmatrix} \quad [2.45]$$

As can be seen, this model is unattractively complex since a set of differential equations is required for each segment. However, since the PPG waveform is only observed in distal sites the intermediary transmission line distributed model is over complex in this application, and will not be developed further.

2.4 Pressure Models and PPG

Section 2.3.3 showed the development of a lumped constant model of the arterial circulation. As discussed, the unforced response of this system was developed, modelling the response of the system to the diastolic portion of the pressure waveform in the time domain. This solution is shown in equation [2.46].

$$P(t) = a_1 + a_2 \exp(-a_3 t) + a_4 \exp(-a_5 t)\cos(a_6 t - a_7) \quad [2.46]$$

The inverse solution for the model parameters of this equation is given in equation [2.47], normalised with respect to peripheral resistance R_P. These are expanded forms of the equations presented in equation

$$\begin{aligned} \frac{L}{R_P} &= \frac{(a_3 + 2a_5)^2}{2a_5\left(\left[a_3 + a_5\right]^2 + a_6^{\,2}\right)} \\ R_P C_M &= \frac{2a_5\left(\left[a_3 + a_5\right]^2 + a_6^{\,2}\right)}{a_3(a_3 + 2a_5)\left(a_5^{\,2} + a_6^{\,2}\right)} \\ R_P C_P &= \frac{1}{(a_3 + 2a_5)} \end{aligned} \quad [2.47]$$

The fundamental assumption of PPG, briefly discussed in Chapter 1, is that a blood volume increase results in a corresponding increase in optical density. Since the arterial vasculature is elastic, quantified with vascular compliance in section 2.3.1, it can be argued an increase in arterial pressure will result in an increase in blood volume due to expansion of the artery, thereby invoking an increase in optical density. Attempts at providing a direct correlation between arterial pressure and arterial PPG have been published in the literature[36,37]. The

Allen paper employed a simple first-order lag transfer function in order to relate the blood pressure to the blood-volume pulse signal, with the transfer function employed in a black-box manner, peripheral arterial blood pressure as input and blood volume pulse as output.

$$G(s)=\frac{K\exp(-sT_d)}{1+\tau s} \qquad [2.48]$$

The equation [2.48] above represents the pressure / PPG transfer function, as described in the frequency (Laplace) domain discussed earlier. Here, K is the input-output gain, τ is the time constant lag; both are continuously variable parameters. Additionally, T_d is the system delay time and is fixed, depending on subject and equipment.

Moreover, more complex generalised transfer functions have been proposed[38] in order to relate arterial PPG to the arterial pulse pressure (defined as the transmural pressure oscillation between the upper systolic and lower diastolic pressure limits), which illustrates the increasing amount of literature in the field providing a direct correlation between arterial pressure and arterial PPG. Qualitatively, proportionality between arterial pulse pressure and PPG seems obvious, since any increase in pressure over quiescent conditions will cause vascular expansion, hence increased blood volume, and thus increased light attenuation that may be monitored using PPG.

It was stated that in the blood pressure model, peripheral resistance R_P is models the total resistance of the peripheral arterial bed. One could argue that the field of view of a PPG probe only inspects a tiny proportion of the overall vascular bed. Therefore, the peripheral resistance analogy breaks down in the case of PPG since the PPG probe is actually monitoring skin haemodynamic resistance, not overall peripheral resistance as seen by the heart. However, inspection of the model shows the peripheral pressure is measured across the peripheral resistance and compliance. It can therefore be argued that the systemic peripheral resistance is formed from set of parallel peripheral resistances incorporating the various elements of peripheral microcirculation throughout the body. In this way, skin haemodynamic resistance, as viewed under the PPG probe, will form a proportion of the overall peripheral resistance, summing in a parallel manner. In the same way, the compliance of the vessels in the field of view of the probe contributes in a parallel manner to the overall peripheral compliance. Figure 2-6 shows this concept diagrammatically.

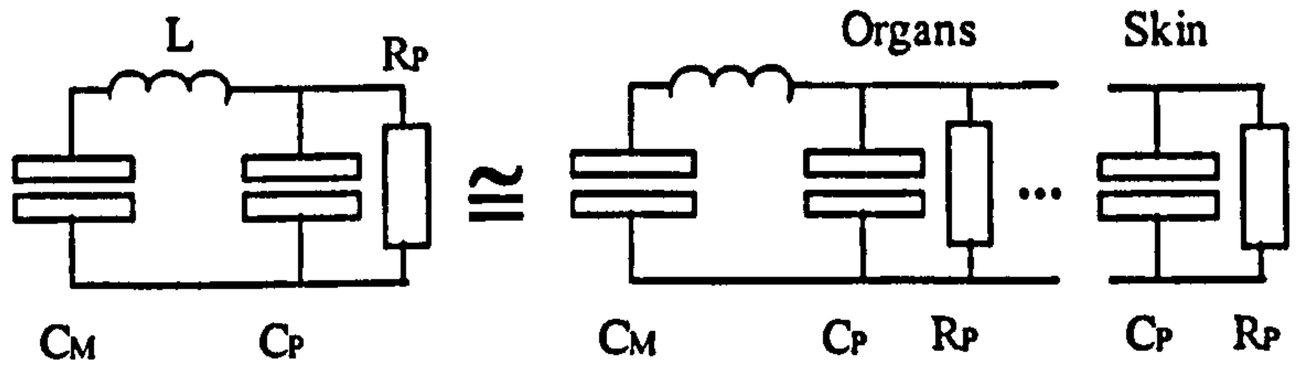

Figure 2-6. Four Element Lumped Parameter Arterial Model, with equivalent decomposition of peripheral elements. Shown are Periperal compliance and resitance for the major internal organs, along with the peripheral compliance and resistance of the skin.

Figure 2-6 illustrates that the simple peripheral compliance and resistance of the model presented in Figure 2-3 may be decomposed to represent the small artery compliance and resistance of several elements of the body. As described above, pressure derived across any of the elements of the periphery is identical across all resistance elements that form the macroscopic peripheral resistance and compliance. Therefore, the analogy between arterial PPG developed above is still valid.

As stated, one of the main advantages of PPG is its non-invasive methodology – most blood pressure sensors require an invasive pressure catheter in order to obtain the pressure waveform. If the limitations of these transfer functions are taken into account, then the field of arterial pressure models may be applied in the context of arterial PPG in order to retrieve information of the subjects vasculature, from the PPG pulse waveform.

2.4.1 Typical Physiological Pressure Values

Typical[24] pressure values obtained from normotensive and hypertensive subjects, detected using a catheter tip pressure sensor located in the brachial artery, are shown in Table 2-2. Corresponding lumped parameter values, obtained from the same source, are also shown. Observation of these results shows a decreased distal vascular compliance time constant R_PC_P, which also explains the increases oscillatory frequency since this is distal compliance dependent, as discussed in approximations, equation [2.42].

Distal vascular resistance R_P may be inferred from the L/R_P time constant since inertance of normotensive and hypertensive subjects is assumed to be approximately equal, discussed in section 2.3.1, as inertance is modelled as a column of blood from the heart to the measuring site, assuming similar vessel dimensions. Accepting these assumptions reveals R_P for hypertensive subjects is approximately 50% greater than for normotensive subjects.

Parameter	Units	Normals	SD ±	Hypertensives	SD ±
a_2	mmHg	103.36	6.75	155.63	18.36
a_3	s^{-1}	0.55	0.11	0.61	0.29
a_4	mmHg	12.12	4.74	13.48	6.69
a_5	s^{-1}	3.95	0.83	17.17	2.68
a_6	Rad s^{-1}	19.17	2.67	44.57	3.61
a_7	Rad	-1.44	0.50	0.04	0.34
$R_P.C_M$	s	1.789	0.386	2.095	1.361
$R_P.C_P$	ms	123	25	29	5
L/R_P	ms	23.3	5	15.45	1

Table 2-2. Lumped Parameter taken from normotensive and hypertensive subjects[24].

2.4.2 Effects of Scaling

Observation of the parameters of the forward model, equation [2.46], shows that system scaling parameters, or initial parameters a_2 and a_4, are *not* required in equation [2.47], meaning only parameters a_3, a_5 and a_6 are used when determining lumped parameter timing values. Consequently, a scaled diastolic contour waveform would still provide information on the lumped model timing parameters using a numerical curve fit, since any scaling constants are unused. Further observation reveals the static pressure a_1 is also unused in determination of lumped model timing parameters. Hence, a pressure waveform may have the offset removed, then scaled to an appropriate level, such as when analogue to digital conversion signal processing, yet still provide a solution for the model parameter time constants after curve fitting.

Examination of the transfer function presented in equation [2.48] shows the pressure waveform can be related to the arterial PPG waveform by a gain K and a time delay τ. Relating the transfer function gain K to the observations made above shows that an arterial PPG waveform could represent the arterial pressure waveform by scaling; the derivation of model parameter time constants from a pressure waveform using a numerical curve fit are unaffected by scaling. We can assume the non-linear arterial compliance, which is dependent on arterial pressure, will be linear within the normotensive and hypertensive ranges; literature[39] shows that the greatest non-linear effects are outside physiological limits. Additionally, the pressure offset parameter a_1 associated with arterial pressure may be

ignored, as in the case of arterial PPG, without affecting the derivation of model timing parameters. We may express these statements in terms of an expression, as shown in equation [2.49].

$$PPG(t_{Diastolic})_{Arterial} \propto P_{Pulse}(t_{Diastolic}, L, C_M, C_P, R_P) \quad [2.49]$$

Equation [2.49] implies that the arterial PPG signal is proportional to the arterial pulse pressure, which is a function of the forward model parameters, during the diastolic period. Therefore, the arterial PPG signal should provide information relating to the compliance of the two arterial groups used in the lumped parameter model. Therefore, numerical curve fits of the third order pressure model, applied to arterial PPG waveforms, should provide physiological system timing parameters using the same methodology as developed in section 2.4.1.

2.5 Conclusion

During this chapter, the concept of modelling has been introduced. Several differing model types have been introduced, ranging from light with tissue interaction models to complex circulatory models.

Specifically in the case of light and tissue models, an expression for the one-dimensional Beer-Lambert light propagation model was developed. This equation models blood-volume changes under the field of view of the PPG probe, but was found lacking since this model does not account for probe coupling effects. Therefore, a more general light-tissue interaction model was developed; in this model the blood volume changes were attributed to a function of the arterial transmural pressure and probe coupling was simply described. This general model has the advantage over the Beer-Lambert model in that physiological subject effects are being partially modelled – this model will be developed further in chapter three in order to determine volume changes in the periphery. It may be possible, using fluid dynamics theory (such as the law of Laplace[40] and the Navier-Stokes equations), to determine the relationship between arterial transmural pressure and blood volume changes, incorporating this relationship into the general model presented here.

Since both the Beer Lambert and general light tissue models do not provide sufficient insight into subject physiology, the field of blood pressure models was investigated. Both lumped parameter models and distributed models were presented; distributed models being discarded in this thesis due to the added complexity not necessarily providing extra useful information. Development of the lumped parameter model continued with analysis of a third order model

using network theory and Laplace transforms, arriving at a diastolic time domain solution whereby the parameters of the lumped model may be inferred by curve fitting of an appropriate pressure waveform.

Investigations regarding arterial PPG and arterial pressure waveforms were performed, with the conclusion that the third order numerical curve fit approach developed above, previously applied to arterial pressure waveforms, may be applied to arterial PPG waveforms in an identical manner in order to obtain the parameters of the lumped model. An argument was developed based on the difference between skin haemodynamic resistance and systemic peripheral resistance, which concluded that pressure determined across the skin haemodynamic resistance was equivalent to pressure determined across systemic peripheral resistance, ensuring the lumped model solution was still valid.

Scaling problems associated with PPG, normally a problem due to the relative nature of arterial PPG waveforms, have been shown not to affect the lumped parameter model, as the arterial PPG waveform is argued to be proportional to the arterial pulse pressure waveform. Typical physiological values obtained by applying the third order numerical curve fit methodology to brachial artery pressure waveforms show marked differences between normotensive and hypertensive subjects. These differences qualitatively fit the expected physiology under these circumstances – i.e. reduced compliances and increased peripheral resistance.

A problem with extraction of vascular parameters from the diastolic portion of the waveform is the normalisation that results. The vascular parameters of interest, major compliance (C_M), peripheral compliance (C_P) and inertance (L), are all normalised with respect to peripheral resistance. Of these parameters, arterial compliance values have the greatest sensitivity to subject physiology. Given that, with blood density being relatively invariant (only affected by the haematocrit value), an approximate inertance, based on body size geometry (since this will be a dominant part of any function describing L) may be derived after statistical analysis of population groups for a given probe placement location. From this, calculation of peripheral resistance may be possible, allowing de-normalisation of the vascular compliances mentioned above. Additionally, using the value of L derived from body geometry as described above, observation of oscillatory peaks in the pressure waveform may allow determination of a_6 alone, without numerical fitting. In this way, determination of peripheral compliance C_P could allow comparative evaluation of arterial health based on arterial compliance.

2.6 Chapter References

[1] Hedong ZHANG, Yutaka TSUCHIYA, "Applicability of Time Integrated Spectroscopy Based on the Microscopic Beer-Lambert Law to Finite Turbid Media with Curved Boundaries", OPTICAL REVIEW Vol. 7, No. 5, pp. 473-478 (2000)

[2] Huabei Jiang, "Optical image reconstruction based on the third-order diffusion equations", Optics Express 4, pp.241-246 (1999)

[3] Aoyagi T, Kishi M, Yamaguchi K, Watanabe S, "Improvement of the ear piece oximeter", Abstracts Jpn. Soc. Med. Electronics Biol. Engineer, pp. 90 – 91 (1974)

[4] Cejnar M, Kohbler H, Hunyor S.N, "Quantative Photoplethysmography: Lambert –Beer law or inverse function incorporating light scatter", J. Biomed. End, 15, pp. 151-154 (1993)

[5] Shimida Y,Yoshiya I, Oka N, Mamaguri K, "Effects of Multiple Scattering and Peripheral Circulation on Arterial Oxygen Saturation, Measured with a Pulse Oximeter", Med. Biol. Eng. Comput., 22, pp. 475-478 (1984)

[6] Steinke J.M, Shepherd A.P, "Role of Light Scattering in Whole Blood Oximetry", IEEE Trans. Biomed. Eng., 33(3), pp. 294-301, (1986)

[7] Hurch A, Hurch R, Kourg V et al., "Limitations of pulse oximetry [letter]", Lancet, 1, pp. 357-359 (1988)

[8] Schmitt J.M, "Simple Photon Diffusion Analysis of the Effects of Multiple Scattering on Pulse Oximetry", IEEE Trans. Biomed. Eng, 38(12), pp.1194-1203 (1991)

[9] Morse P.M, Feshback H, "Methods of Theoretical Physics", McGraw-Hill (1953)

[10] Trafford J. de, Lafferty K, "What does Photoplethysmography Measure? [letter]", Med. Bio;. Eng. Comput., 22, pp.479-480 (1984)

[11] van Bemmelen P.S, van Ramshorst B, Eikelboom B.C, "Photoplethysmography re-examined: lack of correlation with duplex scanning", Surgery, 112:3, pp. 544-548 (1992)

[12] Godje O, Thiel C, Lamm P, Reichenspurner H, Schmitz C, Schutz A, Reichart B, "Less invasive, continuous hemodynamic monitoring during minimally invasive coronary surgery", Ann. Thorac. Surg,, 68(4), pp. 1532-6 (1999)

[13] de Bono D.,"Complications of diagnostic cardiac catheterisation: results from 34,041 patients in the United Kingdom confidential enquiry into cardiac catheter complications", Br Heart J. , Sep;70(3):297-300 (1993)

[14] Hoeksel SA, Jansen JR, Blom JA, Schreuder JJ. "Detection of dicrotic notch in arterial pressure signals", J Clin Monit. Sep;13(5):309-16 (1997)

[15] Lagerstrom, P. A., "Laminar Flow Theorem", Princeton, Princeton University Press, NJ (1964)

[16] Reynolds O, "An experimental investigation of the circumstances which determine whether the motion of water shall be direct or sinus, and of the law of resistance in parallel channels", Trans. Roy. Soc. Lond., 174, pp. 935-82 (1883)

[17] Hales S, "Statistical Essays: Containing Haemostaticks", Innyes & Manby, London, UK, vol. II (1733)

[18] Stevanov M, Baruthio J, Eclancher B, "Fabrication of elastomer arterial models with specified compliance", J. Appl. Physiol, 88, pp. 1291-1294 (2000)

[19] Peterson L.H, "Properties and behaviour of the living vascular wall", Physiol. Rev., 42, pp. 309-337 (1962)

[20] Davies RR, Goldstein LJ, Coady MA, Tittle SL, Rizzo JA, Kopf GS, Elefteriades JA., "Yearly rupture or dissection rates for thoracic aortic aneurysms: simple prediction based on size", Ann. Thorac. Surg, 73(1), pp. 17-27 (2002)

[21] Frank O, "Die Grundform des arteriellen Pulses", Z. f. Biol. 37, pp. 483-526 (1899)

[22] Rashevsky N, "Some medical aspects of Mathematical Biology", Springfield, Illinois, Charles C. Thomas, Ch. 6-14 (1964)

[23] Fry D.L,"The Measurement of pulsatile flow by the computed pressure gradient technique", IRE Trans. Medical Electronics, ME-6, pp. 259-264 (1959)

[24] Watt T.B., Burrus C.S., "Arterial Pressure Contour Analysis for estimating Human Vascular Properties", J. Appl. Physiology, 40(2), pp. 171-176 (1976)

[25] Quick C.M, YoungW.L, Noordergraaf A, "Infinite number of solutions to the hemodynamic inverse problem", Am. J. Physiol. Heart Circ. Physiol., 280, H1472-H1479 (2001)

[26] Nise N.S., "Control Systems Engineering", 3rd Edition, John Wiley and Sons, Ca., USA (2000)

[27] Van Valkenburg M.E., "Network Analysis", Prentice Hall, Englewood Cliffs, N.J., USA (1964)

[28] Newton I.S., "Philosophiæ Naturalis Principia Mathematica", 1st Edition, S. Pepys Publishing, Cambridge University Press, Cambridge (1686)

[29] Rose W.C, Shoukas A.A, "Two-Port Analysis of systemic venous and arterial impedeances", Am. J. Physiol, 265(5 Pt2), H1577:1587 (1993)

[30] Ladyzhenskaya O., "The Mathematical Theory of Viscous Incompressible Flows" (2nd edition),Gordon and Breach (1969)

[31] Goldwyn R.M, Watt T.B, "Arterial Pressure Pulse Contour Analysis via a Mathematical Model for the Clinical Quantification of Human Vascular Properties", IEEE Trans. Bio.Med. Eng, BME-14(1), pp. 11-17 (1967)

[32] Christopoulos C., "The Transmission-Line Modelling Method", John Wiley and Sons, USA (1996)

[33] Moens A.I., "Die Pulskurve", Leiden, Germany, E. J. Brill (1878)

[34] Korteweg D.J., "Über die Fortpflanzungsgschwindigkeit des Schalles in elastichen Röhren", Ann. D. Physik., III, pp. 525-542 (1878)

[35] Chen C.W, Shau Y.W, Wu C.P, "Analog Transmission line model for simulation of systemic circulation", IEEE Trans. Biomed. Eng., 44(1), pp. 90-94 (1997)

[36] Heubach T, Czastrau C, Klysc T, Blazek V, Junger M, Hahn M, "Synchronous Measurements of Capillary Blood Pressure and Arterial Photoplethysmography", Int. J. of Microcir. Clin. Exp., 16(1), pp. 121 (1996)

[37] Allen J, Murray A., "Modelling the relationship between peripheral blood pressure and blood volume pulse using linear and neural network system identification techniques", Physiol. Meas, 20, pp.287-301 (1999)

[38] Millasseau S.C., Guigui F.G., Kelly R.P., Prasad K., Cockcroft J.R., Ritter J.M., Chowienczyk P.J., "Non-invasive assessment of the digital volume pulse. Comparison with the peripheral pressure pulse", Hypertension, Dec 36, pp. 952-6 (2000)

[39] Monson K., "Mechanical and Failure properties of Human Cerebral Blood Vessels", PhD Thesis, University of California, Berkeley (2001)

[40] Laplace P.S., "Théorie l'action capillarie", In Traite de mécanique céleste, Suppliment au livre X, Pais, Coarcien (1806)

Optical Engineering Group
Loughborough University

Chapter Three

Photoplethysmography and Functional Perfusion Diagnostics

3 Introduction to FPD and PPG

Previous chapters introduced both PPG and PVD. The technical aspects behind PPG were introduced and extended, resulting in the development of models describing light and tissue interaction. Finally, a physiological forward model based on the lumped constant blood pressure model was analysed and applied to PPG.

This chapter will investigate these perfusion models further in order to develop a light tissue model that may be used for functional perfusion diagnostics (FPD). FPD will be the term given to the technique of monitoring the circulatory system by means of PPG. FPD will use a relative methodology in order to create a reference structure against which further measurements are compared. This technique should eliminate relative sizing problems usually associated with PPG, providing a measure of perfusion which could be used both in sports science and clinical diagnosis of peripheral vascular disease (PVD). Perfusion investigation in the field of sports science involves the investigation and research of blood flow during both exercise and resting conditions. PVD was introduced in chapter one, with the associated risks and consequences; the conclusion being early diagnosis and treatment of PVD is essential for both increased patient quality of life and longevity.

In this chapter, FPD derived using a simultaneous dual channel PPG methodology in order to perform comparative perfusion monitoring. This methodology has obvious applications in the monitoring of PVD cases, where comparative perfusion monitoring between differing sites is desired.

Furthermore, the lumped pressure model, the solution of which was argued could be applied to PPG, will be developed further in order to determine an inverse model. This inverse model will give a relationship between the arterial PPG waveform and the parameters of the lumped constant model. Finally, the lumped inverse model will be extended in a similar manner to FPD in that simultaneous dual channel PPG will be incorporated into the technique, allowing both comparative symmetric and asymmetric evaluation.

3.1 Dual Channel Photoplethysmography

Generally, studies conducted using PPG have been concerned with blood volume changes as measured from a single site, as discussed in chapter one. This section develops the hypothesis that analysis of PPG signals obtained simultaneously from at least two separate

distal sites may provide better insight into the physiology of the subject, by enabling comparative evaluations to be performed.

Blood volume changes are often registered at the finger for the reasons mentioned in chapter one, i.e. ease of use, good signal to noise (SNR) etc. However, many tests based on PPG technology are conducted at other distal sites, in order to assess differing physiological parameters or faults in the peripheral circulatory system, such as deep vein thrombosis diagnosis using venous PPG[1] or venous insufficiency[2] tests. Pulse oximetry probes are often used on the foot of neonates or the ear[3], with several commercial exercise equipment companies use ear PPG in order to determine heart and respiration rate during exercise, since both the hands and feet are often engaged during exercise.

A proposed novel analysis method using simultaneous dual channel PPG allows comparative evaluation of physiological parameters at two distal sites. The locations of the sites will alter the effect on the test diagnosis conclusion; one site is generally termed a reference site, acting as a base with which to compare changes in the opposing site under investigation. For example, a probe could be employed at both the finger and toe, and comparisons made between the two sites.

3.1.1 Dual Channel PPG FPD Model

In order to develop comparative site evaluations, a simple metric must be developed which would allow quick and easy evaluation of relative perfusion in two sites. For example, as mentioned previously, patients suffering from diabetes may have reduced perfusion in the toes[4], but the perfusion in fingers is usually near normal. By taking a comparative measure between the toe and finger sites, relative perfusion of the toes compared to the fingers could be established, which is an example of asymmetric testing, to be discussed later.

In order to understand this further, a pulse or perfusion index directly related to arterial perfusion must be developed mathematically which encompasses the methods developed previously on single channel PPG.

3.1.1.1 Development of single channel Relative Volume Change (RVC) Index

Returning to the general model, first discussed in chapter two, an expression directly proportional to the pulsatile PPG component was developed, based on manipulating components of the PPG signal, repeated in equation [3.1]. In equation [3.1], the constant κ represents the relative ratio for the coefficients of absorption for both tissue and blood at the chosen illuminating wavelength, with probe coupling coefficient represented by β.

$$RVC = \frac{\Delta I(t)}{I} = \frac{AC(t)}{DC} \cong \frac{\kappa}{\beta} p(t) \propto p(t) \quad [3.1]$$

In equation [3.1], the band limited differential of the PPG signal may be divided by the low pass filtered quasi static PPG, arriving at an expression directly proportional to the pulsatile component *p(t)* of the recovered PPG signal, which was termed relative volume change (RVC). The RVC metric is most suitable when observing *changes* in perfusion. However, as stated, changes in perfusion must occur in order to monitor perfusion levels, which may not be suitable in all monitoring cases, particularly when 'spot' monitoring is desired. Additionally, inter-subject comparative perfusion monitoring will be scaled by the constants, the differing subject constants causing differing scaling effect, thereby subjects scatter plots will be incomparable, reducing the effectiveness of inter-subject comparison. To perform inter-subject comparison and additionally dual site comparative monitoring, extensions to the general PPG model are necessary.

3.1.1.2 Extension of RVC to Dual Channel PPG

The RVC index allows us to monitor time varying blood volume changes beneath the monitoring site. However, absolute values of RVC are scaled by the ratio of blood and tissue absorption coefficients, probe coupling coefficients and source intensity. Development of a dual site comparative investigation methodology must eliminate scaling parameters, allowing relative perfusion monitoring between sites, and inter-subject comparisons to take place. One method for eliminating scaling due to the blood and tissue absorption coefficients is by taking the ratio of the two sites, since the absorption coefficients for tissue and blood in the two sites is expected to be very similar if not identical, unless known pathology negates this assumption. This gives an expression in equation [3.2] for a relative measure of perfusion between the two measuring sites, which shall be termed Perfusion Volume Index (PVI), where site *A* could be a finger and site *B* could be toe.

$$PVI \cdot \gamma = \frac{RVC_A}{RVC_B} = \frac{\frac{\kappa_A}{\beta_A} p_A(t)}{\frac{\kappa_B}{\beta_B} p_B(t)} = \frac{p_A(t)}{p_B(t)} \frac{\beta_B}{\beta_A} \quad [3.2]$$

Examination of the effects of including the coefficients described above in equation [3.2], shows κ will cancel, since the ratio of blood and tissue coefficients of absorption should be near identical in the two sites. Probe coupling coefficients β may be very similar if for example, two identical finger probes are employed on opposite hands[5]. However, in the case

of finger and toe PPG sites, probe design and coupling will be vastly different, causing the PVI to be scaled by a fixed constant value γ, defined as the ratio of β_A and β_B.

In order to eliminate probe coupling scaling, a relative test method must be devised (for example, pre and post exercise tests) which will reduce or eliminate entirely the effects of any probe coupling constants, which we shall call relative peripheral vascular index (RPVI).

[3.3] $$RPVI = \frac{\gamma PVI_{POST}}{\gamma PVI_{PRE}}$$

Equation [3.3] above demonstrates how using pre and post *event* values for PVI will eliminate any probe coupling problems, where *event* is some action or method which will produce a change in perfusion between PVI determinations in time, such as an exercise test. There is a remote possibility that sweating in the post exercise state may affect probe coupling, but this is doubtful since probe coupling is dominated by subject geometry and tissue anatomy. Not only does this methodology allow inspection of relative peripheral perfusion, but also comparative testing functions, which could identify any arterial perfusion problems in a post event state.

The RPVI index allows a single index to provide insight into comparative perfusion between two sites, irrespective of probe geometry, probe coupling coefficients etc. Finally, the constant K, defined as the ratio of tissue and blood coefficients of absorption may differ between sites without affecting the RPVI metric. These points are quite distinct compared to the limitations imposed by earlier metrics, and the advantages are apparent, detailed below.

- RVC metric allows perfusion monitoring in a single site only. Direct inter subject correlation is unadvisable since unknown scaling occurs between subjects, caused by probe coupling. Initial perfusion may be employed as a normalisation factor, necessitating change in perfusion to generate deviation from baseline perfusion.
- PVI allows comparative perfusion monitoring in dual sites using a single measure. Inter subject comparisons are possible provided probe geometries are identical between subjects. Limitations such dual site identical absorption coefficients are also required, otherwise, further scaling will occur.
- RPVI allows comparative perfusion monitoring in dual sites using a single measure. Inter subject comparisons may be freely performed. Differing probe geometries may be employed; hence, differing tissue absorption characteristics. A perfusion change must be invoked in order to allow this general metric to be employed.

3.2 Dual Channel Pressure Derived PPG Models

The lumped parameter pressure model was introduced in chapter two, and a time domain solution for the diastolic portion of the pressure waveform was developed in terms of the system lumped parameters. In order to extend the pressure model for employment in a dual-channel PPG system, the basic concept must be extended, as shown in Figure 3-1, with the two distal perfusion sites noted as site *A* and site *B*.

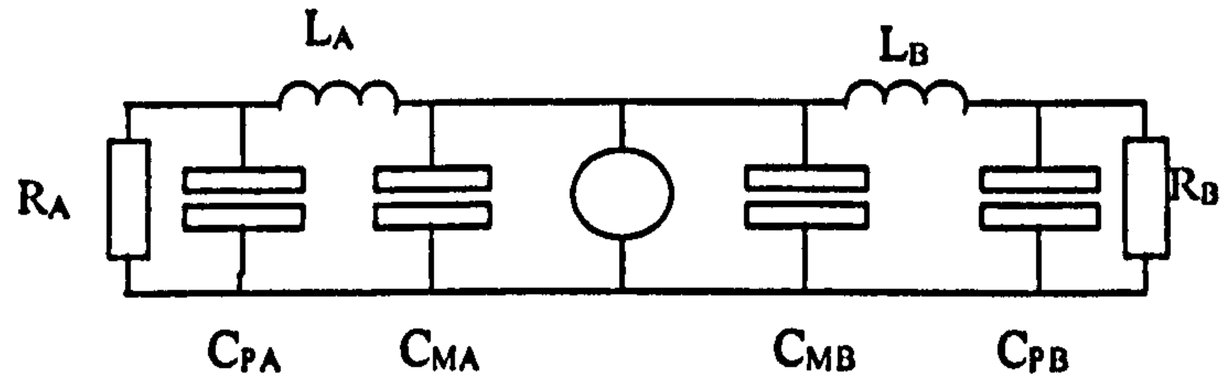

Figure 3-1. Extension of 3rd order Lumped Parameter model for dual Channel PPG.

It is obvious from Figure 3-1 that the lumped constant model has been simply duplicated for both sites *A* and *B*, but employing a common source. Earlier, decomposition of the peripheral model elements was discussed, concluding that the peripheral elements of the model are a parallel summation of the elements throughout the body. This model begins to isolate the peripheral elements of the body in a simplistic manner – now there are two locations in the model where the peripheral resistance *of that area* may be determined, and is a closer approximation to the initial question regarding skin haemodynamic resistance.

Depending on the two sites, diagnostic information on the vascular health of the patient may be revealed. The model developed in chapter two produces vascular parameters, normalised with respect to peripheral resistance R_P. Ratiometric evaluations of the normalised parameters, obtained from curve fitting as discussed in chapter two, will express comparative physiology. The expected ratiometric results are strongly influenced by the dual-channel probe placement sites, and fall into two broad categories – symmetric testing, where the parameters are expected to be equal, and asymmetric testing, where they are not.

3.2.1 Symmetric Comparison

This methodology assumes symmetry between all physiological components. Any ratios constructed between similar parameters should be approximately unity for healthy subjects. If, for example, a subject has ratiometric peripheral compliance close to unity but ratiometric major compliance is not, this indicates reduced compliance of the large arteries in one site. This could be confirmed by examining inertance for both sites, since inertance between sites should be similar; using a table of typical inertance values for given probe placement

locations, as discussed in chapter two. From this, ratiometric determination of peripheral resistance could be performed.

One example of symmetric analysis would be comparative testing using index finger PPG probes, in order to investigate vascular changes which may have occurred as a result of adaptation due to exercise – this will be discussed in chapter five.

3.2.2 Asymmetric Comparison

Here, differing probe placement sites would result in lumped parameter model fit solutions that are markedly different. Any ratios created using the dual channel methodology would be expected to be non-unity, since subject anatomy is dissimilar between sites. To determine the limits of difference between the two measuring sites, comparative statistical analysis would need to be performed on population groups in order to determine known healthy values and deviation due to pathology, correlated with known technologies, such as ABPI, duplex ultrasound etc.

Again, typical inertance, based on suitable population groups for differing probe placement sites, could provide an insight into peripheral resistance ratio, even though the inertance is dissimilar between sites.

One example of asymmetric testing would be comparative testing using finger and toe PPG probes on order to investigate vascular abnormalities – this will be discussed in chapter five.

3.3 Lumped Constant Inverse Model

In chapter two, it was argued that the shape of the PPG waveform is proportional to the transmural arterial pulse pressure waveform. A forward model based on lumped arterial parameters related the mechanical and physical properties of the connective vasculature to the shape of the arterial pressure waveform. As described, the same forward model can be applied to PPG waveform; the coefficients of the diastolic solution were obtained using a numerical fit of the wave shape.

Numerical fits have been criticised[6] for producing false minima, where error convergence occurs on physiologically unrealisable parameters; additionally, some literature[7] suggests the numerical fit approach to physiological systems has an infinite number of solutions, thereby the numerical solution found cannot necessarily be assumed to be the correct solution.

An alternative approach would be to develop an inverse model that could be applied directly to the arterial PPG waveform, giving haemodynamic parameters for the subject's arterial vasculature. This approach may have the added benefit that low cost technology could be

employed to provide insight into the physiological system. Low cost technology is the key to establishing the lumped parameter model in primary healthcare settings, where an inexpensive handheld unit could obtain a PPG waveform and perform an arterial vasculature diagnosis by using the inverse model, rather than the numerical fit.

3.3.1 Diastole Pulse Contour Gradient Analysis

The 3rd order model of circulatory systems was developed in chapter two, the time solution for the diastolic portion of the pressure curve which was developed is shown in equation [3.4] below.

$$P(t) = a_1 + a_2 \exp(-a_3 t) + a_4 \exp(-a_5 t)\cos(a_6 t - a_7) \qquad [3.4]$$

By performing a multi-parameter numerical fit of the diastolic portion of an arterial pressure waveform using equation [3.4], normalised lumped parameter values may be determined by using the a_i values determined in the fit.

An inverse model will be developed, which does not rely on numerical fits, allowing determination of the lumped parameter values by analysis of the arterial diastolic pressure waveform. In order to derive an inverse model, we must re-examine the characteristics of a typical pressure waveform. A representative diastolic arterial pressure waveform is shown in Figure 3-2 was derived from the literature[8] using the forward model parameters shown in Table 3-1, as plotted using equation [3.4] assuming an offset a_0 of zero. The time axis is shown to the value at which the function is no longer monotonically decreasing. The analytic derivative of the waveform is also shown, along with significant points of the derivative, expressed in terms of $(a_6 t - a_7)$, to be discussed later.

Essentially, development of the inverse model requires identification of two significant features, such as peaks or troughs, of the gradient pressure waveform in order to determine a time interval Δt, shown in Figure 3-2. These two significant points, which are related to specific terms of the expression for the gradient waveform, have a corresponding relation to the pressure waveform, and the timing interval Δt between the two points can be determined. The identification of these two features from a typical pressure waveform allows the derivation of an analytic expression for these key points in terms of the a_i parameters of the forward model solution. The time interval expression may then be factored in terms of the lumped parameter coefficients, to express the timing interval in terms of the forward model parameters.

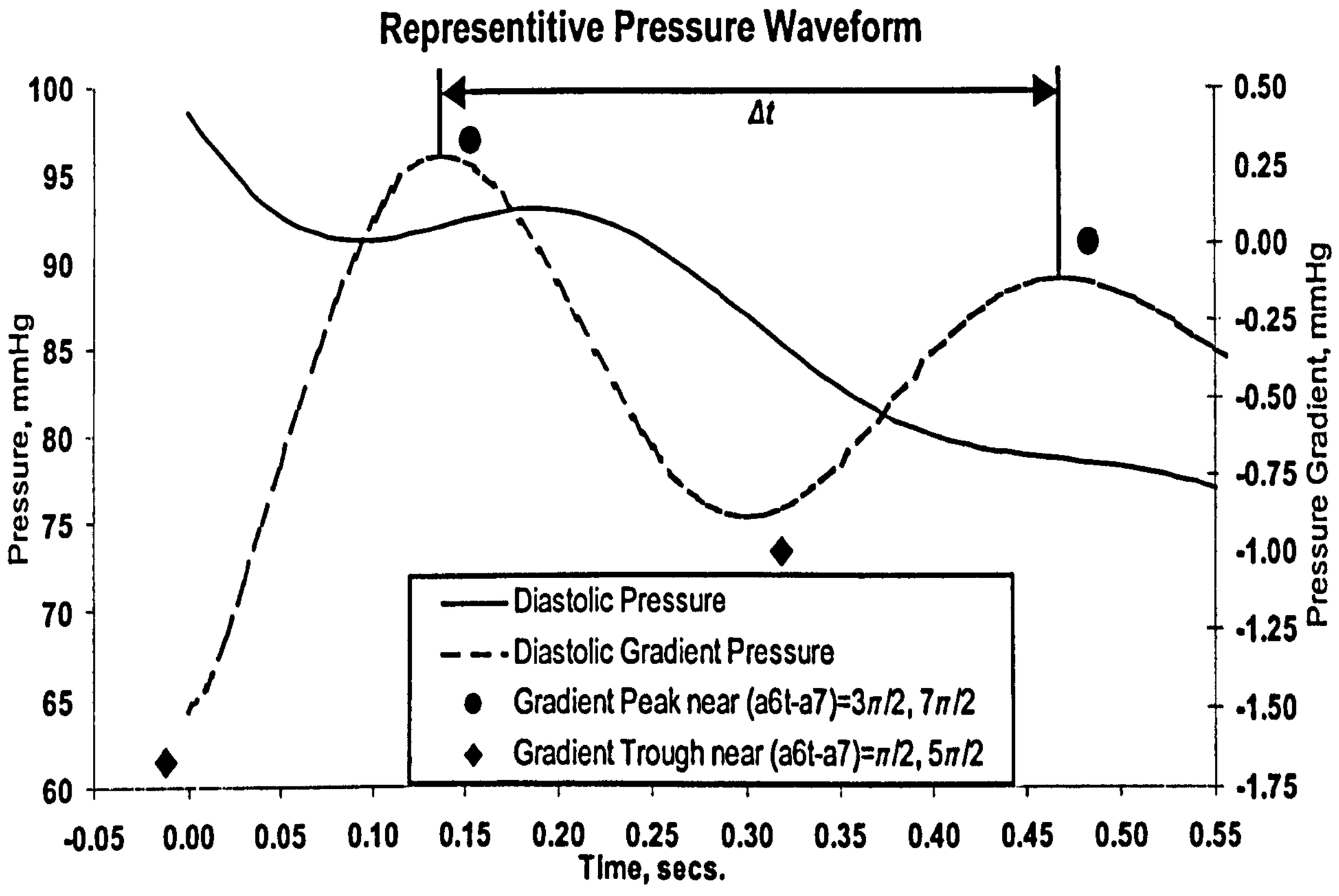

Figure 3-2. Representative Pressure waveform and derivative, shown with gradient turning points. Note *t = 0* represents end of systole.

Parameter	Units	Value
a_2	*mmHg*	100
a_3	s^{-1}	0.5
a_4	*mmHg*	6
a_5	s^{-1}	3
a_6	$Rad.s^{-1}$	19
a_7	*Rad*	-1.8
$C_M R_P$	*s*	1.86
$C_P R_P$	*s*	0.15
L/R_P	*s*	0.02

Table 3-1. Representative coefficients for lumped parameter model, taken from Watt and Burrus[8].

Numerical analysis of a real gradient pressure waveform can reproduce the timing interval using simple signal processing techniques (such as differentiation and peak detection), which can be equated to the expression containing the lumped parameters developed above. shows the gradient and pressure waveforms, annotating the peaks and troughs of the pressure gradient waveform.

3.3.2 Development of an Inverse Model

Development of the inverse model here will concentrate specifically on gradient turning points as the two significant points for which the timing interval is found; although the methodology is not specifically limited to turning points. These waveform turning points may be attributed to the oscillatory components of the expression for the gradient waveform; identification of these components is significant, as will be explained.

Taking two such significant turning points allows a time difference to be formed, the expression for which will be in terms of the a_i parameters of the forward model. This expression may then be factored in terms of the lumped parameters, using the equations developed in chapter two, giving the timing interval expression containing inertance L, major compliance C_M and peripheral compliance C_P.

The significant points for which the timing interval Δt will be derived are both arbitrarily chosen as gradient peaks, as already stated, purely because this results in a more compact expression for the timing interval. The general gradient methodology is in no way restricted to the gradient peak significant points, as will be discussed in the conclusion, but are simply taken for convenience.

The general form of the inverse model is first derived by linearising the gradient waveform about the two significant points of interest. The linearisation process introduces a timing offset τ that is small (a perturbation), being the difference between the *actual* location of the significant point and the *approximate* value of the significant point, as illustrated in Figure 3-3. The expression for the actual location of the significant points of interest will then simply be the approximate timing point determined by inspection plus the linearisation offset τ, the expression for which will be developed.

An analytic expression for the diastolic portion of pressure gradient waveform is given in equation [3.5], in terms of coefficients for the diastolic forward model solution.

[3.5]
$$F(t)=\frac{dP}{dt}=\begin{aligned}&-a_2a_3\exp(-a_3t)\\&-a_4a_5\exp(-a_5t)\cos(a_6t-a_7)\\&-a_4\exp(-a_5t)\sin(a_6t-a_7)a_6\end{aligned}$$

If this expression is plotted, using the representative a_i constants mentioned above and shown in Figure 3-3, then by inspection, gradient peaks will occur close to $(a_6t_{0,1}-a_7)=\frac{3\pi}{2},\frac{7\pi}{2}$, since this is the location of the turning point *maxima* of the gradient.

The location in time of the gradient peaks will be termed t_0 and t_1 respectively.

In order to determine the exact location in time of the gradient peaks, and hence the interval Δt between them, a Maclaurin[9] expansion of the gradient function, equation [3.5], around $t_{0,1}$ (where the gradient peaks occur) will be defined as F_E and is shown in equation [3.6]. The Maclaurin expansion will only be considered to second order, since a quadratic form of the expansion is assumed - this assumption is proved by observation of the derivative waveform at the peaks.

[3.6]
$$F_E(t_{0,1}+\tau)=F(t_{0,1})+\tau\frac{dF(t_{0,1})}{dt}+\tau^2\frac{dF^2(t_{0,1})}{d^2t}=F(t_{0,1})+\tau\dot{F}(t_{0,1})+\tau^2\ddot{F}(t_{0,1})$$

The linear expansion of the gradient waveform presented in equation [3.6] requires the first and second derivatives (with respect to time) of the gradient waveform, represented in equation [3.6] by $\dot{F}$ and $\ddot{F}$ respectively, and shown in equation [3.7] and [3.8] respectively.

[3.7]
$$\dot{F}(t)=\begin{aligned}&a_2a_3^2\exp(-a_3t)+a_4a_5^2\exp(-a_5t)\cos(a_6t-a_7)\\&+2a_4a_5\exp(-a_5t)\sin(a_6t-a_7)a_6\\&-a_4\exp(-a_5t)\cos(a_6t-a_7)a_6^2\end{aligned}$$

[3.8]
$$\ddot{F}(t)=\begin{aligned}&-a_2a_3^3\exp(-a_3t)-a_4a_5^3\exp(-a_5t)\cos(a_6t-a_7)\\&-3a_4a_5^2\exp(-a_5t)\sin(a_6t-a_7)a_6\\&+3a_4a_5\exp(-a_5t)\cos(a_6t-a_7)a_6^2\\&+a_4\exp(-a_5t)\sin(a_6t-a_7)a_6^3\end{aligned}$$

Before substituting the gradient function equation [3.5] and the differentiated gradient equations [3.7] and [3.8] into the expanded linearised equation [3.6], certain simplifications can be performed.

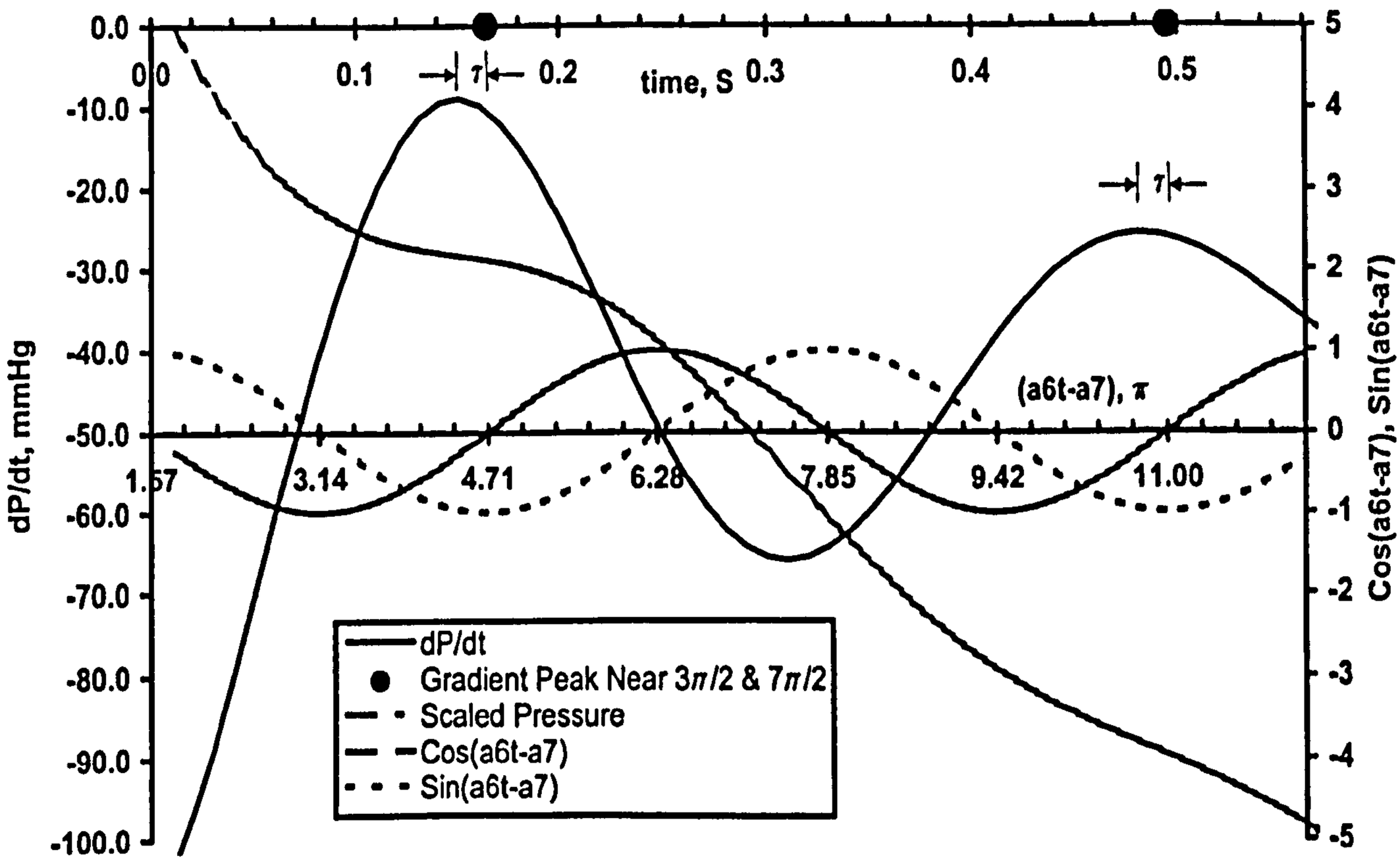

Figure 3-3. Gradient Pressure waveform, with horizontal axis in both seconds (since end of systole) and in terms of $(a_6t\text{-}a_7)$, with units of π. The pressure waveform is shown for reference, arbitrarily scaled. Sine and Cosine components of the gradient are also shown, together with locations of gradient peaks.

At $t_{0,1}$ where $(a_6 t_{0,1} - a_7) = \frac{3\pi}{2}, \frac{7\pi}{2}$, the various waveform oscillatory components are seen to be $\sin(a_6 t_{0,1} - a_7) = -1$ and $\cos(a_6 t_{0,1} - a_7) = 0$, simplifying the forms for the gradient waveforms and derivatives of the gradient waveform. This may be confirmed by inspection of both the $\cos(a_6 t - a_7)$ and $\sin(a_6 t - a_7)$ plots shown in Figure 3-3. Since the linearisation will only be valid around $t_{0,1}$, the general equations [3.5], [3.7] and [3.8] may be simplified in order to form expressions only valid around $t_{0,1}$. The notation reflects the simplified form of the expressions, shown in equations [3.9], [3.10] and [3.11] below, which are only valid around $t_{0,1}$.

[3.9] $$F(t_{0,1}) = -a_2 a_3 \exp(-a_3 t_{0,1}) + a_4 a_5 a_6 \exp(-a_5 t_{0,1})$$

[3.10] $$\dot{F}(t_{0,1}) = a_2 a_3^{\,2} \exp(-a_3 t_{0,1}) - 2 a_4 a_5 a_6 \exp(-a_5 t_{0,1})$$

[3.11] $$\ddot{F}(t_{0,1}) = -a_2 a_3^{\,3} \exp(-a_3 t_{0,1}) + 3 a_4 a_5^{\,2} a_6 \exp(-a_5 t_{0,1}) - a_4 a_6^{\,3} \exp(-a_5 t_{0,1})$$

The Maclaurin expansion F_E presented in equation [3.6] may now be completed using the simplified functions forms for the gradient and gradient derivatives developed above, the resultant expression shown in equation [3.12] below.

$$[3.12] \qquad Fe(t_{0,1}+\tau) = \begin{array}{r} -a_2a_3\exp(-a_3t_{0,1})+a_4a_6\exp(-a_5t_{0,1}) \\ +\tau\left(a_2a_3^{\,2}\exp(-a_3t_{0,1})-2a_4a_5a_6\exp(-a_5t_{0,1})\right) \\ +\tau^2\left[-a_2a_3^{\,2}\exp(-a_3t_{0,1})+a_4a_6\exp(-a_5t_{0,1})\left(3a_5^{\,2}-a_6^{\,2}\right)\right] \end{array}$$

Equation [3.12] above expresses the gradient waveform about time $t_{0,1}$ plus the small offset τ discussed above. In order to determine the offset τ, the differential of the expanded gradient waveform is needed. The differential of the gradient waveform equates to zero at the gradient peak turning points selected (in actual fact any turning point), which can result in an expression for the timing offset τ. Differentiating equation [3.12] with respect to τ gives an expression for turning points, and is shown in equation [3.13].

$$[3.13] \qquad \dot{F}_E(t_{0,1}) = \frac{dF_E(t_{0,1}+\tau)}{d\tau} = \dot{F}(t_{0,1})+2\tau\ddot{F}(t_{0,1})$$

As stated, equating equation [3.13] to zero and solving for τ gives an expression for the offset $\tau_{0,1}$ at times $t_{0,1}$, shown in equation [3.14].

$$[3.14] \qquad \tau_{0,1} = \frac{-\dot{F}(t_{0,1})}{2\ddot{F}(t_{0,1})} = \frac{-\left[a_2a_3^{\,2}\exp(-a_3t_{0,1})-2a_4a_5a_6\exp(-a_5t_{0,1})\right]}{2\left[-a_2a_3^{\,3}\exp(-a_3t_{0,1})+3a_4a_5^{\,2}a_6\exp(-a_5t_{0,1})-a_4a_6^{\,3}\exp(-a_5t_{0,1})\right]}$$

With an analytic expression for timing offset τ being determined, the gradient peaks were defined at $(t_0+\tau_0)$ and $(t_1+\tau_1)$. The timing interval Δt may now be defined in terms of $t_{0,1}$ and $\tau_{0,1}$, as shown in equation [3.15] below.

$$[3.15] \qquad \Delta t = (t_1+\tau_1)-(t_0+\tau_0) = 2\pi/a_6+\tau_1-\tau_0$$

Equation [3.15] above gives a concise analytic expression for the timing interval Δt based on the parameters of the forward model, equation [3.4], using the timing offset τ developed from linearisation, using gradient peaks as the significant events for the timing interval.

3.3.3 Effects of Scaling

The development of the pulse contour gradient technique allows inference of physiological parameters from the pressure pulse waveform – the example shown above is based on the selection of arbitrary points on the representative pressure waveform discussed previously. However, this technique will be applied to PPG, with relative magnitudes used for the forward model transient parameters a_2 and a_4 as shown in equation [3.4]. These parameters of the forward model are responsible for the relative scaling between the dominant decay and the decaying oscillatory component of the pressure waveform. Therefore, the timing interval Δt will be developed from the gradient of the arterial PPG waveform using identical methodology developed above for the pressure waveform. Analysis must be performed to ensure that the relative nature of PPG does not affect the gradient analysis technique when applied to arterial PPG, since the gradient analysis methodology was originally developed from pulse pressure waveforms. Manipulation of the timing offset τ of equation [3.14], in terms of the scaling parameters a_2 and a_4, will give an indication of the effects of changes in these parameters, as shown in equation [3.16].

[3.16]
$$\tau_{0,1} = \frac{a_2 P - a_4 Q}{a_2 R + a_4 S}, \qquad \begin{aligned} P &= a_3^{\,2} \exp(-a_3 t_{0,1}) \\ Q &= 2a_5 a_6 \exp(-a_5 t_{0,1}) \\ R &= 2a_3 P \\ S &= 2a_6 \exp(-a_5 t_{0,1})(a_6^{\,2} - 3a_5^{\,2}) \end{aligned}$$

Equation [3.16] illustrates that the forward model scaling coefficients a_2 and a_4 form a ratio; therefore, any scaling applied to these parameters (such as during PPG signal recovery and manipulation) will not affect the overall timing offset τ, therefore the timing interval Δt will remain unaffected. In the example above, the timing offset τ was developed using gradient peaks as described. However, it is probable that any linearisation using turning points as significant events will result in similar equations for the timing offset τ; with the expression forming a ratio of the forward model scaling parameters. All forms of the gradient analysis method using turning points for significant events are thus rendered insensitive to waveform scaling.

Parameters a_3, a_5, and a_6 are system-timing parameters that are unaffected by scaling of the arterial PPG waveform. Similarly, probe design becomes irrelevant as the probe coupling coefficient β, discussed in light and tissue interaction models, is immaterial in this methodology.

3.3.4 The Inverse Model in terms of Lumped Coefficients

Equation [3.15] above gave an expression in terms of the timing offset τ in order to determine the timing interval Δt. To express the timing interval Δt in terms of the lumped parameter coefficients, the timing offset τ must be factored in terms of the coefficients. To ease this process, elimination of any exponential terms in equation [3.14] would be desirable. Again, a Maclaurin expansion of the exponential terms could be used, truncating to second order as before. Collecting like terms in t, would give a quadratic expression for the timing offset τ of the form shown in equation [3.17].

[3.17] $$\tau_{0,1} = Pt^2 + Qt + R$$

Equation [3.17] shows the timing offset could be determined by a quadratic equation in t at the significant points discussed, taken as gradient peak turning points. The coefficients P, Q and R could be factored in terms of either the exact or approximate equations for the normalised Lumped parameters developed in chapter two.

3.3.5 Sensitivity Analysis of the Inverse Model

In order to determine the sensitivity of the timing interval to the system parameters, typical forward model parameters from published literature[8] must be considered, for both normal and hypertensive subjects. The forward model average a_i parameters, along with the derived lumped parameters and the timing interval using the gradient peak methodology described above, are presented in Table 3-2.

Table 3-2 lists the normalised lumped parameter values and percentage changes between the lumped parameter compliances and inertance between normotensive and hypertensive subject, and additionally the timing interval Δt developed above. An additional column is present, termed 'middletensive', which represents the average values between the normotensive and hypertensive groups. The middletensive group will be used during sensitivity analysis later.

Parameter	Units	Normotensive	Hypertensive	Middletensive
a_2	$mmHg$	103.36	155.63	129.5
a_3	s^{-1}	0.55	0.61	0.58
a_4	$mmHg$	13.12	13.48	13.3
a_5	s^{-1}	3.95	17.17	10.56
a_6	$Rad\ s^{-1}$	19.17	44.57	31.87
a_7	Rad	-1.44	0.04	-0.7
$C_M R_P$	s	1.7205	1.6258	1.6868
$C_M R_P$ Change	%	5.8		
$C_P R_P$	s	0.1183	0.0286	0.0461
$C_P R_P$ Change	%	313.6		
L/R_P	s	0.0233	0.0154	0.0196
L/R_P Change	%	51.3		
Δt	s	0.3285	0.1434	0.1988
Δt Change	%	129.1		

Table 3-2. Normotensive, Hypertensive and average critical parameters, from Watt and Burrus[8].

Examination of Table 3-2 shows a significant change in timing interval Δt between normotensive and hypertensive subjects, and a significant change in normalised peripheral compliance between the two groups. Interpolating between the limits presented in Table 3-2 gives a spread of system a_i values, allowing a progressive evaluation of changes in the lumped parameters. The normalised lumped parameter compliance ($C_M R_P$ and $C_P R_P$) and inertance (L/R_P) can also be determined from the interpolated spread, along with the associated timing interval Δt.

Figure 3-4 shows a plot of the pressure curve using the values presented in Table 3-2, with eight intermediary interpolated pressure curves, with the key giving details of the associated timing interval. It is obvious that both the location in time and the width of the dichrotic notch changes, with the hypertensive curve possessing a narrower dichrotic section, thereby reduced timing interval Δt.

The interpolated starting pressure a_2 can be plotted against timing interval Δt, shown in Figure 3-5, illustrating how the timing interval varies with arterial pressure - which could be equated to Δt against pulse pressure. Figure 3-5 also shows how the timing interval varies with normalised peripheral compliance. From this plot, the timing interval can be seen to

decrease with increased starting pressure, drawing a correlation between blood pressure and timing interval. The increased starting pressure also relates to a reduced normalised peripheral compliance as determined by numerical fitting, which is a reasonable conclusion to draw from hypertensive subjects, as discussed in chapter one. More importantly, the timing interval shows an increased value with increased normalised peripheral compliance, which correlates timing interval and peripheral compliance. These results illustrate how the timing interval alone can be used in assessing both normalised peripheral compliance and hypertensivity in a subject, without resorting to pressure cuffs or invasive procedures.

As briefly stated, Table 3-2 also shows as intermediary '*middletensive*' parameters set, derived from the mean of the normotensive and hypertensive forward model parameters, in order to illustrate the effects of changes in individual forward model a_i parameters on any derived parameters. The effects on timing interval Δt and lumped parameters will be investigated using the middletensive values as initial starting points.

Using the derived mean values for the a_i parameters, the individual parameters a_3, a_5 and a_6 were altered between limits in an attempt to determine the effects of changes in these parameters on the timing interval and the lumped parameter values. While it is appreciated that individual parameter changes just described are very unlikely to occur in real physiology (since changes to the whole parameter set are more probable between patients) individual changes aid understanding of how the various forward model a_i parameters affect the timing interval Δt.

Compilation of these results are shown in Table 3-3, with an '=' sign indicating no change from the middletensive value; additionally, a_i values not shown are identical to the derived middletensive values originally presented in Table 3-2.

Table 3-3 shows that in the context of these single forward model parameter changes, the timing interval Δt is most sensitive to the oscillatory frequency a_6 of the a_i parameter set, producing a very significant change of over 400%. Relating this change in a_6 to the lumped parameters of the model, the system parameter most sensitive to changes in a_6 and thus the timing interval is the lumped inertance, but the change in lumped inertance between subject groups was also significant at over 300%.

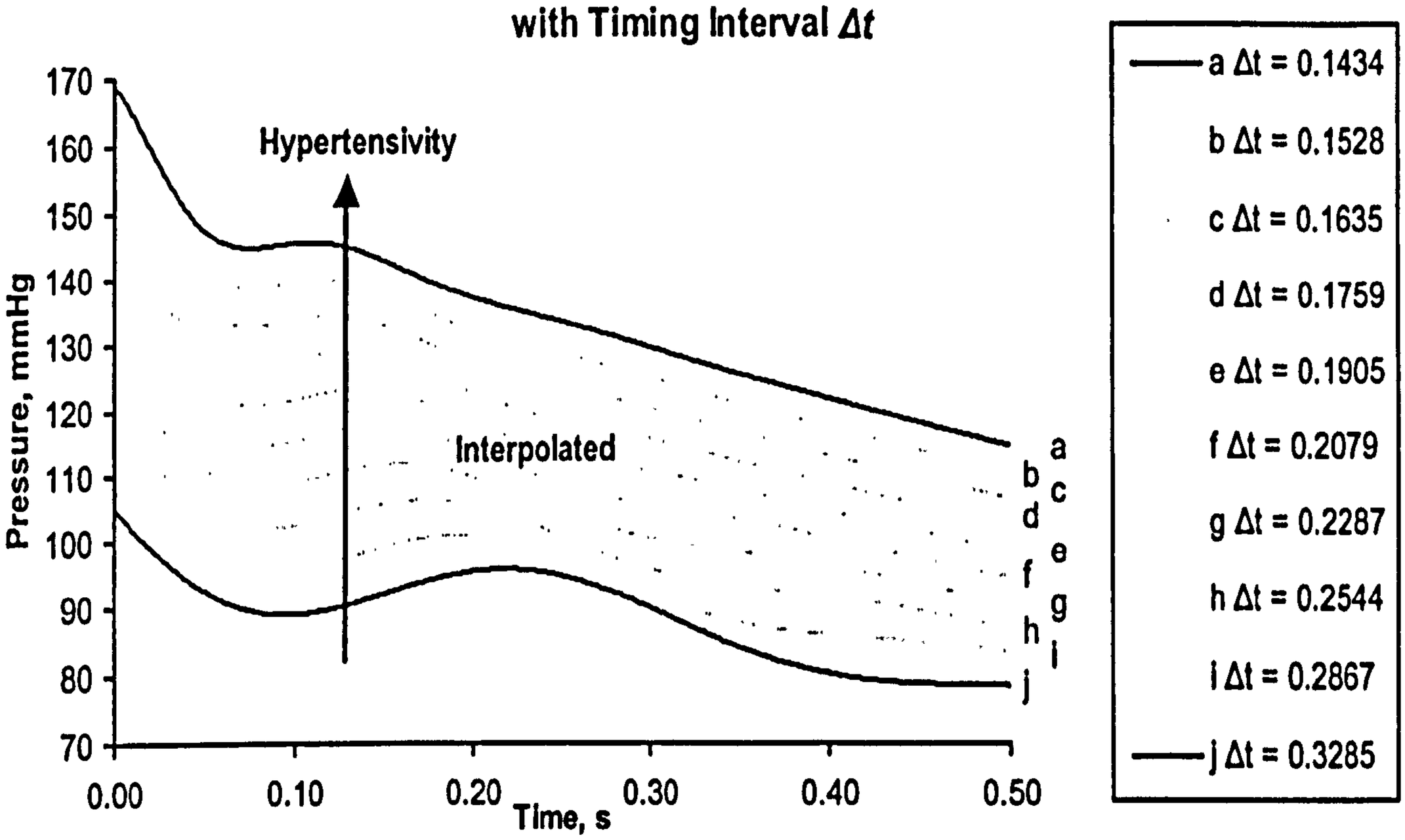

Figure 3-4. Interpolated pressure curve for normotensive and hypertensive subjects, showing associated timing interval.

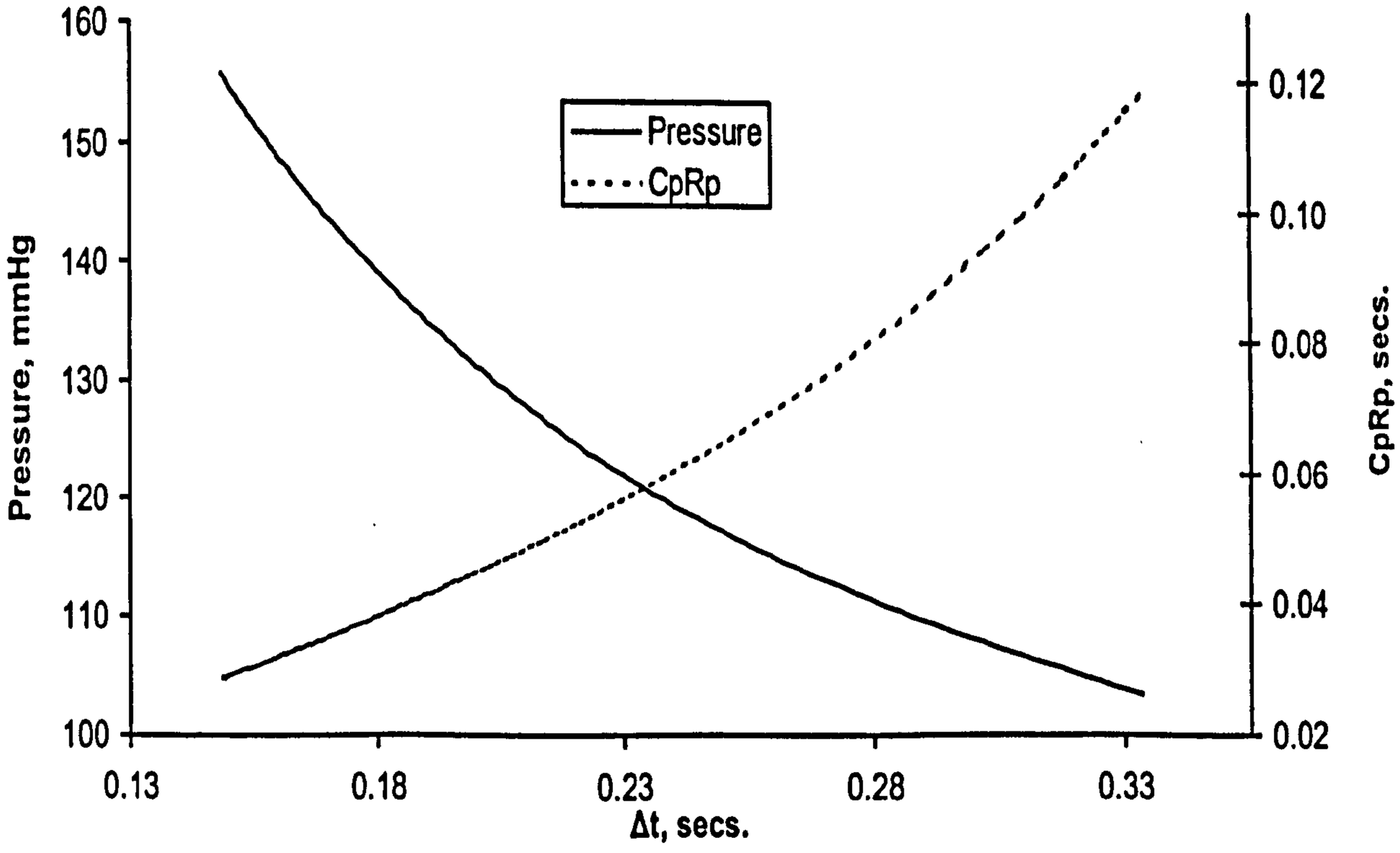

Figure 3-5. Timing interval and pressure/peripheral compliance for interpolated values.

Parameter	a_3 Low	a_3 High	a_5 Low	a_5 High	a_6 Low	a_6 High	a_7 Low	A_7 *High*
$a_3 s^{-1}$	0.55	0.61	=	=	=	=	=	=
$\Delta a_3\%$	10.9		0		0		0	
$a_5 s^{-1}$	=	=	3.95	17.17	=	=	=	=
$\Delta a_5\%$	0		334.6		0		0	
$a_6 s^{-1}$	=	=	=	=	19.17	44.57	=	=
$\Delta a_6\%$	0		0		132.5		0	
$a_7, rad\, s^{-1}$	=	=	=	=	=	=	-1.44	0.04
$C_M R_P S$	1.7908	1.6121	1.6139	1.7217	1.7221	1.6881	=	=
$\Delta C_M R_P\%$	11.1		6.7		2		0	
$C_P R_P S$	=	0.0460	0.1179	0.0286	=	=	=	=
$\Delta C_P R_P\%$	0.2		312		0		0	
$L/R_P S$	0.0195	=	0.0088	0.0267	0.0454	0.0106	=	=
$\Delta L/R_P\%$	0.5		203		328		0	
$\Delta t\, S$	0.1987	0.1990	0.1972	0.2809	0.7611	0.1411	0.1985	0.1992
$\Delta \Delta t\%$	0.2		42.4		439		0.3	

Table 3-3. Changes in lumped constant parameters with associated changes in forward model parameters and timing interval. An '=' indicates no change from the 'Middletensive' value.

The timing interval is appreciably sensitive to changes in a_5, which determines the rate of oscillatory decay, with a change of over 40%. The lumped parameter most sensitive to a_5 is the normalised peripheral compliance, which is especially of interest in hypertensive and other cases where peripheral diagnosis is of concern. The timing interval is insensitive to changes in the dominant decay constant a_3, which mainly affects lumped normalised major compliance, with a change of only 0.2% for an approximately 11% change in normalised major compliance. Table 3-3 also shows the timing interval is practically insensitive to

changes in the phase component over the phase range specified. This is significant as the phase drastically affects the shape of the pressure curve – illustrating that the gradient peaks timing interval is unaffected by changes in the location of the dichrotic peak.

To monitor relative changes in lumped parameters against changes in timing interval, normalisation of the percentage changes presented in Table 3-3 is required. By forming a ratio of the lumped parameter as percentage change divided by percentage change in timing interval Δt, a normalised sensitivity S can be determined.

	Δa_3	Δa_5	Δa_6
$\partial \Delta t$ %	0.2	42.4	439.4
$\partial C_M R_P$ %	11.1	6.7	2
$\partial C_P R_P$ %	0.2	312.2	0
$\partial L/R_P$ %	0.5	203.4	328.3
$S\ C_M R_P / \Delta t$	55.5	0.2	0.01
$S\ C_P R_P / \Delta t$	1	7.4	0
$S\ L/R_P / \Delta t$	2.5	4.8	0.75

Table 3-4. Sensitivity analysis for hypothetical limits of forward model parameters.

Table 3-4 shows in column format the required percentage change required in any of the lumped parameters to produce a one percent change in the timing interval Δt. Table 3-4 must be interpreted with care otherwise false conclusions can be drawn. For example, when the dominant decay parameter a_3 is changed by almost 11%, as was performed in these tests, then a 55.5% change in the major compliance produces a 1% change in the timing interval Δt. In the same way, a 1% change in normalised peripheral compliance produces a 1% change in the timing interval.

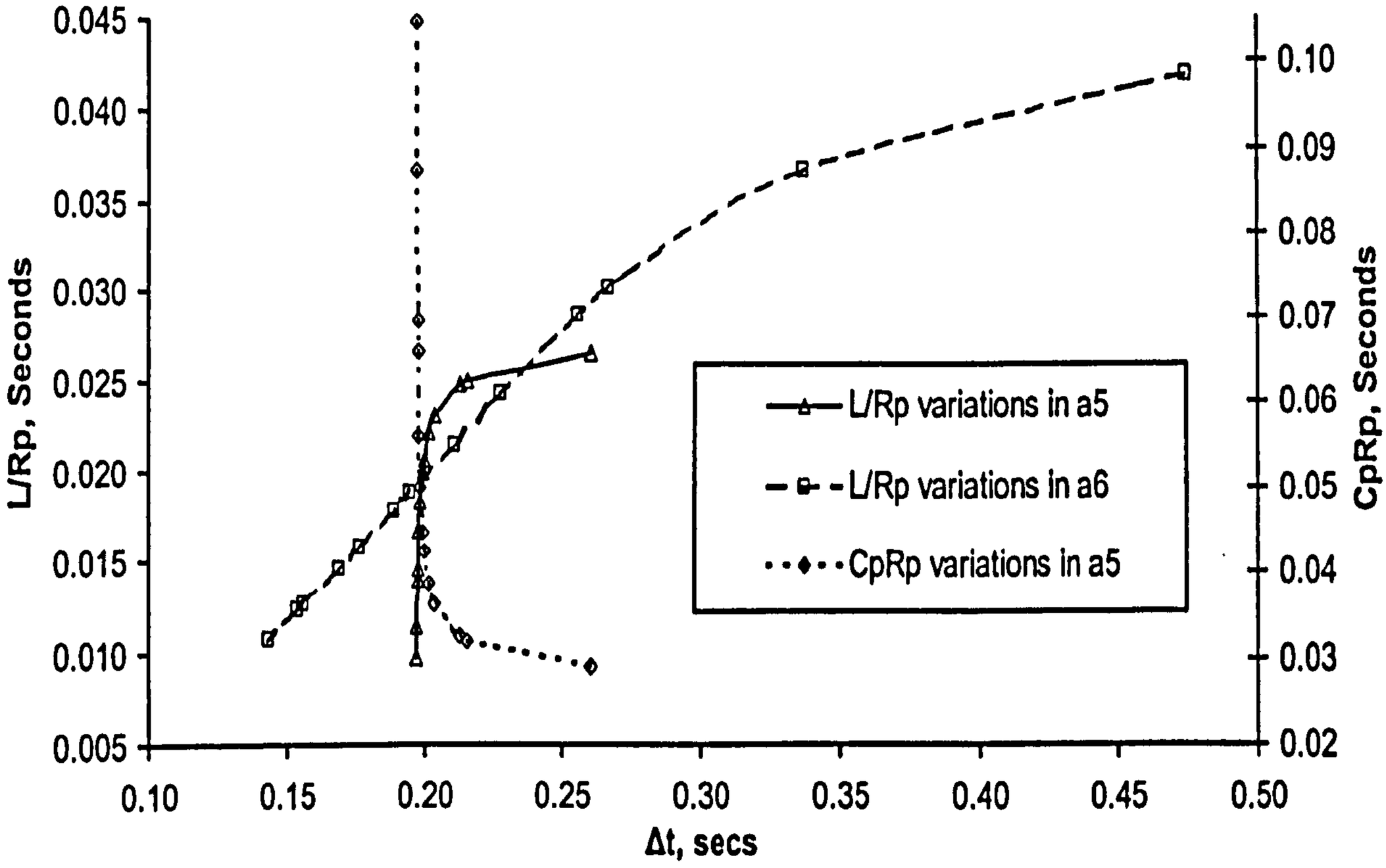

Figure 3-6. System parameter changes with variations on timing interval. Hypertensive subjects have shorter timing interval.

One could assume that the timing interval was more sensitive to changes in normalised peripheral compliance when the parameter a_3 is varied, which it indeed is. However, Table 3-3 shows that normalised major compliance is most sensitive to changes in a_3, indicating therefore that although the normalised peripheral compliance and inertance show greater sensitivity than normalised major compliance to producing a corresponding change in timing interval, these parameters are not significantly altered by changes in a_3.

In order to clarify the lumped parameter most sensitive to changes in the corresponding forward model a_i parameter, Table 3-4 is highlighted to indicate the appropriate lumped constant, confirming the initial observations made above regarding sensitivity.

In order to observe the spread of changes in isolated forward model parameters generated by the interpolation between the hypertensive and normotensive limits described above, any significant lumped parameter and timing interval changes were plotted, shown in Figure 3-6, remembering in this case that shorter timing intervals represent hypertensive subjects, longer timing intervals represent normotensive subjects.

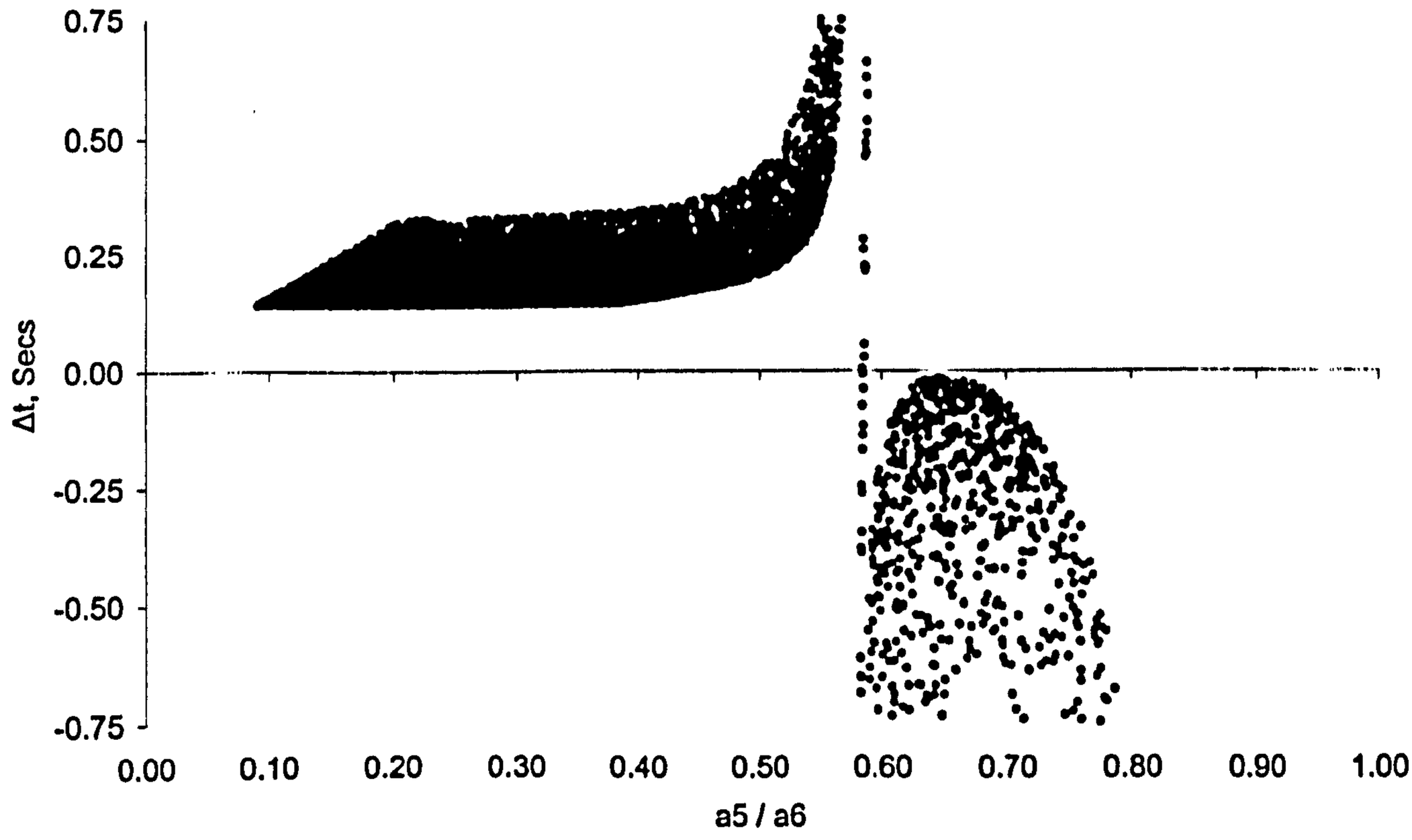

Figure 3-7. Plot of random changes in a_5 and a_6 versus timing interval.

Figure 3-6 further reinforces the observation that the timing interval is most sensitive to the frequency of oscillation a_6. Timing interval changes of approximately 25% are also shown, with corresponding changes in normalised inertance and peripheral compliance. These plots illustrate the dangers of arbitrarily changing isolated forward model parameters; the resultant lumped parameters derived from the synthetic a_i parameters being highly non-linear.

To investigate the limits of isolated changes in forward model parameters on the timing interval Δt, a random test was performed. Here, both the oscillatory decay constant a_5 and the oscillatory frequency a_6 were varied randomly between the normotensive and hypertensive limits establish in Table 3-2. The remaining forward models parameters were fixed at the intermediary middletensive value defined above. A plot of ten thousand random changes in a_5 and a_6 along with the resultant timing interval was generated, shown in Figure 3-7.

Examination of Figure 3-7 shows a discontinuity exists for forward model values where the oscillatory decay a_5 is greater than approximately 55% of the oscillatory frequency a_6. However, since this corresponds to an associated timing interval of more than 0.5 seconds, this discontinuity can be ignored as timing interval values greater than 0.5 seconds will be rare.

3.4 Dual Channel Lumped Constant Inverse Model

Section 3.3 began with the development of an inverse model, based on the forward model solution of a lumped constant pressure model developed in chapter two. This model will be expanded for application in dual channel PPG.

The methodology of performing ratiometric assessment for the two distal sites, *A* and *B*, was first developed in section 3.1.1. This same technique can be applied to the timing interval, developed above, obtained from the two distal sites. A general form of this technique is shown in equation [3.18] below, where the timing interval is developed according to Equation [3.15] above.

[3.18] $$\hat{R} = \frac{\Delta t_A}{\Delta t_B}$$

As discussed previously in section 3.2, comparative evaluation between sites may be performed with this metric. Again, evaluation of this ratio will depend upon whether symmetric or asymmetric testing is performed. Ideally, an appropriate system could describe both ratiometric timing intervals and ratiometric compliances, which would illustrate any differences between the two sites.

3.4.1 Dual Channel Inverse Model Sensitivity Analysis

As before, the effects of changes in the forward model parameters on the timing interval and associated lumped parameters must be evaluated using a dual site, i.e. dual channel methodology. The use of two measuring sites, both employing the forward model presented in section 3.2, implies that two sets of a_i parameters will exist, resulting in two sets of results for major compliance, peripheral compliance, vascular inertance and timing interval.

As stated before, dual channel analysis falls into one of two subgroups: symmetric or asymmetric analysis. In the case of symmetric analysis, deviation between locations indicates changes in vascular parameters. The degree of change will indicate the severity of any underlying pathology.

Asymmetric comparisons will depend heavily on the two probe sites. In order to determine typical and atypical results, statistical analysis with known normal and diseased patients would be required. However, expected results can be simulated, with the corresponding effects on the timing interval observed.

3.4.1.1 Asymmetric Dual Channel Inverse Model Sensitivity Analysis

The hypothetical 'middletensive' values derived earlier will be used as a starting point for both distal locations in this simulation. When considering asymmetric testing, where the two probe locations are finger and toe, then speculative estimations for the lumped parameters can be made, and the forward model resultant a_i parameters determined. From these, timing intervals for any simulated pathology can be found.

In this simulation, it will be assumed that the finger probe will possess the 'middletensive' forward model a_i values described earlier. The toe will also use the 'middletensive' forward model a_i values described earlier, but these will be slightly modified to simulate the differing vasculature. The toe is assumed to possess a greater vascular length than the finger, which will therefore exert both an increased inertance and greater major compliance. Additionally, mild congestive effects will reduce the peripheral compliance slightly. Therefore, toe inertance and major compliance will be increased by approximately 50%, compared to the finger middletensive value, and peripheral compliance will be reduced to only 90% of the finger value. The approximate forms of the lumped parameter equations, developed in chapter two, allow simple modifications of the forward model a_i values to achieve the desired lumped values.

In order to represent a diseased vascular system (for example a diabetic patient with calcified arteries) an additional data set was constructed in the same manner where the major compliance was approximately 2/3 the finger value, the peripheral compliance was only approximately 50% of the finger value and again the inertance was increased by 50%.

These a_i parameters, with the associated lumped parameters and timing interval are shown in Table 3-5, again, middletensive values as shown in Table 3-2 are represented by an '=' sign, along with any unchanging values. The phase parameter a_7 was assigned the middletensive value for normal or near normal locations, and normotensive phase for the diseased leg.

Parameter	Units	Normal Arm	Normal Leg	Diseased leg
a_3	s^{-1}	0.58	0.3929	0.88
a_5	s^{-1}	10.56	12.06	21.7
a_6	$Rad\ s^{-1}$	31.87	27.19	33.31
a_7	Rad	-0.70	-0.70	-1.44
$C_M R_P$	s	1.6968	2.5316	1.1361
$C_M R_P$ Ratio	%	0	149.1	49.3
$C_P R_P$	s	0.0461	0.0408	0.0226
$C_P R_P$ Ratio	%	0	88.5	49
L/R_P	s	0.0196	0.0278	0.0279
L/R_P Ratio	%	0	141.8	142.3
Δt	s	0.1988	0.2382	0.0165
Δt Ratio	%	0	119.8	8.3

Table 3-5. Dual Channel Asymmetric hypothetical sensitivity analysis. Ratio values are toe parameter divided by finger parameter.

Table 3-5 illustrates the power of the dual channel approach. It is evident that the synthetic forward model parameters, derived above, produce significant ratio changes for relatively minor changes in pathology between normal and diseased subjects. Comparisons between the normal toe and finger timing interval ratio and the diseased toe and finger timing ratio illustrates this. Evaluating this technique for a large population group would allow statistical compilation of a database containing representative values for healthy and diseased subjects. These simulations have shown that the gradient peak timing interval is sensitive to the phase parameter a_7. Values of phase greater than 0.425π result in a negative timing interval when using the middletensive forward model a_1 parameter set. Analytically, this is due to the quadratic approximation giving a root less than zero on the time axis. The limits of changes in phase may be observed in Figure 3-8; with the phase set at the upper limit, the assumptions made regarding gradients peaks during inverse model development are invalid. Therefore, diseased leg simulation in Table 3-5 employs the normotensive phase value. Modifying several parameters simultaneously as in this simulation is a more accurate methodology compared to individual parameter changes as performed in section 3.3.5, but interpretation of synthetic results will never be as useful as real population analysis.

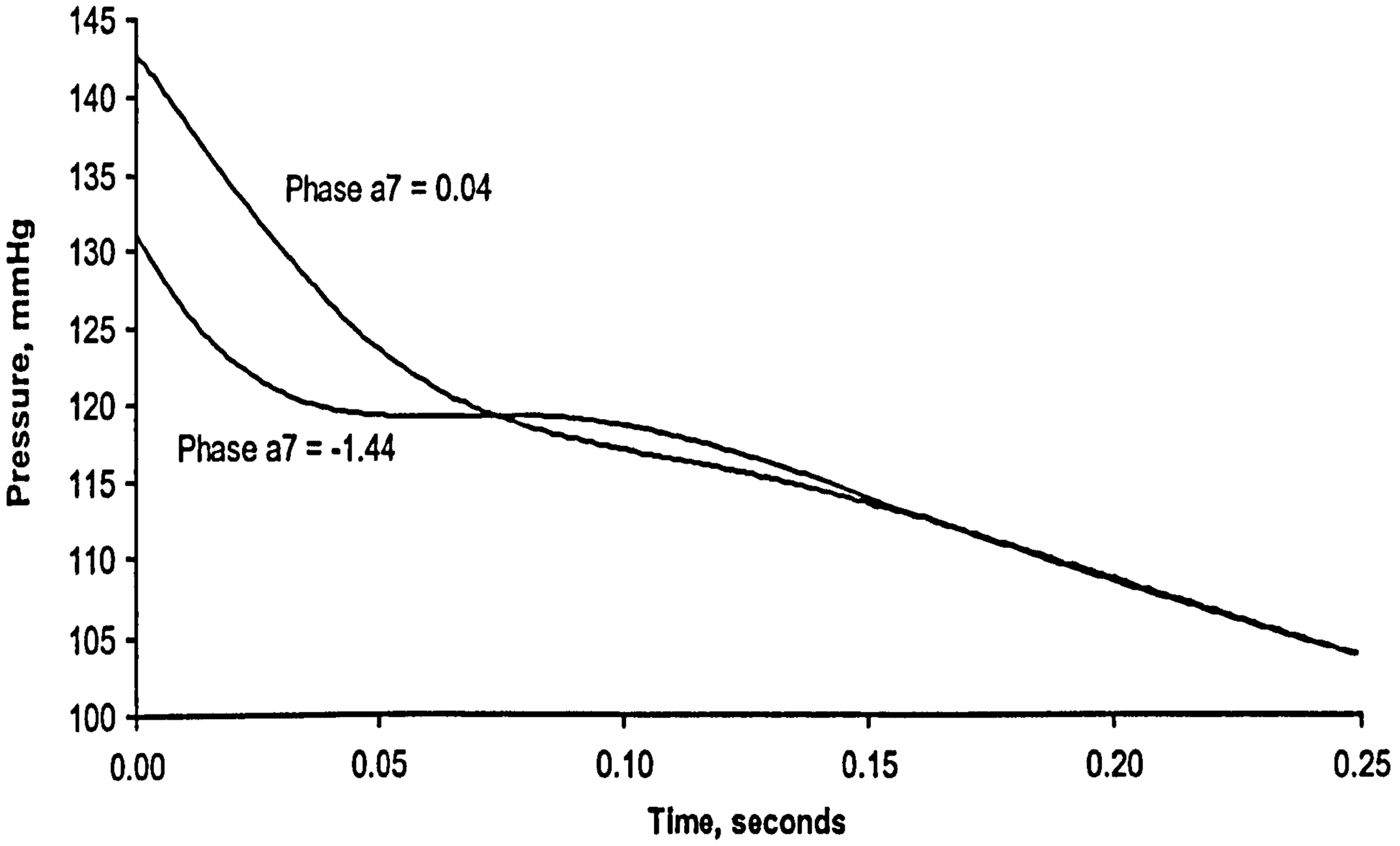

Figure 3-8. Limits of Phase for Simulated Diabetic Toe Pressure Curve.

3.4.1.2 Symmetric Dual Channel Inverse Model Sensitivity Analysis

Symmetric dual channel simulations are more difficult to perform since, by the very nature of the method, any results should be similar if not identical between sites. However, some circumstances can be envisaged where differences will occur between sites. These can be classified under pathology, where an abnormality is the cause of the non-identical parameters, or physiology, where temporary changes to the characteristics of the vasculature are made by the body in response to stimuli. This simulation will assume a typical physiological response to a cold stimulus, and thus peripheral circulatory shutdown.

Again, the 'middletensive' forward model parameters developed above will be used as the starting parameters. The middletensive forward model parameters will be changed in the same manner as changes were made for the asymmetric sensitivity analysis. In this case, peripheral resistance R_P will be increased by approximately 25% in the arm undergoing shutdown. The associated effects this has on both the individual normalised lumped parameters and parameter ratios will be investigated. These modified forward model parameters and derived lumped parameters are shown in Table 3-6; any parameters not shown are identical to the middletensive values.

Parameter	Units	Middletensive 'Normal' Site	Peripheral Shutdown Site
a_3	s^{-1}	0.58	0.47
a_5	s^{-1}	10.56	8.68
a_6	s^{-1}	31.87	33.31
$C_M R_P$	s	1.6968	2.0796
$C_M R_P$ Change	%	122.6	
$C_P R_P$	s	0.0461	0.0561
$C_P R_P$ Change	%	121.7	
L/R_P	s	0.0196	0.0154
L/R_P Change	%	78.6	
Δt	s	0.1988	0.1890
Δt Change	%	95.1	

Table 3-6. Symmetric sensitivity simulation parameters.

This simulation shows that increasing peripheral compliance affects all normalised lumped parameters, since normalisation is performed with respect to peripheral resistance. Table 3-6 shows that both normalised compliances increase and that normalised inertance decreases, as would be expected.

It was established earlier that this implementation of the timing interval is most sensitive to changes in normalised inertance, since inertance is related to the oscillatory frequency. This is obvious since the period of oscillation will have pronounced effects on the gradient peak timing interval. This simulation only provokes a small change in the timing interval Δt. However, the actual inertance will be approximately equal between the two sites so forming the ratio of normalised site inertances could allow determination of the actual peripheral resistance ratio between sites. This could then allow scaling of normalised compliances by the ratio of actual peripheral resistance, giving deeper insight into the lumped parameters of the forward model.

The small change in timing interval would indicate the lumped inertance and compliances have not changed significantly, therefore, the remaining parameter is peripheral resistance. This again illustrates the power of the dual channel methodology; by using a combination of the timing interval and dual channel ratio techniques, coupled with understanding of the

underlying physiology provides a powerful tool for non-invasive assessment of vascular physiology.

3.5 Conclusion

This chapter introduced the concept of both clinical and sport science based vascular assessment using arterial PPG, in order to determine information on subject physiology. Two alternative methods have been described for vascular assessment – perfusion monitoring, where the amplitude of the arterial PPG waveform is significant, but the shape is not, and the inverse model, where the shape of the arterial PPG waveform is significant, but the amplitude is not. These two contrasting methodologies were then expanded allowing simultaneous dual channel monitoring of subject vasculature.

Perfusion monitoring began with a RVC index. The problems associated with this perfusion monitoring procedure were discussed, with possible methodologies for overcoming its limitations (such as perfusion change monitoring) with single channel monitoring considered. The RVC index was extended to dual channel, creating the PVI methodology in order to perform comparative site testing using dual channel techniques. The PVI methodology has the advantages of allowing comparative evaluations between subjects, since model constants are eliminated when using identical equipment. To further extend and generalise perfusion monitoring, the RPVI methodology was introduced. This technique eliminates all constants and dependencies on equipment, since all model parameters are entirely eliminated, allowing perfusion comparisons with different probe designs and settings amongst different subjects.

The lumped parameter model developed in chapter two was extended to dual channel use, by again employing comparative site testing. The feasibility of comparative tests with the sensor located in differing as well as similar distal sites, providing both symmetric and asymmetric testing, has been demonstrated.

Additionally, an inverse model, based on a timing interval metric, was introduced, developed form the lumped parameter model. This technique analyses significant points on the PPG waveform to derive a timing interval measure which can be related to the lumped parameters. An implementation of the timing interval, using gradient peaks for the significant events, was developed and analysed. The timing interval methodology is completely insensitive to both probe design and coupling or any scaling effects associated with PPG signal processing.

Initial results obtained with the inverse model suggest it may be possible to determine a degree of hypertensivity using the timing interval on a single channel without actually determining SBP, as well as non-invasive observations of peripheral compliance.

The time interval inverse model may also be used to provide an insight into the connective vasculature without requiring a time consuming numerical fit, which the lumped parameter model requires. Simulations using hypothetical values have demonstrated the sensitivity of the timing interval to changes in subject physiology.

The timing interval inverse model was further developed for use with dual channel PPG to provide comparative testing between distal sites. Simulations of expected changes between physiologies were performed, with promising results, since the timing interval demonstrated increased sensitivity to pathology changes when using a dual channel approach.

The exact form of the timing interval inverse will require further investigation, to determine the optimum significant events for the actual interval. These may be related to physically observable phenomena, such as incissura or dichrotic notch peak, or may be arbitrary as was the case here. Once the optimum significant events have been determined, based on the desired lumped parameter sensitivity, the full form of the inverse model may be expressed, allowing factorisation of the timing interval in terms of the lumped model parameters.

3.6 Chapter References

[1] Tan Y.K., da Silva A.F., "Digital Photoplethysmography in the Diagnosis of Suspected Lower Limb DVT: Is It Useful?", Eur. J. Vasc. Endovasc. Surg., 18, pp.71-79 (1999)

[2] Sarin S, Shields D.A, Scurr J.H, Coleridge-Smith P.D, "Photoplethysmography: a valuable non-invasive tool in the assessment of venous dysfunction?", J. Vasc. Surg, 16:2, pp. 154-162 (1992)

[3] Aoyogi T, Kishi M, Yamaguchi K, Watanabe S, "Improvements of the Ear Piece Oximeter", Abstracts Jpn. Soc. Med. Electronics Biol. Engineer, pp. 90-91 (1974)

[4] Apelqvist J., Castenfors J., Larsson J., Strenstrom A., Agardh C.D., "Prognostic value of systolic ankle and toe blood pressure levels in outcome of diabetic foot ulcer", Diabetes Care, 12, pp. 373-8 (1989)

[5] Allen J, Murray A, "Similarity in bilateral photoplethysmographic peripheral pulse wave characteristics at the ears, thumbs and toes", Physiol. Meas., 21, pp. 369-377 (2000)

[6] Wilde D.J., Beightler C.S, "Foundations of optimisation", Prentice Hall, N.J., USA (1967)

[7] Quick C.M., Young W.L., Noordergraaf A., "Infinite number of solutions to the hemodynamic inverse problem", Am. J. Heart Circ. Physiol., 280, H1472-1479 (2001)

[8] Watt, T.B, Burrus, C.S, "Arterial pressure contour analysis for estimating human vascular properties", J. Appl. Physiol, 40(2), pp. 171-176 (1976)

[9] Stroud, K.A, "Engineering Mathematics", 3rd Ed, Macmillan, London, England (1987)

Optical Engineering Group
Loughborough University

Chapter Four

FPD: Blood Volume Trials

4 Introduction to Blood Volume Trials

A general expression relating the effects of light and tissue interaction was developed in chapter two. The model was developed into the RVC index, and in subsequent chapters, expanded in both single and dual channel modes to improve the validity, reduce limitations and eliminate constant coefficients.

This chapter will apply the methodologies, developed in chapters two and three, to two separate application trials, under the general heading of Functional Perfusion Diagnostics –vascular diagnosis using blood volume perfusion.

The first trial is an investigative study into the detection of comparative blood volume changes during exercise. Differing exercise states are provoked in the subjects under investigation, with their peripheral perfusion response registered using PPG. This trial will establish the validity of the pulsatile perfusion trend-monitoring scheme, for development in the subsequent blood volume study. Observations and conclusion on the perfusion responses to differing exercise types are made.

The second trial is a clinical study, monitoring peripheral blood volume in order to establish the feasibility of automatic SBP determination. This work is then extended to an investigation of PAD assessment in the legs by PPG; direct correlation being provided with the ABPI measurement technique, introduced in chapter one.

In both these trials, as mentioned previously, the interpretation of changes in the peripheral perfusion of the subject is performed with knowledge of the underlying physiology. This is quite distinct from the lumped parameter model, where quantitative descriptions of vascular properties are indirectly obtained by fitting the forward model to the pulsatile PPG waveform. This approach will be investigated in the next chapter.

4.1.1 Equipment and Initial Analysis

Both trials in this chapter employ a custom built 16-bit dual channel PPG system, connected to a PC parallel port, which was designed and built by the Optical Engineering Group, Loughborough University. Specifications of this system, termed '*WinPPG*', are discussed in Appendix B, while a brief overview is given here. Additionally, several common elements of the protocols in both the clinical and exercise protocols are stated.

The PPG probes employed in both trials were 850nm transmission-mode contra-lateral types (Medilab RK850), commonly employed with Pulse Oximeters. The probe was clamped either side of the digit, LED adjacent to nail matrix, located either on the index finger of the subject or on 2nd toe of the foot under investigation. In the case of toe PPG, the PPG probe was fitted to the second toe, rather than great toe, since a better anatomical fit to the PPG probe was possible, as this toe is more like a finger, hence better optical coupling. The WinPPG hardware amplified the signal from the finger probe, then performed ambient light compensation using a 5Khz LED modulation sample and hold subtraction scheme, reducing the effects of ambient light artefact, allowing the system to be used in non-darkroom conditions. The signal is then hardware filtered at 0.5Hz to extract the AC and quasi-static DC components of the PPG signal, with the AC and DC signals representing arterial and venous, respectively, contributions to optical absorption, the filter limits developed from the literature. A programmable gain block (-3dB frequency of 15Hz) allowed the arterial PPG signals to be scaled and filtered. Hardware filter frequencies were developed from the literature[1]. A 16-bit analogue to digital converter (ADC), allowing up to 65536 quantisation states, converted the analogue arterial and venous waveforms into a binary digital format, performing fifty conversions per second for both the arterial and venous signals. The now digital data was then transferred to a Laptop PC via a bi-directional parallel port using a custom control program, written in Microsoft Visual C++. The control program, operating under Microsoft Windows NT V4.0, allowed full control of LED brightness, sample rates, recording time and gain settings, displaying the recovered PPG waveforms on the PC display, before time stamping and storing the data on the hard disk of the laptop.

Off-line analysis of the stored data was performed using the Matlab[2] programming system. Section 2.1 (modelling) indicated that the overall PPG signal is comprised of two signal components, a pulsatile AC signal, attributable to light absorption by arterial volume change pulsations, and a quasi-static DC signal, which is attributable to light absorption by tissue structures (static component) and venous blood. Isolation of these two signal components was performed in hardware, as described above. Post processing in software included digitally filtering the DC channel, using a four tap Butterworth[3] digital IIR filter (whose –3db cut-off point was 1Hz), processing the PPG data in both the forward and reverse directions, in order to remove any transients such as artefact caused by subject movement. The technique of twice running the data through the filter

effectively doubles the filter order[4] and eliminates phase errors usually attributed to IIR filters. To help reduce high frequency artefacts and baseline wander from the PPG AC channel, a 7 tap IIR maximally flat band-pass (corner frequencies of 1 and 15 Hz) digital filter was applied to the AC data, again applied in both the forward and reverse directions.

As developed in section 2.1, the signals from each probe were normalised by dividing the full-scale AC signal by the DC signal, in order to obtain an arterial absorption waveform termed relative volume change (RVC). The RVC index was then used as the starting point to derive additional metrics for further analysis.

4.2 Study A: Physiological Perfusion Changes During Exercise

This trial is designed to observe the changes in blood volume in the periphery as a result of exercise, using a symmetric dual channel perfusion methodology. This study was designed to test the perfusion models developed in chapter two. The single channel RVC index and dual channel relative indices were developed to allow both bilateral and inter subject comparisons of perfusion.

The subjects and form of exercise investigated was related to tennis players. PPG recordings were taken from both index fingers using a transmission-mode Medilab pulse oximetry finger probe, as discussed at the beginning of this chapter. Two subject groups, named 'Iso' and 'Dyna', undertook isometric and dynamic exercise respectively. Group Iso comprised 15 males aged 26-54 years (mean 37.4, SD 8.9), and group Dyna encompassed 25 males aged 25-61 years old (mean 39.67, SD 6.28). The subjects in both groups were healthy with no known circulatory problems. Group Iso performed maximal isometric handgrip exercise for 1-minute (maximally squeezing a tennis racquet handle), and group Dyna performed two separate 3-minute pre and post aerobic exercise tests, i.e. dynamic aerobic exercise.

4.2.1 Aims

The two groups employed differing protocols in order to compare the effects of the specific exercise type on peripheral perfusion.

Group Iso performed isometric exercise; designed to enable monitoring of peripheral perfusion levels whilst the flexor muscles in the forearms were maximally contracted. These muscles have a direct action on the ulna and radial arteries directly supplying the tissue beneath the PPG finger probe. Dual channel PPG was employed, using identical

probes and placement, in order to use the relaxed non-dominant arm as a control, i.e. symmetric comparative perfusion monitoring, as discussed in chapter three. Since the contraction time was short for this protocol, it was assumed that any perfusion changes would be a result of localised effects rather than systemic or whole body response to this exercise. Perfusion was monitored before, during, and after exercise for completeness.

The second study, performed by group Dyna, was designed to provoke a systemic body response, directly opposite to the Iso trial. Here a whole body reaction was desired, induced by performing dynamic aerobic exercise for longer periods. Again, perfusion was monitored in both the dominant and non-dominant arms, the non-dominant arm being used as a control, in order to compare the effects of a whole body response on perfusion in the peripheral circulation. Although the intensity level of exercise was not controlled, it was assumed that a medium-intensity exercise condition would be invoked in the body of the subject. Any exercise adaptation in the arm of the tennis players may have an effect on peripheral circulation for that arm; this protocol would illustrate this by monitoring relative perfusion levels between arms, identifying asymmetry where present.

4.2.2 Equipment

As discussed, the equipment used in this study is detailed in Appendix B, with a brief description provided at the beginning of this chapter.

4.2.3 Trial Protocol

Before the study took place, informed consent was obtained from all subjects, and the studies conformed to the Decleration of Helsinki set by the World Medical Association. Both subject groups were asked to refrain from stimulants, such as coffee, cigarettes etc for two-hours. During actual data collection, each subject sat upright with both arms resting outstretched in front at approximately heart level, hands resting on a table. The recording station was situated in a sheltered enclosure whose ambient temperature was approximately 23°C, located out of direct sunlight and draughts. During the recording procedure, subjects were asked to refrain from either moving or talking. In an attempt to encourage the subject to relax, each subject was asked to sit quietly in the recording position for 3 minutes before the resting recording began. In order to reduce subject anxiety, the PC screen was placed out of sight of the subject during the procedure. PPG

finger probes (details given above) were placed on the index finger of both the dominant and non-dominant hand.

4.2.3.1 Isometric Exercise Protocol Details

In this study, the subject was asked to hold the handle of a tennis racquet in their dominant hand for a total of three minutes. For the first minute, the subject relaxed. At the end of this relaxation period, the subject then maximally gripped the racquet handle for one minute. Following this one-minute period of sustained maximal gripping of the racquet handle, the subject returned to the relaxed state, with data recording continuing for a further minute. After this third and final minute, the recording was terminated, and the subject left the recording area. Care was taken to ensure the finger probe was not dislodged during the entire protocol. This concluded data gathering for that subject.

4.2.3.2 Aerobic Exercise Protocol Details

In this protocol, dual 3-minute PPG recordings were taken; initially while the subject was in a rested (pre-exercise) state, and secondly in a post-exercise state. The pre-exercise state recording required the subject to rest for 3 minutes, as mentioned above, after which a PPG recording was taken for a further 3 minutes whilst the subject sat motionless. After the initial pre-exercise recording was taken, the subject played tennis, exercising for a minimum of 1 hour. At the end of the exercise period, the subject quickly returned to the testing station, and a post-exercise 3-minute PPG recording was taken. After this three-minute post exercise recording, the recording was terminated, and the subject left the recording area. This concluded data gathering for that subject.

4.2.4 Data Analysis

Analysis for this study conformed to the proven analysis techniques developed in the previous studies. However, in this study, the RVC index was divided into 15-second epochs. This window typically, depending on heart rate, comprised 15 to 20 cycles of the PPG signal, more after exercise, again depending on heart rate.

The intelligent envelope detector specified in Appendix B was used to obtain the envelope of the signal for this period. Since this envelope detector employs band limited tracking and non-linear decay, an excellent approximation to the overall RVC envelope shape was obtained. To obtain a metric for each window position, the mean for each 15-second RVC envelope window was used: this metric being termed the Perfusion Value (PV).

An auto correlation technique, as discussed in Appendix A, was used to determine the subjects' heart rate over each 15-second window. Again, the mean peak-to-peak time interval was used in determining the heart rate over each period.

Further analysis techniques were specific to each subject group, and are discussed individually below.

4.2.4.1 Analysis specific to Isometric protocol subjects

In the case of the isometric exercise study, group Iso, the PV for each arm was simply plotted against time to generate a figure, averaged using 15 seconds epochs. Furthermore, the PV and heart rate values were averaged over one minute periods in order to generate a data table at one-minute intervals.

4.2.4.2 Analysis specific to Dynamic Aerobic exercise subjects

A more sophisticated methodology was employed to analyse the dynamic exercise study undertaken by group Dyna, as comparisons between pre and post-exercise perfusions were desired. Equation [4.1] shows the PEP metric, developed to compare perfusions between the post and pre exercise states.

$$PEP = \frac{\overline{PV}_{After}}{\overline{PV}_{Before}} \qquad [4.1]$$

The Post Exercise Perfusion (PEP) is the ratio of pre and post exercise PV for the same period, expressed as a percentage, and was calculated for both dominant and non-dominant arms. The average PV for each 15-second window was used for calculations in both pre and post exercise states, to provide a degree of stability for the results. If a subject has a PEP of 100% over a certain period, this shows the arm in question (dominant or non-dominant) has the same PV compared to the same arm over the same period during the resting recording, before and after exercise.

An additional metric allows comparison of perfusion between the dominant and non-dominant arm, and is shown in equation [4.2].

$$PERP = \frac{PEP_{Dominant}}{PEP_{Non-Dominant}} \qquad [4.2]$$

The post exercise relative perfusion (PERP) is the ratio of dominant and non-dominant post exercise perfusion (PEPs) over the same time interval, and is again expressed as a percentage. This allows us to compare simultaneous relative perfusion increases between arms. If a subject has a PERP of 100%, this means the dominant arm has the same PV in the post exercise state compared to the non-dominant arm.

Since this study produced data with a wide spread, the results were automatically sorted based on the mean of each subjects mean PERP. This produced two sets of data, group Alpha, where perfusion in each arm was similar, and group Beta where it was not.

4.2.5 Results

The results for both protocols are shown. Tabulated mean results over each minute are shown, and figures displaying the mean trend of each 15-second epoch, along with standard deviation error bars, are provided.

4.2.5.1 Group 'Iso' Study Results

Table 4-1 shows the heart rate details during the isometric exercise procedure, as determined using auto-correlation of the pulsatile PPG waveform. The error shown is the standard deviation of the heart rates. This table also shows the perfusion value PV, discussed above, based on the RVC index developed in chapter two.

	Minute 1 Pre Contraction		Minute 2 During Contraction		Minute 3 Post Contraction	
	Mean	SD	Mean	SD	Mean	SD
Non-Dominant, PV	0.74	0.02	0.73	0.022	0.79	0.014
Dominant, PV	0.47	0.017	0.14	0.076	0.5	0.032
Heart rate, BPM	73.9	0.63	81.5	2.03	75.6	1.05

Table 4-1. Perfusion and heart rates for the Isometric exercise protocol.

Figure 4-1 and Figure 4-2 shows these results graphically; error as shown is the standard deviation of the mean perfusion ratio.

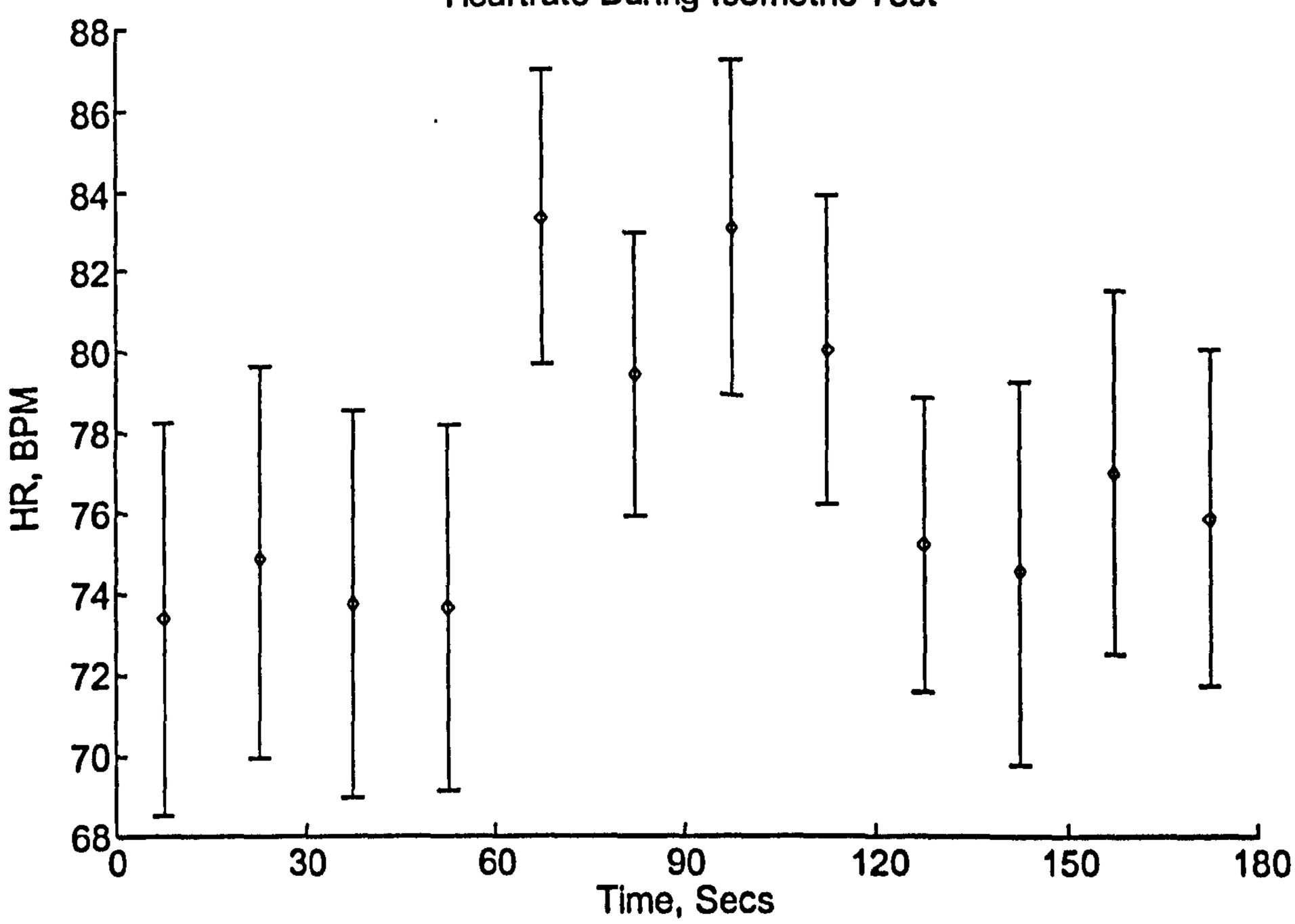

Figure 4-1. Isometric heart rate.

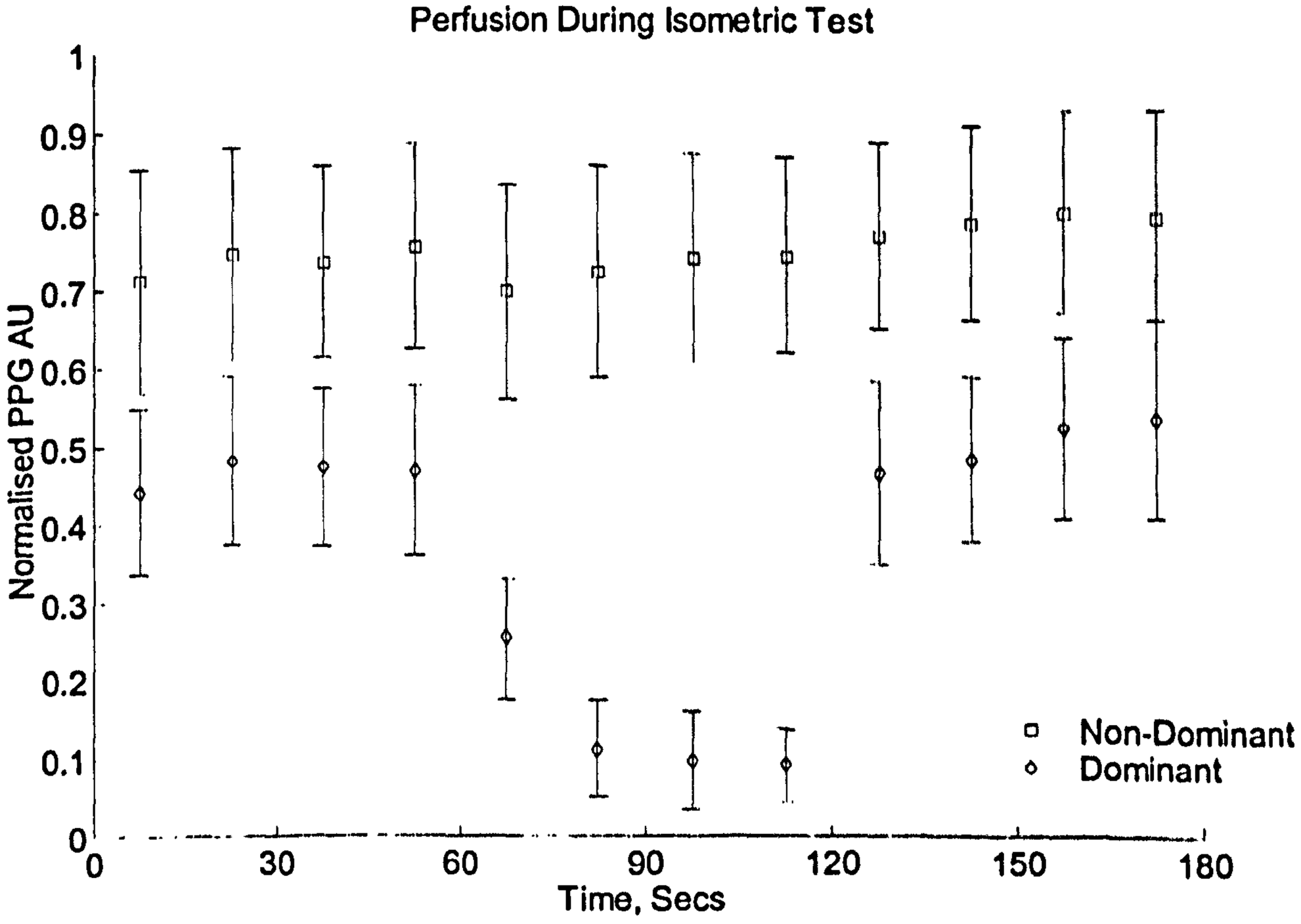

Figure 4-2. Isometric perfusion.

4.2.5.2 Group 'Dyna' Pre/Post Study Results

Tables of mean values for the two groups are shown, with more detailed figures illustrating tabular results are provided.

Heart rates

Table 4-2 show the mean heart rate over time as determined by auto-correlation of the pulsatile PPG signal for each group. shows heart rate over time for the two groups

			Minute 1		Minute 2		Minute 3	
Group	No. Subjs.	HR BPM	Mean	SD	Mean	SD	Mean	SD
Alpha (α)	18	Before	79.4	9.5	80.3	9.0	79.5	9.5
		After	95.3	7.7	93.0	8.4	91.8	7.6
Beta (β)	7	Before	73.3	13.2	74.1	13.2	74.2	12.5
		After	94.5	14.2	92.1	13.6	89.1	12.0

Table 4-2. Dynamic exercise heart rate.

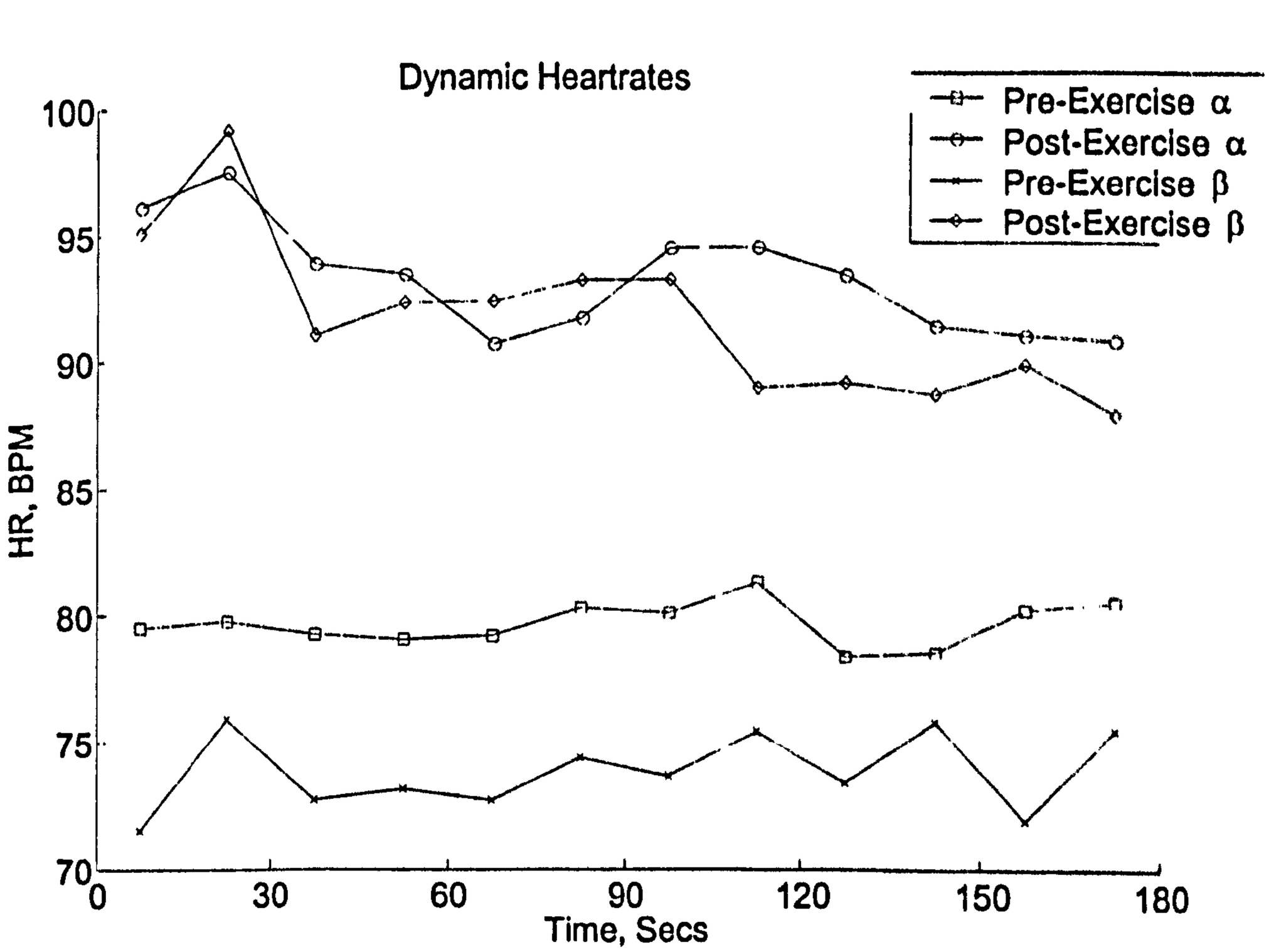

Figure 4-3. Dynamic Exercise Heart rate plot.

Post Exercise Perfusion (PEP)

Figure 4-4 and Figure 4-5 show post exercise perfusion (PEP) for each arm for the two groups Since the PEP for group Alpha in Figure 4-4 overlap, confidence lines are shown on this figure to facilitate understanding. Table 4-3 shows the mean PEP for each group over one-minute periods.

		PEP, %	Minute 1		Minute 2		Minute 3	
Group	No. Subjs.	Arm	Mean	SD	Mean	SD	Mean	SD
Alpha (α)	18	Non	130.7	89.9	119.8	72.2	109.4	67.9
		Dom	134.3	104.1	123.5	87.0	118.1	82.9
Beta (β)	7	Non	91.3	40.6	79.6	18.7	81.9	26.6
		Dom	218.8	95.5	190.9	96.2	171.9	85.7

Table 4-3. PEP for subjects during study

Post Exercise Relative Perfusion (PERP)

Figure 4-6 show post exercise relative perfusion (PERP) increase taken as the ratio of the dominant over non-dominant arm for the two groups. Table 4-4 shows the mean PERP for each group over each one-minute period.

PERP, %		Minute 1		Minute 2		Minute 3	
Group	No. Subs.	Mean	SD	Mean	SD	Mean	SD
Alpha (α)	18	105.1	30.6	104.3	26.8	108.6	26.6
Beta (β)	7	274.3	180.1	244.6	127.7	225.1	133.7

Table 4-4. PERP results for dynamic study.

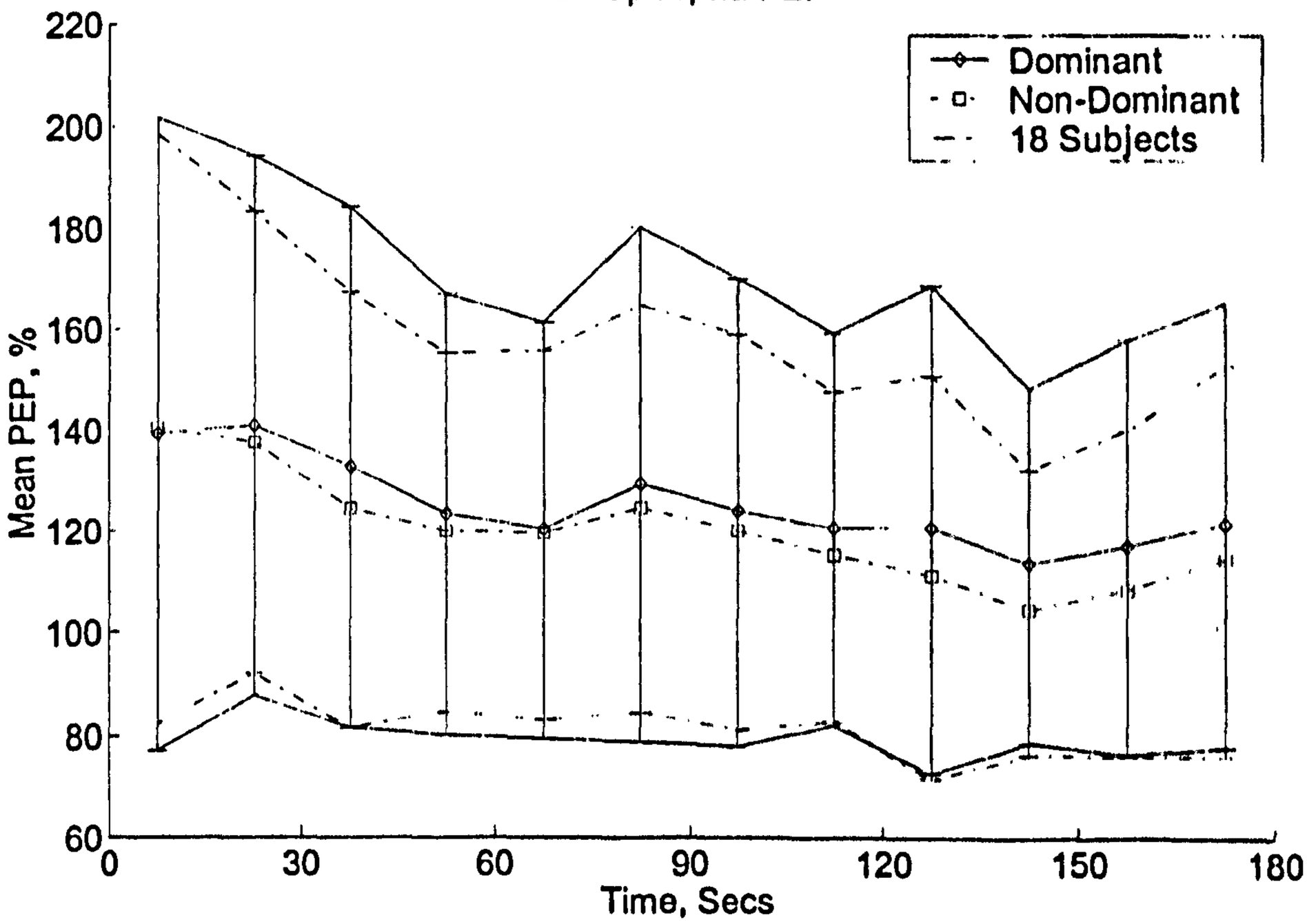

Figure 4-4. Group Alpha PEP.

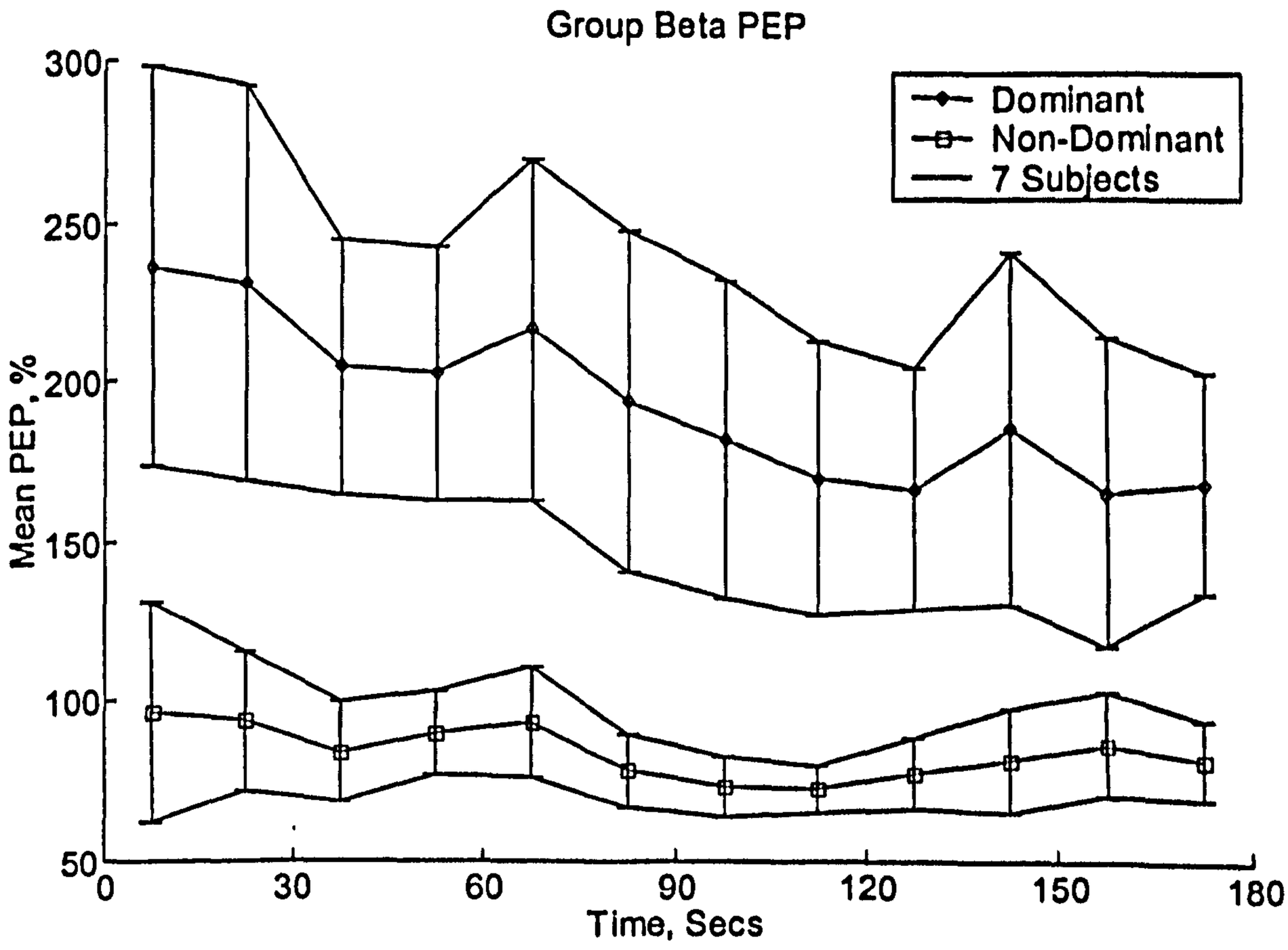

Figure 4-5. Group Beta PEP.

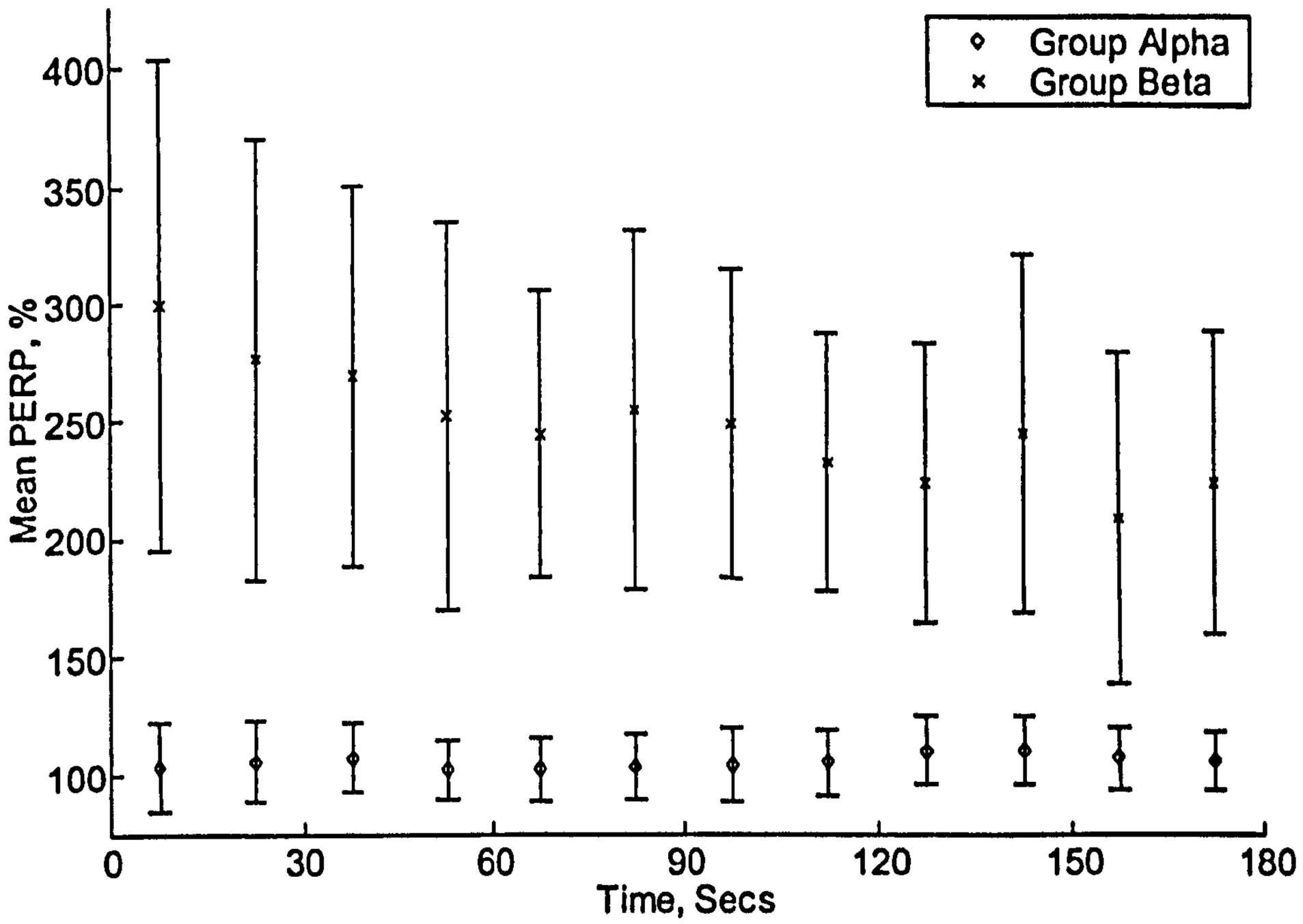

Figure 4-6. Group Alpha and Beta Post Exercise Relative Perfusion.

4.2.6 Result Analysis

This section contains a brief analysis of the results, allowing conclusions to be drawn in the next section.

4.2.6.1 Isometric Exercise Study

Analysis of the figures presented in Table 4-1 reveal several points of interest. For the minute preceding the exercise test, perfusion in the non-dominant arm was almost 57.5% greater than the dominant arm. During the one-minute duration isometric handgrip exercise, the perfusion in the dominant (squeezing) hand dropped to around 30% of its resting perfusion value. Somewhat unexpectedly, perfusion in the non-dominant arm also dropped, but only by around 1.5%.

After the isometric exercise, perfusion increased in both arms. The non-dominant arm shows an increase of around 6.75% and the dominant by 6.38%.

As mentioned, perfusion in the non-dominant arm was greater in the resting state than the dominant arm. In the post exercise state, the non-dominant arm showed an increase in perfusion of 58 %, notably similar to the pre-exercise condition.

The heart rate during the pre-exercise minute remained relatively steady at 74 BPM. During the exercise period, the heart rate climbed to around 81 BPM, an increase of

approximately 10%. During the post exercise period, the heart rate dropped to around 75 BPM, which is less than 2% above the initial pre-exercise heart rate.

4.2.6.2 Dynamic Aerobic Exercise Study

As the subjects participating in this group were of a wide fitness level, the results were wide ranging. As part of the analysis process discussed above, the mean and standard deviation (STD) were determined for each 15-second time period window. To enhance presentation of this data, the subjects were automatically classified into one of two groups. Classification was performed by creating a threshold based on the mean of all subjects PERP over the entire recording period. Subjects with a mean PERP below the mean of all subjects was assigned to group α. Subject with a mean PERP above the threshold was assigned to group β. This produced groups with 18 and 7 members for alpha and beta respectively. The concept behind this was to group subjects possessing similar spread in their post exercise perfusion, which could be equated to similar fitness levels based on heart rate variance.

4.2.7 Discussion

As investigation into skin perfusion revealed, the dynamics of skin blood flow are exceedingly complicated. Since the blood supply to the skin exceeds its metabolic rate by some measure, the skin must be responsible for another function, i.e. thermo-regulation. The body has to balance the requirement for redistributing blood flow from inactive tissue to working muscle, and balance the needs for thermo-regulation[5]. As the core temperature rises, a threshold is reached which is detected by thermo-sensitive cells in the autonomic nervous system. When this threshold is exceeded, both sweating and cutaneous vaso-dilation (i.e. increased blood flow) is initiated, and the rate of these cooling methods increases with increasing core temperature[6]. Increased sweating is only useful when the blood supply to the skin is also increased, otherwise evaporative cooling would only serve to lower skin temperature with little effect on deep body temperature, hence vaso-dilation.

Previous studies have shown a trend of reduced blood flow to the upper extremities during dynamic (as opposed to isometric) leg exercise[7]. This initial vaso-constriction is only initiated when the exercise intensity is large, but a sustained increased temperature threshold is apparent during exercise, observable when the exercise intensity is great[8].

The so-called 'muscle pump' also has an effect on dermal blood flow[9]. The contraction of skeletal muscle has dramatic effects on the vasculature within the muscle tissue, altering compliance, resistance, and other factors. The muscle pump hypothesis is based on the expulsion of blood from venous tissue during muscle contraction[10]. This hypothesis is facilitated by the presence of check valves in the venous system, which prevents back-flow of venous blood. A net vascular flow increase is obtained during rhythmic muscle contraction, since the venous blood is ejected by the contraction, so providing a greater pressure differential across the arterial – venous system. During muscle relaxation, the venous system is refilled[11]. It therefore stands to reason that sustained contraction would reduce overall blood flow since no periodic refilling and emptying mechanism exists.

The type of exercise is also important when discussing peripheral blood flow. The reflex actions discussed above seem not to apply when isometric exercise is taking place[12]. Increase in skin temperature suggests a corresponding increase in skin blood flow[13] during a sustained isometric handgrip exercise. Changes in arterial pressure with a corresponding increase in apparent blood flow[14] indicate a passive change in blood flow, caused by mechanical muscle function rather than reflex actions. This situation was clarified when it was revealed that isometric exercise caused no detectable reflex change in vasomotor tone, regardless of exercise intensity or muscle mass.

4.2.7.1 Group Iso - Isometric Exercise Trial

This study was designed to monitor the effects of localised isometric exercise on limb blood flow. Since isometric exercise is only deemed to cause local effects, this study focused on the changes in blood flow caused by specific muscle groups – in this case, the forearm flexor muscles. Since the subject rested for 3 minutes before the start of the recording period, starting values are assumed as the reference point for any derived calculations.

Although isometric exercise causes minimal reflex actions[15], a heart rate increase of 10% increase was observed. This is in line with previous literature[16,17], with subject anxiety during the procedure in part accounting for this increase. Further work in this area would benefit from a logging ECG monitor to correlate heart rate as determined by PPG against another heart rate recording method.

The actual perfusion index dropped to less than 30% in the case of the dominant arm during the exercise period, taken as the mean of the whole period. For the non-dominant

control arm, perfusion remained relatively consistent during the exercise period. In both cases, the perfusion index increased during the post exercise state for both arms; 6% for both the dominant and non-dominant arm. These effects agree well with published literature[18].

4.2.7.2 Group Dyna - Pre and Post Exercise Trial

This exercise was designed to monitor the systemic effects of exercise on peripheral blood circulation. Additionally, any marked differences in perfusion between the dominant and non-dominant arms in the post exercise state may be attributable to exercise adaptation.

The normalisation procedures employed as part of this trial have been very effective in illustrating perfusion changes, both because of exercise in the same arm and comparative perfusions amongst both arms. Data analysis reveals group alpha has the higher resting heart rate and longer recovery time. Group alpha also shows almost identical perfusions between arms in the post exercise state. These similarities between perfusions are therefore normalised to around unity when analysing the comparative measure PERP. Here, group alpha shows a relatively flat perfusion, when compared to the group beta perfusions, which show a marked perfusion increase that tails off over the recording interval.

Group beta also shows marked differences between perfusion in each arm, with the non-dominant arm showing the least deviation amongst results.

Several conclusions may be drawn from these results. Firstly, since group beta has a lower resting heart rate, it can be concluded that this group is more aerobically adapted, in other words 'fitter', than group beta. This conclusion is reinforced since group beta heart rate also decreases more rapidly than group alpha.

Secondly, group beta has undergone adaptation in the dominant arm through playing tennis. This can be verified since the dominant arm shows increased perfusion in the post exercise state when compared to group alpha, whereas group alpha shows increased perfusion in both arms. Both physiological adaptation and better technique in the case of group beta could illustrate why only the dominant arm displays both increases perfusion, and a more significant perfusion increase than group alpha.

In order to further understand the resulting subject groups alpha and beta, where each subject had been allocated into the appropriate group on the basis of their perfusion, a table of subject details was compiled, shown in Table 4-5.

Group	Age Years		Height Cm		Weight Kg		BMI		Playing Time, Years	
	Mean	Std	Mean	Std	Mean	Std	Mean	Std	Mean	Std
Alpha	40.65	10	179.5	6.6	81.3	9.15	25.3	2.8	7.48	6.5
Beta	33.86	6.12	182	4.5	78.1	5.5	23.6	1.9	9.02	2.5

Table 4-5. Subject details for Dynamic exercise protocol.

Table 4-5 illustrates that group beta has the younger average age of the two groups; group beta also has a lower body mass index, which is a technique for normalising body height against body mass. In addition, group beta has a greater tennis playing time compared to group alpha. These statistics further illustrate why group beta has the lower resting heart rate and decreased recovery time.

Drawing on these conclusions, it can be argued that group beta has displays adaptation of the dominant arm due to the repeated exercise strain induced by playing tennis. These subjects are generally fitter and younger than group alpha, with a longer playing time despite a reduced mean age. Normalising mean playing time with mean age gives 67.2 days and 97.2 days playing time experience per year of age for groups alpha and beta respectively. Group alpha subjects show increased perfusion in both arms immediately after exercise, which is attributed to the overall exercise-induced load placed on the body causing increased peripheral perfusion in order to cool down. This hypothesis is reinforced when investigating the literature[19], which has also found adaptation in the dominant arm of tennis players. Similar adaptation has been observed in other asymmetric sports[20].

To further increase the validity of these observations, both finger tip skin surface and body temperature measurement, recorded before and after exercise, could be taken. This would then allow inspection of body core temperature and skin temperature changes as a result of exercise induced changes. A dominant arm showing similar skin surface temperature to the non-dominant arm, but increased perfusion, could be assumed to have increased perfusion due to increased bloody supply to the muscles of the arm. Conversely, increased perfusion and increased skin surface temperature in both arms, coupled with increased core temperature, could indicate any increased perfusion was an attempt at body temperature regulation.

4.3 Study B: Perfusion Investigations In Subjects with Suspected PAD.

The problems and complications of PAD were introduced in chapter one. Current diagnostic techniques for PAD in the feet, namely the Korotkoff SBP determination method and the ABPI metric for quantifying occlusive PAD severity were also described, along with relevant problems associated with these techniques. This trial will develop screening techniques using PPG, in order to assess occlusive PAD. The ABPI procedure, as discussed in chapter one, has inherent operator variability problems, and is not suited to all patients; patients suffering diabetes mellitus with calcified arteries being one example. Additionally, the specialised nature of performing ABPI measurements, using the 'Doppler and cuff' technique, necessitates examination in a vascular clinic where skilled personnel can perform diagnosis. Clinical screening of PAD using PPG may be possible in the home or at primary healthcare levels, such as a GP surgery, with obvious advantages including reduced patient inconvenience, ease of use and earlier diagnosis of PAD. A trial study was conducted to determine the feasibility of automatic SBP determination using PPG, with SBP forming the basis for ABPI determinations. The aim of this trial was to evaluate the possibility of using pulsatile PPG, rather than the 'Doppler and cuff', to detect systolic blood flow return, thus allowing automatic SBP determination by combining a PPG system and automatic pressure cuff.

Moreover, a dual-channel asymmetric comparative evaluation of peripheral perfusion levels, as discussed in chapter three, was performed in both healthy and diseased subjects. The aim here was to establish the suitability of using a PPG only technique for determining occlusive PAD in the feet, effectively eliminating the need for sphygmomanometry. Comparison of the severity of PAD as determined with the novel PPG based method with conventional ABPI was performed in order to establish the significance of these results.

A PPG system capable of monitoring the progress of arterial disease could form a useful primary healthcare tool, in much the same widespread way that automatic blood pressure monitors have. It is recognised that automatic blood pressure monitors employing oscillometric pressure monitoring techniques are widely available. However, a systolic/ABPI system based on PPG peripheral circulation monitoring could provide a more sensitive system due to the peripheral measurement of SBP, with the possibility that the lumped parameter forward and inverse model could also provide additional

quantitative vascular parameters, as discussed in chapters two and three. PPG has the potential to not only equal the current diagnostic information techniques, but also surpass them with increased sensitivity to PAD and direct physiological parameter such as compliance providing a more complete diagnosis.

4.3.1 Automatic Systolic Blood Pressure Determination using PPG

In this study, a protocol was devised to investigate the feasibility of determining the SBP in the brachial artery using a PPG finger probe. The 'gold standard' method for determining SBP is by invasive arterial pressure sensors; however, the more convenient Korotkoff auscultatory procedure, as discussed earlier, will be used provide an assessment of systemic systolic blood pressure. Since the Korotkoff procedure itself can give rise to blood pressure operator induced subjectivity errors, the degree of agreement between the two methods will be used to determine the feasibility for automatic PPG based SBP determination system.

Nine subjects, SBP 135 to 150mmHg (mean 142.22 mmHg, SD 7.12 mmHg), had their brachial systolic pressure determined using the conventional Korotkoff auscultatory procedure, in the outpatients department of the Vascular Department of Leicester General Hospital, part of the University Hospitals Leicester (UHL) NHS trust. The only deviation from the standard procedure, discussed in chapter one, was a Doppler Ultrasound flow probe placed on the subject's radial artery (instead of using a stethoscope) in order to detect blood flow. The Doppler flow probe affords extra sensitivity compared to a stethoscope, which is essential when monitoring the possibly diseased small arteries in the feet. A PPG finger probe, placed on the index finger of the arm under investigation, allowed a continuous PPG recording to be obtained during the entire Korotkoff cuff inflation and deflation procedure. Evaluation of peripheral blood volume perfusion, throughout the SBP determination procedure, should allow a method to be derived suitable for automatic PPG based SBP detection.

4.3.1.1 Aims

In order to evaluate peripheral perfusion while blood pressure is being found, a complete peripheral perfusion recording is needed during the entire cuff inflation and deflation cycle. From this, a specific peripheral blood perfusion value should be observed at the instant of blood flow return, i.e. systolic pressure, during cuff deflation.

A peripheral perfusion threshold can be determined from statistical analysis of the systolic return threshold for several subjects, allowing an automatic system to determine

SBP if automatic control of cuff pressure and PPG perfusion was possible, probably giving a SBP reading after the cuff inflation-deflation cycle. Operator subjectivity errors, currently associated with the Korotkoff method and other PPG based SBP methods[21], should be eliminated with this approach.

4.3.1.2 Equipment

The WinPPG system employed was briefly discussed at the start of this chapter, with full specifications available in Appendix B. Since the WinPPG system offered full control over the PPG acquisition system, all data recordings employed the same settings (such as gain, LED intensity) to ensure consistency between data sets, as was pointed out in chapter three. However, in this trial study, only one signal channel of the WinPPG system, corresponding to the right index finger PPG probe, of data was analysed.

A CW Doppler Ultrasound system (4Mhz probe) was used on the right radial artery adjacent to the wrist to register arterial pulsatile blood flow. A standard mercury Sphygmomanometer was used to provide a controlled occluding pressure, located around the brachial artery on the upper arm. A vascular technician, with several years experience in obtaining SBP using the Doppler Ultrasound system, obtained the subject's brachial SBP using the usual Korotkoff cuff inflation-deflation technique.

4.3.1.3 Methods

During the cuff inflation and deflation procedure, various significant points, such as maximum pressure, systolic return etc were timed and noted, for subsequent analysis of the resulting PPG waveform. Figure 4-7 depicts an actual waveform, showing the inflation and deflation cycle of the sphygmomanometer cuff and corresponding pulsatile PPG waveform. The points of interest noted are the beginning of cuff inflation, vessel occlusion pressure, maximum applied cuff pressure, systolic return as defined by the technician and cuff full deflation.

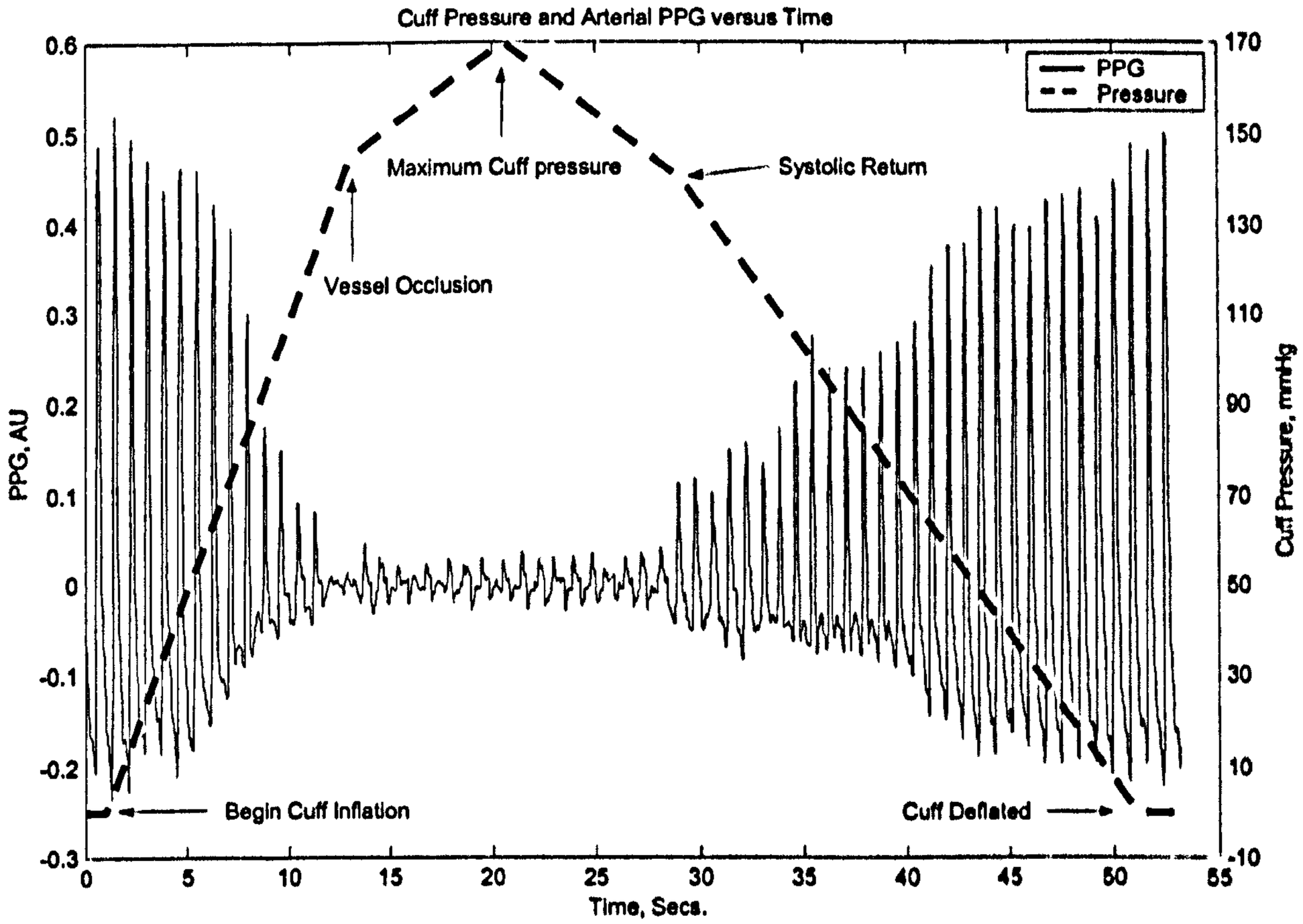

Figure 4-7. Typical cuff inflation/deflation cycle and corresponding pulsatile PPG waveform.

4.3.1.4 Protocol

Ethical approval for the study protocol was obtained from the UHL Ethical Committee. Additionally, informed consent was obtained from all subjects involved, and the studies conformed to the Declaration of Helsinki set by the World Medical Association. Prior to the procedure, each subject reclined on a standard hospital couch for several minutes in order to relax. The ambient temperature of the room was approximately 22°C, with no obvious draughts. During the recording procedure, subjects were asked to remain motionless and refrain from talking, placing their arms by their sides, whilst reclining in the supine position. To help reduce subject anxiety, the PC screen was placed out of sight of the subject during the procedure. The PPG probe was attached to the right index finger, the pressure cuff attached over the brachial artery on the upper arm, and data recording was started. The technician then performed a brachial SBP pressure determination procedure, synchronising the various points of interest with the cuff pressure at that instant. The technician generally inflated the cuff 20mmHg higher than the occlusion pressure before beginning deflation of the cuff. Figure 4-7 shows a linearly interpolated cuff pressures between cuff pressure events, hence a straight-line pressure curve. This procedure was repeated for all nine subjects.

4.3.1.5 Analysis

As described in chapter two, an RVC index was derived from the PPG signal. The RVC index was envelope detected using an intelligent band limited envelope detector developed, shown in the appendix. The envelope waveform was then smoothed using a ½ second symmetric moving average window.

To generate a metric suitable for threshold detection, a 1 second window was used in generating mean Perfusion Values (PV). A PV was determined for the 1 second preceding cuff inflation, then a PV found for a symmetrical period either side of the occlusion pressure point, the maximum pressure point, and the systolic return point. The location of these points were noted during cuff inflation and deflation as part of the protocol. A post deflation 1 second PV was also found for completeness.

In order to normalise against maximum pressure PV and initial PV, an empirical proposition was developed, equation [4.3], which removes the 'baseline' perfusion value present at maximum cuff inflation, and scales between zero and unity.

$$PV_{Normalised} = \frac{\left(\overline{PV} - \overline{PV}_{P_{Max}}\right)}{\left(\overline{PV}_{PreInflation} - \overline{PV}_{P_{Max}}\right)} \qquad [4.3]$$

Normalised PV, equation [4.3], can be expressed as percentage of full scale PV minus maximum pressure perfusion offset, allowing comparison between subjects regardless of relative PV values, as developed in chapter three.

4.3.1.6 Results

Table 4-6 shows normalised PV percentage and pressure for all nine subjects. The normalised PV requires the perfusion offset present at maximum cuff pressure to be removed and is scaled by initial PV before cuff inflation began. This results in a percentage perfusion value with the consequence that initial PV and Maximum PV are not shown since they are used during normalisation. Of the nine subjects, all had SBP at the higher end of the 'normal' range since their average age was greater than sixty years. Basic statistics were calculated for the results, and these are shown in Table 4-6.

Subject	Occlusion		Systolic Return		Post Deflation
	NPV %	Pressure	NPV %	Pressure	NPV %
A	-0.35	145	10.72	140	86.91
B	4.41	150	0.62	145	97.46
C	0.9	135	12.78	150	98.13
D	-0.98	145	5.22	150	100.85
E	4.62	140	22.98	140	103.71
F	-5.19	155	2.15	135	106.2
G	-2.81	150	6.62	140	85.68
H	1.75	140	4.30	130	85.46
I	-0.09	170	6.38	150	91.56
Mean	0.25	147.78	7.98	142.22	95.1
STD	3.17	10.34	6.79	7.12	7.96

Table 4-6. Normalised PV for all nine subjects.

4.3.1.7 Discussion

From the normalised Table 4-6, a threshold for systolic return could be defined as approximately 8% normalised PV. An automated cuff controller and pulsatile PPG system would register pre-inflation PV, occlusion PV, maximum inflation PV and monitor cuff pressure as the cuff is deflated, with maximum pressure being defined as 20mmHg greater than the occlusion pressure. The raw PV threshold relating to 8% of the normalised value would be calculated, then the corresponding cuff pressure determined. This would be the systolic pressure, generated automatically. Analysis of subject results reveals subject E has a systolic return threshold much greater than other subjects, with subjects E and F showing signs of hyperaemia after cuff deflation. If subject E were eliminated from the table, then systolic return threshold would be 6%.

In order to test the theory that a simple perfusion threshold, as applied to a perfusion envelope, allows calculation of systolic pressure, the threshold technique derived above was re-applied to the cuff inflation-deflation envelopes from all nine patients, shown in Table 4-7.

Intermediary pressures were derived by cubic-spline interpolation[22] of the maximum pressure, systolic return and cuff deflation points with the corresponding time point for threshold detection. Additionally, the pressure at the calculated PPG threshold ±

standard deviation was also found in order to aid understanding the pressure spread involved.

Subject	Pressure, mmHg				
	Actual	Interpolated	Error	Minus SD	Plus SD
A	140	140.88	-0.88	159.91	138.4
B	145	136.13	8.87	164.09	133.8
C	150	152.25	-2.25	155.1	148.33
D	150	148.69	1.32	151.67	145.67
E	140	146.1	-6.1	155.4	143.1
F	135	131.58	3.42	148.9	128.72
G	140	139.22	0.78	145.62	117.84
H	130	126.02	3.98	134.66	106.66
I	150	108.44	41.56	148.28	105.5
Mean	147.78	136.59	5.63	151.51	129.73
SD	10.34	13.4	14.11	8.61	16.33

Table 4-7. Threshold Interpolated pressure values.

Table 4-7 shows that a reduced perfusion threshold will produce a greater systolic pressure since the cuff is closer to max pressure – correspondingly, a larger threshold will produce a lower pressure since cuff pressure is closer to cuff deflation, i.e. zero.

The mean error for all nine subjects is less than 6mmHg – this is comparable to the error limit employed by the technician performing the tests, since it is clear the technician rounded to 5mmHg. However, it is apparent that a more rigorous indication of cuff pressure (such as could be provided by direct electronic monitoring of cuff pressure) is needed in evaluating this methodology, along with either more accurate Korotkoff auscultatory derived SBP values or an alternative SBP measure. Furthermore, a more rigorous protocol that is more closely synchronised with technician-derived events would be advantageous, but the current protocol had to be integrated into a working vascular clinic without intruding into its operation. Nevertheless, these initial results are encouraging, showing that pulsatile PPG derived SBP show good agreement with technician derived SBP. This opens up the prospect for further diagnosis using PPG derived SBP values.

4.3.2 PPG Derived ABPI and Functional Perfusion Diagnostics

The automatic SBP technique using PPG, developed in section 4.3.1 above, may be extended for automatic determination of ABPI using PPG. The automatic SBP study in section 4.3.1 above was conducted on the brachial artery of normotensive subjects. This study will apply the automatic SBP technique to toe and finger pulsatile PPG in order to obtain automatic SBP and therefore generate automatic ABPI values, as determined by PPG. The added complexity of hypertensive subjects and claudicants will also be investigated, with the effects of these complications noted on the automatic SBP determination technique.

Comparison between technician derived ABPI values and this automatic technique will reveal the suitability of this procedure to non-specialised ischaemia screening at the GP level.

Additionally, investigations into functional perfusion diagnostics (FPD) will be undertaken, using the technician generated ABPI index for correlation. This proposed technique has the advantage of dispensing with the occluding sphygmomanometer and cuff, greatly simplifying the determination of limb ischaemia. This could allow non-specialised personnel in the primary healthcare environment (GP level) to perform initial occlusive PAD screening, as opposed to current the situation that requires patients to attend vascular diagnosis clinics.

4.3.2.1 Aims

This trial has two broad aims. These are discussed in detail below.

- SBP will be found in the limbs of subjects using both standard 'cuff and Doppler' techniques and the automatic PPG derived SBP technique discussed in section 4.3.1 above. From this, ABPI metrics will be calculated, and compared with PPG derived ABPI values. It is assumed that PPG derived values will show increased sensitivity since pulsatile perfusion registration is detected in the periphery, rather than larger arteries as used in the conventional ABPI protocol.
- Additionally, a Relative Peripheral Vascular Index (RPVI) will be determined, based on the perfusion value of the patient before cuff inflation in both the pre and post exercise state. This technique eliminates any probe coupling associated problems as developed in chapter three. The assumption here is that patient suffering occlusive PAD will have reduced peripheral perfusion, resulting in a non-existent or small perfusion change in the post exercise state. Healthy

patients will produce a large perfusion change between pre and post exercise. Comparison of the various techniques employed in this study will reveal the suitability of these techniques to early ischaemia screening.

4.3.2.2 Equipment

The same equipment as used previously was employed in this study, utilising dual channel simultaneous recording of both the index finger and second toe.

Those patients undergoing exercise tests use the Stu-Ert Stress'ter calf ergometer[23]. The advantages of using the Stress'ter calf ergometer is that during exercise the pedal ergometer promotes a more localised physiological response, when compared to treadmill testing, allowing exercise tests to be performed on subjects who cannot undertake treadmill tests[24], for example patients with aortic aneurisms. Additionally, post exercise pressure readings can be performed more quickly using the pedal ergometer, as the subject does not have to move from a treadmill to a reclining couch for measurement, increasing the sensitivity of the ABPI measurement.

4.3.2.3 Methods

Since this study is an extension of the one presented in section 4.3.1, the methods will be very similar. However, an extension to that method will be the determination of a RPVI index calculated before cuff inflation. This will be a measure of the subject's perfusion level, discussed in detail in section 4.3.2.5 below. The RPVI is calculated from recorded PPG before cuff inflation, and has been integrated into the standard vascular clinic protocol for determining ABPI. In addition, FPD using RPVI is quite distinct from ABPI, as this technique uses peripheral vasculature as opposed to the major arteries investigated using ABPI.

Toe probe SBP readings derived using PPG will be compared to ankle SBP readings derived using the Doppler and cuff technique. Finger probe SBP readings derived using PPG will be compared to brachial SBP readings taken using the Doppler and cuff technique. From these readings, PPG and Doppler ABPI metrics will be derived, and compared with one another. This methodology should reveal the degree of agreement between the two SBP measuring techniques, and shows if PPG derived ABPI can displays increased sensitivity.

4.3.2.4 Protocol

Ethical approval for the study protocol was obtained from the UHL Ethical Committee. Additionally, informed consent was obtained from all subjects involved, with the studies conformed to the Declaration of Helsinki set by the World Medical Association. The protocol for this study was designed to integrate with and extend the standard ABPI protocol employed in a vascular clinic where the subjects were being evaluated. The protocol is therefore minimally intrusive into the normal ABPI procedure, relying solely on passive data logging and recording of significant events and technician derived SBP. As such, the majority of the protocol is as described in section 4.3.1.4. However, before the technician began determination of resting pressures, a PPG probe was attached to the index finger of the patient's right arm. Another PPG probe was attached to the second toe of the leg under investigation. The cable to the PPG probe on the foot was secured using surgical tape attached to the dorsum in order to reduce probe movements during exercise, hence reducing PPG movement artefact. Once the probes were applied, the PPG device began simultaneous recording from both toe and finger, and the technician began the procedure for obtaining ABPI.

After the brachial SBP was determined as described above, the pressure cuff was then relocated to the calf of the leg under investigation. When correctly placed, three ankle SBP determinations were taken using the Doppler and wand technique, sequentially determining SBP in the dorsalis pedis, posterior tibial and peroneal (poplital) arteries. The largest ankle SBP was then divided by the brachial SBP determined above in order to obtain the resting ABPI. If only resting pressures are required, that concludes the monitoring of that leg; the procedure may be repeated if ABPI readings are required for both legs.

If pre and post exercise ABPI readings are required, after determining the resting ABPI the subject then performs exercise, with the intention of dilating the arteries supplying the calf muscle. As mentioned, subjects performed dorsoflex extensions using the Stu'ert Stresster calf ergometer as the load, one dorsoflex extensions per second for two minutes. This generated the post exercise state locally, rather than promoting a systemic response.

After the two-minute exercise period, ankle SBP was determined from the artery producing the greatest pressure in the foot from the pre exercise SBP determination. This must be performed quickly before the patient's vasculature has time to recover.

With determination of ankle SBP complete, the cuff was relocated to the brachial artery and the post exercise brachial SBP would then determined, in order to ensure no systemic SBP change has occurred. From these two values, the post exercise ABPI may be determined. The PPG data logging was then terminated for that subject, or the procedure may be repeated using the other leg.

4.3.2.5 Analysis

Most of the analysis techniques were described in the analysis section of the previous trial. Here, normalised PV was required in order to determine SBP. The procedure involved monitoring envelope detected PV, searching for the systolic return threshold during cuff deflation, with the associated cuff pressure being prescribed as SBP. However, this study requires an additional FPD metric to be developed which will provide insight into comparative blood volume changes, in an attempt to eliminate the need for sphygmomanometry.

Previously, the notion of PV was developed as a mean envelope detected RVC index over a given timescale. A peripheral vascular index (PVI) can be defined as the ratio of mean PV at two PPG measurement sites, described in equation [4.4].

$$PVI = \frac{\overline{PV}_{Toe}}{\overline{PV}_{Finger}} \qquad [4.4]$$

The Peripheral Vascular Index is a ratio of relative volume changes, since the mean PV is the ratio of envelope detected pulsatile (AC) PPG over venous (DC) PPG as described in modelling. However, calibration factors exist due to probe coupling constants and any possible non-linearity between channels. In order to reduce these effects, a relative measure may be determined, as described in equation [4.5].

$$RPVI = \frac{PVI_{PostExercise}}{PVI_{PreExercise}} \qquad [4.5]$$

The relative Peripheral Vascular Index (RPVI) is defined as the ratio between the post exercise PVI and pre exercise PVI. This calibration method will obviously only be useful in pre and post exercise tests, but will eliminate scaling problems discussed previously.

4.3.2.6 Results

In total, 34 brachial and 99 ankle systolic blood pressure readings were obtained from 14 subjects. Eleven subjects undertook pre and post exercise tests and three undertook only resting ABPI determination. The use of three ankle arteries in determining resting foot SBP explains the larger number of ankle as opposed to brachial pressure readings. The results are presented in two sections: pressure and ABPI determination using PPG, and comparison between FPD and ABPI.

4.3.2.6.1 Pressure Determination

Table 4-8 shows mean SBP as determined by both PPG and conventionally in pre and post exercise states, for toe (ankle) and finger (brachial) probe sites. Also shown are standard deviations, and the coefficient of determination (regression error or R^2 error), representing quality of fit, taken from their associated figures.

Figure 4-8 and Figure 4-9 show plots of PPG and conventionally derived pressures for brachial and ankle respectively, taken in both pre and post exercise states. Also shown on both plots are a linear regression and quality of fit R^2. Figure 4-10 and Figure 4-11 show Bland-Altman[25] plots for Brachial and Ankle determination procedures respectively.

Table 4-9 shows mean ABPI parameters as determined using conventional and PPG derived pressures. Mean and standard deviations are provided, with regression error also shown. Additionally, relative ABPI (RABPI) is also shown, defined as the ratio of both pre and post exercise ABPI, and is given for both methods. The RABPI index will be less than unity if the post exercise ABPI value is lower than the pre-exercise ABPI value.

Figure 4-12 show a comparison plot of ABPI values obtained both conventionally and using PPG methods for pre and post exercise states, with Figure 4-13 showing the RABPI scatterplot. Figure 4-14 shows the Bland-Altman plot for the ABPI determination methods, with Figure 4-15 showing the Bland-Altman plot for RABPI.

4.3.2.6.2 FPD Tests

In total, 19 FPD determinations were performed. A statistical analysis of RPVI and PVI for both locations was undertaken to determine the significance of these metrics with pre, post, and relative exercise ABPI.

An RABPI metric was defined as the ratio of pre and post exercise ABPI; since ABPI often drops in the post exercise state when PAD is present, enhancing the significance

of this event, given in Table 4-10. Regression coefficients and twin-tailed paired Student-T test (TTPST) were determined, along with both raw PVI and RPVI and the natural logarithm of APV and BPV used for calculating both PVI and RPVI.

Site and Method		No	Conventional		PPG		R^2
			Mean	SD	Mean	SD	
Pre Exercise	Brachial	14	160.64	15.54	155.54	16.16	0.67
	Ankle	80	151.54	30.62	138.10	35.39	0.46
Post Exercise	Brachial	21	159.19	17.83	156.61	20.42	0.39
	Ankle	19	137.05	39.27	135.66	38.65	0.85

Table 4-8. SBP Pressure determination results obtained from pre and post exercise tests.

ABPI Method	No	Conventional		PPG		R^2
		Mean	SD	Mean	SD	
Pre	80	0.95	0.18	0.90	0.23	0.47
Post	19	0.88	0.21	0.87	0.22	0.47
RABPI	18	0.91	0.3	.98	0.33	0.62

Table 4-9. ABPI values obtained from pre and post exercise tests

Method	Pre Exercise ABPI		Post Exercise ABPI		RABPI	
	TTPST	R^2	TTPST	R^2	TTPST	R^2
PVI	7.2e-19	0.03	6.8e-4	0.43	1.39e-5	0.08
Log(PVI)	2.6e-22	0.11	3.6e-7	0.04	1.11e-3	0.01
RPVI	0.88	0.06	0.16	0.02	0.82	0.08
Log(RPVI)	0.57	0.09	0.32	0.10	0.6	0.01

Table 4-10. FPD Results.

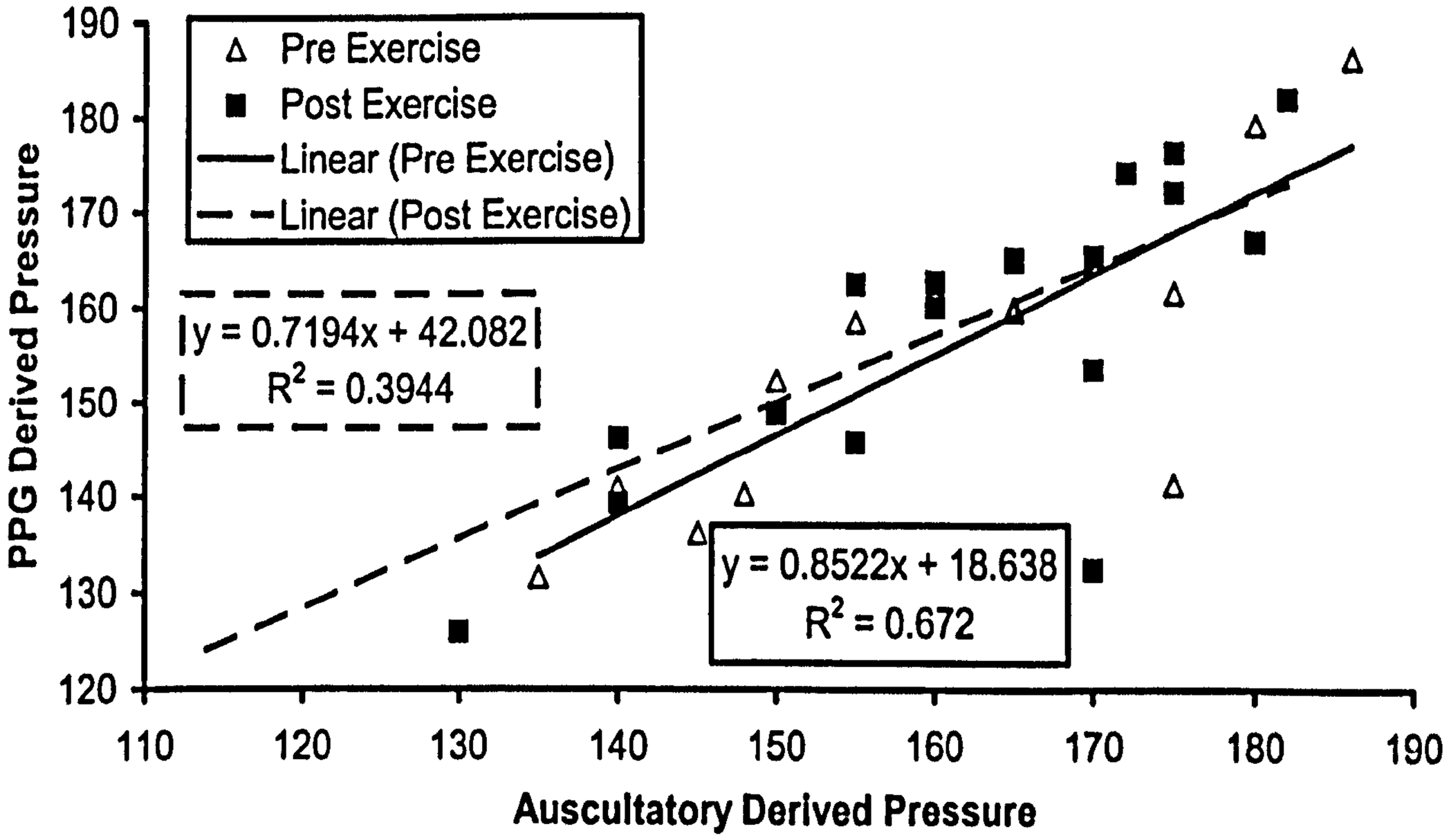

Figure 4-8. Comparison between Conventional and PPG derived Brachial SBP.

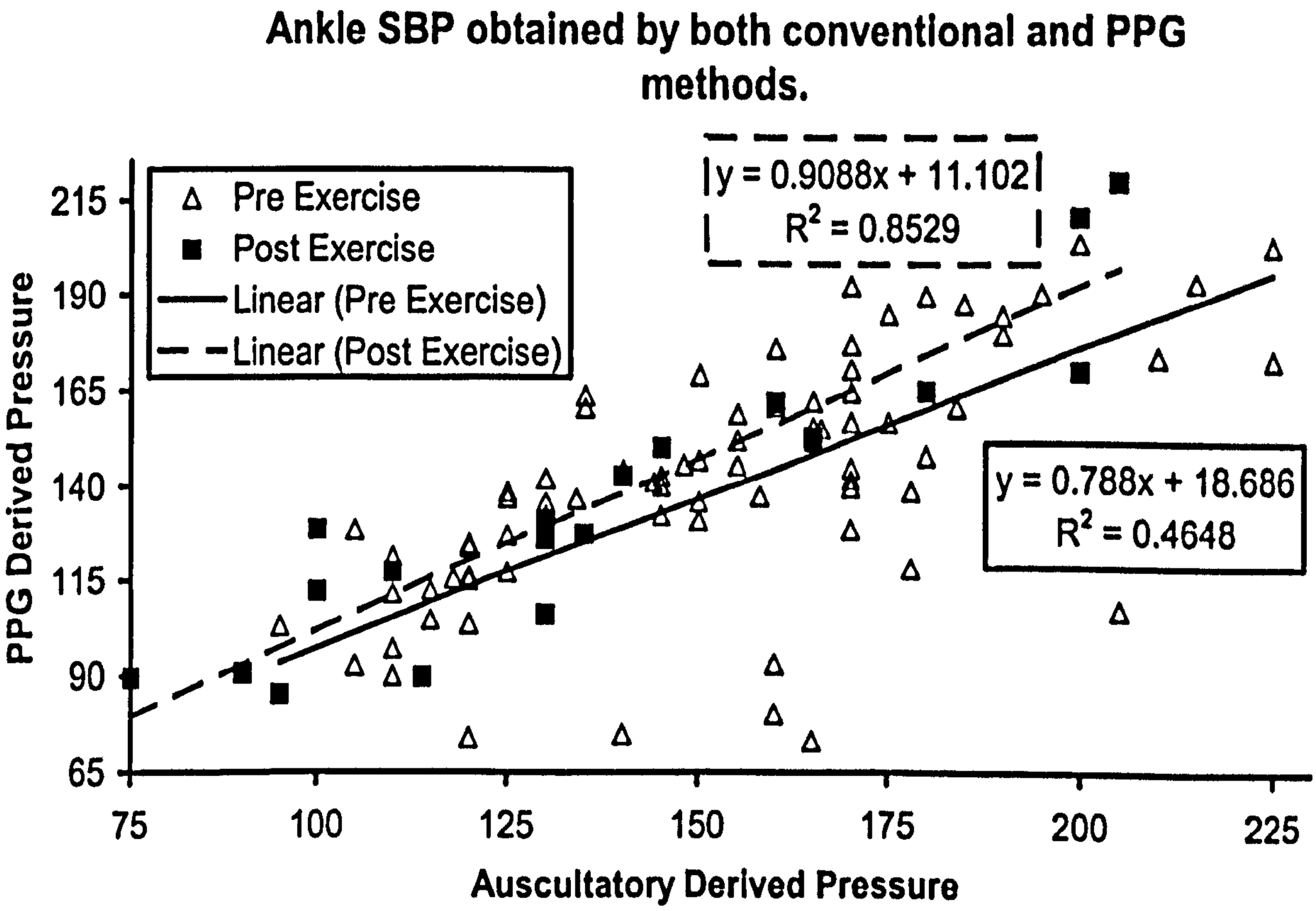

Figure 4-9. Comparison between Conventional and PPG derived Ankle SBP.

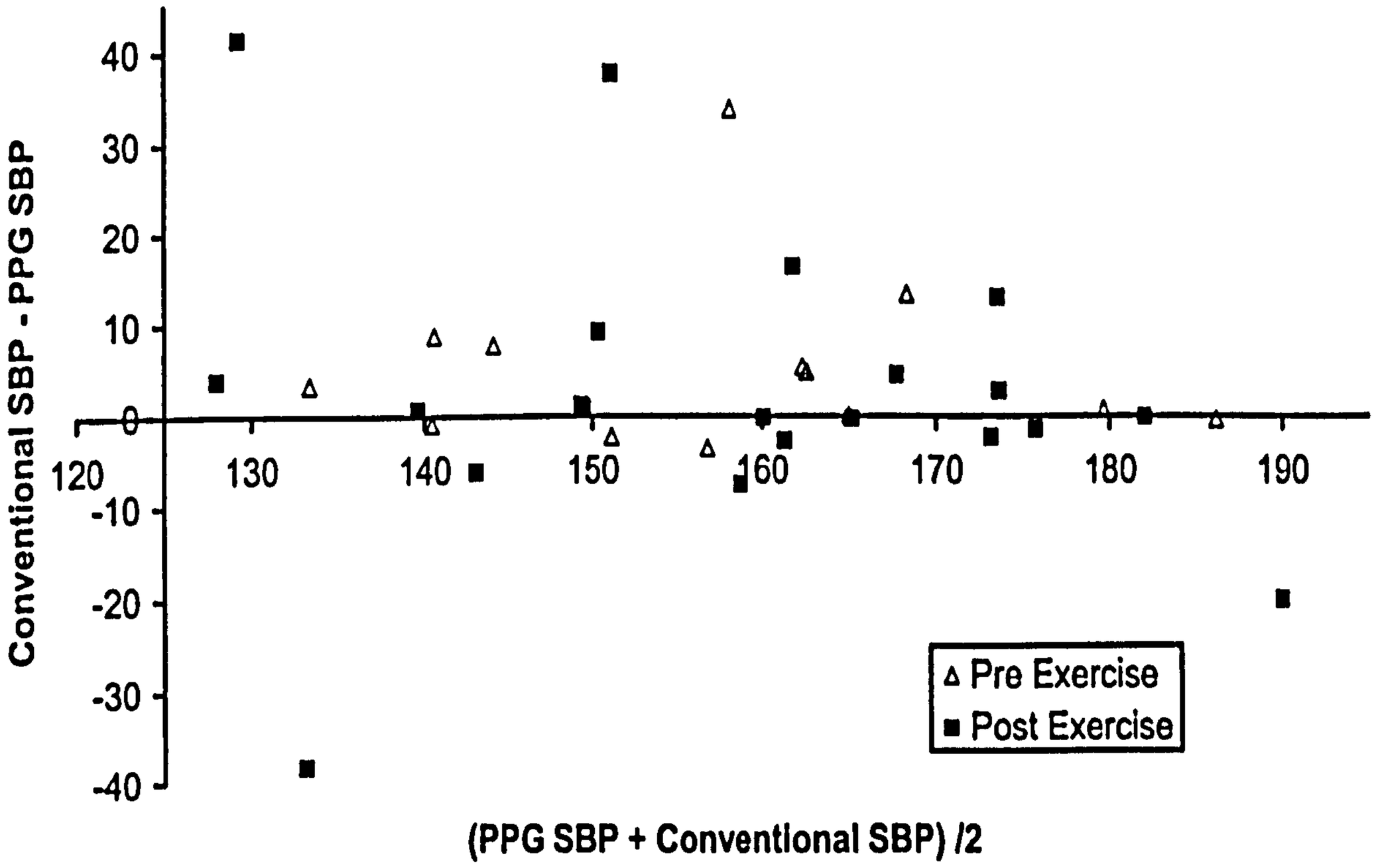

Figure 4-10. Bland-Altman plot for Brachial SBP Determination methods.

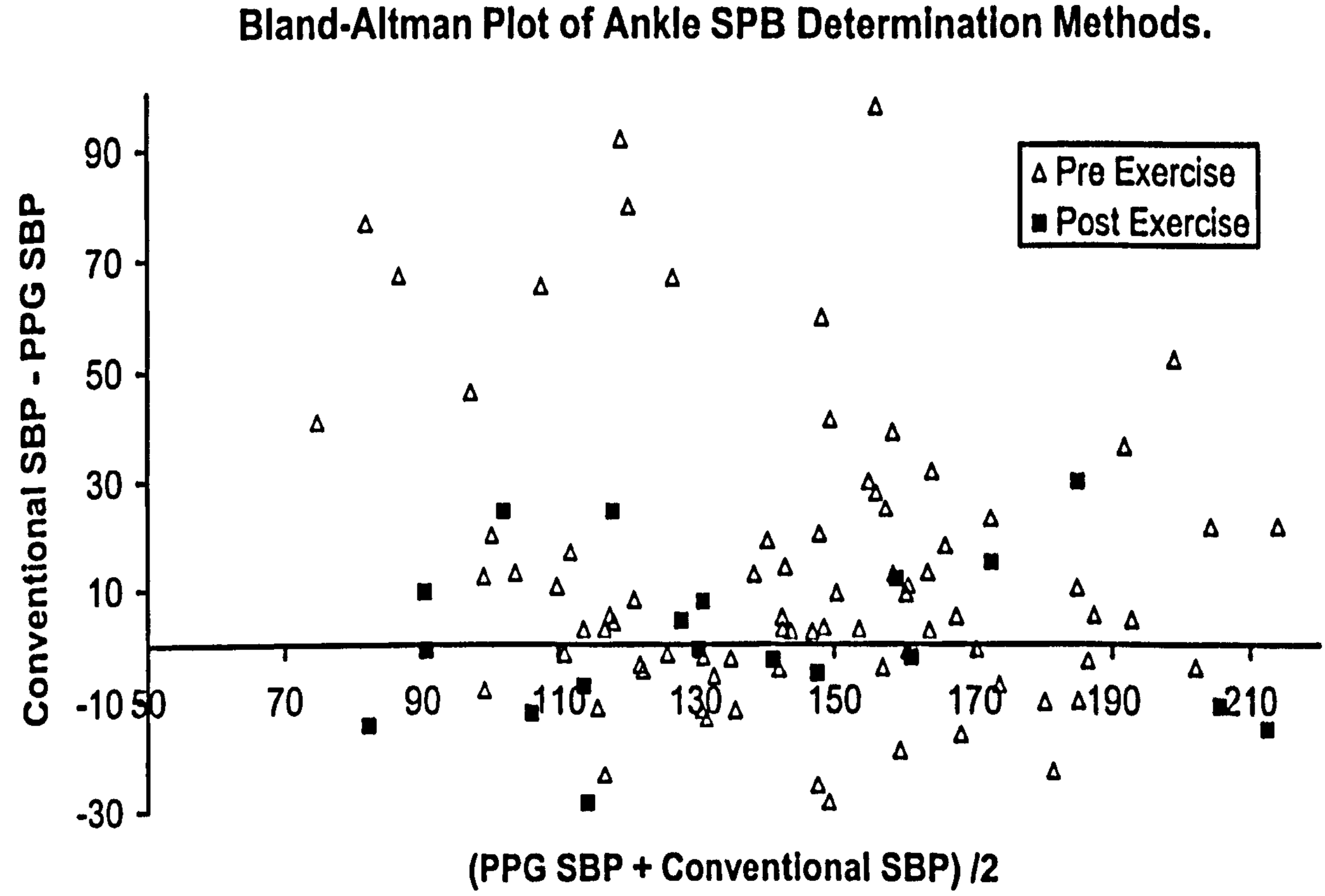

Figure 4-11. Bland-Altman plot for Ankle SBP Determination methods.

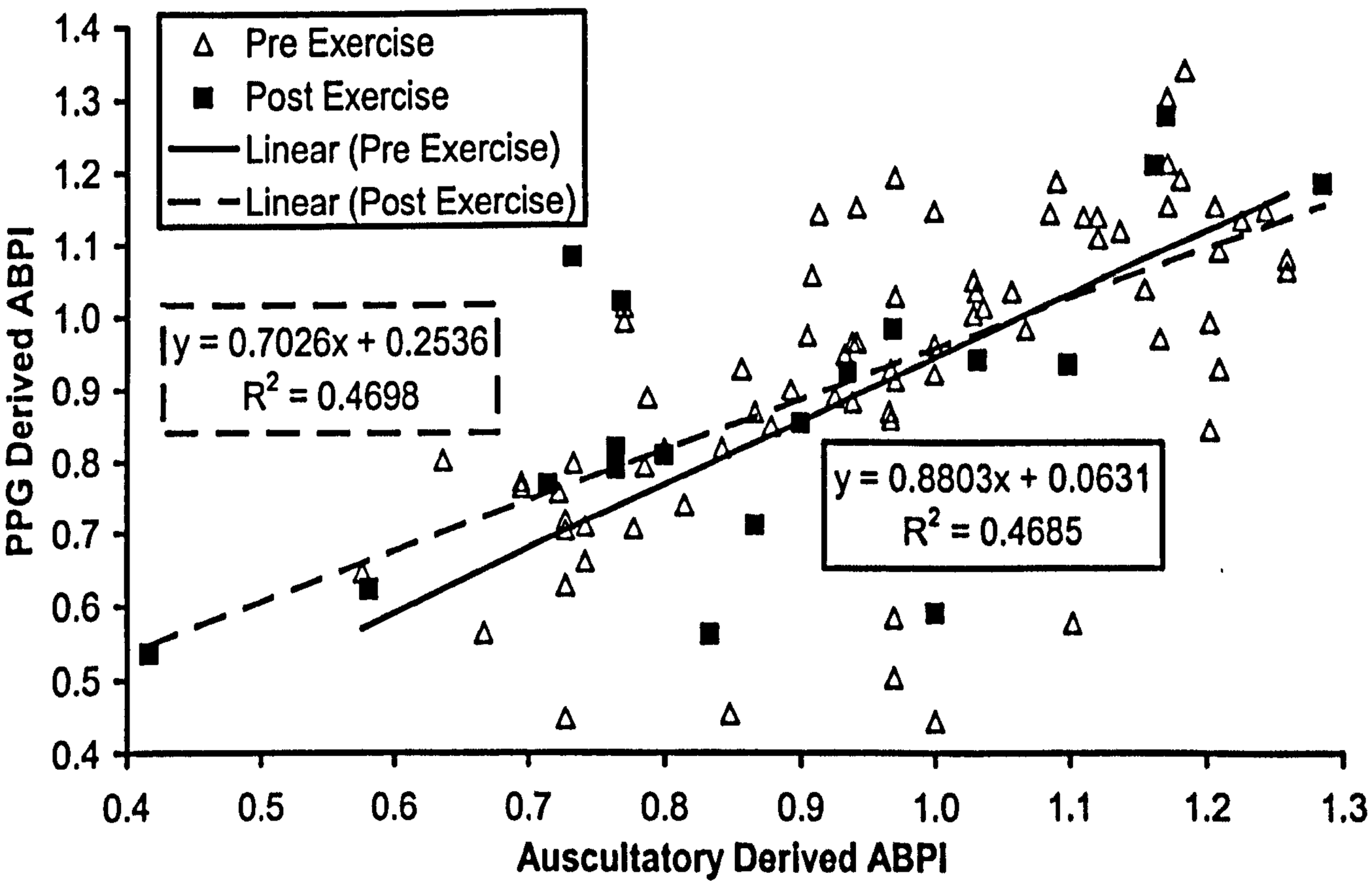

Figure 4-12. Comparison between conventional and PPG derived ABPI.

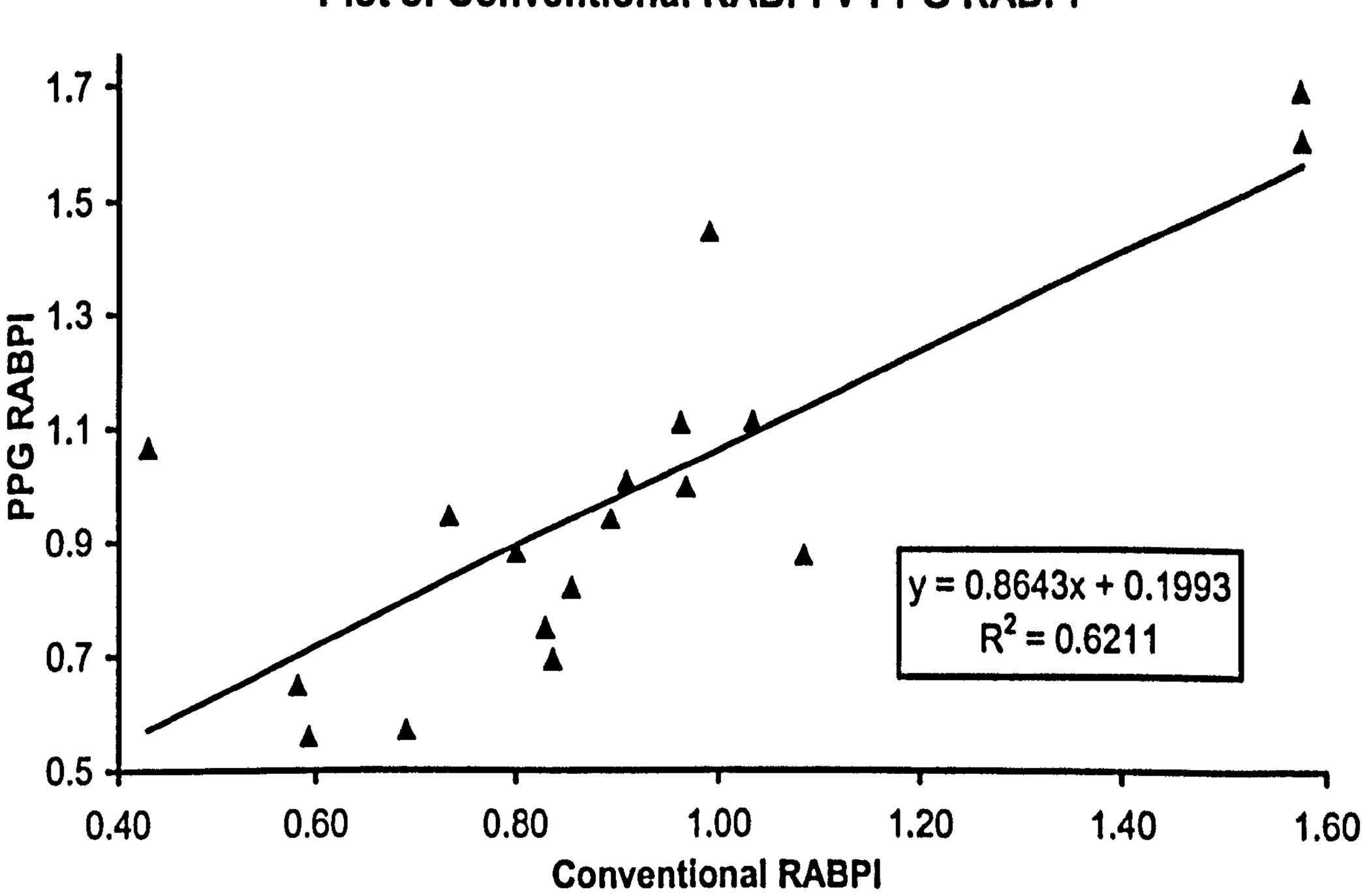

Figure 4-13. Comparison between Conventional RABPI and PPG derived RABPI.

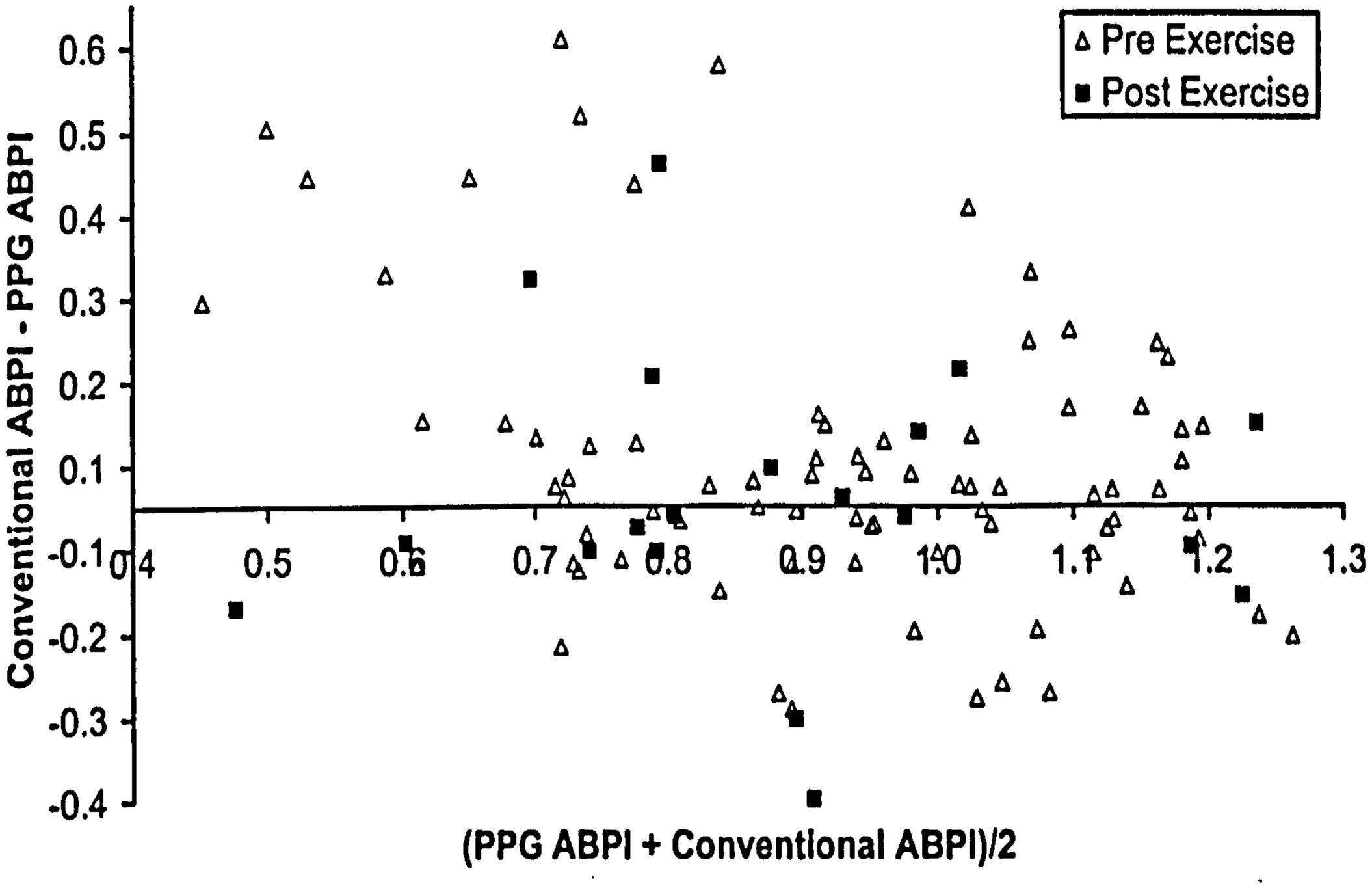

Figure 4-14. ABPI Bland Altman Plot for conventional and PPG derived methods.

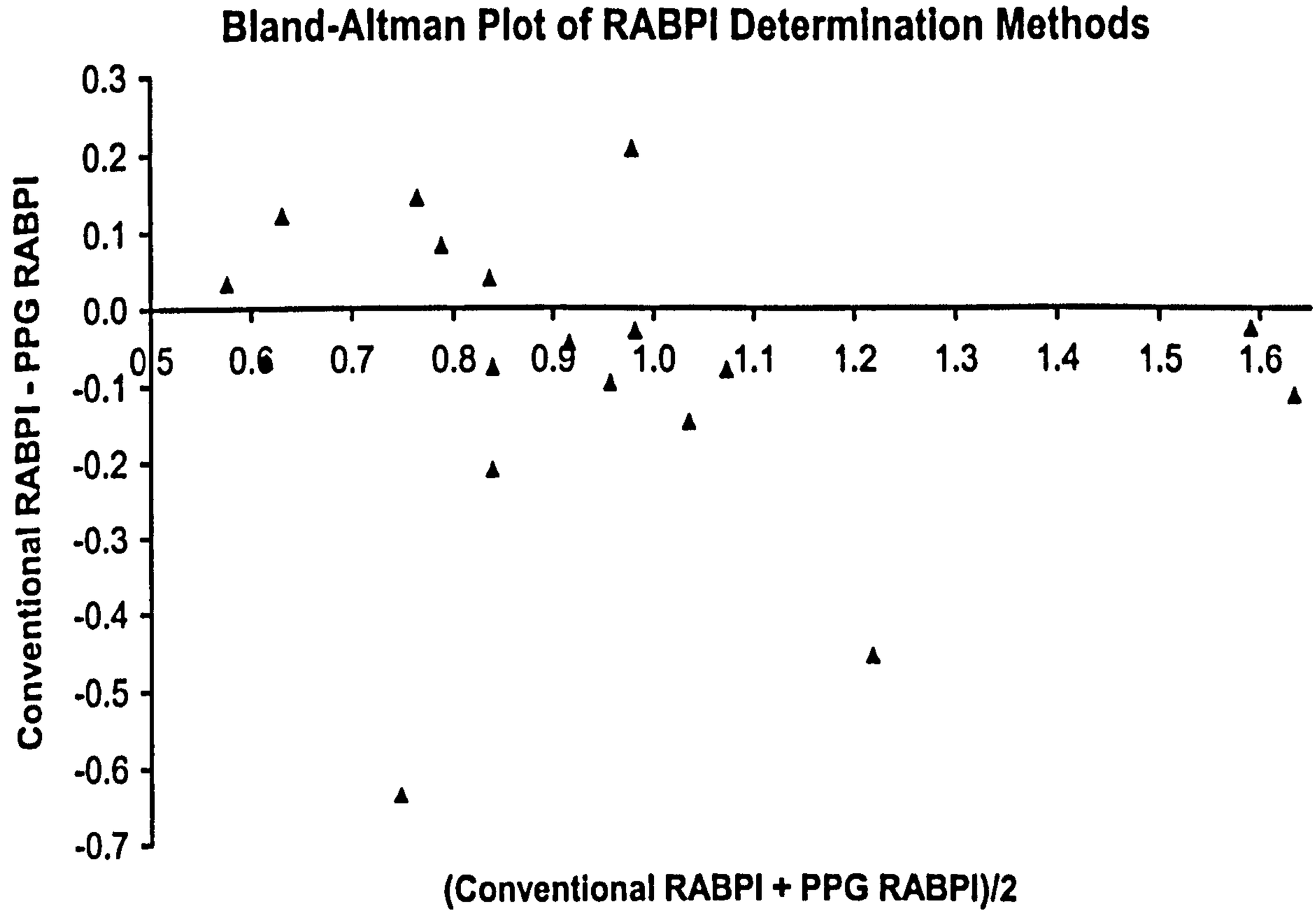

Figure 4-15. RABPI Bland-Altman Plot for conventional and PPG derived Methods.

4.3.2.7 Discussion

As this trial was complex and had several distinct aims, discussion is presented in several section.

4.3.2.7.1 SBP Determination using threshold pulsatile PPG.

Referring to Table 4-8, the automatic SBP produces encouraging results for the small sample set of subjects employed in this study. Post exercise values are especially encouraging, as the mean error differs by only a few mmHg compared to the technician derived SBP values, with similar deviation spreads. Referring to the scatter plots, where Figure 4-8 shows brachial SBP and Figure 4-9 shows foot SBP, it is apparent that a strong correlation is observed between the two methods. Outliers may be attributed to poor probe coupling. Additionally, since this threshold PPG method employs peripheral perfusion, it could be argued that this technique is more sensitive to the localised perfusion of the patient. The possibility exists that patients producing a low PPG derived foot SBP have poor perfusion of the extremities where the PPG probe is placed, but have better perfusion where the Doppler flow probe registers systolic return, explaining the reduced mean SBP values as determined by PPG. This would therefore mean that threshold PPG SBP could identify the onset of PAD before conventional Korotkoff derived ABPI techniques, screening these subjects for further diagnosis such as Duplex Ultrasound Imaging. Further evidence for this hypothesis is provided from the pressure Bland-Altman plots. Both Figure 4-10 and Figure 4-11 consistently show the PPG derived pressure is lower than the conventionally derived pressure readings – much more so in the feet, which can be suffering PAD, than in the arm, which is generally disease free.

Improvements to this study are numerous. A more advanced protocol employing an improved toe probe design and more effective monitoring of cuff pressure, along with more accurate derived conventional SBP values would eliminate most of the technical problems in this study. From this, statistical analysis of large population groups with follow up work over a longer period would confirm the accuracy of this work, identifying if the PPG methodology does indeed give greater sensitivity.

4.3.2.7.2 ABPI Determination using threshold Arterial SBP

Referring to Table 4-9 it is apparent that the statistical results are encouraging. Figure 4-12 shows good agreement between the ABPI values for both pre and post exercise states. The increased sensitivity of the automatic PPG SBP determination has propagated through to indicate lower PPG derived ABPI measurements, as can be

shown in the Bland-Altman plot of Figure 4-14, since the ABPI readings are slightly lower for the PPG derived method. This is significant since the ABPI measurement is defined as the ratio of foot SBP over brachial SBP, and brachial SBP is assumed to remain relatively constant, implying the pressure drop as registered using the Automatic SBP method is more pronounced.

Figure 4-12 also shows that, generally, reduced PPG derived ABPI in the outliers could be attributed to the increased sensitivity of this technique, as the corresponding conventional ABPI values are not so low.

Inspection of the mean RABPI values in Table 4-9 and the scatter plot of Figure 4-13 show an improved correlation when compared to raw ABPI values. This is due to the post exercise pressure drop trend in subjects suffering PAD, and is registered by both conventional and PPG derived ABPI techniques. This is illustrated in the Bland-Altman plot of figure Figure 4-15, since there is no obvious trend for either for the conventional or PPG methodologies.

The enhancement to the SBP procedure to obtain more accurate PPG SBP values, suggested above, would serve to clarify any sensitivity issues, along with a secondary correlation of conventional PAD diagnosis technique.

The correspondence between RABPI in both PPG derived and conventionally derived results could possibly be improved if a more rigid toe better patient interface was employed. These feasibility studies employed a finger probe affixed to the toe, which is far from ideal. After exercise, the probe may have become fractionally dislocated, which could affect the field of view of the probe. A more secure probe to patient interface could be developed which would reduce problems of probe movement. However, this has implications of hygiene problems if an enveloping probe is used. Alternatively, remote PPG could be implemented into this technique in order to determine SBP and thus ABPI without a patient interface.

4.3.2.7.3 FPD and ABPI

The aim of using FPD was to eliminate the requirement for pressure tests when identifying occlusive PAD in the toes. The hypothesis was that subjects suffering occlusive PAD would not display significant perfusion changes in the toe following exercise, whereas healthy subjects would show increased peripheral perfusion in the toe due to dilation of major arteries supplying the lower leg and periphery. Normalisation would be performed using the perfusion level from the finger in order to eliminate any

relative scaling problems, since the finger perfusion level should remain relatively constant.

These results are less encouraging. Table 4-10 details the R^2 error for a linear fit against the ABPI baseline in various states. The low value of the Student T Test in the first two rows indicates the data is statistically significant, whereas the remaining two rows show the data is not.

This trial is therefore inconclusive. The improvements in probe design mentioned above and a larger population set would be needed to confirm whether elimination of the pressure cuff in occlusive PAD diagnosis using PPG is viable.

4.4 Conclusion

This chapter has applied the techniques established previously relating skin and tissue blood perfusion to two separate applications, namely clinical trials and sport science.

This chapter investigated perfusion monitoring of a sport science trial. Two differing exercise states were invoked in the subjects, and the effects on the subject's peripheral vasculature observed. Models and techniques developed in earlier chapters allowed comparative perfusion evaluations using dual channel PPG technology. Both single session and dual session trials were performed, proving the validity of the techniques developed earlier for monitoring perfusion in subjects.

The isometric exercise trial involving monitoring reduced perfusion caused by the action of the forearm muscles constricting arterial vasculature feeding the periphery; comparative evaluations were performed using a reference finger as the normal. The dynamic exercise trial identified two subject groups from a population based, solely on peripheral perfusion changes. When the characteristics of these groups were reviewed, marked differences between the two groups experience and body physiology was observed. Further investigations could be performed using a correlatory technique, such as duplex ultrasound, in order to relate peripheral perfusion changes with arterial changes feeding the major muscle groups.

A novel automatic method of determining SBP in the periphery has been shown, which, is argued, possesses greater sensitivity to the changes in perfusion caused by the onset of occlusive PAD. In addition, the automated system increases accuracy by reducing operator-induced error in determining SBP.

The new method of determining SBP was applied to the technique of diagnosing occlusive PAD in the toes, and compared to the existing standard ABPI measurement method. The new methodology can again be argued to show increased sensitivity, and again reduce errors due to operator variability and subjectivity. This new method for determining toe occlusive PAD severity has the potential to be employed in primary healthcare, offering increased effectiveness and ease of diagnosis without requiring referral to a vascular clinic. This has the possibility to reduce subject inconvenience, and provide immediate diagnosis without the usual delays associated with waiting times and referrals.

An attempt has been made at diagnosing PAD in the toe using only PPG. Here, a dual-channel PPG technology would allow comparative evaluations between the suspected site, the toe, and a known good site, such as the finger. This methodology has the potential to remove the need for sphygmomanometry, and its associated problems, such as aneroid sphygmomanometer calibration and mercury sphygmomanometers toxicity. The assumption was that lower limb exercise would cause increased peripheral perfusion in the case of non-claudicants, with claudicants showing reduced perfusion. Initial results have proved inconclusive, necessitating further work. Suggestions for developments and improvements to both protocol and equipment have been made, with employment of remote PPG being ideal, since this would eliminate both patient-probe interface and hygiene problems, as well as enhancing the usability of the system by providing reduced diagnosis time.

This chapter has shown the perfusion techniques developed earlier regarding single and dual channel PPG may be successfully applied in differing methodologies. Dual channel PPG is especially interesting since the applications of this technique are only just becoming apparent. No-doubt other normalisation techniques will be developed, but essentially the comparative evaluatory technique is a significant novelty of this thesis. Dual channel perfusion monitoring, coupled with the forward and inverse pressure based models discussed in the following chapter, have the potential for making PPG a valuable tool in assessing both vascular perfusion and health in many differing applications.

4.5 Chapter References

[1] Allen J, Murray A, "Similarity in bilateral Photoplethysmography peripheral pulse wave characteristics at the ears, thumbs and toes", Physiol. Meas., 21, pp.369-377 (2000)

[2] Matlab, The Mathworks Inc, 1999

[3] Ifeachor E.C, Jervis B.W., "Digital Signal Processing – A Practical Approach", 2nd Ed, Addison Wesley, Massachusetts, USA (1993)

[4] Oppenheim, A.V., Schafer R.W., "Discrete-Time Signal Processing", Englewood Cliffs, NJ: Prentice Hall, pp. 311-312 (1989)

[5] Kellogg D.L, Johnson J.M, Kosiba W.A, "Competition between the Cutaneous Active Vasoconstrictor and Vasodilator Systems during Exercise in Man", Am. J. Physiol., 261 (Heart. Circ. Physiol.), H1194-1189 (1991)

[6] Benzinger, T.H., "On Physical Heat Regulation and the Sense of Temperature in Man", Proc. Natl. Acad. Si. USA, 45, pp.645-649 (1959)

[7] Bevegard, B.S., Shepherd J.T., "Reaction in Man of resistance and capacity vessels in Forearm and Hand to Leg Exercise", J. Appl. Physiol. 21, pp. 122-132 (1966)

[8] Taylor W.F., Johnson J.M., Kosiba W.A., Kwan C.M., "Graded Cutaneous Vascular Responses to Dynamic Leg Exercise", J. Appl. Physiol., 64, pp. 1803-1809 (1988)

[9] Tschakovsky M.E, Shoemaker J.K, Hughson R.L, "Vaso-dilation and Muscle Pump Contribution to Immediate Exercise Hyperemia", Am. J. Physiol, 271, H1697-H1701 (1996)

[10] Laughlin, M.H., "Skeletal Muscle Blood Flow Capacity: Role of Muscle Pump in Exercise Hyperemia", Am. J. Physiol., 253, H993-H1004 (1987)

[11] Folkow, B.U., Haglund U, Jodal M., Waaler B.A., "Blood Flow through Limb Muscles during Heavy Rhythmic Exercise", Acta. Physiol. Scand., 81, pp.61-72 (1970)

[12] Kamiya A., Daisaku M, Qi F, Yuki N, Satoshi I, Tadaaki M, Akio S, "Static handgrip exercise modifies arterial baroreflex control of vascular sympathetic outflow in humans", Am. J. Physiol. Regulatory Integrative Comp. Physiol, 281, R1134-R1139 (2001)

[13] Kilbom A, Brundin T., "Circulatory Effects of Isometric Muscle Contractions, Performed Separately and in Combination with Dynamic Exercise", Eur. J. Appl. Physiol, 36, pp. 7-17 (1976)

[14] Taylor W.F., Johnson J.M., Kosiba W.A., "Cutaneous Vascular Responses to Isometric Handgrip Exercise", J. Appl. Physiol., 66, pp. 1586-1592 (1989)

[15] Taylor W.F., Johnson J.M., Kosiba W.A., "Roles of Absolute and Relative Load in Skin Vasoconstrictor Responses to Exercise ", J. Appl. Physiol. , 69, pp. 1131-1136 (1990)

[16] Smolander J, Aminofdf T, Korhonen I, Tervo M, Shen N, Korhonen O, Louhevaara V, "Heart Rate and blood pressure responses to isometric exercise in young and older men", Eur. J. Appl. Physiol. Occup. Physiol, 77(5), pp. 439-444 (1998)

[17] Kamiya A, Daisaku M, Qi Fu, Niimi Y, Iwase S, Mano T, Suzumura A, "Static handgrip exercise modifies arterial baroreflex control of vascular sympathetic outflow in humans", Am J Physiol Regulatory Integrative Comp Physiol, 281, R1134-R1139 (2001)

[18] Bystrom S.E., Kilbom A., "Physiological response in the forearm during and after isometric intermittent handgrip", Eur. J. Physiol. Occup. Physiol., 60(6), pp.457-466 (1990)

[19] König D, Huonker M, Schmid A, Halle M, Berg A, Keul J, "Cardiovascular, metabolic, and hormonal parameters in professional tennis players", Med. Sci. Sports Exerc., Vol. 33(4), pp. 654-658 (2001)

[20] Margonato V, Roi G.S., Cerizza C, Galdabino G.L., "Maximal Isometric force and muscle cross-sectional area of the forearm in fencers", J. Sports Sci, 12(6), pp. 562-572 (1994)

[21] Nielson P.E., Pulson H.L., Gyntelberg F., "Arterial Blood pressure in the skin measured by photoelectric probe and external counter-pressure", Vasa, 3, pp. 65-74 (1973)

[22] de Boor, C, "A Practical Guide to Splines", Springer-Verlag New York (1978)

[23] Cameron A.E.P, Porter A., Rosser S., da Silva A.E.C., "A new device for the assessment of claudication", Br. J. Surg. Vol. 84, Supp.1 (1997)

[24] Manning B.J., McGreol G., Crowles H, "Prospective comparison of conventional treadmill testing with pedal ergometry in patients with suspected claudication ", Br. J. Surg, Vol. 87, Suppl 1 (2000)

[25] Altman D.G., Bland J.M., "Measurement in Medicine: the Analysis of Method Comparison Studies", The Statistician, 32, pp. 307-317 (1983)

Optical Engineering Group
Loughborough University

Chapter Five

Lumped Parameter Trials

5 Lumped Parameter Pressure and arterial PPG.

Chapter two introduced the lumped parameter pressure model, and illustrated how this model could be applied to an arterial PPG waveform. Numerical fitting of the forward model allows indirect determination of quantitative vascular parameters for the connective arterial vasculature between the heart and the probe location.

Chapter three introduced the inverse lumped parameter model, developed from the solution of the forward lumped parameter model. This technique developed a timing interval between significant features of the arterial PPG waveform, with the chosen implementation allowing direct determination of peripheral compliance. Sensitivity analysis was performed, showing how variations in the forward model solution parameters can affect the inverse model results.

The concept of dual channel comparative testing was also introduced in chapter three. Simulation was performed in order to investigate the effects of changes in forward model parameters on both the timing interval and also comparative results, as applied to both symmetric and asymmetric probe placement schemes.

This chapter will apply the techniques developed in chapters two and three, namely the lumped parameter forward and inverse models, along with parameter based comparative evaluation. A pilot study with known subject characteristics will have numerical fits performed on their pulsatile PPG data, and the inverse model timing interval will be determined for the same pulsatile PPG data. A further study with a larger population containing both diseased and healthy subjects will also be investigated, with the aim of determining the effects of PAD on vascular parameters.

5.1 Common Methods Applied to Numerically Fitting the Lumped Model

Since this chapter is exclusively devoted to trials employing the lumped parameter forward and inverse model, as applied to real data, common equipment and analysis techniques are presented here in order to avoid repetition.

5.1.1 Equipment

The equipment and initial analysis techniques are identical to the equipment and methods as described in section 4.4.1. To recap, a dual channel PPG system, termed WinPPG, specifications of which are given in the appendix B was employed to record PPG waveforms simultaneously in up to two locations. The WinPPG system offered full

control of source intensity and PPG gains, recording dual channel data using 16-bit quantisation onto a PC hard disk with a variable sample rate. PPG probes were standard Viamed pulse oximetry probes, applied to the index finger or second toe.

Initial analysis was performed using the Matlab[1] programming system. Digital filtering of both AC and DC channels, corresponding to arterial and venous PPG, was performed in order to reduce the effects of artefacts. Normalisation was performed using the procedures developed in section 4.1.1 to eliminate the effects venous changes on the arterial PPG waveform.

Once a filtered, normalised arterial PPG waveform was obtained, from either one or both locations, the waveform periodicity was identified using the algorithm described in Appendix A. This allowed the identification of individual peaks and troughs of each cardiac cycle, and thus the extraction of the diastolic portion of the PPG waveform for each pulse. Each diastolic pulse waveform was truncated at the point where the waveform was no longer monotonically decreasing, in order to reduce the effects of baseline wander. The diastolic portion of each cycle to be analysed was normalised by removing any offset, then scaled so the waveform was between zero and unity. This scaling and offset removal, as discussed in chapter two, does not affect the forward model numerical fit nor does it affect the inverse model, since they are both insensitive to scaling effects.

5.1.2 Analysis - Fitting

Each diastolic section of the pulsatile PPG waveform was then fitted using a 7-parameter equation, as first proposed in chapter two, which is the solution to the lumped parameter forward model, shown in equation [5.1].

$$P(t) = a_1 + a_2 \exp(-a_3 t) + a_4 \exp(-a_5 t)\cos(a_6 t - a_7) \qquad [5.1]$$

From the parameters of the forward model, the normalised vascular parameters shown in equation [5.2] may be calculated, assuming peripheral compliance is much smaller than major compliance. As stated, these parameters are normalised with respect to peripheral resistance R_P, and have units of seconds.

$$\frac{L}{R_P} = \frac{(a_3 + 2a_5)^2}{2a_5\left([a_3 + a_5]^2 + a_6{}^2\right)}$$

$$R_P C_M = \frac{2a_5\left([a_3 + a_5]^2 + a_6{}^2\right)}{a_3(a_3 + 2a_5)\left(a_5{}^2 + a_6{}^2\right)} \qquad [5.2]$$

$$R_P C_P = \frac{1}{(a_3 + 2a_5)}$$

A Nelder-Mead[2] simplex search algorithm was used to implement the numerical fit using the error between the real, diastolic PPG waveform and a synthetic diastolic PPG waveform generated using the supplied seven a_l parameters of the forward model. This algorithm does not require derivatives, since a cost-function produces a dimensionless error array in N, in this case seven (a_1 to a_7), dimensions, and the a_l parameters producing minimum error returned, based on supplied starting parameters from which the algorithm searches around. A significant advantage of the Nelder-Mead minimisation method is its ability to handle non-linearities and discontinuities in the error space. This facility is necessary if the coefficients are to be bounded, in order to ensure the solution does not converge on error minima that are physiologically unrealisable. Although it may be argued that quicker, more elegant numerical optimisation algorithms are available, this was immaterial since off-line processing was performed.

Previous implementations of the fit algorithm reported in the literature[3] used a simple error function between the synthetic (obtained from the passed parameter coefficients of the model) and actual diastolic portion of the pressure waveform. However, tests performed using this technique resulted in sub-optimal fits. Any minor oscillation present in the lower portion of the PPG curve formed a small component of the overall error, when using simple error functions. These minor oscillations are significant, since observation of equation [5.2] shows the oscillatory component of the diastolic waveform is involved in two of the three lumped parameter values. Figure 5-1 shows a typical fit using an RMS error function; the slight variation in the real hypertensive waveform at around $t = 0.25$ shows the synthetic waveform does not accurately follow this trend correctly, despite the similarities around main peak of the waveform, therefore producing low error. For the normotensive waveform, the oscillatory component is fitted with relative accuracy because the dichrotic notch forms a significant feature in the waveform.

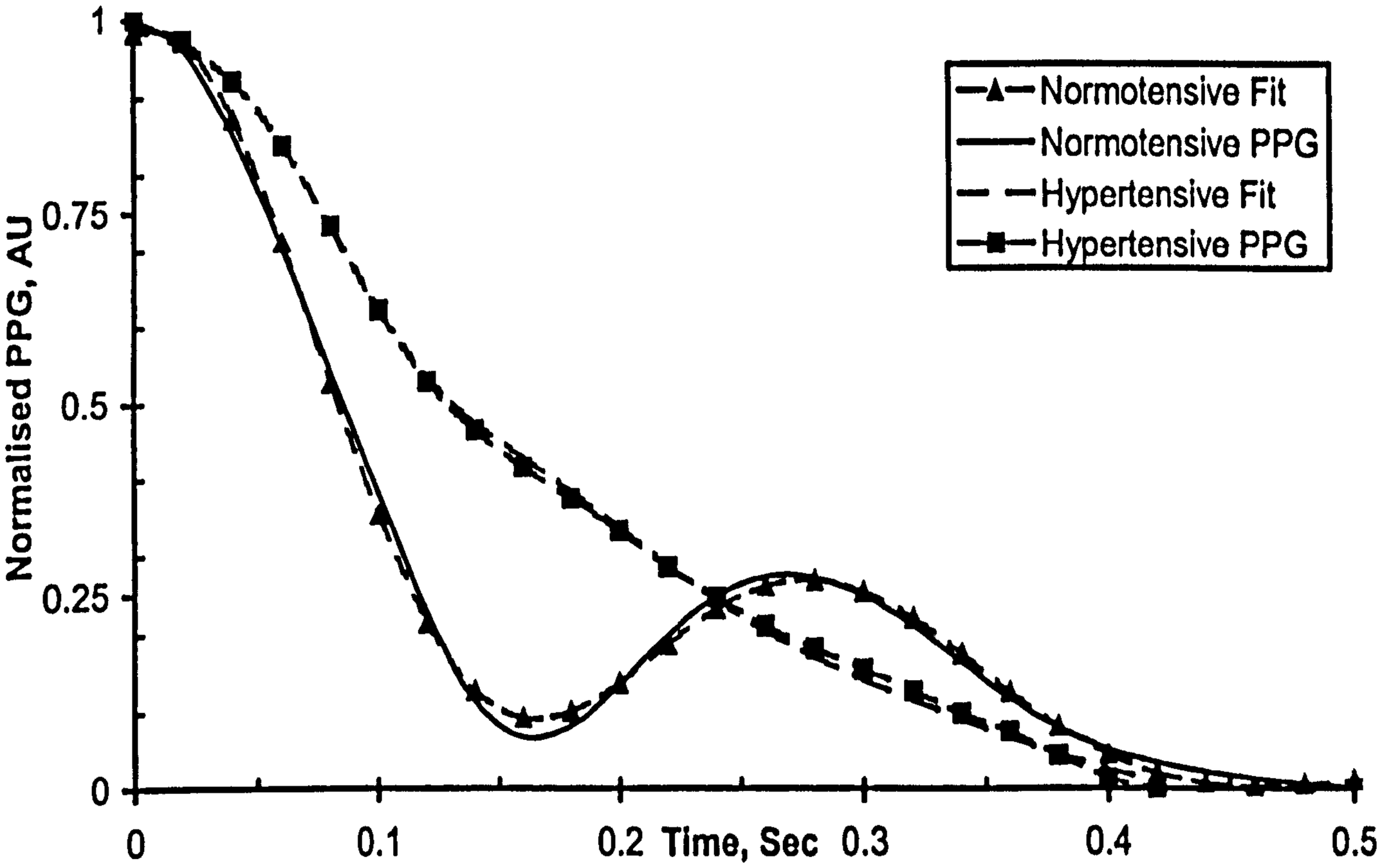

Figure 5-1. Fitted data for normotensive and hypertensive subjects.

The a_1 parameter set produced from the hypertensive fit has appropriate values for all forward model parameters apart from the oscillatory frequency component a_6 and oscillatory decay a_5, which may be highly inappropriate.

Referring to equation [5.2] the oscillatory component a_6 has a dominant effect in determining normalised inertance; inertance could prove instrumental in both symmetric and asymmetric comparative evaluations, as discussed in chapter three, so it is imperative to attain an accurate value. Additionally, errors in the decay for the oscillatory component a_5, which will be affected by inaccuracies in the oscillatory frequency, will further compound errors, both in normalised inertance and also by introducing error in normalised peripheral compliance.

To counteract this, a novel error function was developed, specifically designed to highlight the forward model parameters responsible for obtaining vascular parameters. In the novel error function, the diastolic waveform is split into the component parts of waveform, based on superposition assumption.

In addition to insensitivity to crucial curve features, a simple error cost function does not evaluate the effects of the parameters being fitted. For example, in this case the peripheral compliance should always be smaller than the major compliance, due to the mechanical properties and dimensions of the large arteries compared with the small

arteries modelled by the lumped peripheral compliance. It is conceivable that the solution will converge on a region of values that, though fitting the diastolic waveform with low error, will results in a_i values producing physiologically unrealisable lumped parameters; for example, a physically unrealisable solution could be if the resulting peripheral compliance is larger than the major compliance. If the starting values are poor, then the Nelder-Mead algorithm will produce results that are a relatively poor fit. Convergence still occurs as, although the error is large, a fit may still be found by searching which produces less error than the starting values supplied – termed local-minima. Incorporating bounds within the error function to check the parameters against typical subject physiology and to check against poor starting values ensures more reliable data fits will occur.

Referring to equation [5.1], the diastolic portion of the PPG waveform is modelled using three components: a static term, represented by a_1, the dominant decay term, modelled using forward model parameters a_2 and a_3, and the exponentially decaying oscillatory component term, modelled using the remaining a_4 to a_7 forward model parameters. To separate the real diastolic waveform into its fundamental components, the novel error function subtracts both the synthetic offset a_1 and the synthetic dominant decaying component, modelled using a_4 to a_7, from the real diastolic PPG data series. The resultant residual waveform should be the oscillatory component term of the real diastolic waveform. The component parts of this algorithm are shown in Figure 5-2, with the diastolic portion, the dominant decay and residual error showing the principles of the algorithm.

The novel error function returns the sum square error between the residual diastolic portion (which should be the decaying oscillatory component for the actual vasculature under investigation) and the decaying oscillatory component of the synthetic waveform, generated using passed a_4 to a_7 forward model parameters. This algorithm gives greater sensitivity to the shape of the oscillatory component of the diastolic waveform; resulting in more accurately derived vascular parameters. The dominant diastolic portion of the waveform is also correct since any errors in the dominant portion will have a marked effect on the residual proportion of the diastolic waveform after subtraction. In this case, poor dominant parameters a_2 and a_3 will result in an error value that is mainly a function of the dominant decay parameters.

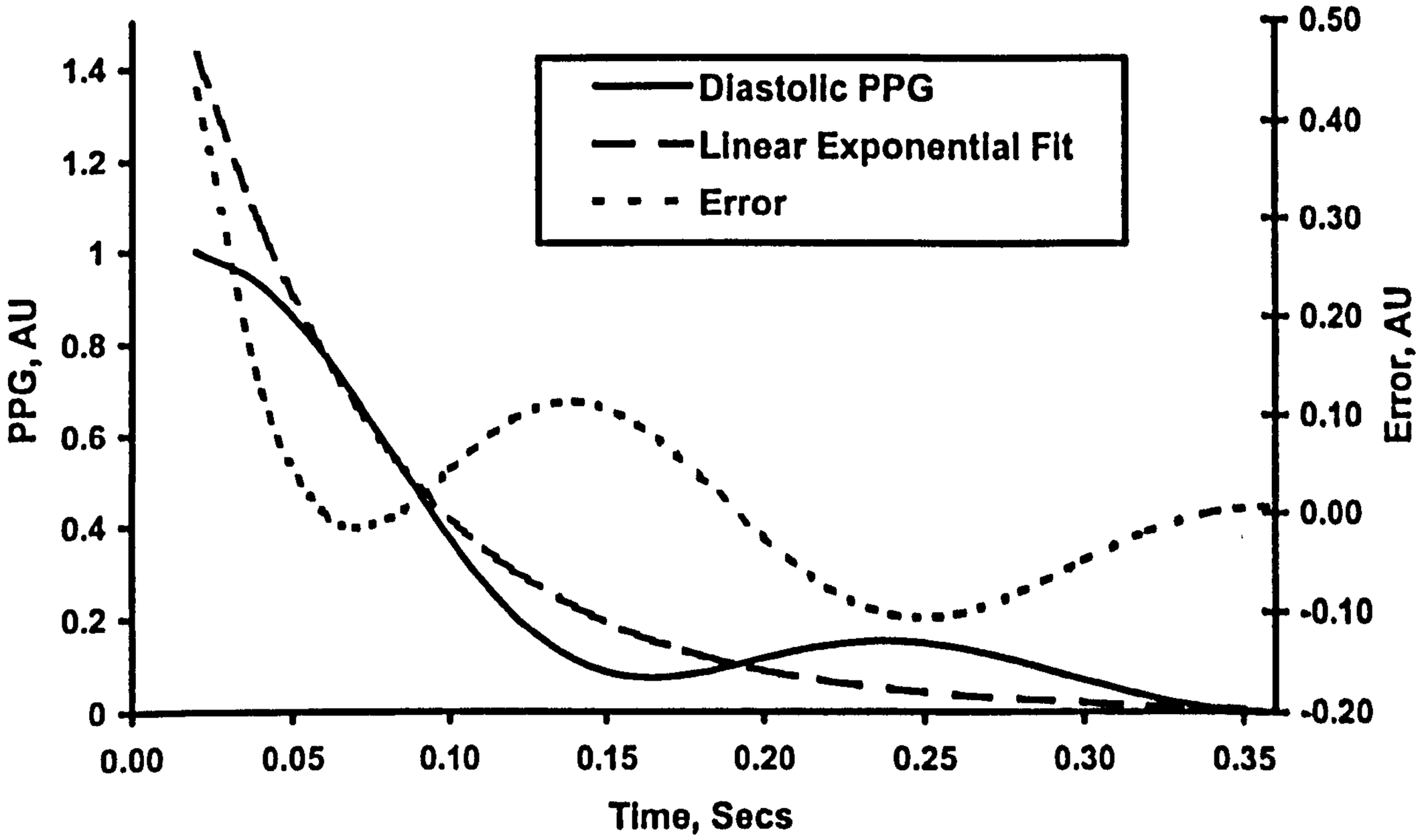

Figure 5-2. Diastolic portion of PPG waveform, Linear fit and residual error.

5.1.3 Analysis – Starting Parameters

All 'fit' functions require good (i.e. close to actual) initial values for starting conditions in order to ensure accurate convergence – obviously, an arbitrary fit must search through an infinite number of individual parameters. In this application, there are seven parameters, thus seven dimensions and therefore seven infinities. The Nelder-Mead simplex search is especially sensitive to starting parameters, since the algorithm does not require a rate of change of error function, therefore the algorithm can converge on local error minima. Consequently, it is essential that good initial estimates of starting parameters are used, so the iterative nature of the simplex search can find a minima in the novel error function as discussed.

If only occasional diastolic PPG waveforms are to be fitted, then manual assignment of starting parameters may be employed, based on the physiological limitations described above. However, this approach is wholly unsatisfactory for an automatic system or where many pulses are to be analysed, so an algorithm must be developed which will provide satisfactory starting values. This section described the algorithm adopted during this thesis for starting values.

As stated, the PPG waveform is normalised by the removal of any offset then scaled to lie within zero and one. The normalisation process assists the determination of starting

parameters, as limits are placed on the magnitude of the various scaling components. Taking the natural logarithm of the diastolic portion of the PPG waveform allows a linear least squares straight line fit to be approximated to the PPG waveform. The resultant straight-line fit parameters are then converted to anti logarithm i.e. exponential form, in order determine the dominant oscillatory component magnitude and decay time constants, a_2 and a_3 respectively. Two of the seven forward model a_i parameters are therefore now approximately defined.

Subtracting the synthetic exponential fit from the PPG waveform will produce a difference residual waveform, based on the contribution of the decaying oscillatory component. The timing interval between peaks will give an approximate indication of oscillatory component, a_6. The magnitude of the oscillatory component, a_4, may be inferred by the magnitude of the error waveform. Inspection of Figure 5-2 shows typical waveforms obtained during the starting parameter determination algorithm.

The decay time constant of the oscillatory component, a_5, may be inferred by following the magnitude trend of the error waveform, giving an approximate indication of the value.

The remaining component, a_7, which is the phase of the oscillatory component, may be deduced by examining the positioning of the error waveform peaks from time $t = zero$.

Although this technique may seem a protracted method for obtaining reasonable starting parameters for the Nelder-Mead search fit, only a minimal number of calculations are required to derive acceptable starting parameters. As previously described, good starting parameters are required in order to achieve optimal convergence. The novel error function, described above, employs similar principles to the starting parameter determination algorithm just described.

5.2 Lumped Pilot Study

As the proposed idea of employing models derived for the purpose of analysing pressure pulse waveforms is novel and has never previously been applied to arterial PPG, a pilot study was conducted in order to evaluate this technique. The technique of numerically fitting a model to invasive pressure curves has been previously demonstrated[3] when a pilot study involving normotensive and hypertensive subjects was conducted. Here, the arterial PPG waveform obtained from the brachial artery was analysed using the lumped parameter fit technique, and observations on these results made.

Performing a pilot study with numerical fitting of the pulsatile PPG waveform, taken from the fingertip of both normotensive and hypertensive subjects, would allow comparison between any results obtained from the PPG study with the results obtained from the pressure study literature.

The concept of symmetric and asymmetric comparative testing using dual channel PPG was introduced in chapter three, with several hypothetical scenarios being presented in order to analyse the sensitivity of this technique. An evaluation of this technique using real subjects, rather than simulations, would determine the validity of this process. Therefore, simultaneous dual channel arterial PPG recordings were obtained in order to determine vascular parameters from multiple sites. The effects of symmetric and asymmetric sites on vascular parameters and the inverse model timing interval, developed earlier, could be compared by observing results obtained from finger and toe probes and dual finger probes for asymmetric and symmetric evaluations respectively. Additionally, the effects of aging on the arterial vasculature of subjects could be observed by comparing vascular parameters obtained from both elderly and young subjects.

5.2.1 Lumped Pilot Study Overview

To test the premise of applying numerical fits of the pressure derived forward model to arterial PPG waveforms, several subject groups had arterial PPG waveforms analysed using the pressure derived forward model described previously. Several subject groups were investigated, with differing aims.

To investigate the effects of hypertension on vascular properties, a subject group had PPG waveforms recorded. The group comprised four (treated) hypertensive subjects (SBP mean 183 SD 3.2 mmHg) and four aged matched normotensive subjects (SBP mean 139 SD 2.1mmHg). All subjects had arterial PPG recordings taken from the index finger of one hand, and vascular parameters derived from this recording.

To test the validity of extending the single channel lumped constant model to dual channel PPG, a trial was performed on the both left and right hands of four male normotensive subjects, who were tennis players. The purpose of the study was to observe variance between parameters of the lumped constant model in near identical sites. The subjects mean weight was 82.75kg SD ±9.3kg, mean height 183.75cm SD ±10cm. The subjects (mean age 28.5 SD 3.1 years, mean BMI 24.5) were assumed healthy without any reported vascular complications. With identical probes placed on

matching measuring sites, it was expected similar vascular parameters (though not identical due to some adaptation of the dominant arm) would be obtained.

To investigate the effects of differing measurement sites on vascular parameters obtained using dual channel PPG, a trial was performed using group of four normotensive subjects who had asymmetric arterial PPG recordings taken simultaneously from the index finger and toe. Differences in vascular compliance and inverse model timing interval were especially of interest.

The average age of the normotensive/hypertensive group and finger/toe group was more than 60 years old, with the dual channel tennis players average age being approximately half this. Additionally comparisons could therefore be performed between vascular parameters derived from the index finger of the elderly groups and the vascular parameters derived from the index fingers of the tennis players. Comparison of vascular parameters between subject groups should show the effects of aging on the vascular parameters.

5.2.2 Aim

The pilot study had four main aims, using three subject groups.

1. To observe the effects of hypertension on vascular parameters. To do this, age matched normotensive and hypertensive subject groups (four in each group) will have a single channel PPG taken from their index finger. From the PPG recording, vascular parameters will be derived and compared.
2. To observe the degree of similarity of vascular parameters obtained from identical sites. To do this, four normotensive subjects will have a dual channel arterial PPG taken simultaneously from both index fingers. From these PPG recordings, vascular parameters will be derived and compared.
3. To observe the degree of similarity of vascular parameters obtained from differing sites. To do this, four normotensive subjects will have a dual channel arterial PPG taken simultaneously from the both index finger and toe. From these PPG recordings, vascular parameters will be derived and compared between the two sites.
4. To observe the effects of aging on vascular parameters. By comparing vascular parameters derived from the PPG recording obtained from the index finger of

two normotensive groups, one young and one old. Vascular parameters derived from the PPG recording will allow comparison between age groups.

The normotensive tennis player group did not have brachial blood pressure taken, but were known to be normotensive after discussion with each subject. Additionally, the subjects performing the hand and foot evaluations were normotensive but had mild PAD, as the foot pressures show. The effects of this must be considered when evaluating any results.

5.2.3 Protocol

As several subject groups were analysed, several slightly differing protocols were required. The common methods between trials are discussed first.

All subjects gave informed consent for the trials. The studies conformed to the Declaration of Helsinki set by the World Medical Association. Ethical approval for the clinical studies was obtained from the UHL Ethical comitte.

The toe and finger probes were Viamed P856 pulse oximetry probes, wavelength 956nm. The probe was located on the index finger where required, or the 2nd toe, in both cases the illuminating LED facing the nail matrix. During the recording period, the hands were held in a relaxed position whether resting on a desk at approximately heart level for the tennis players, or laying beside the prone subject otherwise; in both circumstances palms facing downwards. The subject relaxed for several minutes before recording began, in an attempt to reduce subject anxiety. The ambient temperature during recording was approximately 22°C. Any restrictions around the wrists and arms or leg, such as watches or bracelets or socks/stockings were removed before the recording. The subjects were asked to remain motionless and refrain from speaking during the duration of the recording. The PPG system was a proprietary 16 bit unit designed and built in the Optical engineering group, detailed in section 4.1.1, full specifications of which are given in appendix B. The sampling rate was 50Hz, and a hard disk recording mechanism was employed for each of the channels. The controlling laptop PC was situated so that the subject could not see any recording traces, again in an attempt to reduce subject anxiety.

1. To obtain the symmetric dual channel PPG recording, four subjects (tennis players) each had a 3-minute PPG recording taken simultaneously from the index finger of both hands. The shaded recording area was situated outdoors away from any obvious wind draughts. Common gain and LED setting was employed for all subjects. The subject sat motionless during the recording period; at the end of which the subject removed the finger probe and left.

2. The normotensive/hypertensive and asymmetric dual channel finger/toe studies followed very similar protocols. Eight subjects, four normotensive and four hypertensive, were involved in the normotensive and hypertensive trial. Four normotensive subjects were involved in the asymmetric finger/toe trial. All subjects reclined on a standard medical couch in a temperature-controlled room. Each subject reclined on a couch for approximately 2 minutes prior to recording to relax, during which the PPG probes were attached, to either the index finger alone in the case of normotensive/hypertensive subjects or finger and toe for asymmetric dual channel subjects. To help reduce movement artefact, the cable of the PPG probe was taped to the dorsum of the foot or back of the hand using surgical tape. The subject reclined with legs outstretched during the PPG recording. The PPG system recorded the PPG for one minute; following recording SBP was determined using a Doppler Ultrasound probe (instead of a stethoscope) to detect blood flow return. The Doppler probe is generally more sensitive to blood flow return when compared to the stethoscope, especially when monitoring the small arteries in the feet. In the case of brachial pressure determination, the occluding cuff was placed around the forearm, and the Doppler probe applied to the radial artery, with standard cuff inflation and deflation following the Korotkoff procedure. Pressure determination in the feet was conducted with the cuff placed around the calf, just above the ankle. SBP was determined three times using the dorsalis pedis artery, posterior tibial and peroneal artery. Recorded foot SBP was determined as the mean of the three arterial SBP values.

5.2.4 Analysis

The arterial PPG waveform was normalised as described in chapter two, to reduce the effects of venous blood volume changes. A continuous sequence of five pulsatile events were extracted from approximately the centre of each data run, when the subject had relaxed into the protocol. If dual channel PPG was employed, the same continuous sequence of pulses was employed for both channels. The diastolic portion of each pulsatile waveform was identified using the algorithm described in appendix A and a seven parameter numerical fit using the solution of the third order pressure model described in equation [5.1] above was numerically fitted to the diastolic portion of the PPG curve. A Nelder-Mead fitting algorithm, using a novel error function described previously, formed the error between the synthesised and real data set, in order to determine a solution set for the supplied data. Hard limits were implemented into the algorithm to prevent any negative coefficients and also reduce the likelihood of non-physiological parameters, such as complex results, inappropriate values and such.

Once the coefficients of the diastolic portion of the PPG curve were determined, the mean over the five pulses was taken to reduce parameter instability. To obtain physiological parameters from the forward model solution obtained by fitting, the equations shown in equation [5.2] were used to determine the inertance, major and minor arterial compliances, all normalised with respect to peripheral resistance.

The same forward model parameters were used in the expression developed for the lumped inverse model to form a timing interval for the significant events, as developed in chapter three, in this case using gradient peaks as the significant events. Comparisons of the timing interval of the various subject groups and fitted vascular parameters will establish the viability of the timing interval metric as a useful inverse model.

5.2.5 Results

Table 5-1 shows the mean and standard deviation for the both solution and model parameters obtained from the mean of the numerical fits to all subjects in each case. Also shown is a measure of the quality of fit of the synthesised PPG waveform, taken as one minus the correlation coefficient (ρ) multiplied by 100. Additionally, the derived forward model parameters $C_M R_P$, $C_P R_P$ and timing interval Δt were plotted on a chart with standard deviation for all subject groups, shown in Figure 5-3.

Table 5-1. Pilot Study Lumped significant parameters.

Parameter	Tennis Players				Clinical Index Finger				Clinical Finger/Toe			
	Right		Left		Normotensive		Hypertensive		Finger		Toe	
	Mean	SD	Mean	SD	Mean	SD	Mean	SD	Mean	SD	Mean	SD
a_3 ,s	4.34	1.63	4.68	1.23	7.88	1.05	5.45	0.69	8.01	1.08	7.29	2.64
a_5 ,s	5.52	0.54	5.61	0.98	9.23	0.81	10.17	1.39	9.49	1.13	9.39	1.9
a_6 ,s	22.99	1.44	23.72	0.89	24.43	2.24	33.86	5.48	24.38	2.23	29.3	9.36
$C_M R_P$,s	0.23	0.12	0.19	0.08	0.12	0.01	0.16	0.02	0.12	0.01	0.14	0.04
$C_P R_P$,s	0.066	0.009	0.064	0.009	0.038	0.004	0.039	0.004	0.038	0.005	0.039	0.005
L/R_P ,s	0.034	0.007	0.034	0.005	0.042	0.005	0.025	0.007	0.043	0.005	0.036	0.016
Δt ,s	0.28	0.02	0.27	0.01	0.27	0.02	0.2	0.03	0.27	0.02	0.24	0.05
P, mmHg	Na				139	2. 1	183	3.2	138.8	2.2	108.9	8.6
100*(1-ρ)	0.1127	0.1845	0.1483	0.2399	0.0474	0.0471	0.0677	0.0607	0.0419	0.0467	0.1899	0.2331

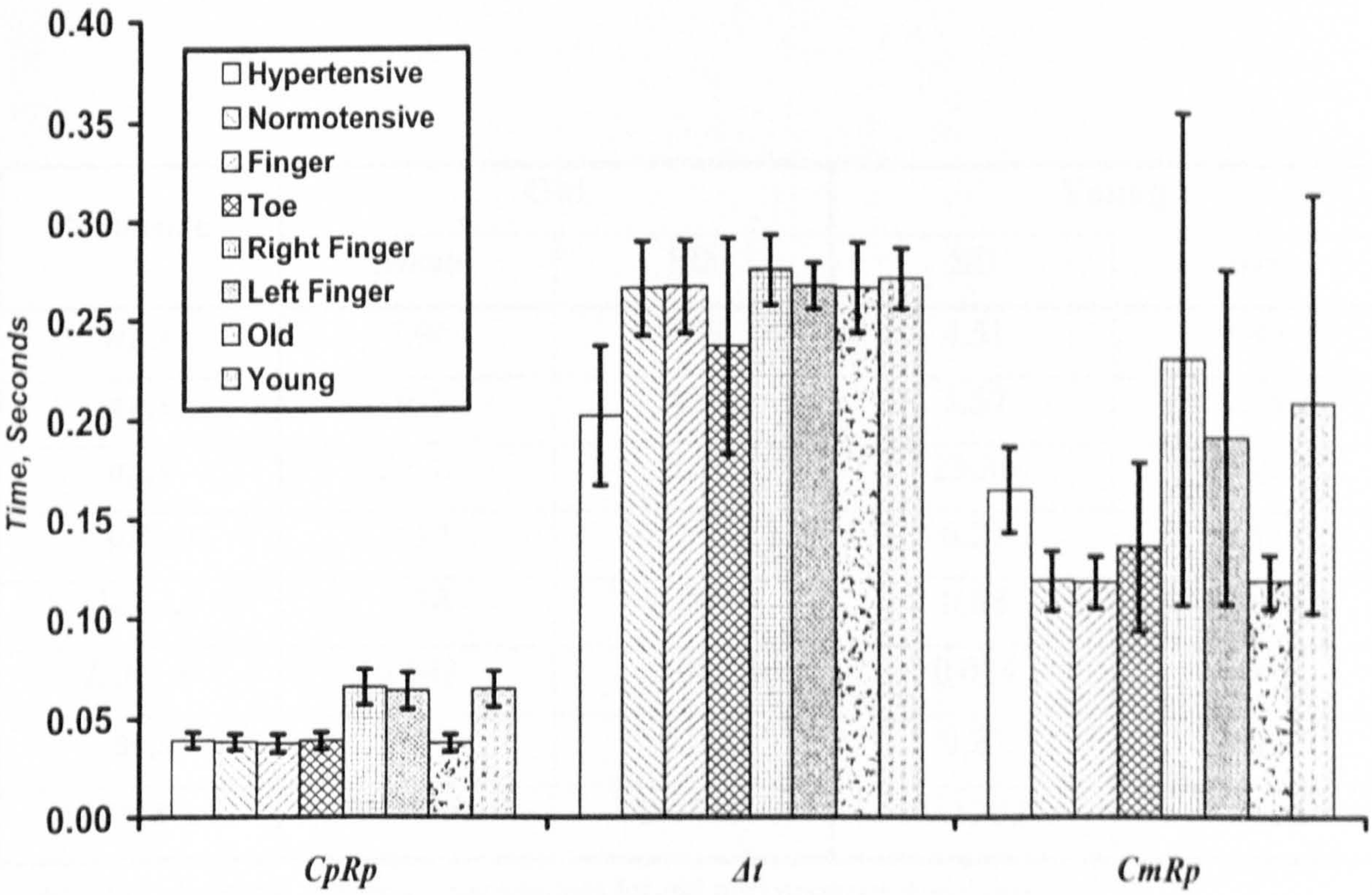

Figure 5-3. Lumped Trial Significant Parameter plot.

To compare the effects of ageing on both the vascular parameters and the timing interval, a set of typical vascular parameters was generated from the mean of the data from the tennis players index fingers, representing young subjects, and the mean of both the normotensive subjects and the finger data from the finger/toe subjects, who were approximately twice the age. These results are shown separately in Table 5-2.

Table 5-3 shows the ratios of the mean significant parameters. For the ratio measurement, the denominator was taken as the reference value, since the numerator was expected to change. For the tennis players, the numerator was the right hand, as adaptation may be present. Hypertensive subjects were expected to have differing vascular characteristics compared to normotensive subjects. For the comparative finger and toe, the finger was made the reference.

Parameter	Old		Young	
	Mean	SD	SD	SD
a_3 ,s	7.96	1.03	4.51	1.43
a_5 ,s	9.4	0.99	5.57	0.79
a_6 ,s	24.41	2.2	23.36	1.23
$C_M R_P$,s	0.12	0.1	0.21	0.11
$C_P R_P$,s	0.38	0.004	0.65	0.009
L/R_P ,s	0.043	0.005	0.034	0.006
Δt ,s	0.27	0.02	0.27	0.02
100*(1-ρ)	0.04465	0.0469	0.1305	0.2122

Table 5-2. Average significant parameters for old and young subject groups.

Ratio	$\frac{Right}{Left}$	$\frac{Hypertensive}{Normotensive}$	$\frac{Toe}{Finger}$	$\frac{Old}{Young}$
$C_M R_P$	1.21	1.39	1.15	0.57
$C_P R_P$	1.03	1.02	1.04	0.58
L/R_P	1.02	0.583	0.85	1.25
Δt	1.03	0.76	0.89	0.98

Table 5-3. Lumped Pilot Study Mean Significant parameter ratios.

5.2.6 Lumped Pilot Study Discussion

The lumped pilot study was undertaken to investigate the technique of applying the lumped parameter forward model numerical fit, developed in chapter two, to the diastolic portion of the arterial PPG waveform. In addition, the feasibility of applying the lumped parameter inverse model, developed in chapter three, to arterial PPG waveforms was also to be determined. Finally, the effects of extending both techniques to dual channel simultaneous arterial PPG was to be investigated.

To fully scrutinize the effects of differing subject physiology on both the numerical fit and inverse model, several subject groups were analysed. Clear aims were established for each group before analysis in order to cohere any derived results. In order to evaluate these aims, comparison by inspection of absolute vascular parameters between differing subject groups was performed. Additionally, ratios of significant parameters for the groups were determined, in order to evaluate the dual channel technique. Ratiometric comparison may be performed assuming similarity of parameters in identical probe placement sites, simplifying interpretation of results, as discussed in chapter three.

5.2.6.1 The Effects of Hypertension on Lumped Parameter PPG

The first aim was to observe the effects of hypertension on the vascular parameters of subjects. Two groups of age matched elderly subject had arterial PPG recordings taken, which were then numerically fitted in order to establish the vascular parameters. The timing interval was determined using diastolic gradient peaks. Examining Table 5-2 shows the lumped normalised parameters for the normotensive and hypertensive subjects. Ratios between hypertensive and normotensive subjects for the lumped model parameters are shown in Table 5-2.

The effects of hypertension are assumed to be reduced arterial compliance and increased arterial resistance, as was discussed in chapter one and two. Examining the major compliance parameter, considerable difference is observed between hypertensive and normotensive subjects – the hypertensive value is approximately 40% larger. On first inspection, this result would seem to contradict the previous statement regarding reduced compliance in hypertensives. However, these parameters are *normalised* with respect to the peripheral resistance, so if the compliance is reduced slightly and resistance increases significantly, then the overall normalised value will increase. This

is what appears to have happened here. The same phenomenon appears to have occurred in the literature[3].

The peripheral resistance may be deduced by comparing normalised inertance. The normalised inertance is divided by peripheral resistance, with variations in actual inertance for identical probe placement sites unlikely, as discussed in chapter two. This therefore implies that the peripheral resistance for the hypertensive subjects is some 50% larger than the normotensives, since a larger peripheral resistance will result in a smaller normalised inertance. Inspection of normalised peripheral compliance shows approximately equal values. However, since it is argued that peripheral resistance is greatly increased in the hypertensive subjects, then it follows that actual peripheral compliance must be greatly reduced in hypertensive subjects; approximately half that of normotensives.

These results are encouraging as the overall trend follows what was expected.

5.2.6.2 The Effects of Symmetry on Dual Channel Lumped Parameter PPG

The second aim was to evaluate the dual channel methodology in symmetrical sites. Here, young tennis players were analysed using dual channel arterial PPG, taken from the fingertips. The ratio of results should be approximately unity, since the derived parameters are expected to be identical, due to the symmetrical nature of the measurement.

Inspection of Table 5-2 shows the normalised major compliance is greater for the right finger than the left by approximately 20%. As already stated, it was expected these values would be approximately unity, but a 20% change is significant. The change may be attributable to either increased compliance or increased peripheral resistance. Again inspecting the normalised inertance shows an identical inertance values. This implies that the right arm has increased compliance when compared to the left arm. These tennis players were right hand dominant, so it can be argued that the increased exercise the right arm performs has increased the compliance of the major arteries in this arm.

The normalised peripheral compliance is approximately equal, being a few percent greater in the right finger than the left. This again could be because of the increased peripheral compliance brought on by exercise, but the similarity is interesting.

5.2.6.3 The Effects of Asymmetry on Dual Channel Lumped Parameter PPG

The third aim was to investigate the effects of applying the lumped parameter numerical fit to asymmetric dual channel PPG. To do this, two groups of elderly subjects had arterial PPG waveforms taken from the index finger and the toe. These subjects were suffering from PAD, since the mean ABPI was 0.78.

Inspection of normalised major compliance between the two sites shows an increased value in the toe by approximately 15%. This too was expected, since the longer vasculature would provide increased compliance.

However, since the probe placement sites are no longer identical, difficulties arise when attempting to interpret changes. Previously, when comparing symmetric probe placement sites, the inertance could be examined in order to infer scaling of the peripheral resistance. However, since, in asymmetric testing, the inertance will vary considerably between sites, simple one to one correlations cannot be performed.

By assuming actual inertance of the toe site is double the finger site, based on body geometry assessment, it can be argued that the peripheral resistance in the toe is more than twice the peripheral resistance in the finger. Taking into account the toe site peripheral resistance, argued above, when examining normalised peripheral compliance, the data implies reduced actual peripheral compliance in the toe site. These initial results are again encouraging since it can be argued that the effects stated are symptomatic of PAD, i.e. reduced peripheral perfusion and reduced compliance, which could be caused by either congestion of the smaller arteries or the effects of an up-stream stenosis.

5.2.6.4 The Effects of Ageing on Lumped Parameter PPG

The final trial study aim was to investigate the effect on aging on vascular parameters. The vascular parameter results obtained from both tennis subject sites were averaged to provide the young data set. The vascular parameters from the normotensive finger site for the normotensive/hypertensive subjects and the finger parameters from the finger/toe subjects were averaged to provide the elderly data set, since the mean age of the tennis player was less than half the elderly subjects. These results are displayed separately in Table 5-3. Comparison of normalised major compliance shows a greatly reduced value for the older subjects. This could be expected if actual major compliance is reduced but peripheral compliance is not affected, as in the case of normotensive subjects.

Inspection of normalised inertance shows the older subjects have an approximately 25% increased value compared to younger subjects. This is unexpected since it is assumed that actual inertance between subjects is similar, necessitating here that the older subjects have a reduced actual peripheral resistance. This could however explain the low value of both normalised major and peripheral compliance. Normalised peripheral compliance is greatly reduced in the older subject group, but again this can be argued as the product of reduced actual peripheral compliance and an equivalent peripheral resistance.

5.2.6.5 Lumped Parameter and Timing Interval Comparison across Subject Groups

To compare across subject groups, Figure 5-3 may be inspected. Doing so requires de-normalisation to be performed, which can be performed by simply assuming actual peripheral resistance is unity, allowing comparison in terms of compliance alone. Little variation is shown between sites for values of peripheral compliance belonging to the hypertensive, normotensive, finger and toe subjects. The tennis player subjects gave approximately equal normalised peripheral compliances, the value being roughly 75% greater, as shown when comparing the peripheral compliance between the grouped old and younger subjects.

The normalised major compliance value shows considerable variability between subject groups. The mean value also shows significant deviation amongst individual subjects, even individual beats. The approximate equation for normalised major compliance, given in chapter two, is simply the reciprocal of the dominant decay forward model parameter a_3. Since this is a reciprocal term, even slight variations in a_3 will form large variations in normalised peripheral compliance, which goes some way to explaining the large deviation. The large normalised major compliance of the tennis players, compared to the remaining subjects, is attributed to the youth and fitness level of these subjects. The normalised values of the remaining subjects are either diseased, elderly or both; therefore possessing reduced normalised major compliance.

Figure 5-3 also shows the mean timing interval of groups. The mean timing interval amongst subject groups, taken at rest, displays relatively little variance. The timing interval for all subject groups is approximately equal when taken from the index finger for normotensive subjects. In the remaining results, taken from hypertensive and toe subjects, a significant variation can be observed. Referring to the dual channel

comparative results table, timing intervals amongst the tennis players are approximately equal; within a few percent. The mean timing interval between young and older subjects is also within a few percent. However, significant changes exist in mean timing interval obtained from both hypertensive subjects and also the toe of subjects suffering PAD. Table 5-3 shows the relative values of timing interval, as can be derived when performing dual channel PPG. Here, the hypertensive subject group has a significant change in timing interval, indicating some pathology since both probes are in identical locations. The toe and finger probe locations also show difference in mean timing interval. However, the exact nature of the timing interval in asymmetric testing cannot be defined unless correlation is performed between healthy and pathological subjects, since the difference in timing interval may be perfectly normal. However, with the lumped parameter analysis described above, it is likely the timing interval has been affected by the subject pathology that causes occlusive PAD, as these subjects were diagnosed with an ABPI value of 0.78.

Unexpectedly, the mean timing interval between older and young subjects was approximately equal. It was assumed that the vascular changes associated with ageing would have an effect on timing interval, but it clearly does not. For healthy subjects, there is little change in either inertance or normalised inertance, regardless of age; only compliance changes with age. Chapter three identified inertance as being most sensitive to the oscillatory frequency component (a_6) of the forward model. The timing interval implemented here is also most sensitive to this parameter; the oscillatory frequency will affect the location of gradient peaks.

5.2.6.6 Lumped Pilot Study Conclusion

This initial pilot study has raised many questions, with only partial answers being provided here. A more rigorous study providing correlation to vascular parameters must be performed. One method of correlation could be duplex imaging ultrasonography – this could give a visual assessment of major arteries, from which assessment of compliance (change in volume) and inertance (vessel dimensions) could be determined. This approach is non-invasive and would help reduce or even eliminate normalisation from the normalised lumped parameter set.

In the literature[3], indicator dilution[4] was performed in order to determine peripheral resistance via cardiac output[5]. However, determination of actual peripheral resistance in

this trial was deemed impractical due to the associated risks[6]. It is possible that pulse wave velocity (PWV) could be used to correlate arterial compliance, using the principle of increased travelling wave velocity of the pressure pulse in an artery possessing stiffer walls[7]. This approach has been applied to PPG with some success[8], implying a system using arterial PPG could be designed which will perform numerical fits, timing interval calculations and PWV determination using a single probe, cross correlating using the alternative techniques. However, to provide a correlation of fitting derived major compliance, an invasive catheter probe or an imaging system as described would be required, since the major arteries are inaccessible to PPG, as the penetration depth of PPG is a few millimetres at most, as discussed in chapter one.

The results for the inverse model implementation developed here show a sensitivity to subject pathology, both individually and in a dual channel sense. To further enhance the usability of this technique, a database would need creating by statistical population analysis, where the varying severity of arterial disease would be known and compared against the timing interval. This could allow either partial diagnosis or initial screenings to be performed in the primary healthcare regime or in the home. In this application, the gradient peaks were chosen in as the significant markers for the inverse model. However, the optimum inverse model significant events, and how they relate to subject physiology, are one area where further work could be applied to the inverse model timing interval methodology.

5.3 Comparative Evaluation of Vascular Parameters with Peripheral Arterial Disease.

The previous study investigated several aspects of the lumped parameter forward model when applied to arterial PPG, such as individual lumped parameter values, relative values and the inverse model timing interval.

However, the previous study was a trial involving a small population group. This study will compare relative values obtained using dual channel PPG in a larger population group. The population group will include normotensive and hypertensive subjects, with some subjects suffering occlusive PAD in the feet.

To perform this study, 15 elderly subjects had toe and index finger PPG probes placed to capture a pulsatile PPG sequence in the resting state. A forward model numerical fit was performed on the diastolic portion of the PPG waveform, with the lumped parameter inertance, major and minor compliances derived from the forward model parameters obtained by the numerical fit. Additionally, the inverse model-timing interval, developed in chapter three, for gradient peaks was calculated from the forward model parameters for both probe sites.

In order to provide correlation, each subject had an ABPI reading determined in the resting state. This involved measuring the resting in both the arm and the foot, obtained using the Doppler and probe technique discussed in chapter one.

5.3.1 Vascular Parameters and PAD Overview

This study is more complete that the previous trial as subjects of differing pathology participated. The group comprised 15 subjects overall, with a mean SBP of 155mmHg, SD 12.6mmHg. The overall mean ABPI was 0.997, SD 0.181 indicating the subject group was predominantly healthy. Toe and finger PPG was obtained, prior to performing an ABPI determination involving conventional Doppler and cuff sphygmomanometry in order to determine SBP. The SBP readings can be used to correlate individual site lumped parameters, obtained from numerical fitting, and provide an indication of the effects of SBP on the inverse model timing interval. Additionally, dual channel comparative evaluations can be performed; using ABPI to correlate both numerical fit lumped model parameters and also the dual channel inverse model timing methodology.

5.3.2 Aim

This study had several distinct aims. An incremental approach was taken to verifying assumptions, which could be built on in later arguments.

1. To compare lumped parameter values of inertance and compliance, obtained by numerical fitting, from widely differing subject groups. The lumped parameters, derived from differing subjects groups, can be compared against a known diagnosis, such as hypertension, and the effects on the spread of parameters observed. Additionally, since two measurement sites with vastly differing geometry were used, the effects of probe placement on the lumped parameters can be observed.
2. To compare the inverse model-timing interval to numerical fit lumped parameters amongst differing subject groups. Localised timing intervals for finger and toe can be compared against the localised lumped parameters. As the actual inertance for the toe is expected to be significantly greater than finger inertance, and the timing interval using gradient peaks is especially sensitive to inertance, as discussed in chapter three, the effects on the timing interval for the two site locations must be observed.
3. To investigate dual channel analysis methodologies for both lumped parameter numerical fits and the inverse model timing interval, for a wide range of subjects. The methods for dual channel comparative evaluations, discussed in chapter three, for the numerical fit lumped parameters will be investigated, and the effects of differing subject pathology observed. The dual channel methodology for the inverse model-timing interval will also be investigated, using both dual channel numerical fit correlation of lumped parameters and the ABPI measurement.

5.3.3 Protocol

The initial analysis and equipment used was almost identical to section 4.1.1, but a brief review is given here. The PPG recording system was the WinPPG system, details of which were given at the beginning of this chapter, full specifications of which are given in appendix B.

The protocol tracked closely the procedure followed by the finger and toe subjects, detailed in section 5.2.3. Each subject had PPG recording taken simultaneously from the

index finger of the right hand and from the right foot, 2nd toe – using a Viamed P856 pulse oximetry probe, wavelength 956nm. The second toe was used since better anatomical fit to the finger probe could be achieved.

Each subject reclined on a standard hospital examining couch for approximately 2 minutes prior to the start of any PPG recordings, to allow the subject to relax. A PPG recording was taken for one minute simultaneously from the finger and toe. Immediately following the PPG recording, an ABPI measurement was performed by taking ankle SBP then brachial SBP. Several SBP determinations were performed for the three arteries in the feet, as mentioned in section 5.2.3, but in this case, the greatest ankle SBP was used in determining ABPI.

5.3.4 Analysis

The PPG waveform was then normalised as described in section 4.1.1, to reduce the effects of venous blood volume changes. A continuous sequence of five pulsatile events was extracted from each channel. for both the hand and foot, the same time sequence used for both channels.

Numerical fitting of the data and smoothing over the five continuous sequences was performed as described in section 5.2.4.

The sensitivity of the timing interval to lumped inertance was also discussed in chapter three. The previous trial study discussed the concept of normalising in asymmetric studies such as this using toe normalised inertance divided by twice the normalised inertance of the arm, since an arbitrary ration of 2:1 was assumed for differences in actual inertance between the two sites. Taking ratio of these two inertances will give an indication of the relative nature of peripheral resistance in the two measuring sites.

$$\frac{L/R_{P\,Foot}}{L/R_{P\,Arm}} = \frac{L_F/R_{PF}}{L_A/R_{PA}} = \frac{2L_A}{R_{PF}}\frac{R_{PA}}{L_A} = 2\,R_{PA}/R_{PF} \qquad [5.3]$$

Equation [5.3] shows that by equating actual toe inertance to twice arm inertance, the ratio of normalised inertance will reveal the ratio of actual peripheral multiplied by two. This allows direct comparison of peripheral resistance if congestive PAD is suspected in one of the measuring sites.

The subjects were grouped according to ABPI value and systemic blood pressure, according to Table 5-4.

ABPI	Systemic SBP	Group
ABPI ≤ 0.8	SBP ≥ 150 mmHg	Hypertensive Severe PAD
	SBP < 150 mmHg	Normotensive Severe PAD
0.8 < ABPI ≤ 0.95	SBP ≥ 150 mmHg	Hypertensive Mild PAD
	SBP < 150 mmHg	Normotensive Mild PAD
ABPI > 0.95	SBP ≥ 150 mmHg	Normal Hypertensive
	SBP < 150 mmHg	Normal Normotensive

Table 5-4. Subject Classification for PAD study.

Note that although the onset of hypertension in this study was regarded as a SBP of 150mmHg, which may seem a little high, but this was due to the advanced age of the subjects, who were all over sixty years old.

5.3.5 Results

Results presentation was organised according to the ABPI reading obtained from each subject. As described in chapter one, the ABPI metric gives an indication of occlusive PAD based on the pressure drop caused by an upstream stenosis. Subjects were grouped into two broad categories:- hypertensive and normotensive. These two main groups were further sub grouped depending on occlusive PAD severity, decided by the ABPI value. Collated lumped parameters from the forward model fit, for both finger and toe probe locations, along with the inverse model timing interval using gradient peaks, are shown in Table 5-5

A scatter-plot of timing interval versus peripheral compliance for numerical fits of the finger PPG data is shown in Figure 5-4. This graph compares well with the simulation of timing interval and peripheral compliance given in chapter three. An exponential fit is also shown with regression error.

Chapter three discussed the dual channel methodology of forming rations between parameters obtained from differing sites. Significant ratios are shown in Table 5-6, with the finger probe taken as reference.

The analysis section discussed deriving peripheral resistance ratio using normalised inertance ratios. A plot of timing interval ratio and normalised inertance ratio is shown in Figure 5-5, with the inertance ratio being calculated as toe inertance divided by twice the finger inertance. This ratio eliminates the scaling constant present in equation [5.3].

PAD Group	No. Sub.	ABPI		Toe				Finger					
				$\Delta t, s$	SBP	C_pR_p s	L/R_p s	C_MR_P	$\Delta t, s$	SBP	C_pR_p s	L/R_p s	C_MR_P
H Severe	1	Mean	0.6	0.144	99	0.025	0.02	0.084	0.198	165.0	0.035	0.026	0.135
		SD	0	0.002	0	0.001	0.001	0.007	0.004	0	0.002	0.001	0.004
N Severe	2	Mean	0.719	0.241	102.81	0.071	0.027	0.179	0.279	142.86	0.039	0.040	0.116
		SD	0.009	0.622	4.87	0.021	0.010	0.06	0.040	4.88	0.001	0.01	.0.100
H Mild	4	Mean	0.916	0.243	144.75	0.044	0.034	0.141	0.333	158.12	0.047	0.055	0.138
		SD	0.017	0.045	4.54	0.013	0.084	0.022	0.054	4.79	0.013	0.011	0.029
N Mild	2	Mean	0.892	0.259	128.25	0.049	0.037	0.145	0.343	144.0	0.056	0.050	0.187
		SD	0.035	0.067	2.465	0.010	0.014	0.044	0.035	8.22	0.011	0.006	0.043
H Normal	4	Mean	1.116	0.281	189.34	0.061	0.039	0.173	0.228	168.71	0.041	0.032	0.150
		SD	0.112	0.076	31.81	0.033	0.017	0.068	0.050	10.6	0.005	0.012	0.032
N Normal	3	Mean	1.168	0.262	168.3	0.063	0.032	0.219	0.279	144.2	0.042	0.041	.0160
		SD	0.081	0.081	11.52	0.035	0.017	0.095	0.046	3.53	0.007	0.007	0.088

Table 5-5. Significant parameters for PAD study.

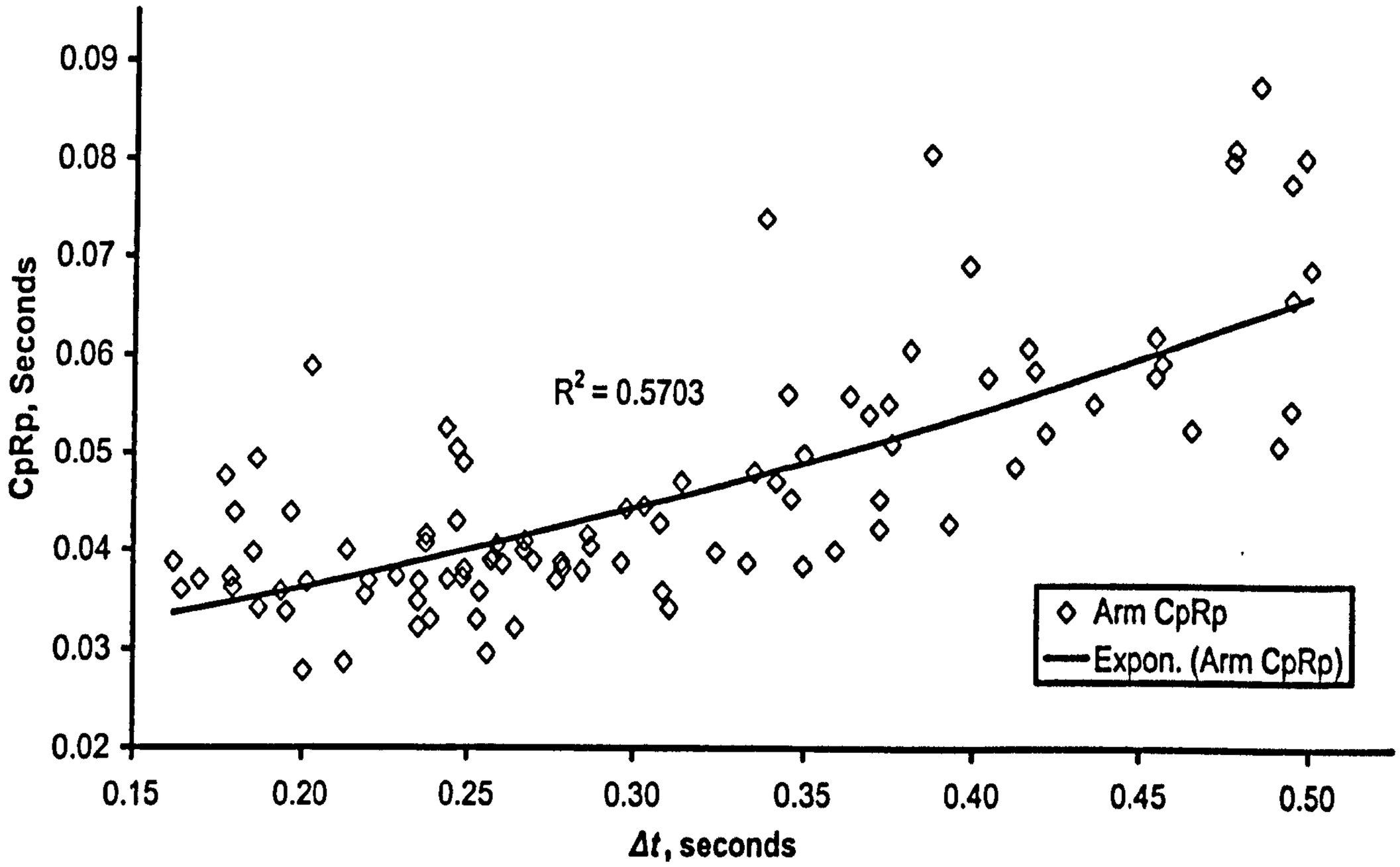

Figure 5-4. Scatter plot of Timing interval Vs Peripheral Compliance for PAD study.

PAD Group	No. Subjects		$\frac{\Delta t_{Foot}}{\Delta t_{Arm}}$	ABPI	$\frac{C_P R_{P\,Foot}}{C_P R_{P\,Arm}}$	$\frac{L/R_{P\,Foot}}{L/R_{P\,Arm}}$	$\frac{C_M R_{P\,Foot}}{C_M R_{P\,Arm}}$
H Severe	1	Mean	0.723	0.6	0.7087	0.778	0.6276
		SD	0.0074	0	0.0719	0.0274	0.0716
N Severe	2	Mean	0.8838	0.7194	1.8256	0.6208	1.5598
		SD	0.2049	0.0093	0.545	0.3036	0.5197
H Mild	4	Mean	0.739	0.9155	1.0165	0.6234	1.0646
		SD	0.133	0.0169	0.3724	0.1642	0.2742
N Mild	2	Mean	0.7549	0.8922	0.9061	0.7145	0.8152
		SD	0.1947	0.0345	0.2274	0.2329	0.3225
H Normal	4	Mean	1.3256	1.1165	1.5336	1.5101	1.1812
		SD	0.5465	0.1119	0.8599	0.9852	0.5223
N Normal	3	Mean	0.9728	1.1675	1.5236	0.8242	1.483
		SD	0.3791	0.0809	0.7667	0.5152	0.6788

Table 5-6. Mean of ratios for PAD study.

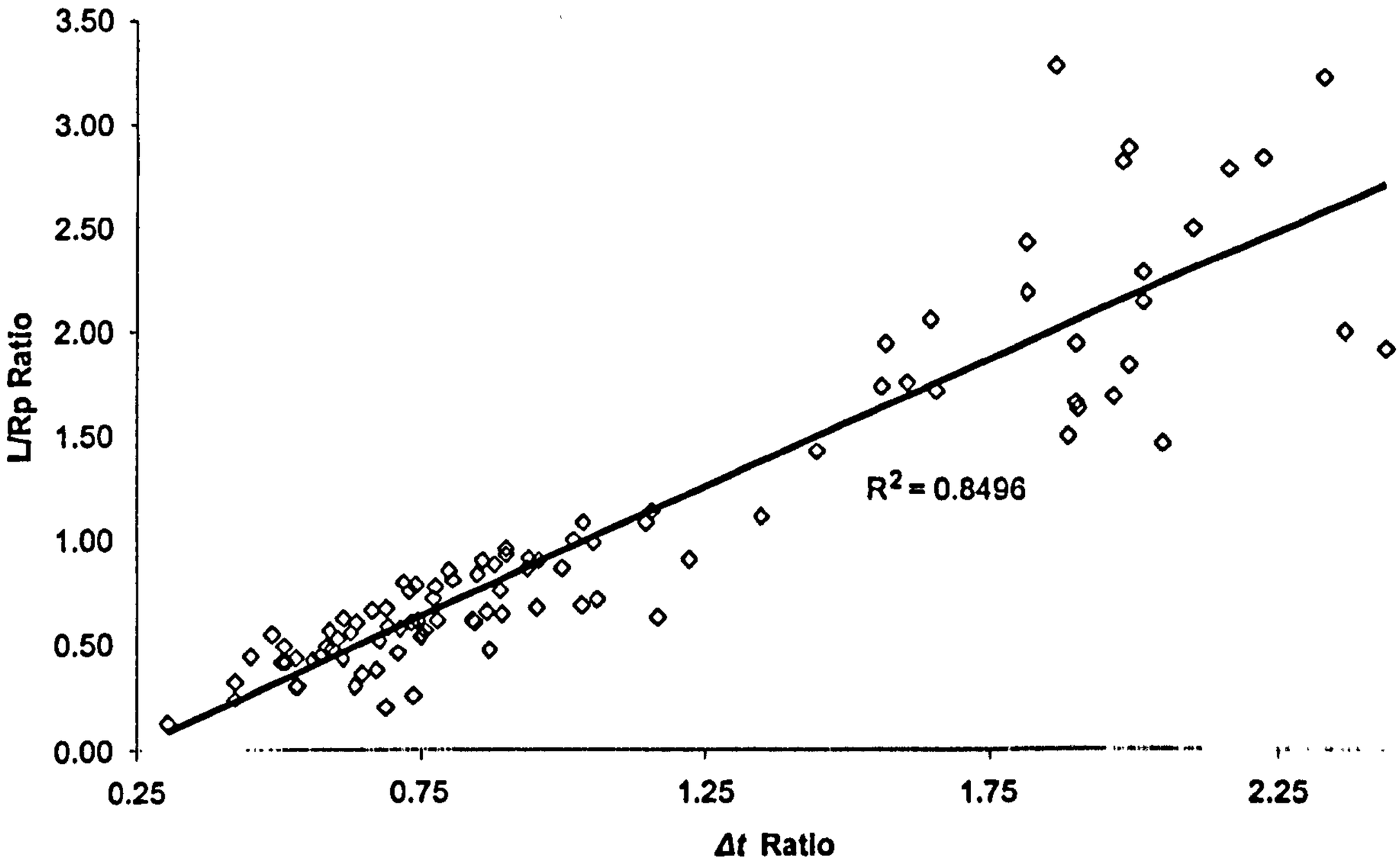

Figure 5-5. Timing interval Ratio and Normalised inertance Ratio scatter plot.

5.3.6 Discussion

Interpretation of results for this trial is complex, so has been broken into several parts based on the initial aims of the trial.

5.3.6.1 Lumped Parameter Comparisons

Comparing values derived from the numerical fitting of the forward model is possible between same site locations. These parameters are normalised with respect to peripheral resistance as described previously, so care must be taken when interpreting results.

Lumped parameters derived from the Toe

Reassuringly, the lowest toe peripheral compliance value was recorded from the hypertensive subject suffering the most severe PAD, determined by the lowest value of ABPI. However, the greatest value of normalised toe peripheral compliance was recorded from the normotensive subjects suffering severe PAD. The normotensive and hypertensive subjects suffering mild PAD record the mid value for normalised toe peripheral compliance. The normal subjects, both hypertensive and normotensive, register what would be the largest value of normalised toe peripheral compliance if it wasn't for the large normalised peripheral compliance recorded from the severe PAD

normotensive subjects just discussed. It is suspected that the effects of peripheral resistance are involved here; an inference of changes in peripheral resistance may be determined by examining normalised inertance, discussed below. In the majority of cases, hypertensive subjects show reduced normalised peripheral compliance compared to normotensive subjects.

The normalised major compliance shows a similar trend to the normalised minor compliance. Here, subjects without PAD show the largest value of normalised major compliance in both normotensive and hypertensive subjects. The hypertensive subject suffering severe PAD shows the lowest major compliance value. Again, the normotensive subjects suffering severe PAD show an anomalous high major compliance. Once more, both normotensive and hypertensive subjects suffering mild PAD show intermediary value of normalised major compliance. Although the normotensive subject suffering severe PAD is an exception, these results for normalised major compliance agree with the argument that PAD causes reduced compliance in both the major and minor arteries. In the majority of cases, hypertensive subjects show reduced compliance when compared to normotensive subjects.

When examining normalised inertance, it can be assumed that the actual inertance is similar between subjects, with variations in body geometry being the only cause of change, as discussed in chapter two. The normalised inertance is the ratio of peripheral actual inertance divided by actual peripheral resistance. Therefore, a smaller normalised inertance indicates a larger peripheral resistance. This arguments holds for the majority of inertance results obtained from the toe. Subjects suffering severe PAD show the least value of normalised inertance, and healthy subjects show larger values of normalised inertance. Again, the hypertensive subject suffering severe PAD has the lowest inertance, indicating highest peripheral resistance. Some variability exists between subjects suffering mild PAD and subjects without PAD, but these variations may be attributed to both slight variations in actual inertance between subjects and also the fact that mild PAD only shows slightly reduced actual peripheral resistance. Again, in the majority of cases, hypertensive subjects show an increased peripheral resistance compared to normotensive subjects in the same group.

Lumped parameters derived from the Finger

Examining the lumped parameters derived from the finger probe, it is apparent that less clear trends exists. This is because PAD seldom affects the finger, and with lesser severity than toes, which is why the upper body pressure is used as the reference in the

ABPI measurement. However, some variations do exists, but are less pronounced when compared to the parameters obtained from the toe.

Comparing normalised peripheral compliance in the finger between subjects, hypertensive subjects show reduced compliance in each respective group. The subject with the least normalised finger peripheral compliance is the subject suffering severe PAD. This could indicate therefore that this subject's entire arterial vasculature has reduced compliance, since reduced normalised compliance was observed in two locations. The normotensive subjects with severe PAD also show reduced normalised peripheral compliance in the finger when compared to the other subjects. The subjects showing greatest normalised peripheral compliance are the subjects suffering mild PAD. This was somewhat unexpected, but as stated, PAD is less severe in the upper body than the lower, indicating the subjects suffering mild PAD and normal subjects have relatively healthy peripheral compliance.

Inspecting the normalised finger major compliance shows a similar trend. The normalised compliance for the two subjects suffering severe PAD is the lowest; the remaining subjects show larger normalised major compliance. This again indicates that although PAD mainly affects the periphery, the effects on larger arteries can also be observed, but to a lesser degree.

Viewing the normalised finger inertance, the hypertensive subject suffering severe PAD shows the lowest value. This is as expected, based on the argument above that increased peripheral resistance produced a reduced normalised inertance, implying that the subjects with severe PAD also has PAD in the fingers as well as toes. The values of normalised inertance for the remaining subjects are less simplistic in their interpretation. The normal subjects do not show the greatest values of normalised inertance; the value of normalised inertance for the hypertensive normals are quite low, which could imply that these subjects are suffering some arterial congestion. Alternatively, these variability may be attributable to anatomical variability between subjects, or possibly a combination of factors.

5.3.6.2 Inverse Model Timing Interval Comparisons

Comparison of the inverse model timing interval is possible between the same probe location. The implementation here of the inverse model employs gradient peaks as significant events, and it was found in chapter three that the timing interval using gradient peaks is sensitive to the lumped inertance. Evaluation of the timing interval must be restricted to locations where the lumped inertance is approximately equal; in this case performing comparison of either toe timing intervals or of finger timing intervals.

Chapter three showed an instance where the timing interval based on gradient peaks can vary as a function of hypertension. The stiffer arterial walls, a result of the arteries being stretched closer to their elastic limit by the increased blood pressure, produce a resonant frequency which is higher than the resonant frequency of normotensive subjects. This means the oscillatory frequency component of a_6, in equation [5.1], will be larger. The implications of a higher resonant frequency are that the dichrotic notch undulation, a key feature of both the arterial PPG and arterial pressure waveform, will be narrower, since the higher frequency has a reduced period. The inverse model implemented here uses gradient peaks as the significant event for determination of the interval, which means the timing interval will be narrower for hypertensive subjects compared to normotensive subjects. This argument was proved in chapter three using interpolation to demonstrate how changes in the forward model parameters resulting from hypertension would result in a reduced timing interval.

However, for subjects suffering occlusive PAD, the SBP is actually lower in limbs affected by PAD, since an upstream stenosis causes a downstream pressure drop. Therefore, the implied assumption that the timing interval is a function of SBP is not valid in all cases – the timing interval is a function of the lumped inertance and both compliances. This was also illustrated in chapter three, with variations in peripheral compliance showing variations in timing interval. The timing interval was shown to be most sensitive to lumped inertance, but it was expected that variations in inertance would not be found, as described above.

Comparisons between timing interval and normalised peripheral compliance can be performed, with the plot of finger timing interval and normalised finger peripheral compliance shown in Figure 5-4. This figure can be compared against the equivalent

figure for simulations shown in chapter three. It can be seen that, irrespective of SBP, the timing interval gives a direct correlation between normalised peripheral compliance, as was shown in the figure using the exponential regression fit. The mean toe normalised peripheral compliance values approximately follow the same trend, since the hypertensive subject suffering severe PAD has the smallest timing interval. This is reasonable since the effects of both reduced compliance due to arterial wall thickening and reduced compliance due to hypertension are in play.

The timing interval for the toe is less straightforward. The mean values follow the trend since increasing timing interval corresponds to increasing normalised peripheral compliance approximately, though with a lower correlation when compared to the finger peripheral compliance. It can be argued that, as the timing interval is more sensitive to inertance than compliance, toe-timing intervals are affected more by the anatomy of the subjects rather than the peripheral compliance. It is suspected that the mean length of an adult arm will have much less deviation than the mean deviation in length of an adult leg. This explains why the timing interval for the finger has a greater correlation to peripheral compliance than the toe. What is needed is a way of eliminating the effects of changes in inertance from the timing interval.

5.3.6.3 Dual Channel Comparisons

Chapter three discussed the concept of dual channel comparative evaluations, where numerical fits could be applied to the PPG waveform in two separate distal sites. Symmetric comparison and asymmetric comparisons could be performed. In the case of symmetric comparisons, deviation from unity would indicate possible subject pathology, as investigated in the pilot study above. Here, asymmetric comparisons must be performed, but this requires care since differences will exist between lumped parameter ratios as the connective vasculature is asymmetric for each probe site, therefore the derived lumped parameters will also be different.

A table of means of the ratios between the two probe sites is shown in Table 5-6. No clear relationship exists between the timing interval and normalised peripheral compliance ratio, nor any clear relationship between timing interval and normalised major compliance. However, by assuming that actual leg inertance, measured at the toe, is twice actual arm inertance, measured at the finger, as shown in equation [5.3], then forming the ratio between normalised inertances will, in reality, give the ratio between

actual peripheral resistance for the two sites. This plot of timing interval ratio and ratio of toe normalised inertance divided by twice finger normalised inertance is shown in Figure 5-5. A strong correlation between ratios is observed, allowing determination of relative peripheral resistance between the two finger and toe sites.

Knowing the relationship between normalised inertance ratios allows evaluation of actual peripheral compliance for each subject group. Referring to Table 5-6, the normotensive subject with severe PAD has the lowest ratio value. According to equation [5.3], this value will be twice the ratio of actual finger peripheral resistance and toe peripheral resistance. Increased resistance could be a result of congestive build-up, since the normotensive severe PAD subject therefore has a toe peripheral resistance more than two and a half times the finger peripheral resistance. The remaining subjects suffering PAD also have drastically increased peripheral resistance in the toe. The normals show much greater ratio values, approximately double the diseased subjects, indicating that, considering the advanced subject age, toe peripheral resistance is approximately one third more than finger peripheral resistance, which is less significant.

5.3.6.4 Comparative Evaluations of Vascular Parameters with PAD Conclusion

This trial has applied numerical fitting of the forward model in order to derive lumped parameter information from a wide range of subjects, in two sites. Hypertensive and normotensive subjects with varying degrees of PAD in the toes were analysed, and the results correlated by the ABPI protocol for assessing PAD in the toes.

Inspection of lumped parameter results obtained from individual sites agrees with physiological symptoms attributable to vascular disease, namely PAD. Combining information from several lumped parameters, such as reviewing both normalised peripheral compliance and normalised inertance, rather than reviewing each parameter in isolation allows a more thorough understanding of the connective vasculature to be developed.

Evaluations of the inverse model timing interval, developed in chapter three for gradient peaks, shows that in each localised site, the inverse model timing interval displays a relatively good correlation to normalised peripheral vascular compliance. Since normalised peripheral vascular compliance is affected by SBP, the timing interval is also sensitive to SBP.

Comparative evaluations using dual channel PPG were performed, by forming ratios of the lumped model parameters and timing interval. An argument was presented to determine the ratio of actual peripheral resistance between sites, using the normalised inertance parameter obtained from each site. The ratio of inverse model timing intervals was found to bear a strong correlation to the ratio of peripheral resistance between sites.

5.4 Chapter Conclusion

Using combinations of the techniques presented above, it is possible to determine an accurate picture of the subject's vasculature by interpreting data from two sites. Two possible methodologies can be employed, one using a combination of numerical fitting and the inverse model timing interval, and one solely using the timing interval.

Combined Approach

In depth vascular assessment is possible using a combination of numerical fitting and the timing interval inverse model. As has been argued, variations in inertance are unlikely to occur in the arm, since the length of adult arms are subject to less variability in length than the legs. An anatomical table could be employed which would give typical inertance values based on arm length, allowing determination of actual peripheral resistance from the value of normalised inertance obtained by numerically fitting the forward model to the finger arterial PPG waveform. With the actual peripheral resistance found, de-normalisation of the finger compliance parameters is possible, giving both major and minor compliances for the finger.

Using the dual channel methodology, it is possible to find the ratio of finger peripheral resistance to toe peripheral resistance. As the value of actual finger peripheral resistance was determined anatomically as described, the value of toe peripheral resistance can be determined. Again, de-normalisation of the remaining parameters is now possible, including a check that can be performed on the ratio of actual toe inertance to finger inertance, used in determining toe actual peripheral resistance.

All the lumped model parameters in un-normalised form are now available. Evaluations of the parameters can be performed against a database, including evaluations of the two major compliance components. These compliances can give an indication of the health of the large arteries using a peripheral probe system.

Lumped Parameter Inverse Model Approach

A speculative conjecture exists that PAD screening may be performed using the timing interval alone. While this approach may not provide a complete vascular assessment as described previously, it may allow assessment of PAD quickly and with comparative ease.

This methodology does not employ numerical fitting. Normalised peripheral compliance may be determined from the inverse model timing interval using the correlation shown in Figure 5-4 or a similar technique, for both finger and toe locations, by statistical means. Normalised peripheral compliance has now been determined in both locations. The timing interval inverse model ratio can now be taken, from this the ratio of peripheral compliance determined, as in Figure 5-5. The finger probe site will be assumed free from PAD, which can be confirmed by inspection of the value of normalised peripheral resistance obtained from Figure 5-4, and the ABPI procedure uses the arm for pressure reference when determining PAD in the feet using sphygmomanometry.

This methodology will therefore give both finger and toe normalised peripheral compliance, and the ratio of peripheral resistance between sites. If normalised toe peripheral compliance is evaluated with the actual peripheral resistance ratio, then compared to finger peripheral compliance, an evaluation of toe peripheral resistance and peripheral compliance can be performed. This approach could provide adequate information necessary to perform primary screening of PAD without using the sphygomanometry, eliminating the associated errors and specialist operator requirements. Investigations into the sensitivity and specificity of this approach is required in order to fully evaluate this hypothesis.

5.5 Chapter References

[1] Matlab, The Mathworks Inc, 1999

[2] Nelder, J. A., R. Mead, "A Simplex Method for Function Minimization", *Computer Journal*, Vol. 7, pp. 308-313 (1965)

[3] Watt, T.B, Burrus, C.S, "Arterial pressure contour analysis for estimating human vascular properties", J. Appl. Physiol, 40(2), pp. 171-176 (1976)

[4] Dow O, "Estimation of Cardiac Output and Central Blood volume by Dye Dilution", Physiological Reviews, 36, pp. 77-102 (1956)

[5] Editorial, "Measurement of Cardiac Output", The Lancet, 2, pp. 257-258 (1988)

[6] Connors A.F., Speroff T, Dawson N.V, et al, "The effectiveness of right heart catheterisation in the initial care of critically ill patients", J. AMA, 276, pp. 889-897 (1996)

[7] Asmar R, Benetos A, Topouchian J, Laurent P, Pannier B, Brisac A-M, Target R, Levy B.I, "Assessment of arterial distensibility by automatic pulse wave velocity measurement: validation and clinical application studies", Hypertension, 26, pp. 485-90 (1995)

[8] Shimazu H, Yamakoshi K, Kamiya A, "Non-invasive measurement of the volume elastic modulus in finger arteries using photoelectric plethysmography", IEEE Trans. Biomed. Eng., BME-33, 8, pp 795-798 (1986)

Optical Engineering Group
Loughborough University

Chapter Six

Conclusion

6 Conclusions

This thesis has dealt exclusively with the difficulties of performing vascular assessment using photoplethysmography. The technology of photoplethysmography has been discussed in full, giving current successful applications. An application of vascular assessment, arterial disease diagnosis, was discussed, identifying problems with current diagnostic techniques.

To increase the functionality of PPG, models were developed, and then extended for use with both single and dual-channel pulsatile PPG, based on either vascular perfusion or indirect vascular parameters identification. An inverse model was developed for direct assessment of vascular parameters from the pulsatile PPG signal.

In order to investigate the consistency of the techniques developed for vascular assessment, several prospective experimental studies were performed in an attempt to assess the effect of differing subject physiology on the derived methods and techniques.

This chapter will distil content of this thesis into a single concise delivery. Details of speculative extensions and modifications to the work will also be suggested.

6.1 Discussion

The aim of this thesis was bring the advantages of PPG technology, such as the non-invasive nature and ease of use, to the problem of vascular assessment. Biomedical monitoring and diagnosis using photoplethysmography has been impeded by the lack of quantification when using this technology, in that the relative nature of the pulsatile PPG signals has limited both its use and acceptance. The established methods of performing clinical vascular assessment have been shown to be somewhat unreliable and clumsy. In order to perform vascular assessment using pulsatile PPG, two alternative avenues were pursued:

1. Perfusion monitoring, where the shape of the pulsatile PPG waveform is inconsequential, and the magnitude or trend of the pulsatile PPG waveform was used in generating a perfusion metric.
2. Identification of quantitative vascular parameters, where the magnitude of the pulsatile PPG waveform is inconsequential, but the shape of the pulsatile PPG waveform is used in performing quantitative assessment of vascular parameters.

6.1.1 Assessment of Vascular Perfusion by PPG

In the first instance, a simple forward model enabling monitoring of vascular perfusion was developed. Performing magnitude trend analysis of the normalised pulsatile PPG waveform, obtained using the simple model, allowed insight into localised subject perfusion changes to be gained.

The perfusion model was extended to allow dual channel, dual distal site pulsatile PPG based perfusion monitoring. This technique allows normalisation of perfusion values, permitting assessment between subjects. An experimental feasibility trial employing the dual channel methodology was employed to monitor changes in vascular perfusion due to exercise. This trial successfully identified changes in perfusion caused by exercise, which was attributed to physiological adaptation in the vasculature of tennis players.

An implementation of the perfusion trend methodology was used to develop a more objective method of determining SBP. To do so, an automatic SBP determination procedure was proposed that would increase SBP accuracy, or reduce error, by eliminating operator variability. Prospective feasibility assessment of the automatic SBP technique was performed using a trial study group, obtaining SBP in the arms, providing results which validated the feasibility of the automatic procedure, showing this technique is worthy of further research. It was argued that a consequence of performing automatic SBP by monitoring the periphery for pulsatile return is that increased sensitivity to subject physiology should be found, as pulsatile PPG registers perfusion changes in the periphery. This too is worthy of further investigation.

Incorporation of the PPG based automatic SBP determination technique into a modified ABPI procedure for determining occlusive PAD severity allowed the benefits of the PPG based automatic SBP determination technique to be brought to ABPI measurement. A clinical prospective assessment of the modified automatic ABPI protocol was performed to assess occlusive PAD in the toes, returning encouraging results. The automatic ABPI protocol eliminates the requirement for specialised operator training required in conventional ABPI determination, which could allow this technology to be used for primary healthcare screening of suspected occlusive PAD cases.

6.1.2 Quantitative Vascular Assessment Using PPG

Limitations in the perfusion models led to the development and application of a 3rd order lumped parameter model to pulsatile PPG. This technique initially required numerical fitting of the diastolic portion of the pulsatile PPG waveform, indirectly allowing derivation of quantitative normalised vascular parameters. A prospective experimental trial was performed on a variety of subject groups in order to assess both age related and hypertension related changes in vascular parameter. The normalised results obtained from this study were consistent with the expected quantitative changes in physiology caused by differing pathology. Techniques were discussed allowing de-normalisation of quantitative vascular parameters, based on subject anatomical information and the invariability of vascular inertance. This technique could allow quantitative determination of the actual vascular parameters employed in the 3rd order lumped forward model.

The indirect lumped parameter model numerical fitting technique was extended with application to dual-channel pulsatile PPG. The dual-channel extension allows self-normalisation of the normalised vascular parameters, permitting relative vascular assessment between sites to be performed. A small experimental trial applied this technique to subjects suffering occlusive PAD. Comparative results obtained from the dual-channel fit showed the validity of lumped relative vascular assessment was, at least in part, feasible.

An inverse model, based on the solution to the third order lumped forward model, was developed to allow direct vascular assessment without the need for numerical fitting. The inverse model required extraction of a timing interval from the pulsatile PPG waveform. An implementation of the inverse model was developed, giving normalised peripheral vascular compliance by direct relationship. The inverse model was extended to dual-channel pulsatile PPG, with the chosen implementation allowing direct determination of relative peripheral resistance between sites. An experimental trial was performed on subjects suffering varying degrees of PAD, with correlation provided by both numerical fits and conventional ABPI measurements. Significant changes in vascular parameters between subject PAD severities were found, confirming the usability of the timing interval inverse model.

The availability of vascular parameters simplifies interpretation of vascular physiology when assessing pathology. In this case, investigations into PVD, specifically PAD, were performed, but it is speculated that quantification of vascular parameters will be a powerful tool in the diagnosis of many pathological conditions.

6.2 Recommendations for Further work

This section outlines suggestions for further work. Both extensions to existing work and proposed novel concepts are discussed.

6.2.1 Extended models

Several models were presented as part of this thesis, with each model possessing inherent advantages and disadvantages. To extend the work here, an entirely new model for use in pulsatile PPG is proposed, incorporating the features of several models.

A rudimentary procedure for extending the single channel pulsatile PPG models to dual-channel pulsatile PPG was presented in this thesis, where simple ratio type normalisation was performed. The general concept was one channel would form a reference signal, against which the other channel was normalised. The single to dual channel normalisation procedure could be extended in order to increase desired sensitivity. There are countless normalisation methods that could be performed, which is why the simplest ratio procedure was performed in this thesis. The exact form of an extended normalisation procedure would be prescribed by the desired parameter sensitivity. However, a novel dual channel normalisation technique could be employed to increase the usability of the dual channel PPG system.

6.2.1.1 Unified PPG Model

A speculative new PPG model is proposed, based on background reading performed by the author, and would unify differing areas of research in PPG and vascular dynamics. This description is by no means exhaustive, and could take many years of research to complete.

The most general model for PPG analysis would be a so-called Unified PPG Model. This model would incorporate aspects of the simple perfusion model, where blood volume changes are registered, with the features of Lumped Model, where the characteristics of the connective vasculature shape the PPG waveform.

The unified model could incorporate the laws developed by Laplace[1], who recognised the properties of vessel wall tension to applied pressure, in order to determine arterial

distensibility, and thus volume change. The Navier-Stokes[2] equations could be incorporated to model inertia effects in an elastic walled artery filled with blood, which could indicate the driving energy involved. The Moens[3]-Koertweg[4] transmission line models could be incorporated in order to describe a segmented, distributed arterial system that would more accurately model the arterial vasculature, which would indicate how the shape of the PPG waveform changed over the vascular system. The haemodynamic changes within the vasculature would modulate the PPG light source; incorporation of light and tissue interaction models such as the Beer-Lambert[5] Law or Diffusion theory[6] would complete the proposed model.

Inversion of the Unified PPG model would be equally if not more difficult than deriving the forward model. It is possible inversions could be solved for both vascular parameters or cardiac output, enabling determination of quantitative haemodynamic parameters or cardiac output from a non-invasive peripheral PPG probe.

6.2.1.2 Lumped Parameter Model

Currently, the lumped parameter forward model requires numerical fitting in order to derive normalised lumped model parameters. Increasing the efficiency of the numerical fit could increase the overall accuracy, overall speed or both speed and accuracy, allowing enhanced derivation of the normalised lumped parameters.

All numerical fits require starting parameters close to the actual solution. A basic methodology was presented in the form of an algorithm that could derive starting parameters by quick and simple analysis of the PPG waveform to be fitted. This starting parameter derivation algorithm could be extended to create a superior starting parameter algorithm, allowing faster convergence by the numerical fit algorithm.

The numerical fit algorithm employed in this thesis was the Nelder-Mead[7] simplex search, that although slow is trivial to implement. Fit algorithms that are more efficient, such as Gauss-Newton, are available which could substantially decrease the number of convergence iterations. However, it must be ensured that any fit algorithm converges on a physiologically unique solution, by for example the implementation of limits.

The Nelder-Mead fitting algorithm employed an error function that attempted to ensure convergence on physiological minima by decomposition of the PPG waveform into its component parts. This methodology too could be extended further in order to allow quicker, more accurate convergence.

6.2.1.3 Inverse model

The general form of the inverse model was presented in chapter three, in that a timing interval was extracted from the pulsatile PPG waveform, based on identification of significant points of the diastolic portion of the PPG waveform.

An implementation using gradient peaks was developed, and analysed for lumped parameter sensitivity. It was found that the gradient peak timing interval is most sensitive to lumped inertance. However, it was argued that large variations in inertance were unlikely between subjects for identical probe sites. Further investigation would be required to confirm this, but if so, a method of denormalising may be performed by statistical population analysis.

Furthermore, a method was suggested in chapter three for factoring the timing interval expression in terms of the lumped model parameters, but a solution of this form could not be found for the gradient peak implementation.

Implementations of the inverse model may exist (using differing significant points to the example developed) that are sensitive to differing lumped parameter components. The exact form of the implementation will depend on the desired sensitivity – for example, an implementation may be desired where the timing interval is most sensitive to major compliance. Alternatively, an implementation may be desired where the timing interval is most sensitive to peripheral compliance. These forms of the timing interval may be found analytically or empirically by working through the various combinations of significant events. Once the implementation most sensitive to the desired lumped parameter is found, this may then be factored using the methodology given in chapter three.

6.2.2 Experimental Trials

Clearly, and deliberately, the trials contained within this thesis are limited. An exhaustive clinical trial would require many more subjects, correlating results obtained via PPG models with ready establish, conventional techniques. The aim of this thesis was to develop and expand models applicable for PPG – thorough validation of these models would require a separate thesis. The specific trials mentioned in this thesis will be discussed, with suggestions for improvements made for each trial.

6.2.2.1 Exercise Based Perfusion Monitoring

This study, presented in chapter four, was an initial evaluation of the perfusion-based model, and the specific techniques developed for trend analysis. As such, no direct correlations were performed during this trial. Statistical analysis of subject groups was performed as part of the conclusions, based on the experience and age of the participants.

To determine the true nature of the perfusion changes caused by exercise, Duplex Ultrasound imaging could be performed on the brachial arteries of the subjects, allowing determination of volume flow rates in pre and post exercise states. Differences in dominant and non-dominant arms could be monitored, allowing determination of adaptation in trained subjects.

6.2.2.2 Determination of SBP and ABPI using PPG

This trial, presented in chapter four, would mainly benefit from additional subjects in order to investigate the limits of the technology. Increased experimental rigour could be provided by electronic monitoring of sphygmomanometer cuff pressure, which would provide more accurate pressure determination rather than relying on human interpreted pressure readings. Electronic monitoring of the Doppler Ultrasound system output would allow synchronisation of Doppler determined systolic return to exact cuff pressure, recorded electronically. Additionally, monitoring of cuff pressure for oscillatory variation, as is perfumed in many automatic blood pressure monitoring devices, would provide an additional correlation of pulsatile flow.

An increased reliability of SBP determination would transfer to the modified ABPI protocol, incorporating PPG derived determination of SBP. The hypothesis that the peripheral nature of PPG could provide increased sensitivity to the onset of PAD would need a follow up trial in order to resolve. A study incorporating ABPI assessment at regular intervals would allow monitoring of the progress of PAD, and hence determine PPG derived ABPI measurement sensitivity.

6.2.2.3 Lumped Parameter Trials

The trial study presented in chapter five was an initial investigation into the feasibility of employing the lumped parameter forward model to the pulsatile PPG waveform. Several subject groups were employed in order to observe the effects on the indirectly

derived lumped parameters, and to investigate the effects of PAD on the lumped parameters. The effects of differing subject groups on the timing interval inverse model was also assessed, again with effects of PAD being of interest.

To improve the validity of these studies, larger subject groups would be required, ideally ranging in age from children to the elderly. In the case of the feasibility trial, age matched subject hypertensive subjects would also be tested. Pulsatile PPG recordings would be taken simultaneously in both fingers and in the finger and toe, in order to perform isolated, symmetric and asymmetric dual channel comparisons. Ideally, a wide range of subjects suffering PAD would participate, and these too would be both normotensive and hypertensive. The range of both SBP and PAD severity would be uniformly distributed throughout the known range, from lower normotensive to upper hypertensive in the case of SBP and from extremely severe to normal in the case of PAD.

The massive amounts of data required to perform this study, ideally having several hundred subjects, would take considerable time to analyse, emphasising the significance of optimised numerical fitting. Statistical analysis of the resulting data would both compartmentalise the returned parameters and also confirm validation of the technique. For example, the resultant data could be organised in terms of both increasing blood pressure and increasing PAD severity, providing an overview of the effects of both hypertension and PAD on the vasculature and the inverse model timing interval.

6.3 Chapter Reference

[1] Laplace P.S., "Théorie l'action capillarie", In Traite de mécanique céleste, Suppliment au livre X, Pais, Coarcien (1806)

[2] Ladyzhenskaya O., "The Mathematical Theory of Viscous Incompressible Flows" (2nd edition),Gordon and Breach (1969)

[3] Moens A.I., "Die Pulskurve", Leiden, Germany, E. J. Brill (1878)

[4] Korteweg D.J., "Über die Fortpflanzungsgschwindigkeit des Schalles in elastichen Röhren", Ann. D. Physik., III, pp. 525-542 (1878)

[5] Cejnar M, Kohbler H, Hunyor S.N, "Quantative Photoplethysmography: Lambert –Beer law or inverse function incorporating light scatter", J. Biomed. Eng., 15, pp. 151-154 (1993)

[6] Schmitt J.M, "Simple Photon Diffusion Analysis of the Effects of Multiple Scattering on Pulse Oximetry", IEEE Trans. Biomed. Eng, 38(12), pp.1194-1203 (1991)

[7] Nelder, J. A., R. Mead, "A Simplex Method for Function Minimization", *Computer Journal*, Vol. 7, pp. 308-313 (1965)

Optical Engineering Group
Loughborough University

Appendix A

Photoplethysmograpy Feature Extraction

A Introduction to Feature Extraction

This appendix discusses current and novel ways of analysing the PPG waveform. A brief overview of typical analysis techniques are given with examples related to PPG. Disadvantages with current methods are discussed, hence the introduction of novel methods. This section is placed as an appendix due to the algorithmic nature of the methods employed, which are unsuitable for incorporation into the main body of the thesis.

A.1 Classification of Signals

Previous chapters were concerned with the generating and obtaining the PPG signal, and what physiological effects could be attributed to the PPG waveform. Extraction of parameters from any physiological waveform is non trivial. Brief descriptions of several physiological parameters often monitored either in intensive care or in ambulatory monitors are shown in Table A-1.

Name	Typical Use	Classification
Arterial plethysmography	Pulse oximetry.	Periodic
Impedance Plethysmography	Pneumography.	Periodic
Electrocardiography (ECG)	Heart muscle monitoring.	Periodic
Arterial Pressure	Hypertension monitoring.	Periodic
Venous Plethysmography	Venous insufficiency tests.	Transient
Electromyography (EMG)	Muscle function analysis.	Transient
Electroencephalography (EEG)	Diagnosis of epilepsy.	Trend
Acidity (pH)	Digestive tract monitoring.	Trend
Intra-Cranial pressure	Cerebral pressure monitoring.	Trend

Table A-1. Typical Physiological Signal analysis trends.

The by no mean exhaustive Table A-1 shows a majority of periodic signals. However, it is interesting to recognise these signals may be broadly classified as either periodic, transient or trend. The definition of these terms is given below.

- Periodic implies a repeated waveform; in the above examples, usually a peak in the signal signifies the beginning of the period, followed by a period of inactivity or 'lull'. Any analysis software must detect these peaks, identifying each period and extracting relevant data from this.
- Transient analysis implies background inactivity followed by a period of activity, returning to inactivity. Extraction of the transient event is relatively trivial since it can be clearly defined against the background, assuming a modest signal to noise ration.
- Trend analysis may be performed by breaking the signal into discrete time samples, or 'chunks'. A figure or metric is usually derived from each sample group or epoch, and these metrics are compared against other sample epochs.

However, since pulsatile PPG is periodic, we will concentrate mainly on algorithms that may be applied to periodic signals. All the following algorithms assume the physiological signal has been appropriately signal conditioned, filtered and sampled into a data set vector ready for analysis.

A.1 Simple Analysis

This section briefly describes analysis methods used to determine basic information about the signals, and their application to feature extraction of PPG waveforms. Most of these analysis techniques utilise a sliding window technique where only a portion of the data set is analysed. This technique lends itself to pseudo real time analysis, since a small buffer can be filled with perhaps a few seconds worth of data, then analysed to give information about preceding two seconds data.

A.1.1 Gradient Analysis

One of the most common methods of detecting waveform peaks is by gradient analysis. The first derivative of the waveform is obtained either electronically or numerically. Typically, the gradient zero-crossing points are identified to recognize turning points of the original waveform.

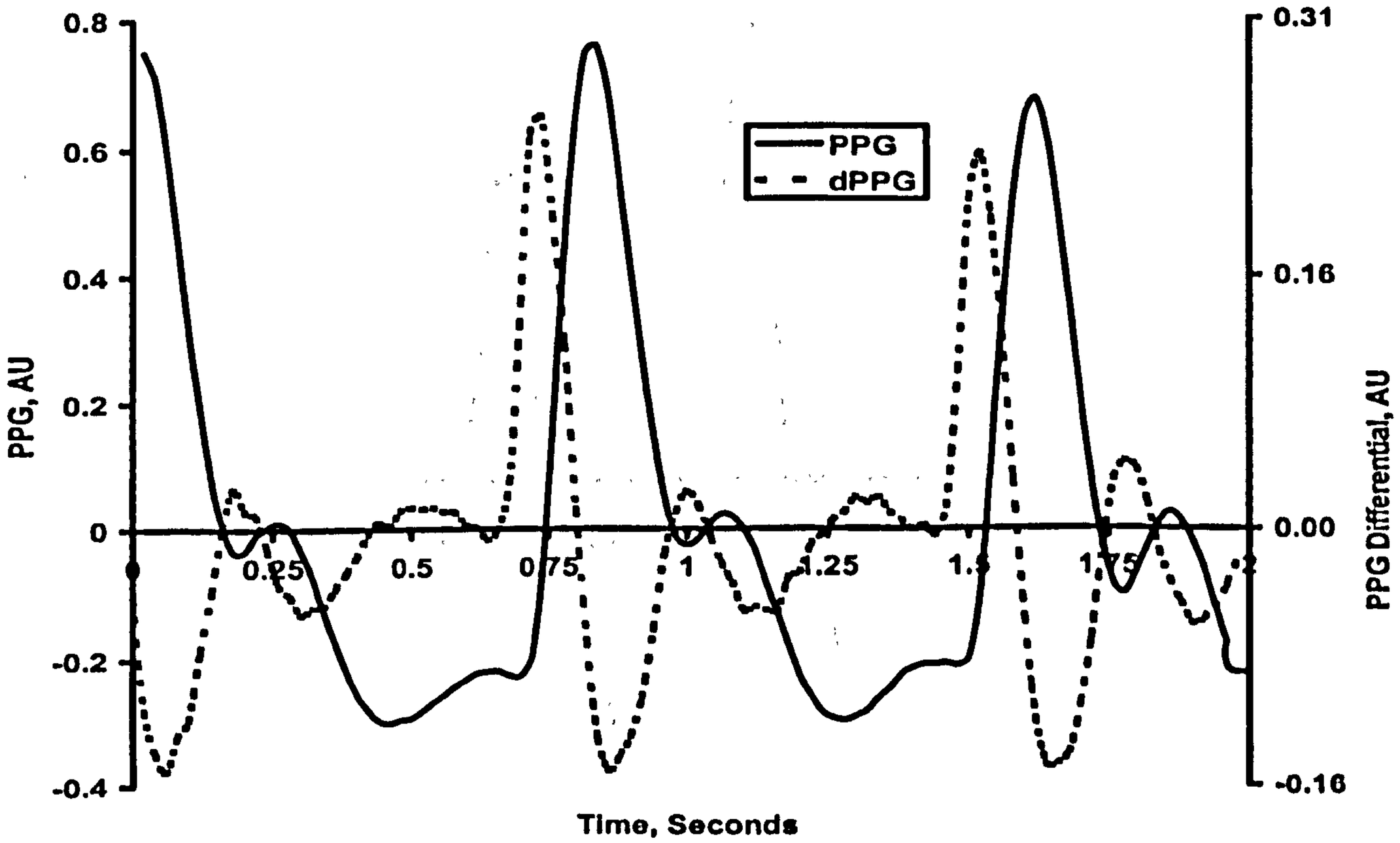

Figure A-1. Typical arterial PPG waveform and first derivative. The noisy nature of the derivative process is illustrated by the ragged trace of the first derivative curve.

Figure A-1 shows a typical windowed pulsatile PPG signal and its numerical gradient illustrating these points. Each gradient zero crossing point indicates a signal sign change; a +ve to –ve sign change indicates a local peak and a –ve to +ve sign change indicates a local trough. Analysis of the initial waveforms with observation of the derivative zero crossing point determination of the fundamental peak or trough.

Obviously, any noise present on the signal will produce extraneous local peaks and troughs whose presence will be exacerbated by the derivative process. This feature is an inherent disadvantages when performing gradient analysis. An actual rugged implementations of this technique require smoothed data and careful adaptive thresholding in order to obtain useful information.. One approach to generating noise free data is to heavily filter the data, either by using a conventional low pass circuit in the electronics front end or using a digital low pass filter on the digital data.

The hardware solution requires more complex electronic circuitry, and the digital solution requires more processing time or more processing power. Both solutions also affect the timing of any peaks detected because of the phase delay of the filters. To counteract this, a more ruggedised algorithm can be developed which double checks the peak detected by the gradient using the values of the original waveform.

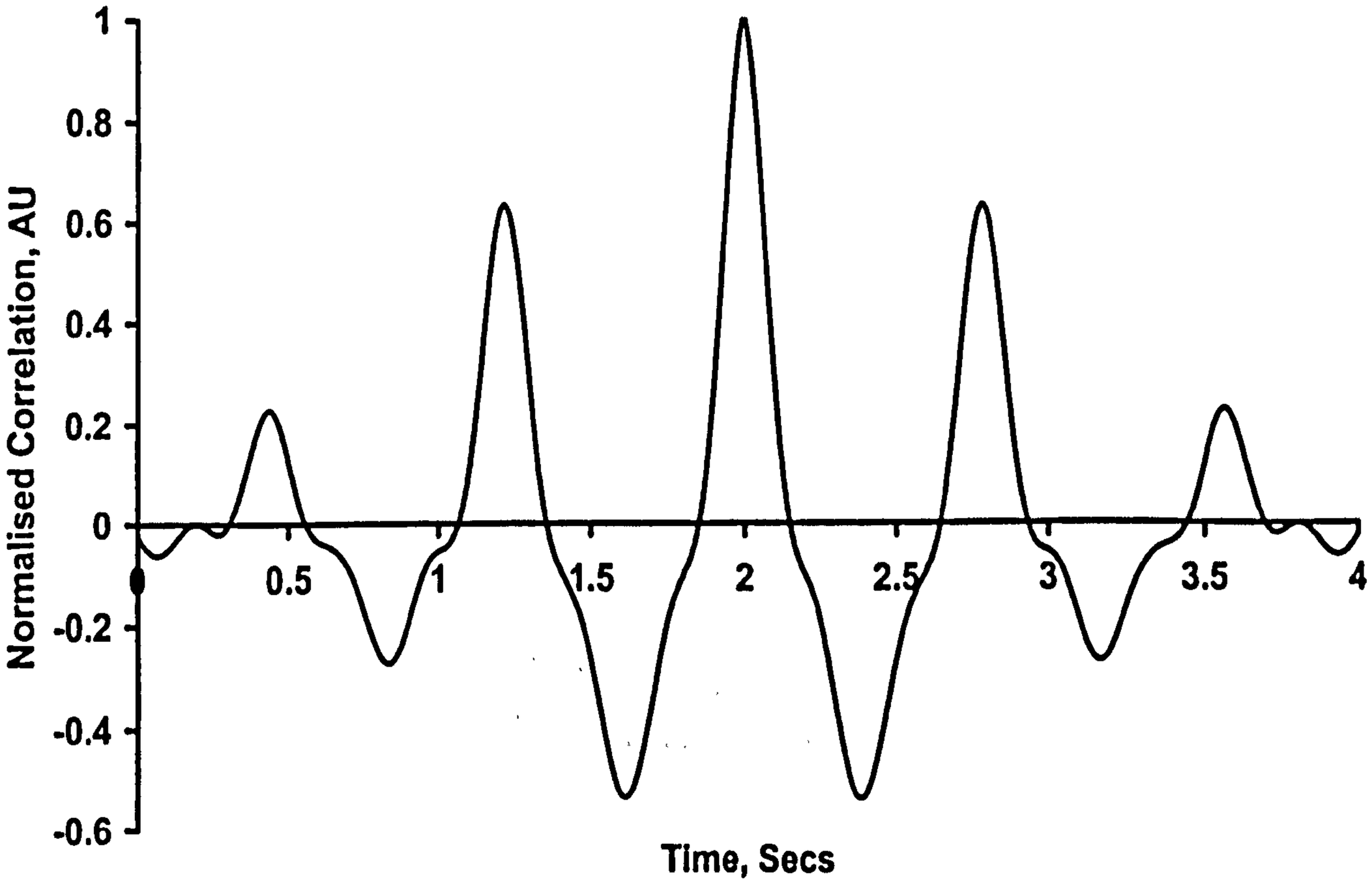

Figure A-2. Auto-correlation waveform of typical arterial PPG.

Here, data points from the original waveform adjacent to the differential zero crossing point are checked. The value of these two points should be less than the value of the zero crossing point to indicate a peak. When the fundamental peaks of the periodic waveform are found, the peak to peak periodicity may be determined by monitoring the time interval between successive peaks. In the case of PPG, the beat to beat heart rate (amongst other things) may be determined by this.

A.1.2 Correlation and Auto-Correlation

Correlation is a classical signal processing technique, often implemented as a correlation filter or as the cross correlation of a data series with itself. In practice, only a finite part of the data set can be analysed at any time (i.e. a windowed data series), which may result in convolution errors. The purpose of both matched filter correlation and auto-correlation is to produce a signal whose features have been accentuated. Running an adaptive peak detection algorithm over the correlated data series should allow the features of the waveform to be detected in a similar manner discussed above, but with greater robustness since noise will have been reduced. Figure A-2 shows the auto-correlation waveform of the arterial PPG signal shown in Figure A-1. Notice the two-second PPG series has been doubled in time, which must be accounted for.

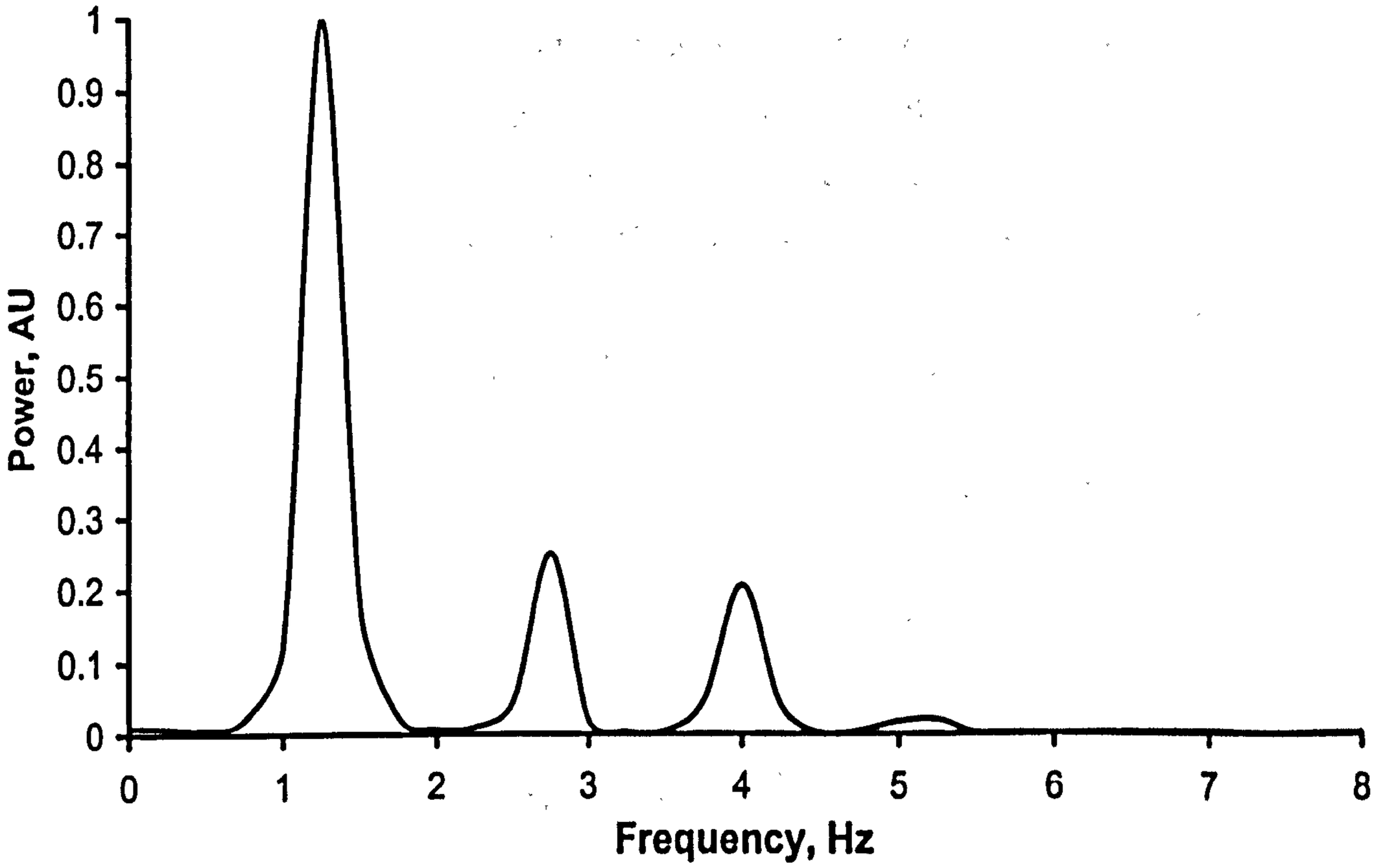

Figure A-3. Power spectrum of a typical arterial PPG waveform.

Correlation can be relatively insensitive to noise compared to the gradient analysis method, since the signal to noise ratio of the correlated waveform is enhanced compared to the initial waveform. An additional peak detection post analysis process is required, however.

A.1.3 Discrete Fourier Transform

The discrete Fourier transform is another classical signal processing technique. The purpose of the Fourier transform in this context is to decompose a time domain series into components of frequency and associated phase. The square of the magnitude gives an indication of the power in each frequency component, termed the power spectrum. The power spectrum fundamental will be the periodicity, and multiples of this will give extra information. Figure A-3 shows the first four harmonics of the arterial PPG waveform of Figure A-1.

Problems with the Fourier transform are its processing time, hence the development of the Fast Fourier Transform (FFT) algorithm, which can only work on a data sequence a power of 2 in length. However, more significant implementation problems arise when processing data with the Fourier transform. The fundamental resolution of the transform is limited by the size of the input vector. This is best illustrated with typical heart rate determination example.

If a PPG signal has a sample rate of 50Hz, then the maximum frequency component available from this is 25 Hz, from the Shannon sampling theorem[1]. If we have 1-minute vector of data samples for analysis, then we will have 3000 samples in total. Taking a discrete Fourier transform (not a FFT since the length is not radix-two) will give a data transform of length 3000 but only half of this is used in deriving a power spectrum. From this, the spectral resolution will be 25/1500, which is 16.67mHz. When using the discrete Fourier transform to obtain the fundamental thus heart rate over the sampling period, this equates to a resolution of 1 Beat per Minute (BPM). Clearly, the heart rate can vary over this one-minute period, so the fundamental will have wider lobes indicating variability about this point. The relationship between sample frequency, number of samples and heart rate resolution is shown in equation [A.1].

$$[A.1] \quad \frac{Fs}{No.Samples} \times 60 = \frac{Fs}{Fs \times SampleTime, s} \times 60 = \frac{60}{SampleTime, s} = \text{Resolution}, BPM$$

Equation [A.1] above shows the limitation when using the Fourier Transform method for obtaining information from the PPG.

Additionally, convolution problems apply when performing the Fourier transform of a windowed data series, since a simple rectangular window produces windowing errors in the transform caused by the convolution of a rectangular window with the data. Various windowing schemes, such as Blackman, Gaussian, Chebychev etc are used to reduce these errors, as discussed in the literature[1]. However, care must be taken to ensure that any interpretation of the Fourier transform is taken as the transform of the actual PPG signal and not the transform of the window.

A.2 Novel Analysis

Because of the inadequacies of the above methods, two methods for identifying parts of the PPG waveform were developed.

A.2.1 Envelope Detection

Since the PPG signal gives a measure of overall perfusion in the site being monitored, it may be used to detect changes in perfusion over time. In this case, the periodicity element of the PPG waveform is irrelevant, and the overall trend or envelope of the signal is of more interest. We can then monitor the trend of the waveform to determine relative perfusion changes in the periphery.

Traditional envelope detectors, based on a non-linear diode model, have limitations since the so called half wave rectification needs excessive low pass filtering (smoothing), which reduces temporal resolution. Full wave rectification is better, but similar problems still apply.

A non-linear band limited envelope detection algorithm was developed which follows the magnitude trend of the PPG waveform, allowing evaluation of relative perfusion changes in the area of interest. This algorithm eliminates phasing problems associated with low pass filtering or averaging of the waveform, which is another method for determining the envelope. Another common problem with envelope detectors is spike sensitivity; this algorithm employs a band-limited approach that reduces errors in the resultant envelope due to noise spikes.

A.2.1.1 Algorithm Parameters

Section A.4 details the envelope detection as pseudo-code, with an apostrophe used to indicate comment to end of line. The algorithm operates over the length of a data vector. The algorithm uses three parameters to control the output: `Tau`, `dRateMax` and `IncRate`. `Tau` is the analogue of a time constant as applied to a first order RC circuit, and controls the envelope rate of decay after a peak in the signal. The parameter `dRateMax` controls the sensitivity of the adaptive threshold for peak limiting. The value `IncRate` is the sensitivity to adaption of the peaks.

A.2.1.2 Algorithm Description

After initialisation, the algorithm checks if the current data value is greater than the previous one. This splits the algorithm into two basic states: tracking, where the output is following the input usually occurring on a rising edge; and falling, where the output is decaying governed by the time constant `Tau`.

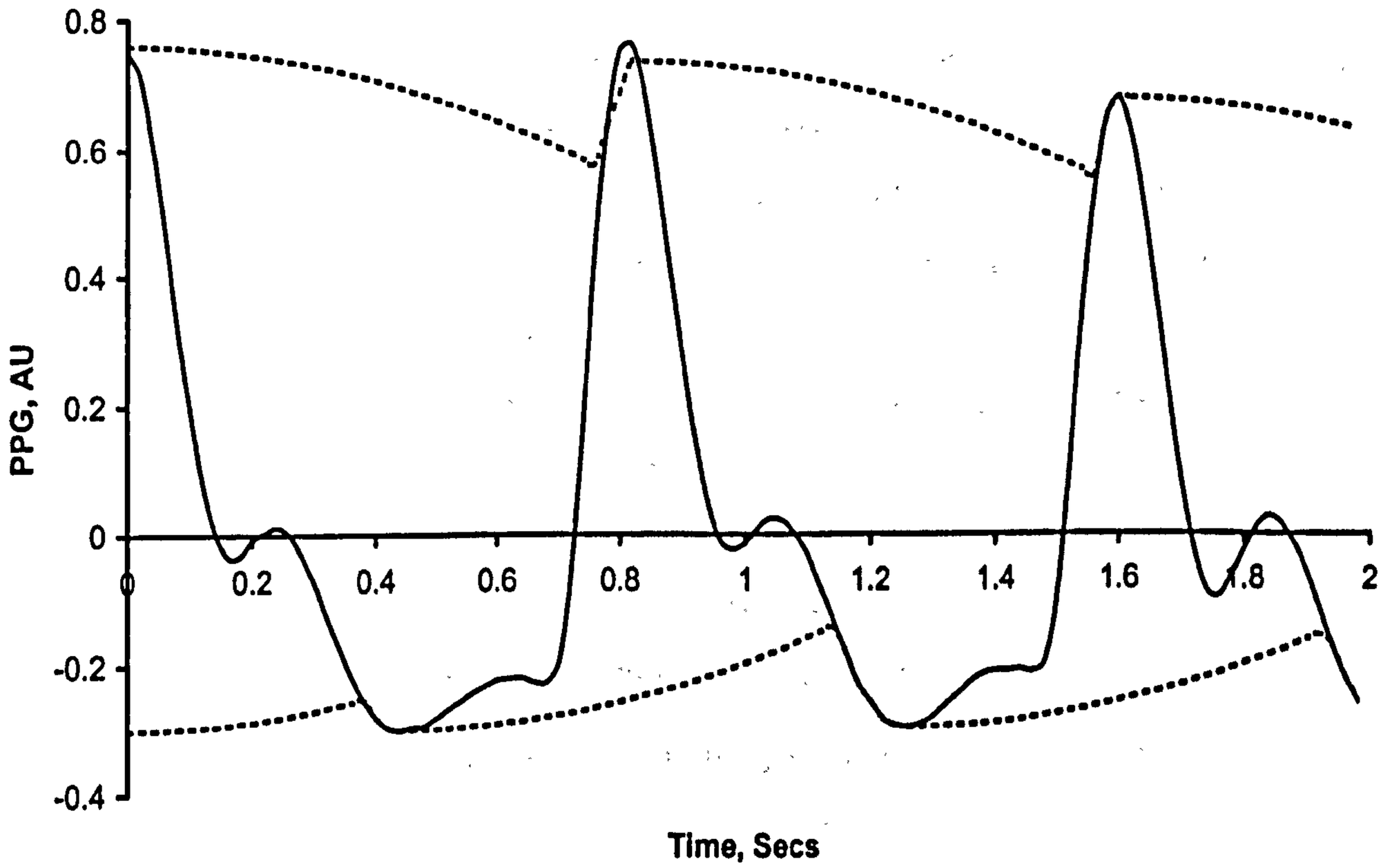

Figure A-4. Application of novel envelope detection to arterial PPG waveform. Rising envelope limiting is visible around 0.8 seconds, and tracking is observed at around 1.6 seconds.

A.2.1.2.1 Tracking Mode

If the current data value is greater than the previous value, the algorithm is in tracking mode. Tracking mode means the output envelope follows the contours of the data series, and a flag is set indicating track mode and the time of the currently tracked point.

However, if the rate of change of the wave-shape is greater than a predetermined threshold, the output envelope will be limited to that threshold. The threshold is a predetermined parameter, and this threshold may be modified by the other algorithm state. A flag is also set to indicate limiting took place.

A.2.1.2.2 Fall Mode

This algorithm state is entered when the current data value is less than the previous envelope value. Now, the output envelope is calculated using the Tau time constant based on the distance between the current and last tracked point.

If both the track and limit flags are set, then the limit value is increased. This is done so automatic adaptation can be performed by the algorithm; rapidly changing transients use a greater maximum rate of change threshold than slow changing waveforms. This helps reduce noise spikes. If the tracking flag was set but limiting flag not set, then the maximum rate of change limit is reset to its default value.

Finally, the track flag is cleared if it was set.

A.2.1.3 Advantages of the Algorithm

This algorithm as described provides a general contour for PPG waveforms, making the trend analysis method available to PPG waveforms. The algorithm does not introduce phase delay problems, unlike filtering techniques, and still provides temporal information, unlike integral techniques. The algorithm reduces spurious noise spikes due to its band limiting nature. A demonstration of the algorithm is shown in Figure A-4; this figure was produced by running both a positive and negative version of the algorithm over the data set used in Figure A-1 with appropriate parameters. Limiting is visible when in the resultant envelope when following, and it is clear this limiting will occur any transient spikes. A case where the envelope algorithm is also demonstrated where the envelope simply tracks the PPG waveform.

A.2.2 Non-Linear Sliding Window Image Generation

Although the novel envelope detector developed previously is useful for monitoring the trend of a waveform, it does not allow us to analyse individual pulsatile events from the PPG waveform. This section develops a non-linear sliding window method that is able to recognise features of the PPG waveform.

This approach produces an image of the PPG waveform that is then subsequently processed to detect features from the data, using common analysis techniques such as thresholding. As with other algorithms presented here, this algorithm uses a sliding window. The difference between this algorithm and previous algorithms discussed is that this algorithm uses a rectangular window in both the y (PPG amplitude) and x (time) axis, whereas previous algorithms have used a window in time.

The size of the window depends on the sensitivity required, and the window slides down the data set in the y-axis from the upper y-limit to the lower y-limit before moving across in the x (time) direction, where it then repeats. This algorithm is designed for processing raw data as it arrives from an analogue to digital converter. For example, if a signed 16-bit analogue to digital converter is used to quantise the PPG signal, the upper and lower limits of the signal will be 2^{15} and $1\text{-}2^{15}$ respectively. These represent the limits of the quantiser, so the upper and lower window limits in the y direction as used by the algorithm are set to these limits. The generated image will be the width of the data set to be analysed (i.e. columns) and will be full-scale magnitude / Δy tall (i.e. rows).

A.2.2.1 Algorithm Description

Section A.5 gives full pseudo code for the algorithm, with Figure A-5 showing the notation as used in the following algorithm description.

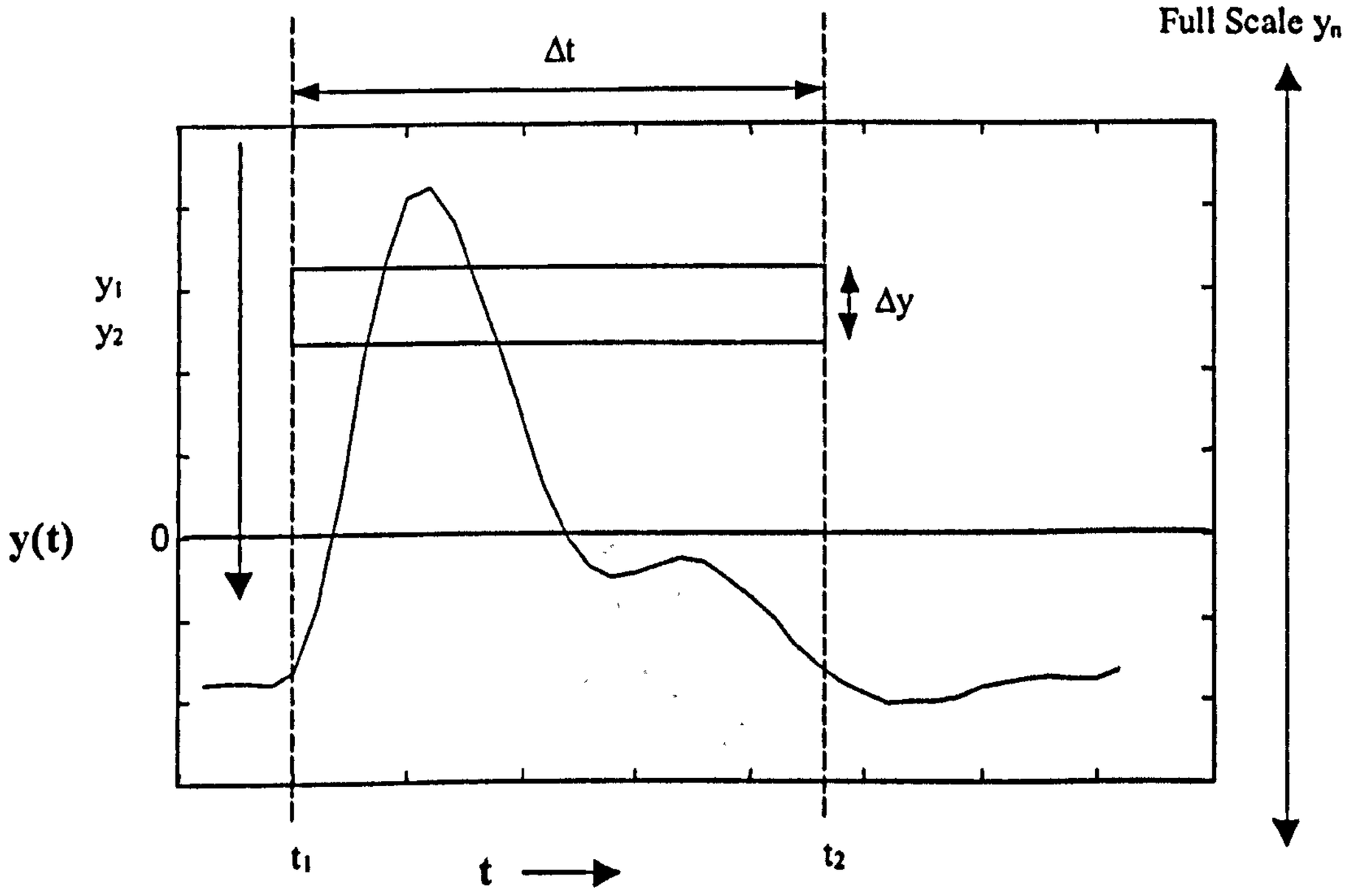

Figure A-5. Non-Linear Sliding window nomenclature.

As the sliding window traverses down the data vector in the y – direction, it extracts a 'window' of the data who's maximum amplitude is Δy and whose width is Δt, as shown in Figure A-6.

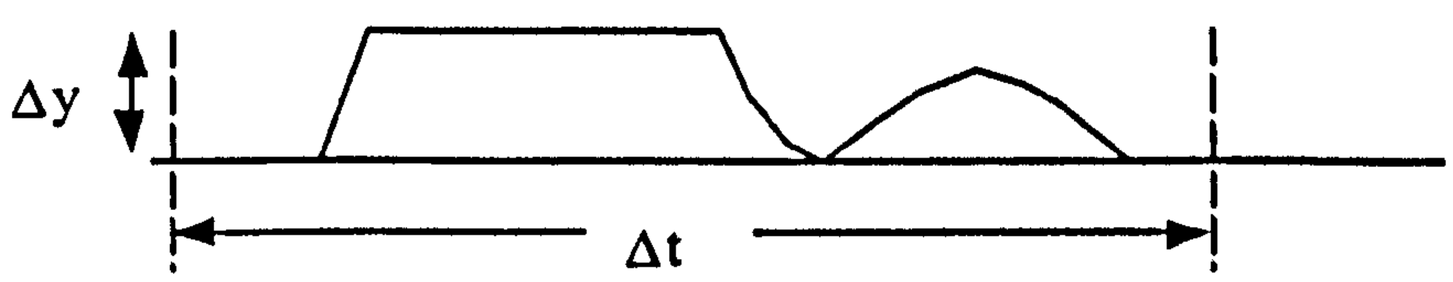

Figure A-6. Close of of sliding window.

If this segment is either all zero or all Δy, then the corresponding point in the resulting image is marked as uninteresting, usually a zero. However, if this is not the case, then the gradient of the window array is found. By analysing the relative positions of the maxima and minima of this gradient, a peak or trough may be detected. If the ratios of the peak and trough values exceed a given threshold, then the resulting image point is

marked with a 1 for a peak or a –1 for a trough. If the ratio threshold is not exceeded or the positions of the maxima and minima do not correspond to anything of interest, then the resulting point is marked uninteresting. This gives a 3 level image, typically shown in Figure A-7.

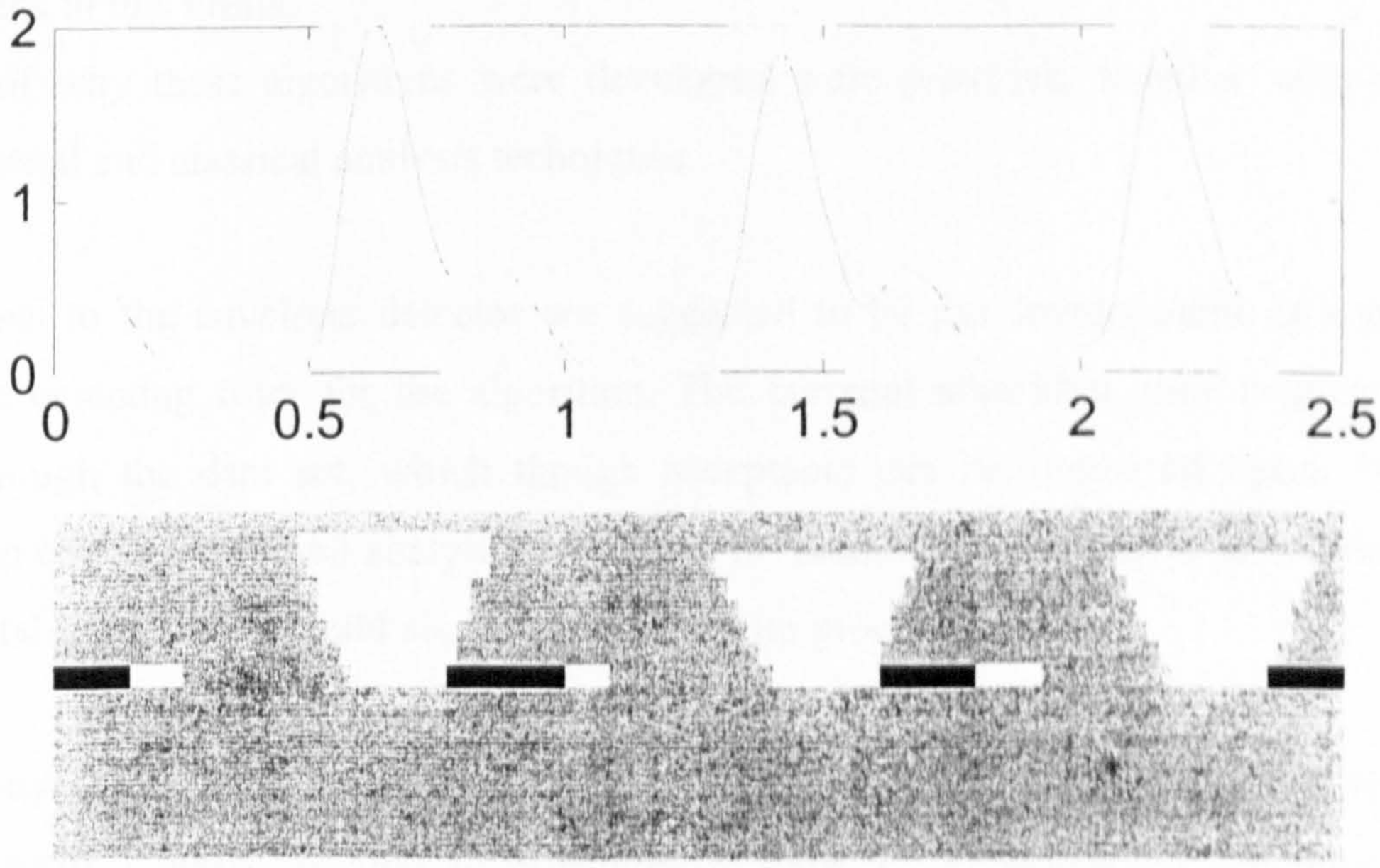

Figure A-7. Application of non-linear sliding window to typical arterial PPG waveform. Top figure shows arterial PPG waveform, bottom figure is resultant image. White areas show peaks, black areas show trough.

A.2.2.2 Advantages of the Algorithm

Figure A-7 illustrates the power of this algorithm. A normalised PPG waveform is shown, and the resulting is shown underneath, with a window width of 0.4 seconds and 16 rows per image. Any peaks are represented by a white section of the image, and any trough by the black section of the image. Simple thresholding of the columns of this image allows peak detection, as illustrated by the block PPG image on the PPG time waveform, but other algorithms may be applied to the image in order to determine other factors.

A.3 Conclusion

This appendix has described the novel analysis method used for determining the both envelope and the location of peaks and troughs as used during analysis of pulsatile PPG waveforms in this thesis.

Details of why these algorithms were developed were provided, together with more conventional and classical analysis techniques.

Extensions to the envelope detector are suggested to be the development of a novel envelope detecting filter for the algorithm. The curreant alkorithm must sequentially walk through the data set, which though acceptable can be improved upon. If the algorithm can be expressed analytically, it may be possible to implement the algorithm as a digital filter, which could significantly speed up processing times.

Extensions to the sliding window technique are similar to the proposed novel envelope filter described above applied to a sliding window filter, enhancing the speed of operation. Additonally, the implementation suggested here only produced a tri-level image to identify peaks and troughs, but the flexibility of the algorithm lends itself to numerous image processing techniques for more complete identification of the PPG waveform.

A.4 Pseudo Code for Novel Envelope Detector

```
' Input is Data vector, output is Envelope vector.
' Control parameters are time constant Tau for delayed falloff, and
' dRateMax for maximum rate of change for rising edges,
' finally, IncRate is change in rising limit.

' Make counter to run through data vector
For t = start to length(Data)

      ' Check for a rising or falling edge, If rising, track data.
      ' If falling, use a delayed tail off
      If data(t) > Envelope(t-1)
            ' We are on a potential rising edge, so set flag
            Set Track_Flag
            ' We need to establish adaptive threshold,
            ' based on previous envelope value plus a function
            ' of dRateMax and a limit counter.
            Thresh = Envelope(t-1) + dRateMax*Limit_Counter
      ' Check data is not greater than limit
      If Data(t) < Thresh
            ' Its OK, Track Data
            Envelope(t) = Data(t)
            ' Not currently limiting, so…
            Clear Limit_Flag
      Else  ' Threshold if
            ' Data too high, could be spike, so limit
            Envelope(t) = Thresh
            ' We are limiting, so
            Set Limit_Flag
      Fi    ' End of threshold check if
            ' Now record time as last tracked point
            Last_Tracked_Point = t
Else  ' Associated with rise/fall if
```

```
' We are falling, so use time const parameter
Envelope(t) = Envelope(t-1) - Tau*(t-Last_Tracked_Point)
' If we are tracking, clear tracking flag
' Since we are now on the falling waveform
If Track_Flag
      Clear Track_Flag
      ' Check to see If we are limiting
      If Limit_Flag
            ' We are limiting, so increase rate of change
            Limit_Counter += IncRate
      Else  ' Limit if
            '  Since  we  are  not  limiting,  clear  Limit
            Counter
            Limit_Counter = 1
      Fi    ' End of If limit
   Fi    ' End of Tracking if
Fi ' End of rising/falling If
Rof   ' End of loop counter for.

' End of Novel Envelope Detector
```

A.5 Pseudo Code for Novel Non-Linear Sliding Window Image Generation

```
' Input is Data vector, output is an Image, Out.
' Out has dimensions (Y Full Scale) / dy tall and length(data) wide.
' Control parameters are dt, dy and Threshhold.

 ' Make counter to run through data vector
For t = start to length(Data)
Seg = 1                 ' Image Y position counter
yn = Y_Upper_Limit
t2 = t + dt/2, t1 = t - dt/2    ' Upper and Lower x Limit

Do                                  ' Loop for Y axis window walk
      ' Setup rectangular window
      y2 = yn , y1 = yn - dY              ' Upper and Lower y Limit
      ' Counter for x axis walkthrough
      For Count = t1 to t2
            ' Make vector
            If y(t) ≥ y2
                  yout(Count) = dy
            elseif y(t) ≥ y1
                  yout(Count) = y(t) - y1
            else
                  yout(Count) = 0
            Fi    ' End of limit check if
Rof   ' end of x walker counter

' Now we have vector, analyse it.
If Sum(yout) == 0                   ' Check for empty vector
      Out( t, Seg ) = 0
ElseIf Sum(yout) == dt*dy           ' Check for full vector
      Out( t, Seg ) = 0
Else
```

```
' Check locations of max gradients to determine
' type of curve using positions of max and min
' values of gradient
dyOut = gradient(yOut)      ' Get Gradient of vector
If position(max( dyOut)) < position(min(dyOut))

' We have a possible Peak, perform a threshold
' check to eliminate noise
If abs( min(dyOut) / max( dyOut) ) > thresh
            out( t, seg) = 1   ' Mark peak
      Else  ' Probably noise
            out( t, seg) = 0   ' Mark not interesting
      Fi

' Check for trough in same manner as above
ElseIf position(max(dyOut)) > position(min(dyOut))
      ' Again, use threshold to check for noise
If abs(min(dyOut)/max(dyOut)) > thresh
            out( t, seg) = -1 ' Mark trough
      Else  ' Probably noise
                  out( t, seg) = 0   ' Mark not interesting
            Fi    ' Trough Threshold if
      Else  ' All other cases result in
            out( t, seg) = 0   ' Mark not interesting
      Fi          ' gradient positions if
   Fi             ' Vector analysis if
   Seg = Seg + 1  ' Increment Y counter
' Loop until Y window position is at bottom limit
While y1 > Y_Lower_Limit
' Now move window in x direction and repeat
Rof   ' End of for

' End of Novel Non Linear Sliding Window Pseudo Code
```

A.6 Appendix A References

[1] Oppenheim A.V, Schafer R.W, "Discrete-Time Signal Processing", Englewood Cliffs, NJ: Prentice Hall, pp. 311-312 (1989)

Optical Engineering Group
Loughborough University

Appendix B

WinPPG Hardware Description

B Application of Simple PPG Analysis

The trials in this thesis employed a sophisticated dual channel PPG system, termed WinPPG, allowing recovery of both pulsatile (arterial) and quasi-static (venous) PPG signals from a variety of PPG probes. Full ambient light artefact compensation and a high-resolution quantisation system allowed PPG waveforms to be captured and recorded onto a PC with great accuracy.

This section describes the design and construction of both hardware and software components of the system. Although these two areas, the hardware and software, could fill each a thesis individually with technical detail, enough information is presented here to allow construction of a similar unit should it be desired.

B.1 Introduction

Before any trials were conducted, investigation of available PPG recording hardware revealed unknown signal processing components within the hardware that could affect subsequent analysis. Furthermore, many systems employ auto-normalisation schemes, since it was assumed the magnitude of the pulsatile PPG waveform is un-calibrated, therefore not required. Finally, most PPG systems offered either venous waveforms or pulsatile waveforms, at that time a system offering both outputs was unavailable. The field of dual channel systems was also extremely limited.

Consequently, a high resolution dual channel PPG recording system, offering full control of LED intensities and full high resolution capture of both venous and pulsatile components of the PPG system was constructed. The system comprised two components; the hardware, developed using the PPG analogue to digital data acquisition subsystem presented as part of the PhD thesis of Mathew Hayes[1], a digital interface board, which allows the PPG sub-system to communicate with a PC via the printer port, and a control program, written to communicate and control the hardware via the parallel port under Microsoft Windows NT/2000 or Windows 95/98.

B.2 WinPPG Hardware

The WinPPG hardware is comprised of three blocks, PPG analogue to digital subsystem, interface card and power supply.

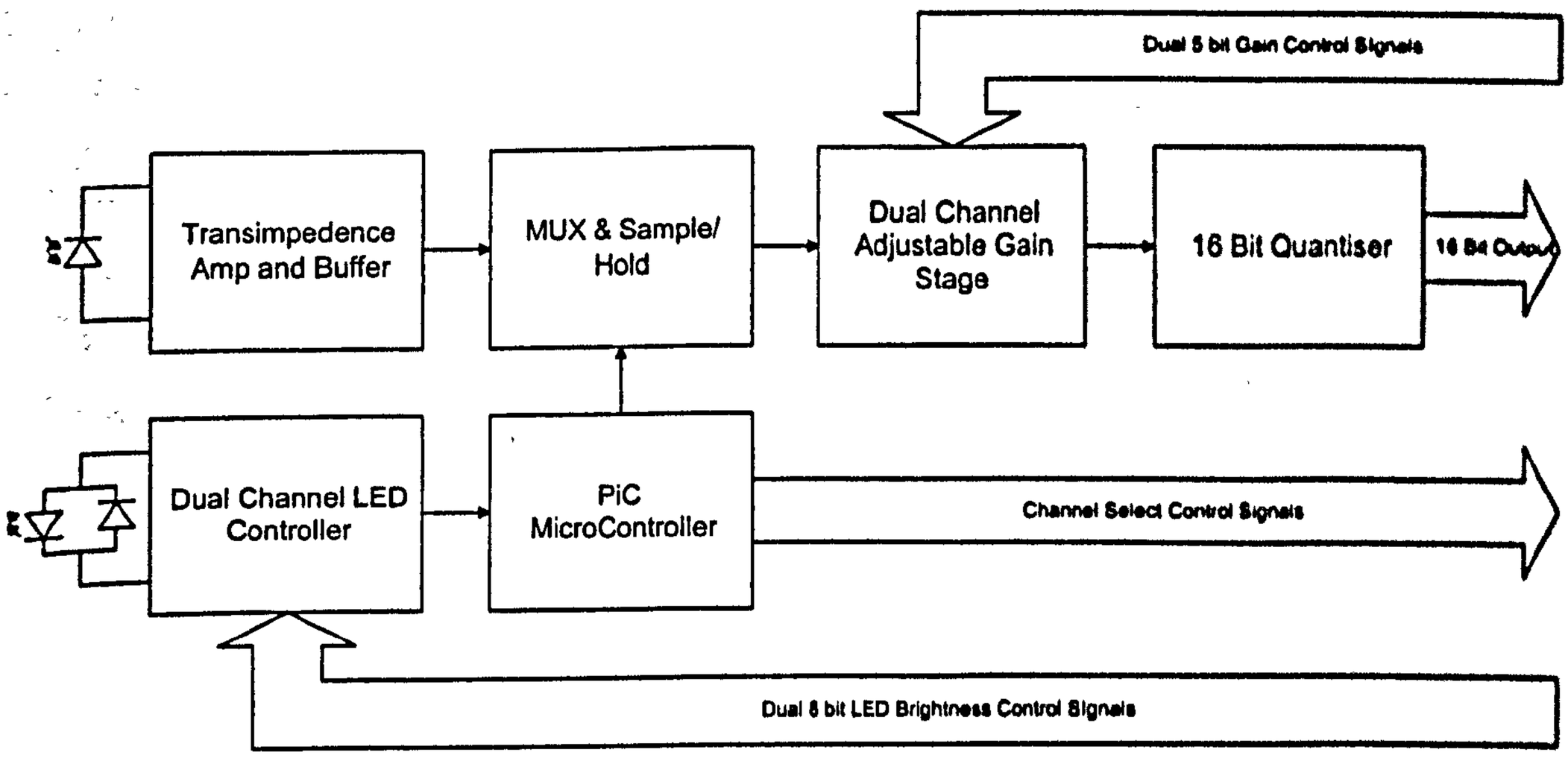

Figure B-1. Block Diagram of the PPG Data Acquisition Subsystem.

The PPG subsystem is a digitally controllable data acquisition system, specifically designed for precision PPG signal recovery. Designed by Dr Mathew Hayes, the PPG data acquisition subsystem is detailed in full as an appendix in his thesis[1] but an overview is included here for completion.

The PPG subsystem is a digitally controlled, dual-channel 16-bit ambient light compensating, signal-conditioning data acquisition card, offering digital control of internal gain stages. A microcontroller synchronously controls both ambient light subtraction, sample and hold circuitry and a digitally controlled dual channel LED driver circuit. A block diagram of the PPG system is shown in Figure B-1.

The PPG subsystem shown in Figure B-1 converts a photodiode current sink output from a standard Pulse Oximetry PPG probe into multi-channel ambient light compensated PPG data signals. Sample and hold circuits are used to obtain both quasi-static (venous) PPG signals and amplified dynamic (arterial) PPG signals for both LED channels, both of which are ambient light compensated.

Brief specifications of the PPG card are described in Table B-1.

PPG Analogue to Digital Data Acquisition Subsystem	
Normalised frequency Response	0.9 to 4Hz
Fixed Gain Stages, Linear Phase response	
Transimpedence Resistor	10Kohms
Buffer Amplifier gain	20dB
Adjustable Gain stage	12-72dB, 31 Steps mean step size 1.8752dB
Quantisation Stages	
16 Bit D/A Converter Speed	5050 samples per second
D/A Converter Specifications	
LED Driver	
Programmable constant current LED Drivers	0-50mA in 256 steps

Table B-1. PPG analogue to digital subsystem specifications.

B.2.1 PPG Card Digital Output format.

The PPG data aquistion subsystem provides a 16-bit data bus and data channel active strobes for simple system interfacing. A Data Valid (DV) positive clock is provided along with strobes (DV0-5) for the appropriate channel to signal what data is present on the shared 16-bit data bus. A timing diagram illustrates this more clearly, as shown in Figure B-2. Note there are 5050 DV pulses per second.

DV is the data valid clock strobe. Whenever DV is high, valid data is present on the data bus, shown by a stable data bus (DB) period on the timing diagram, with the appropriate channel data presented on the data bus. DV0 to 5 are valid data strobes indicating which of the six channels are currently available.

Notice that in this implementation, channels 4 and 5 are unused since channel 4 represents the ambient light intensity level and channel 5 is spare.

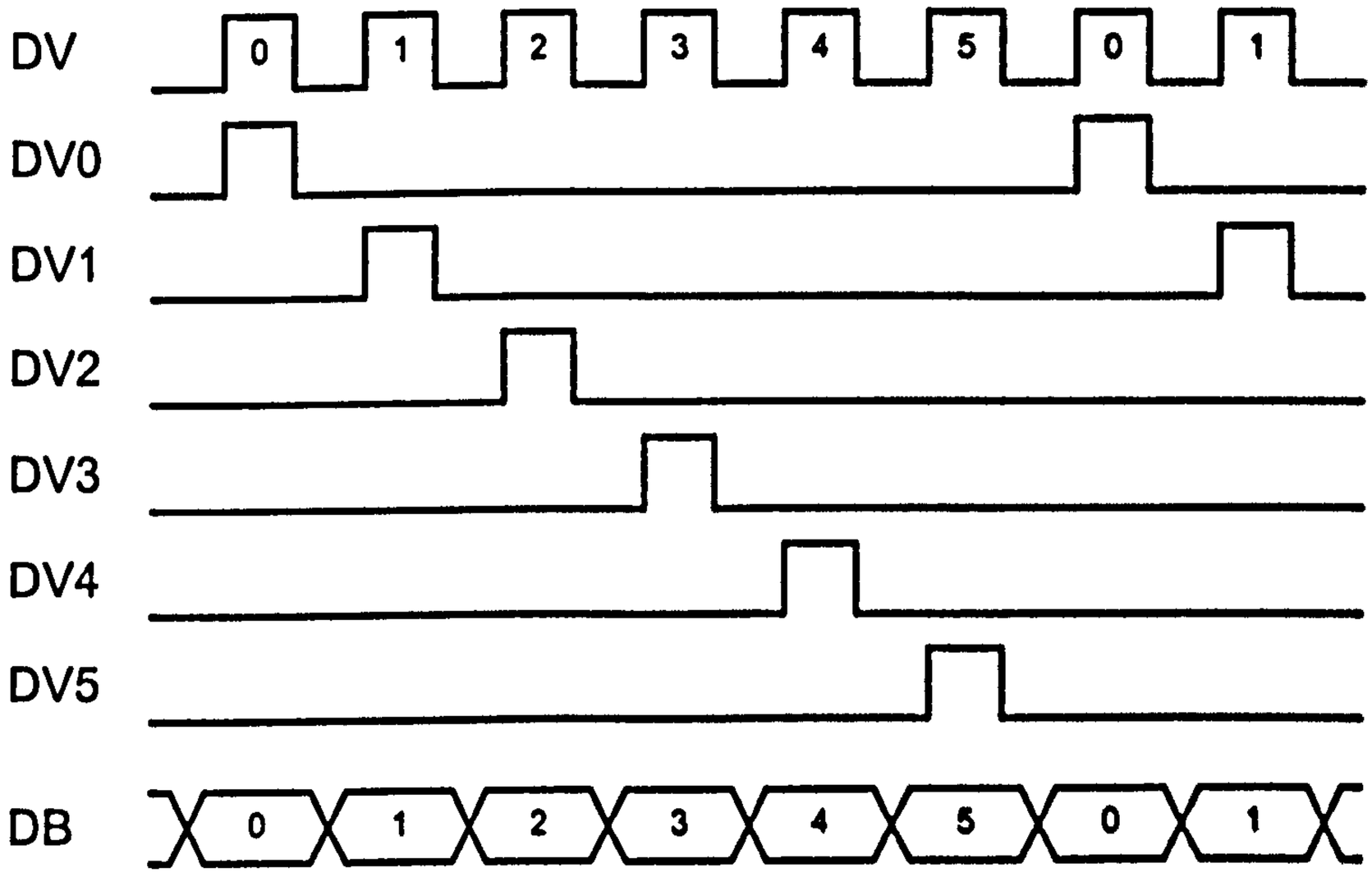

Figure B-2. PPG Data Acquistion subsytem timing diagram.

B.2.2 Interface Card

The interface card is responsible for converting the channel number and 16 bit data generated by the PPG card into a format suitable for communication with a PC. Since data timing is very important in this application, a PC parallel port operating in bi-directional mode was used to transfer data in 8 bit chunks, between WinPPG and the PC, using a hardware interrupt process. When the interface card sets an interrupt request, a dedicated thread program running on the PC (the interrupt service routine) responds to this signal, copying the four channels currently stored in into buffers in the PC. The thread then returns to the interrupted program, allowing the PC to resume normal processing, in this application displaying PPG waveforms.

So as not to overload the PC, a 4-channel hardware buffer was implemented in the PPG interface card to reduce the interrupt overhead by four, along with a decimation circuit, allowing control over the interrupt frequency. This scheme buffered each of the four channels before requesting an interrupt, whereby all four data channels were transferred.

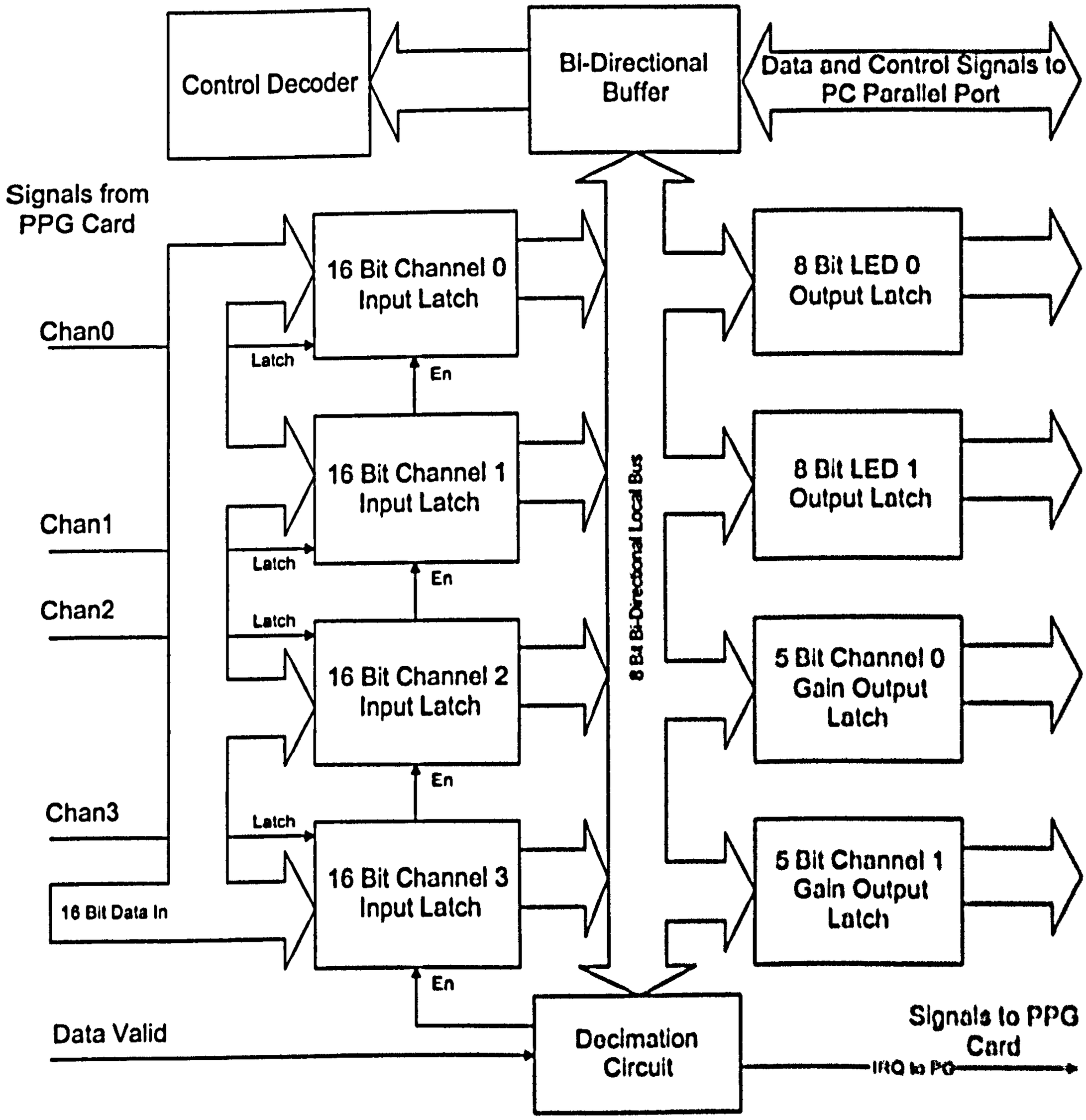

Figure B-3. Block diagram of the PPG interface card.

The decimation circuit was necessary since the data valid (DV) clock rate is fixed by the PPG Card microcontroller at 5050Hz, which is too rapid an interrupt request rate for a bi-directional parallel port on the majority of PCs. However, the decimation circuit allows control of the PC interrupt rate to a more suitable frequency when using a slow PC host machine. Effectively reduces the sample frequency, and the appropriate decimation level must be considered for each application.

A block diagram of the interface card is shown in Figure B-3, illustrating the input latches, the common internal 8-bit bus and the data output latches that control the PPG card.

The PC is responsible for selecting the destination of any data on the internal bus. If the PC is writing to either the LED, Gain or Decimation output latches, the input latches are disabled. If the PC is reading from the input latches, then the output latches will not respond.

Figure B-4 shows the master schematic of the WinPPG system, and is a more detailed version of Figure B-3. The master schematic

Figure B-4 is a hierarchical drawing, and each block represents a sheet, with each page of the hierarchy are also shown from Figure B-5 to Figure B-9.

B.2.3 Basic operation

The PPG card presents data to the input latch circuitry in the sequence shown in timing diagram Figure B-2.

These latches act as memory elements as previously described, storing the current 16 bit value of the associated channel into two 8 bit latches. The I²C is able to read any of these latches in a byte wide format by selecting the appropriate channel on the control lines of the parallel port, thereby enabling the appropriate 8 bit latch output. This then drives the internal data bus, which is then applied to the parallel port via the buffer circuitry. The latch control channel select logic is decoded by the decoder schematic, Figure B-8, half of the 16 possible decoded as inputs and the other half are decoded as outputs using, standard TTL de-multiplexers (74HCT138 and 74HCT238). The decoded output from the control line causes data on the internal bus to be latched by the output latch circuitry, which is responsible for two channels of LED brightness and two channels of Gain control. Notice the gain controls only use the lower 5-bits of the byte wide output port, achieving 32 possible gain levels.

Because of the great variety of differing PC system architectures available, the decimation circuit was devised. If the raw interrupts requests were applied to the parallel port at 5050Hz, it is quite possible this would overwhelm most PC systems with a slower response. The decimation circuit acts as a programmable divider, only creating an interrupt request after a pre-determined number of interrupts.

Examining the decimation circuit in Figure B-7, this is achieved in the following way. The activation of the DV3 signal indicates that Channel 3 data is currently valid, thereby implying channels 0 to 3 have recently been updated, as the timing diagram in Figure B-2 shows. DV3 goes to an 8-bit counter chip (74HCT590) which increments on the negative edge; notice signal DV also goes to the counter and updates the internal output latches of the counter. The byte wide count output from the counter chip is analysed using an 8-bit magnitude comparater (75HCT688) which compares this count value with a pre-assigned divisor value from a latch (74HCT574) controlled by the output decoding circuitry. This latch is loaded on system start-up with the appropriate frequency divisor. If the two values are equal, then the counter is reset and a flip-flop (74F74) is set, signalling a valid Interrupt Request (IRQ) into the PC acknowledge line (ACK), which then generates an interrupt if enabled. At the same time, the DV signals DV0-3 which usually latch data into the appropriate 16 bit-input latches are disabled using the LATCH_EN signal, thereby freezing the memory (latch contents) at the time the IRQ occurred. At this point, the responding Interrupt service routine (ISR) running in software on the PC should quickly read and store all 8 input latches forming four 16-bit words from them, then clear the flip-flop re-enabling the input latches. A dummy write output control is used to clear the flip-flop and reset the IRQ condition.

B.2.4 Power Supply Circuitry

The WinPPG System employs a conventional linear power supply, to feed both the logic and analogue circuitry. Linear supplies, though less efficient, generate much less power line noise, which is essential in this operation. Additionally, reduced EMI is an asset, requiring less counter screening measures. The PPG data acquisition system has its own on board regulation circuitry for digital sections of the circuitry. The exact power supply ratings are described in Table B-2,

Voltage	Rating	Requirement
+12V	1.25A	Data Acquisition analogue, digital and LED Power
-12V	250ma	Data Acquisition analogue Power
+5V	250ma	Interface Card digital Power

Table B-2. Power Supply requirements.

B.3 WinPPG Software

This section will discuss the controlling software side of the WinPPG system. The software was written using Microsoft Visual C++ V5.0 for operation under Microsoft Windows 95/98 and Windows NT V4/2000. The PC compatible computer used in this thesis had 16MB of memory and a 233MHz Pentium MMX processor. This was adequate for a 50Hz sample rate. However, a greater specification PC is required for faster sample rates.

A full program breakdown, including class and function description, data flow diagrams and program operation flowcharts would require several hundred pages to describe. Therefore, a basic program overview and functional description is provided. If further program operational details are required, the source code may be consulted, which is fully commented.

B.3.1 Program Overview

This, like many Windows application, was written using object-oriented programming. The programming language C++ is object oriented, allowing the benefits of this programming methodology to be appreciated. Figure B-10 shows the dialog box as it appears when the program is first started.

B.3.1.1 Slider Bars

The program uses a Dialog box strategy, which eliminates the associated event handlers required for single and multiple document interfaces. Slider controls are provided to control the brightness of up to two source LEDs, with an 8 bit, or 256 level controls representing a linear current range of 0 to 50 ma. Slider controls are provided to control the gain on both pulsatile PPG channels, with a 5 bit or 32 level control of gain from 12 to 72 dB. Sample frequency is also controllable from 20 to 255Hz in steps of 1Hz. The start up default usually provides reasonable settings for the majority of Pulse oximetry probes.

A section of the dialog box allows joint control of either LED brightness or gain settings by locking the sliders together.

B.3.1.2 Hardware Configuration

Upon program start up, the program checks the number of printer ports registered, and the printer port zero is made the default. This facility will only work on standard printer

ports that occupy input-output locations of 378, 278, or 3BC in hexadecimal, usually representing LPT1, LPT2 or LPT3. Soft printer ports, which are usually employed by USB devices or PCMCIA devices, will not be accessible.

The interrupt request for the chosen printer port must now be selected. This is often IRQ 7 for LPT1 printers or IRQ 5 for LPT2 printers. This IRQ must match the hardware configuration of the computer otherwise; the system may at worst crash or at least not function correctly.

B.3.1.3 PPG Display

Two panels each contain large black rectangular boxes. These are the waveform viewer windows. The smaller box displays the quasi-static DC waveform, which is useful to ensure the LED brightness settings are adequate and not saturating the photodiode. The larger rectangular window display the pulsatile AC waveforms, generally attributed to arterial effects.

On the left of the AC waveform display are horizontal four bar graph displays – these display the actual value of the AC and DC components for each of the channels. These values are also displayed numerically below the four bar graphs. Above the four bar graphs is the recording display section, which gives an indication of the recording buffer status both as a percentage and numerically, discussed later.

B.3.1.4 Control Buttons

On the upper right of the dialog box are control buttons. The 'About' and 'Quit' buttons are self explanatory. The 'Init' button is used when the system temporarily locks up, which is possible on some older systems. If, when the system is first enabled by selecting the 'Enable Comms' checkbox, nothing happens, clicking this button sometimes clears any stuck latches. However, it is usually best to switch to an alternative machine.

The 'Event', 'Dump' and 'Rec' buttons will be discussed in the recording section below.

B.3.1.5 Display Configuration

The 'Config' button display a configuration dialog box, shown in Figure B-11.

The lower part of the configuration box allows selection of which traces to display. Additionally, sideways scrolling model, emulating a chart recorder, or overwrite mode, emulating an oscilloscope, are the two display options. All traces and scroll mode are the default options.The size of the display rectangles may be adjusted using the appropriate text boxes. Smaller height values allow zooming in of the waveforms, and

the width is given in samples. The update text box allows control over the number of screen refreshes. If this is too fast, reduced system performance will result, hence the low value. More updates per second will reduce display flicker.

The buffer control sets the size of the recording buffer, in samples. Below that, a text fields calculates total recording time, based on the sample rate provided.

A slider bar and checkbox control the sound output of the WinPPG system. If the 'sound' checkbox is enabled, the WinPPG system will emulate a Doppler ultrasound system, with the volume modulated by the mean of the pulsatile waveform magnitude. The 'volume' slider bar controls the overall volume. More details on this feature will be discussed later.

Of the three buttons, two are self-explanatory. The default button will reset the values to the ones displayed. If any values are outside pre-defined limits, the user will be alerted.

B.3.1.6 Recording Mode

With the record buffer size set, the user may select the 'Rec' button once the program is activated by clicking 'Enabling Comms'. Once recording is activated, the 'Rec' button will change to a 'Stop' button. The horizontal slider bar on the WinPPG dialog box will show overall record buffer progress, with a numerical value indicating recording time below.

The 'Event' button and event counter may now be activated, since they are disabled during non-recording mode. Each time the 'Event' button is clicked, the current record time, down to the actual sample number, is logged in memory. This allows event logging during PPG recording, which is a useful feature. When the record buffer is full, recording will be automatically halted.

At any time the system is not recording, the record buffer may be saved to disk by clicking the 'Dump' button. This will display a standard windows file name request box. Both PPG channels, including AC and DC sections, are logged during recording. The saved file includes a time and date header, control settings header and an event log header, followed by the actual PPG data, comma separated.

B.3.2 Interrupts and TVicHW32

Handling interrupts under Windows based programs is notoriously difficult, even more so with Windows NT and 2000. The problem is Windows operates in Protected mode, and only certain programs are allowed to directly access the hardware. While this is

very useful for a multi-user system, it makes things considerably more difficult if hardware engineering is required.

Devoice driver are the class of programs which are allowed to access hardware, both ports and interrupts. Normally, a device driver would be required to access the hardware and control the interrupts. Device drivers under Window are notoriously difficult to write due to the lack of official information freely available.

Fortunately, a generic device driver was found written by Victor Ishikeev[2], available for a very modest fee. This device driver 'sits' at the correct level to access hardware and monitor interrupts. A user level program such as this can communicate with the device driver, asking the device driver to perform the hardware access. This approach avoids protection faults which would otherwise occur.

One disadvantage with this approach is the reduced speed available – each time the user program asks the device driver to speak to the hardware, the device driver must switch operational modes, perform the task, then switch back and report success or failure.

Furthermore, the device driver cannot call a user mode interrupt service routine. Normally in an application such as this, the interrupt service routine would reside in the device driver, servicing interrupts and storing recovered data in a large buffer. When the user mode program was ready, it would empty the buffer when it received its allocated time slot.

However, the interrupt service routine here exists as a user mode program. Consequently, this cannot be called by the device driver when it receives an interrupt. In this system, a worker thread with the highest execution priority continuously polls the device driver, asking it if it has received an interrupt. If it has, the ISR routine is called to communicate with the WinPPG hardware, recovering the data for the PPG channels. The user ISR routine then places this data into the display buffer and recording buffer, if activated.

Consequently, using this approach, the maximum interrupt rate is limited to a much lower value than would be possible if the time critical code ran from the device driver. Furthermore, even when the program is not executing interrupts, the available time for the operating system to perform other tasks is limited, since the ISR monitoring thread is active, continuously asking the device driver if it has received an interrupt. While these disadvantages are far from ideal, this approach allowed a system to be designed and operational in much less time than would have been possible if a custom device driver had to be written from scratch. Additionally, since the maximum desired sample

rate when performing PPG is at most only a few hundred hertz, this approach is practical on the condition that other applications are prevented from running while the WinPPG application is recording data.

One consequence of this approach is the system can be unfriendly to other parallel port peripherals, such as scanners, external CD ROM drives etc. The TVicHW32 device driver will control the parallel port regardless of whether it is already in use by another application. This at best could cause loss of data or at worst case a system crash, so care must be taken to ensure nothing else will attempt to use the parallel port. This usually means disconnecting and uninstalling all parallel port peripherals, including printers.

A brief description of the TvicHW32 class is given below.

B.3.3 Program Operation

The program employs several classes, as would be expected. The main class is named *CNewPPGApp*. This class is quite simple, and just instantiates instances of the other classes, discussed below, displays the instance of the *CNewPPGDlg* class, and if the user quits, releases the various class's it has set up up, freeing memory as it goes. Each of these classes will be further described in more detail.

B.3.3.1 CEventLL

This class is responsible for controlling the events. It does so using a linked list scheme, where each event has a pointer to the previous and next event, each event knows what number event it is and also the associated sample for that event. This approach allows an unlimited number of possible events, as long as the system has enough memory.

This class will automatically release any memory allocated for the linked lists upon program closure.

B.3.3.2 CPPGConf

This class contains the configuration dialog box. It fills the dialog box with the current values upon creation, and check the dialog box values against bounds when the user clicks OK. The Windows DDX (Dynamic Data Exchange) subsystem is used to do this.

B.3.3.3 CWavPlay

This class is responsible for controlling the noise option of the WinPPG software. This class allows the program to load a sound sample of 'Wav' file format. The wav file is a pink noise wav file – pink noise is 'deeper' in tone than white noise, and simulates a Doppler Ultrasound wand with more realism. The wav file is checked to ensure it is the correct format and the system can play it. The wav file is then started playing in an

endless loop. The WinPPG program then controls the volume using the mixer setting, discussed later.

When the program exits, the wav file is stopped from playing, and all associated memory freed. It is important to stop the wav file from playing, since it will not stop otherwise.

B.3.3.4 CNewPPGDlg

This class is effectively the main execution loop, if it were to be viewed as a sequential program. When the class initialises, it checks that the TvicHW32 device driver is available. If so, the class interrogates the system using the device driver to check how many parallel ports are available.

The class then initialises all the components of the dialog box, such as the sliders, windows etc to the default values.

A periodic Windows timer is then set up, which call a timer service routine (TSR) every 50ms. The TSR is the key to this application. The TSR effectively acts as a task scheduler. Each time the TSR is activated, the TSR checks the position of the slider to determine if they have moved since the last TSR activation. It also checks the display buffers to update the display windows. If so, the new value is calculated to pass to the hardware, and any changes made to the dialog box which may need updating. Note the display windows may be scrolled several times before they are actually updated.

If the appropriate update period has passed, the TSR activates the Windows machinery to redraw the dialog box. This is the time consuming part of displaying things under Windows, which is why it is advised to keep to a minimum, so as not to affect the ISR.

If sound is enabled, the TSR also calculates the new volume level, based on high pass filtering the pulsatile PPG data using a small IIR filter. This volume control scheme and the pink noise wav file effectively mimic a Doppler ultrasound wand.

This class also handles the buttons and checkboxes, making the appropriate responses as required, such as event control, communications etc. When the 'Conf; button is pressed, this class displays the configuration dialog box. When it closes, if the recording buffer has changes, memory is reallocated for the new buffer size. If the buffer size is not possible, a warning message is displayed.

This class also displays the about box when 'About' is clicked, which displays the program Version, author information and also what platform the application it thinks it is running on – either Windows 95 for Win95/98 or Windows NT for NT V4/2000.

Finally, this class writes the output file to disk, searching through the events, and writing the data in comma separated format after obtaining the file name using a standard Windows file name requester.

B.3.3.5 CISRData and ISR.CPP

These two items, the class and the source file, are the parts of the application that deal with the interrupts. The class contains the data buffers and the display buffers, and the source file contains the actual ISR. There are two threads and one ISR, in the source file. The two threads, one for use under Windows NT and one for Windows 98, poll the device driver to determine if it has received an interrupt. If it has, it calls the ISR routine. The ISR routine is responsible for placing the data recovered from the WinPPG hardware into the appropriate places in the display and record buffer. The ISR must follow the correct protocol to access the hardware components, using a combination of data bus and control line signalling.

The class and the ISR are separate from all other classes since the ISR and threads are run asynchronously compared to the main application. This causes synchronisation problems, so the whole ISR class is defined as volatile, forcing the compiler to access the class memory for each read. This definition is essential, otherwise an optimising compiler may optimise out two successive reads if the compiler decides no change has been made to the class. However, the asynchronous ISR may have made changes which the compiler would not know about.

B.3.3.6 TVichHW32

This class contains the device driver wrapper functions. This class can interrogate hardware, initialise interrupts and worker threads to simulate hardware ISRs.

Upon initialisation, the class will load the correct operating system device driver, and start the correct thread to monitor interrupts if desired. All port access is performed through this class via the device driver too. As stated, it is not an optimum speed solution, but is adequate for this application.

B.4 Conclusion

This appendix has detailed the WinPPG hardware, used for all the studies in this thesis. The WinPPG system was designed and built since its entire operation in known and characterised, allowing full interpretation of recovered results. This is in contrast to most commercial PPG devices, which give either a relative, automatically scaled pulsatile output, or are designed for venous analysis.

The WinPPG system has been described in full, both in hardware and software terms. While a full description of such a complex system could fill a whole thesis, enough information is provided to understand the basic operation.

B.4.1 Suggestions for Improvement

Improvements to any complex system are inevitably numerous. For this system, they can be hardware, software or both, ranging from refinement to redesign.

Therefore, improvements to the WinPPG system are given below, in ascending order of complexity.

B.4.1.1 Development of Software

The current software version has been adequate for the trials conducted in this thesis. However, optimisation is required in some areas. For example, the Doppler Ultrasound simulation is not fully rugged – any transients cause the noise source to saturate. This is as a result of the IIR filter system for volume control, and could be refined. Additionally, the concept of using the Windows Mixer for volume control is non-ideal, since it affects all sound sources on the computer. A better approach would be to modulate the volume of the sample directly in memory. Regarding the pink noise wav file, this is currently loaded into memory, but it would be relatively simple to derive a sample in code using a random bit generator, eliminating the requirements to load the file.

Further optimisation would be the development of a real device driver. All time critical code and buffer would reside in the device driver, allowing the application to recover data from the device driver buffers every, say, 100ms. This would remove a tremendous load from the OS, since it is currently polling the device driver to determine if it has received an interrupt. The new computational power could allows the system to add extra functionality to the WinPPG system, such as calculate timing intervals, or even perform numerical fits. Development of a real device driver could follow official Microsoft guidlelines, an eliminate any compatability issues as discussed earlier.

B.4.1.2 Development of Hardware

The interface card was designed using conventional TTL techniques. While adequate for this application, a more ruggedised alternative could be developed using a CPLD or FPGA. The entire TTL arrangement could be fitted into a CPLD package, which would have made the system less sensitive to transient spikes and reduced EMI.

Furthermore, it would have been desirable in some of these trials to incorporate a pressure sensor capable of monitoring sphygmomanometer cuff pressure. A spare channel on the PPG data acquisition system could convert the output of an analogue sensor into a digital format. However, the current interface card only has sufficient memory for the two channels, AC and DC. If the interface card was incorporated into a CPLD, extra analogue channels could be available for further monitoring facilities. Furthermore, other parameters could be monitored in subsequent studies, such as finger-tip temperature, Doppler Ulttrasound velocity output etc. Some modifications in the communication protocol would probably be required.

When the WinPPG device was designed over winter 1998/99, the fastest method of communicating was via the parallel port. High-speed serial ports were deemed too slow and too processor intensive. While the chosen generic device driver approach is not the fastest solution, a change in software using a real device driver could substantially increase the throughput and efficiency of the system. If the WinPPG system were to be designed now, a Universal Serial Bus solution would probably be sought. The USB solution offers high speed connectivity, compact connectors and the possibility of interfacing to several target machines by writing software applications alone. A compact USB micro-controller would interface the PPG data acquisition system to the PC, providing a small fully controlled PPG system. A real device driver would be required for this application, but the advantages would outweigh the technical difficulties involved, especially since device driver writing information is becoming increasingly more available.

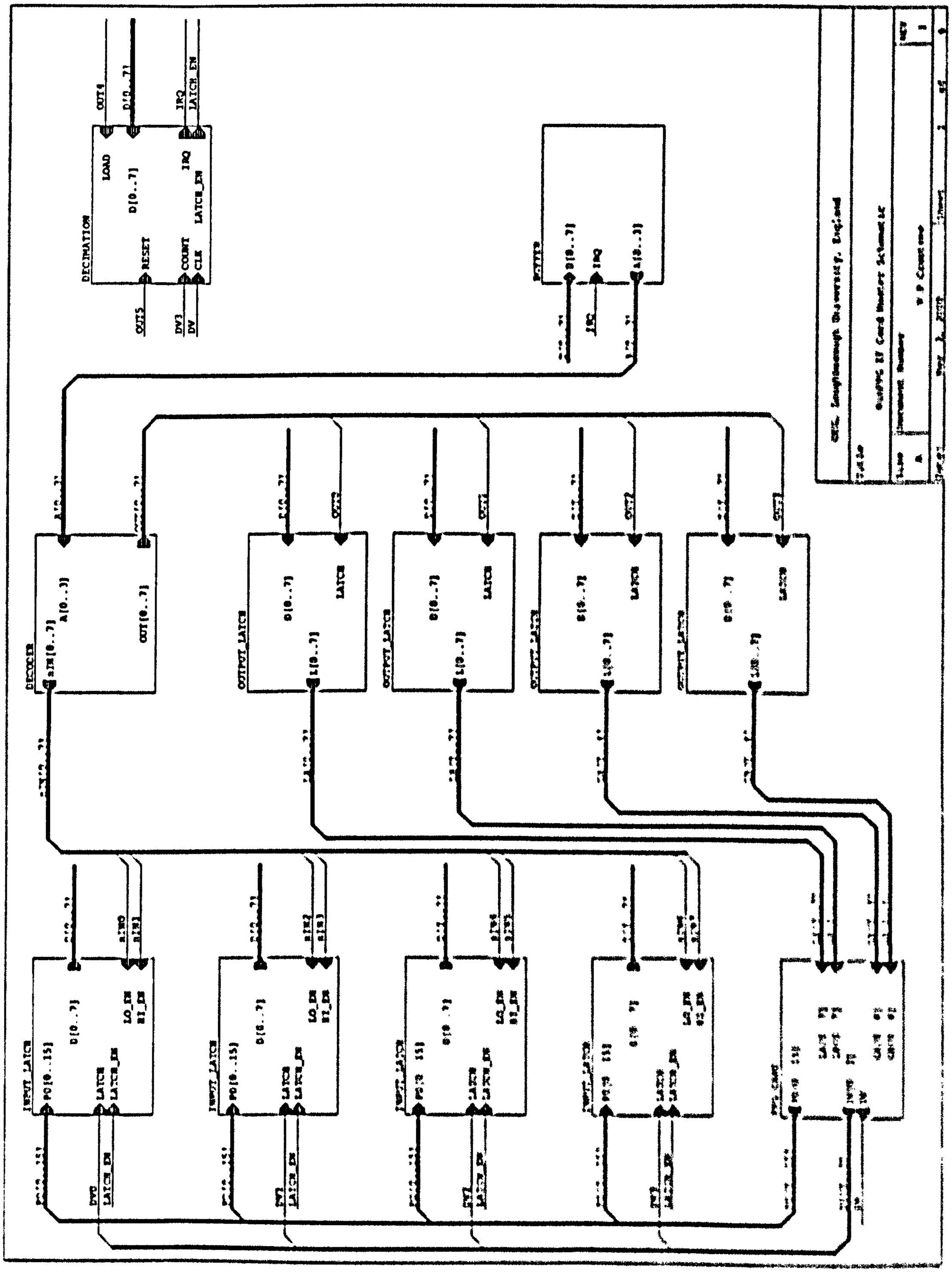

Figure B-4. Master Hierarchical View of PPG Interface Card.

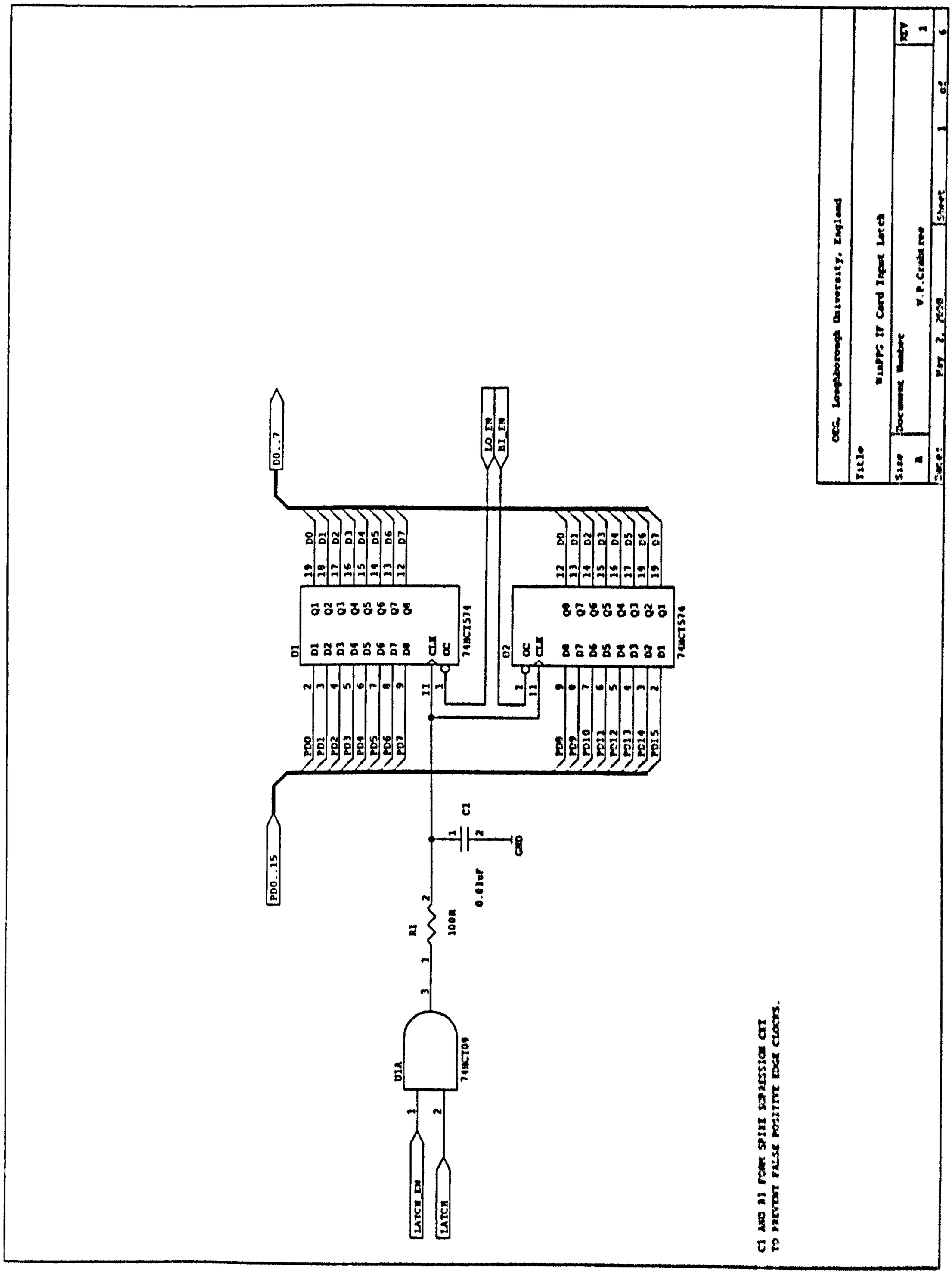

Figure B-5. WinPPG Input Latch.

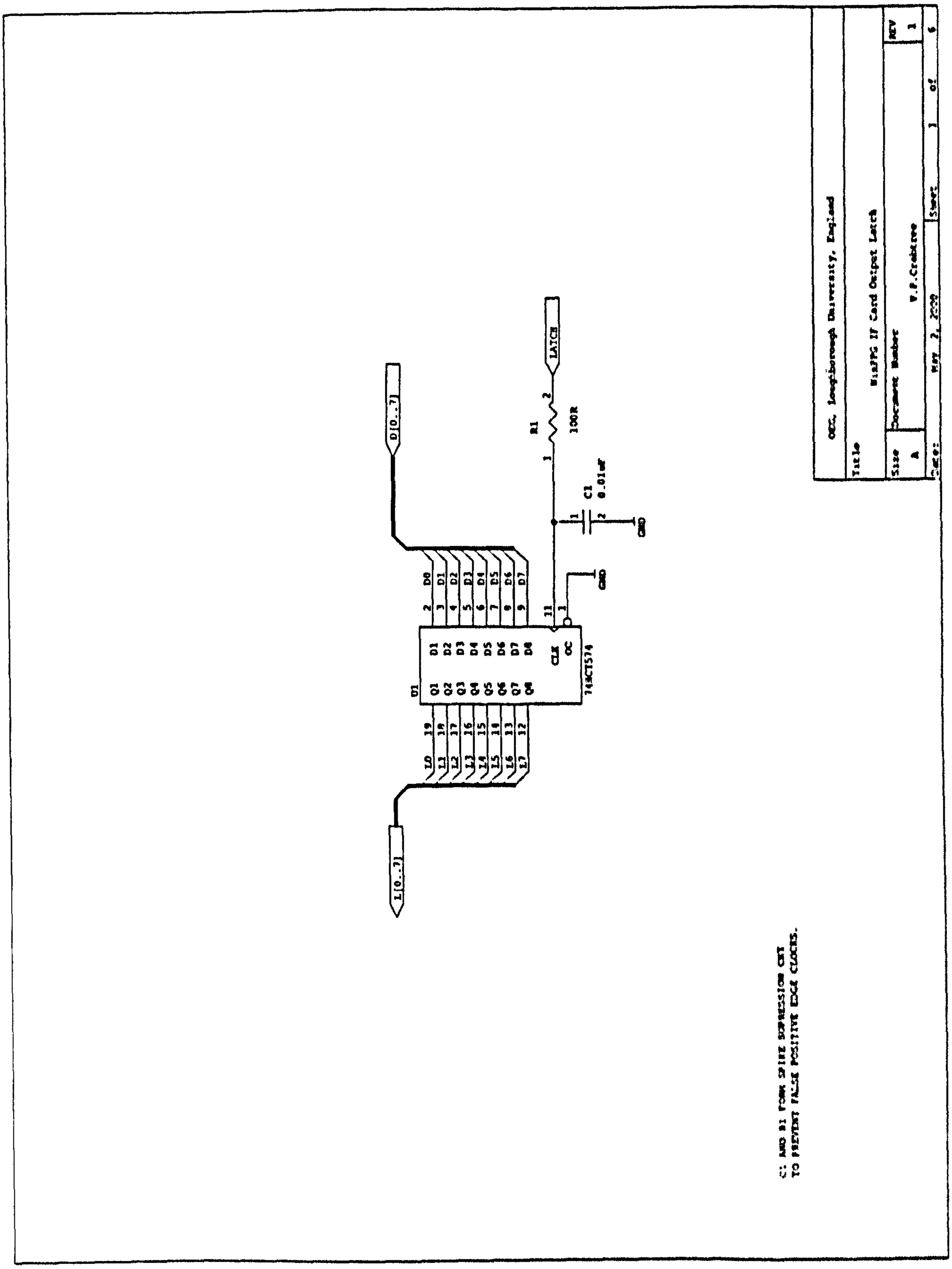

Figure B-6. WinPPG Output Latch.

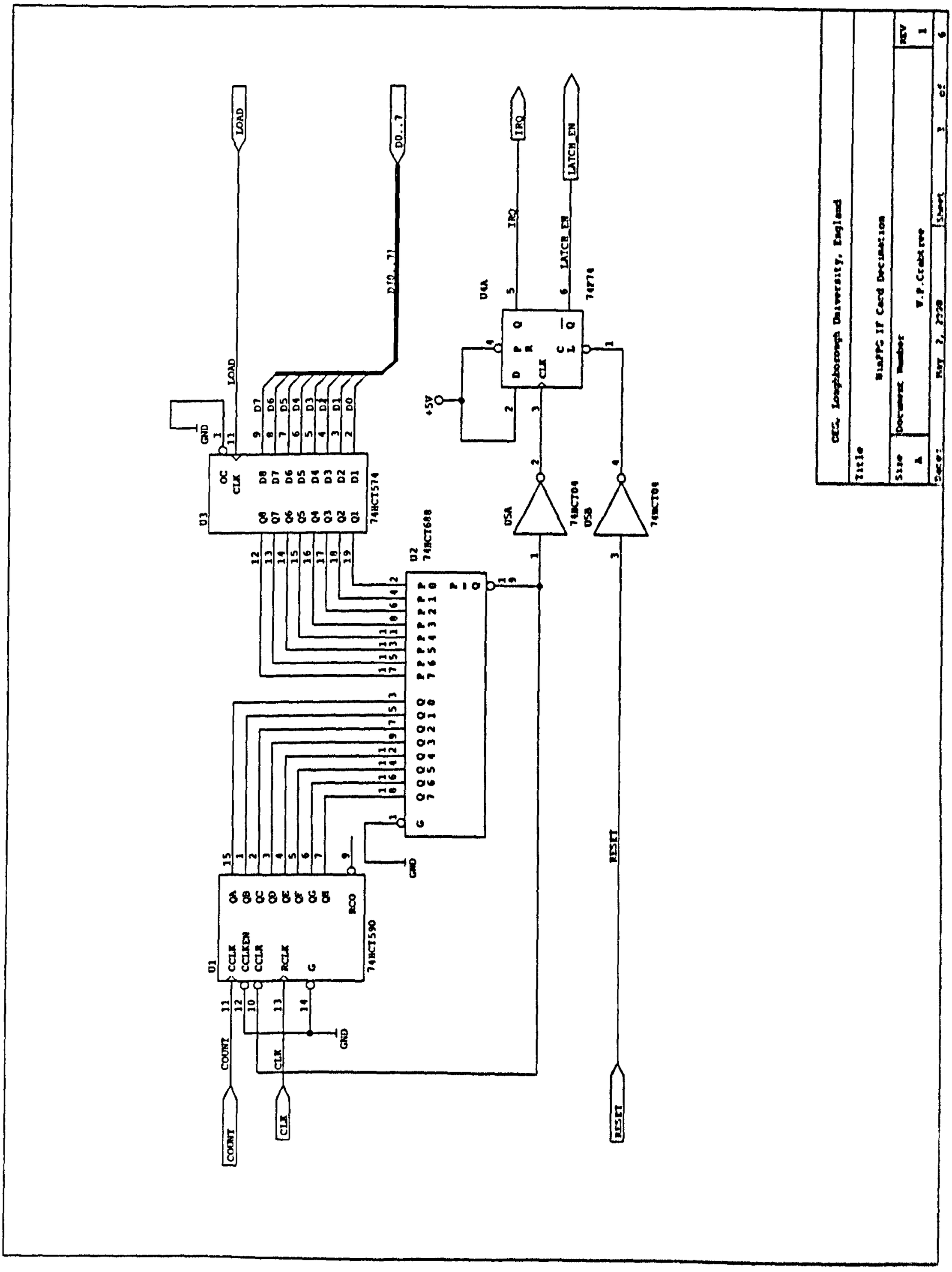

Figure B-7. WinPPG Decimation Circuitry.

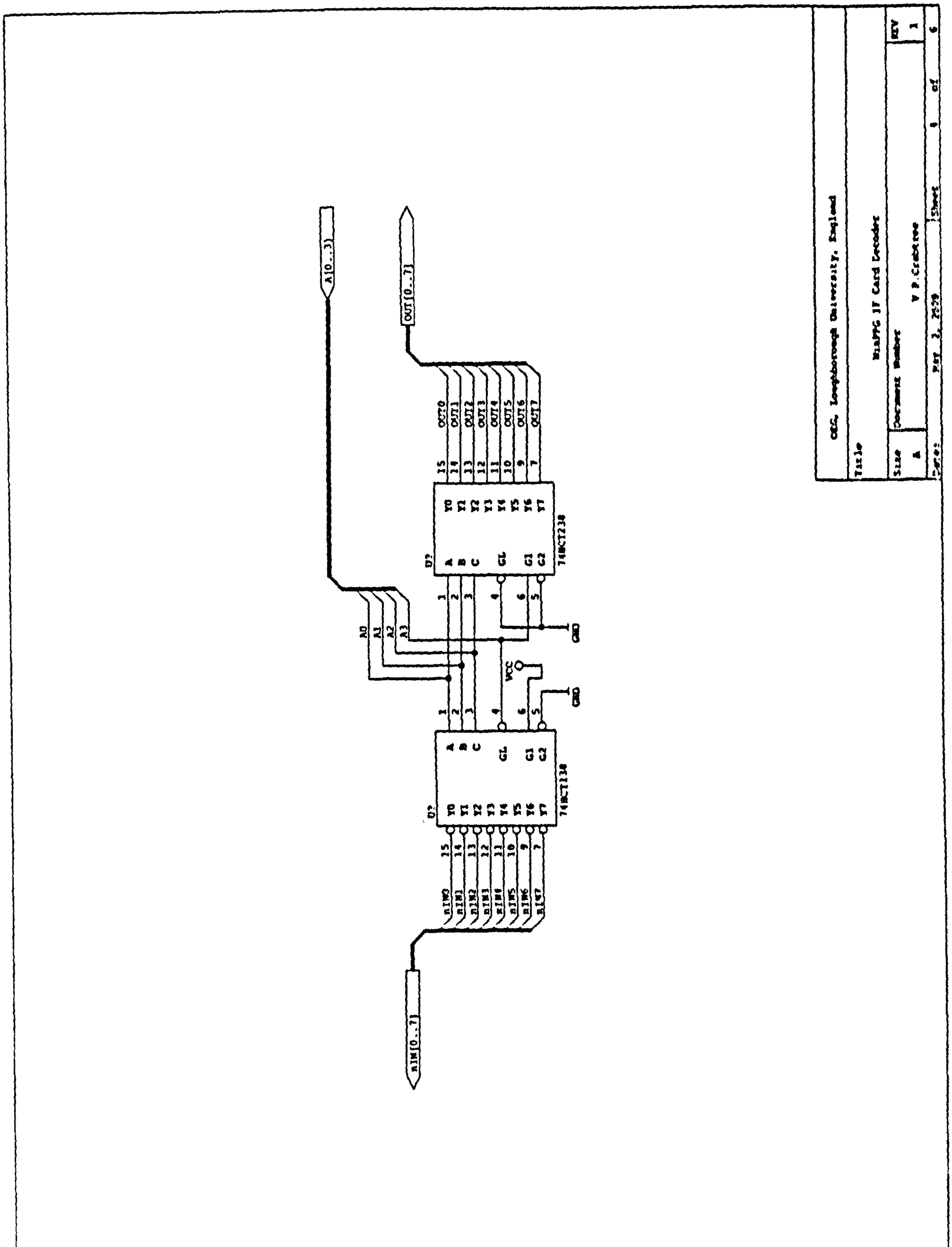

Figure B-8. WinPPG Latch Decoder Circuitry.

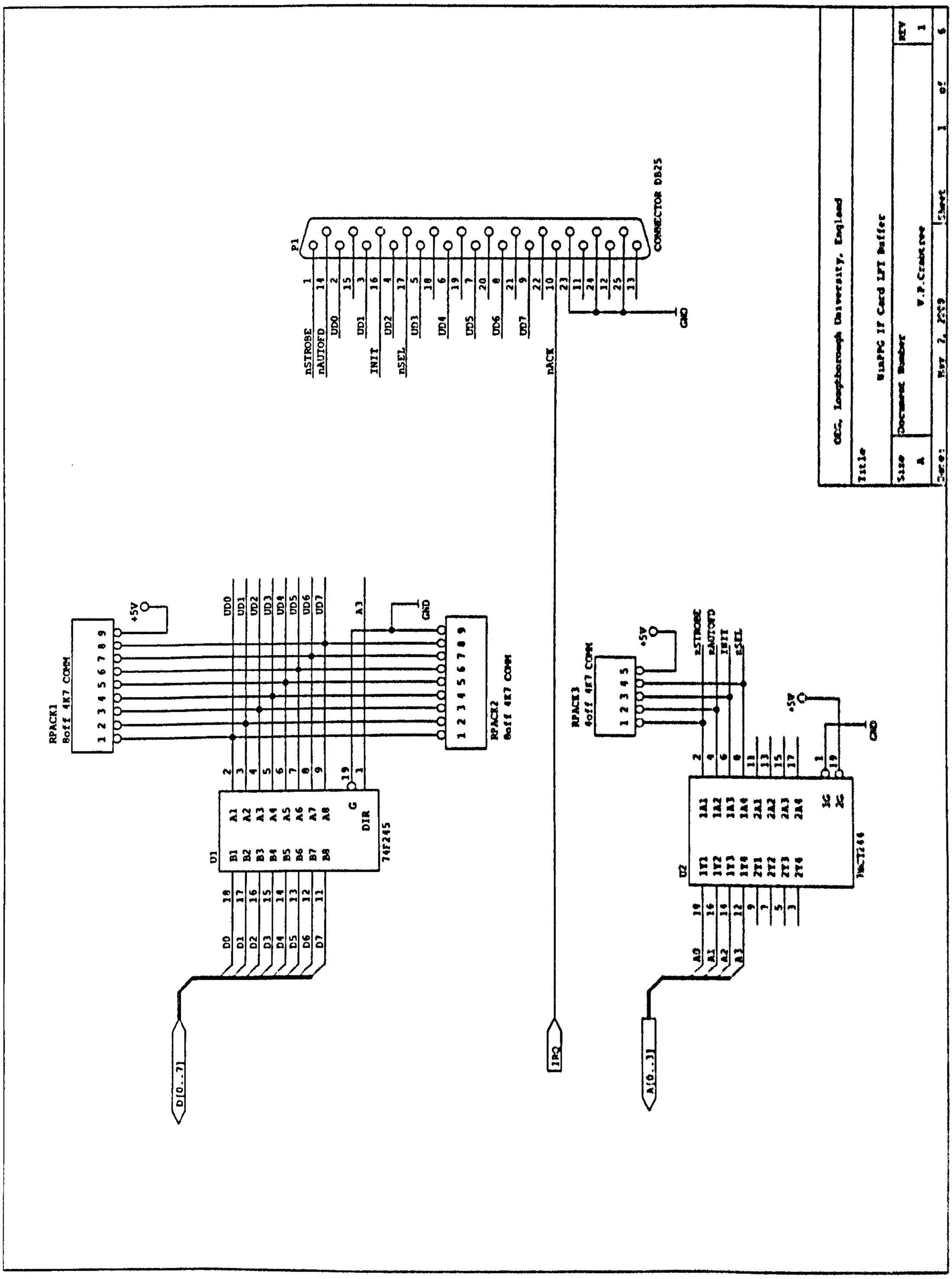

Figure B-9. WinPPG LPT Driver Circuitry.

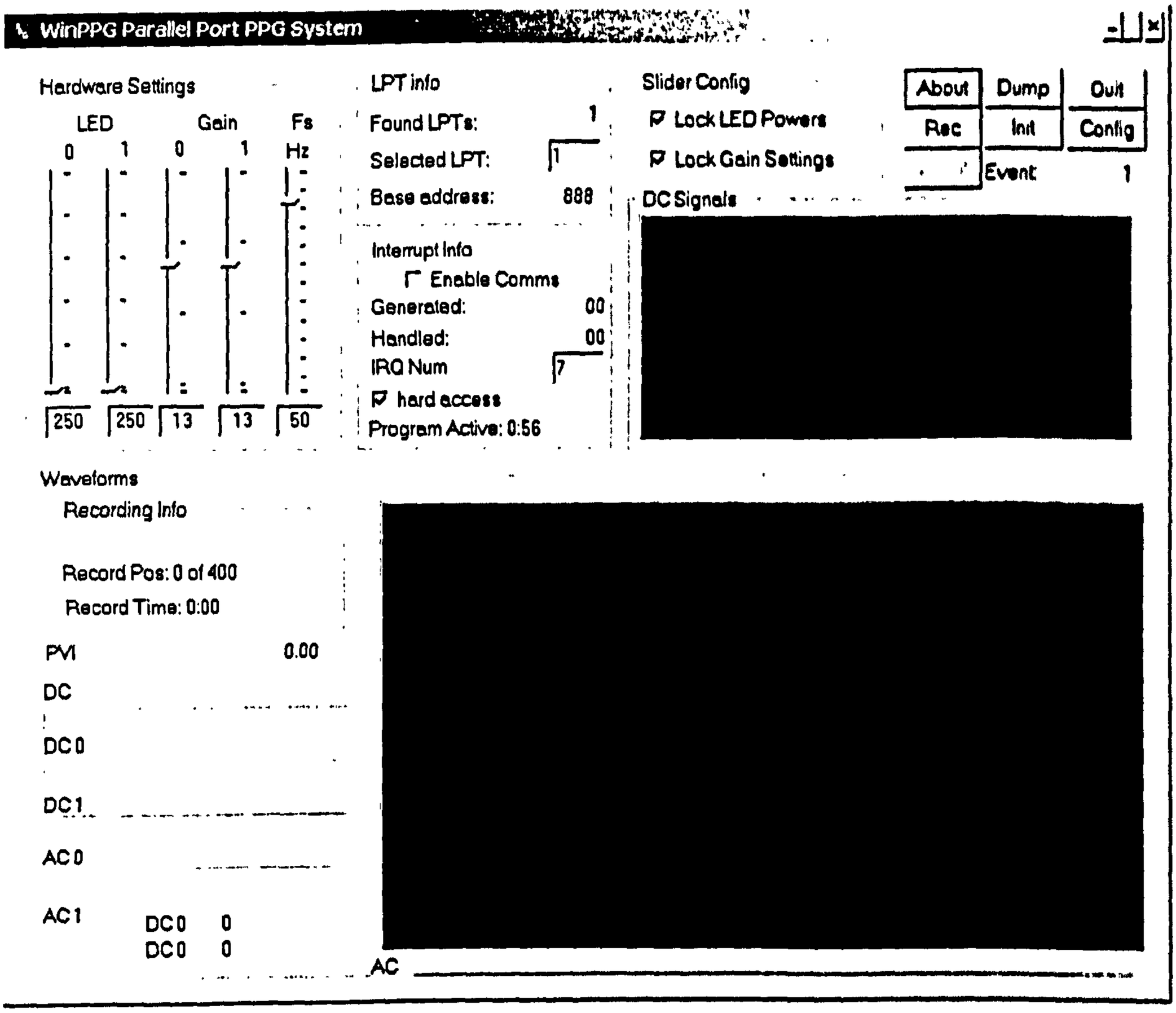

Figure B-10. WinPPG Dialog Box

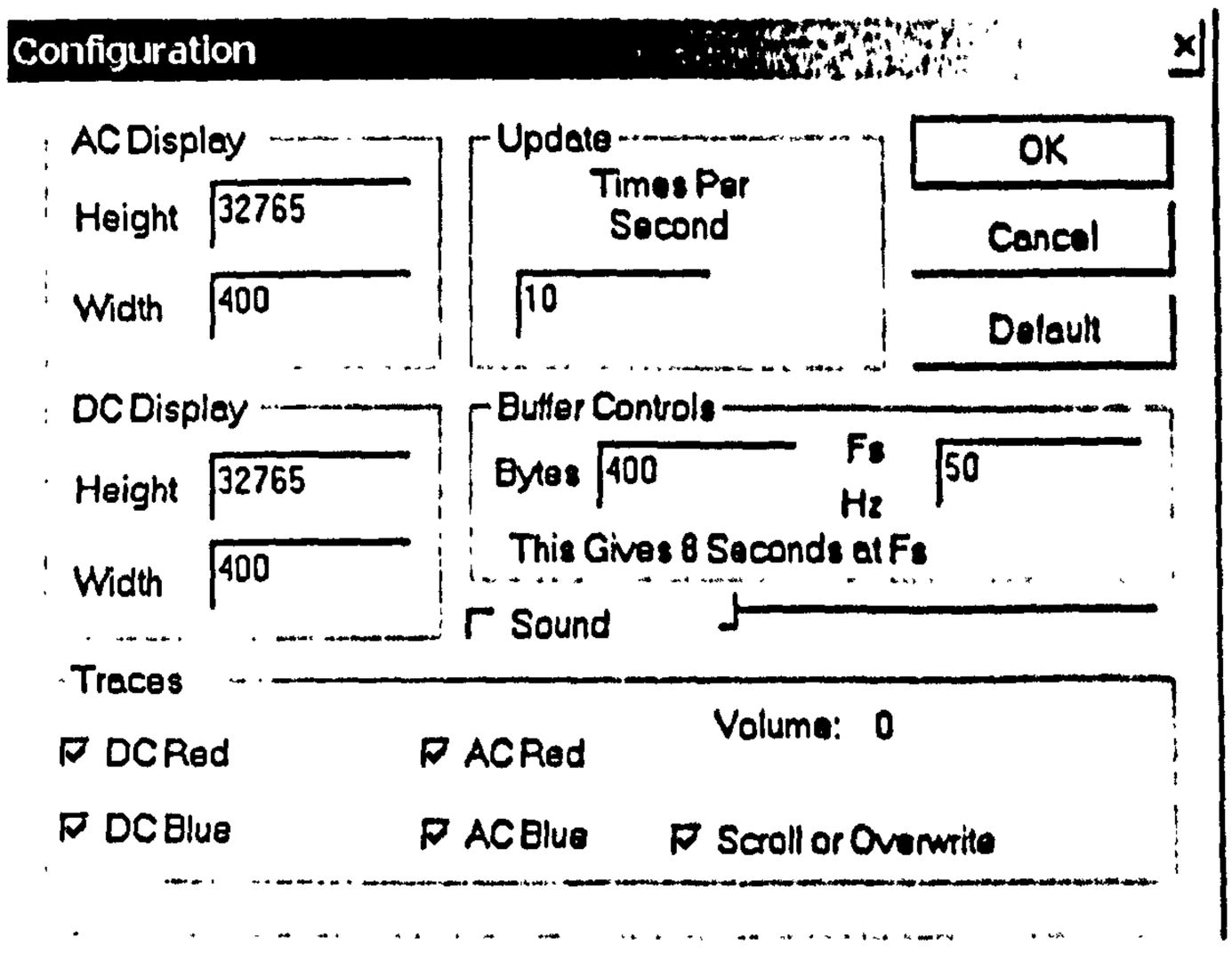

Figure B-11. WinPPG Configuration Dialog

B.5 Appendix B References

[1] Hayes M., "Artefact Reduction in Photoplethysmography", PhD Thesis, Loughborough University, England (1998)

[2] TVicHW32 V3.0, Copyright 1998 Victor Ishikeev, http://www.entechatiwan.com